Petrologic evolution and stratigraphy of the eruptive products from the 7.7ka (^{14}C) Kurile Lake caldera eruption, southern Kamchatka, Russia.

by
Peter G. Rinkleff

Submitted in Partial Fulfillment of the Requirements
for the Degree of Master of Science in Geology
September, 1999

Department of Earth and Environmental Science
New Mexico Institute of Mining and Technology
Socorro, New Mexico

ABSTRACT

The 7.7ka old Kurile Lake eruption in southern Kamchatka, Russia, deposited pyroclastic fall and surge deposits and a thick, unwelded ignimbrite sheet. The initial stages of the eruption are characterized by either pyroclastic surge or phreatoplinian fall deposit and widespread lapilli pumice fall from a central vent. Fall units are followed by laminar to weakly crossbedded surge beds and the final stage of the eruption produced a thick and extensive ignimbrite.

Individual pumice clasts from the fall and surge deposits range from dacite to rhyolite, whereas the composition of pumice and scoria clasts in the ignimbrite range from rhyolite (73% SiO_2) to basaltic andesite (51% SiO_2). Ignimbrite exposures south and west of the caldera are dominantly rhyolite, with minor dacite clasts. Exposures north and east of the caldera are chemically zoned from rhyolite at the base of the exposure to basaltic andesite mid-section, and back to rhyolite at the top.

Black scoria comingled with white pumice is common in clasts from the ignimbrite where it shows zoning. Electron microprobe analyses of banded clasts, however, shows a complete range in composition from 60-76% SiO_2, indicating mixing occurred. The mingled textures are interpreted to be a short interval event, imprinted on a longer time scale mixing event. Homogeneous samples have one glass composition in contrast to the range contained in banded clasts.

Plagioclase is the dominant phenocryst followed by orthopyroxene, clinopyroxene, magnetite, ilmenite, amphibole and apatite. Plagioclase found in dacites and rhyolites can be euhedral and complexly zoned or unzoned, and range from An_{72} to An_{32}. In andesites and basaltic andesites plagioclase is compositionally similar to those

found in dacites and rhyolites. However, in andesites, some sieve textured, unzoned An_{93-43} plagioclase have overgrowth rims of more evolved feldspar compositions. Most samples contain orthopyroxene and clinopyroxene, but rhyolite ashfall pumice only have clinopyroxene. Pyroxenes are euhedral to subhedral and unzoned. Magnetite and ilmenite are unzoned and are commonly subhedral and rarely anhedral. Temperature determinations made using a magnetite-ilmenite geobarometer range from 920 to 780°C. Euhedral amphibole is found in early deposited fall rhyolites. Amphibole geobarometery suggest crystallization occured at pressures of 2.2-2.8kbar. Rare euhedral to anhedral apatite was found in all samples.

Least-squares mass balance models show that the entire suite may have evolved by fractional crystallization from the most basic basaltic andesite. These models suggest that only 25% of the magma chamber may have erupted. Mineral abundances calculated in these models agree with estimates of modal abundances observed in clasts.

Chamber geometry, complex venting or drawdown processes of a compositionally zoned magma chamber may be responsible for the compositional zonation seen in outcrops in the field area. Textures observed in hand sample and microscopic analysis are interpreted to be the result of comingling of magmas during eruption. Long period mixing may have been taking place as is evidenced by the range of glass compositions in banded clasts. Fractional crystallization was responsible for forming at least the basaltic andesite and andesite magmas. It is possible that mixing of andesitic magma and a partial melt rhyolite may be responsible for the formation of dacite magma.

Acknowledgements

This study of the Kurile Lake eruption was suggested by Dr. Philip R. Kyle who was my academic and thesis advisor. His instruction in the field was invaluable to this study. Philip also provided the funds to conduct the INAA and XRF analyses, as well as transportation to and from Kamchatka. Without Dr. Kyle's help with data interpretation and many, many manuscript reviews, I would have not been able to begin to describe the Kurile Lake eruption. This work would not have been possible without the assistance of Dr. Vera Ponomareva and Oleg Dirksen of the Institute of Volcanic Geology and Geochemistry, Russian Academy of Science, Far East Division, in Petropavlovsk-Kamchatsky. They were a great help in matters of field logistics as well as my source of information from Russian language journals. Their extensive planning made field work in the remoteness of Kamchatka comfortable and efficient. Field work in Kamchatka was supported by a grant from the National Geographic Society to Dr. Ponomareva. The generous assistance of Dr. Nelia W. Dunbar of the New Mexico Bureau of Mines and Mineral Resources in accomplishing the electron microprobe analyses as well as answering my questions about interpretation and presentation and reviewing my manuscript is greatly appreciated. Sarah Lundberg provided much needed assistance with the operation of the electron microprobe during my first days of analyses. Her hand-holding during that time allowed me to work efficiently and acquire the excellent data set contained in this thesis. NSF grant STI-9413900 partially funded the purchase of the electron microprobe. Dr. Kent Condie reviewed the manuscript for this thesis. His insightful (and difficult) questions kept me honest in interpretation of data. I also thank Dr. Chang Hwa-Chen of the Department of Earth Science, Academica Sinica, Taipei,

Taiwan, for providing Sr and Nd isotopic data. These data made it possible to interpret magma source and history. Funds provided by the Research and Development Division of New Mexico Institute of Mining and Technology (NMIMT), along with funding from the Geophysical Institute of the University of Alaska allowed me to present preliminary results of this work at the Kamchatkan-Aleutian Workshop in Petropavlovsk-Kamchatsky and conduct further field work during the summer of 1998. I also received a two year teaching assistanceship from NMIMT as well as a grant during the summer of 1997, which helped defray tuition and personal expenses during my time at NMIMT. Hourly work and a research assistance with Dr. Dunbar and Dr. Kyle provided income after the teaching assistanceship expired.

Outside of all the technical, scientific and financial assistance I received, many others made it possible to complete this work. Namely my friends and family who kept me on an even keel and helped me maintain perspective. I should also thank the excellent office staff, Patci Mills, Connie Apache and Joni Mauldin for their sense of humor as well as expertise and patience. During the field work in Kamchatka, Shelly Rourke provided much needed humor and random weirdness to break-up the mood-killing wetness and strain. I also would like to thank Natasha, Alya, Sasha, Kolya and Alexi, the field assistants who cooked, cleaned, made tea, dug holes, hauled water and rock samples, and taught me enough Russian to get in trouble.

TABLE OF CONTENTS

TABLE OF FIGURES

TABLE OF TABLES

CHAPTER ONE

INTRODUCTION

Study of pyroclastic rocks, particularly ignimbrites, from caldera forming eruptions has contributed greatly to understanding the physical and chemical processes accompanying growth and differentiation of silicic magma bodies (e.g. Druitt and Bacon, 1988; Hildreth, 1983; Nakamura, 1995). Large ignimbrite eruptions sample a parental magma chamber during its formation, whereas plutons are frozen magma bodies, which have cooled over long periods of time (Bacon, 1983, Wilson, 1993). Pyroclastic materials provide quenched, unaltered magmatic liquid and crystals. Ignimbrite producing eruptions can erupt tens to hundreds of cubic kilometers of magma, tapping levels down to 2km in a chamber (Smith, 1979).

Magma mixing has often been cited as an important process in the development of igneous rocks (e.g. Hildreth, 1981; Wilson, 1989; Bacon, 1983; Sakuyama, 1981; Didier and Barbarin, 1991). Hybridization, fractionation and internal mixing are part of the pre-eruptive history of any long-lived intermediate to silicic magmatic system (Hildreth, 1981; Sakuyama, 1981; DePaolo 1981). In intrusive igneous rocks, the evidence of mixing is often obscured in long-lived plutons due to chemical and thermal diffusion over time (Wilson, 1993). Indeed, mixing of magmas may be a triggering mechanism for eruptions (Sparks and Sigurdsson 1977). For example, as hot, mafic magma is intruded into a cooler, intermediate or silicic magma, simultaneous vigorous convection, changes in volatile solubility, quench crystallization and superheating occur.

The 7.7ka B.P. (^{14}C) Kurile Lake eruption (KLE) deposited over 200km^3 of pyroclastic material which consists predominantly of rhyolite and dacite pumice. Porphyritic andesite and basaltic andesite clasts were also ejected during the eruption. The eruption was the largest Holocene eruption in the Kamchatka Peninsula (Braitseva et al., 1998).

The objective of this work is to present stratigraphic and geochemical data and present models for the caldera-forming eruption and petrogenesis. Geochemical analyses of 92 whole rock samples and electron microprobe analyses of phenocrysts and glass are used to model the petrologic evolution of a zoned magma chamber and constrain the conditions during the 7.7ka B.P. Kurile Lake eruption. Clasts in the Kurile Lake pyroclastic deposits commonly show banded pumice due to mixing of dacitic and basaltic andesite magma, and provide clear examples of syn-eruptive magma mingling (Smith, 1979). Disequilibrium textured mineral phases observed in Kurile Lake pumices may indicate addition of mafic magma into a fractionating magma chamber, or may be a result of quench crystallization.

Samples used in this study were collected during the 1996, '97 and '98 field seasons. Field descriptions of 32 outcrops and pits were made while collecting samples for geochemical analysis. A general section, including the fall, surge and pyroclastic flow units is developed to illustrate the eruptive sequence and to show compositional zonation present within the deposit. The eruption produced a thick sequence (up to 200m) of pyroclastic materials, which are interpreted to represent deposition from a plinian column, surge due to column collapse and ending with ignimbrite from pyroclastic flows.

CHAPTER TWO

REGIONAL GEOLOGY

Introduction

Kurile Lake is located at the southern end of the Kamchatka Peninsula and the Eastern Volcanic Front (EVF), the easternmost volcanic chain in Kamchatka (Fig. 2.1). The Kurile-Kamchatka arc extends from the western end of the Aleutian arc to northern Japan. Volcanism along this arc results from the subduction of the Pacific plate underneath the Okhotsk and the North American plate (Gorbatov et al., 1997). Seismicity is common along the arc, producing sizeable subduction related earthquakes such as the magnitude 7.7 Kronotsky earthquake of December 5, 1997 (Gordeev et al., 1998). Kurile Lake is located in the Southern Kamchatka volcanic group of the EVF (Fig 2.2) and occupies a caldera formed in the 7.7ka B.P. eruption (Braitseva et al., 1995). Dikii Greben and Illinsky, two post-caldera eruptive centers, flank the Kurile Lake caldera. Zheltovsky, Koshalev and Kambalny in the southern volcanic group were all active prior to the Kurile Lake eruption. Today, all the volcanoes in the southern Kamchatka volcanic group are considered active (Fedotov and Mauserenkov, 1991 and references therein; Bindemann and Bailey, 1994). The basement in southern Kamchatka is a volcanic sequence forming from Late Miocene to the present and represents a typical calc-alkaline series (Zonenshain et al., 1990; Erlich and Ghorskov, 1979).

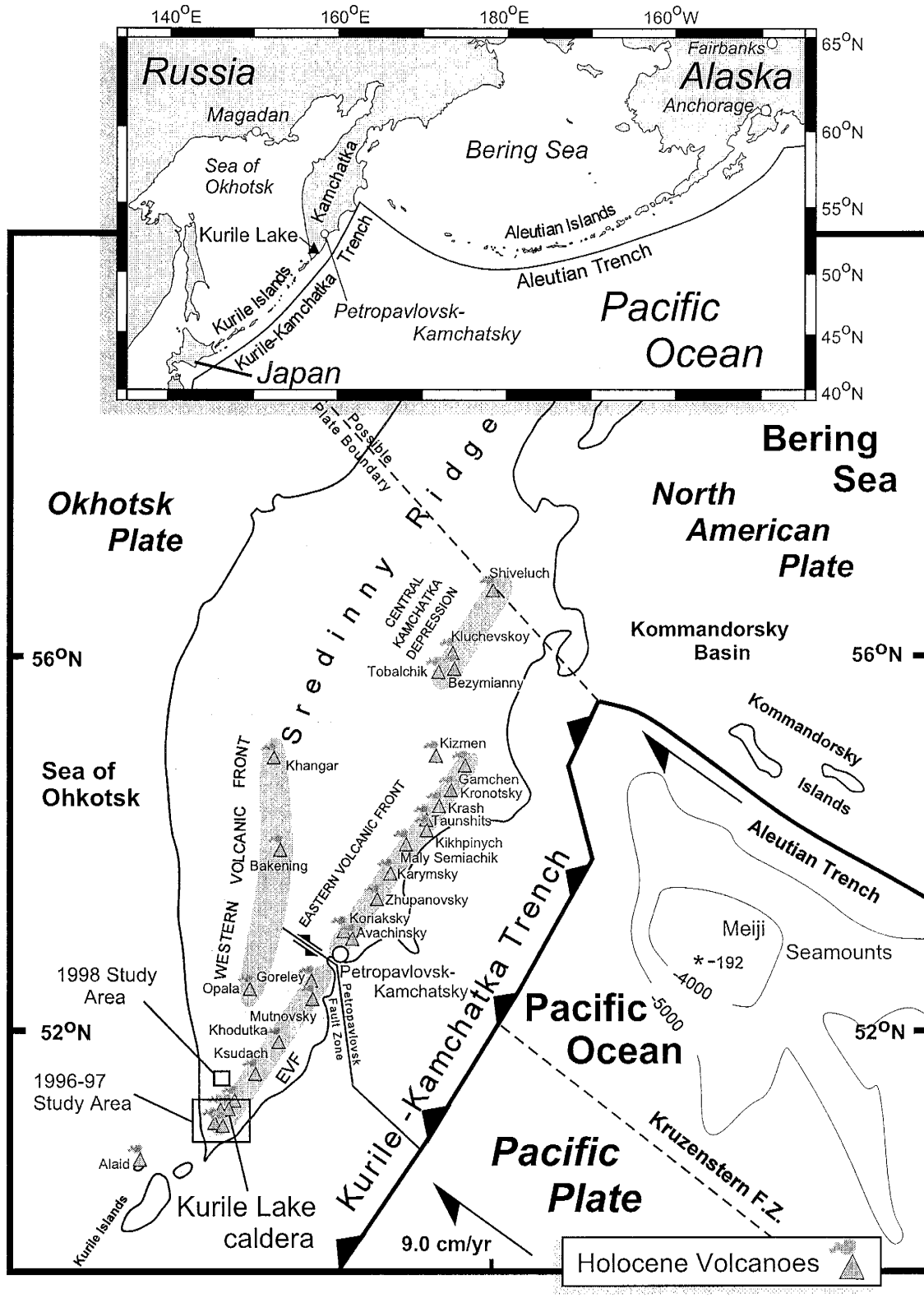

Figure 2.1. Tectonics and Holocene volcanoes of Kamchatka modified from Ponomareva (1998). EVF-Eastern Volcanic Front

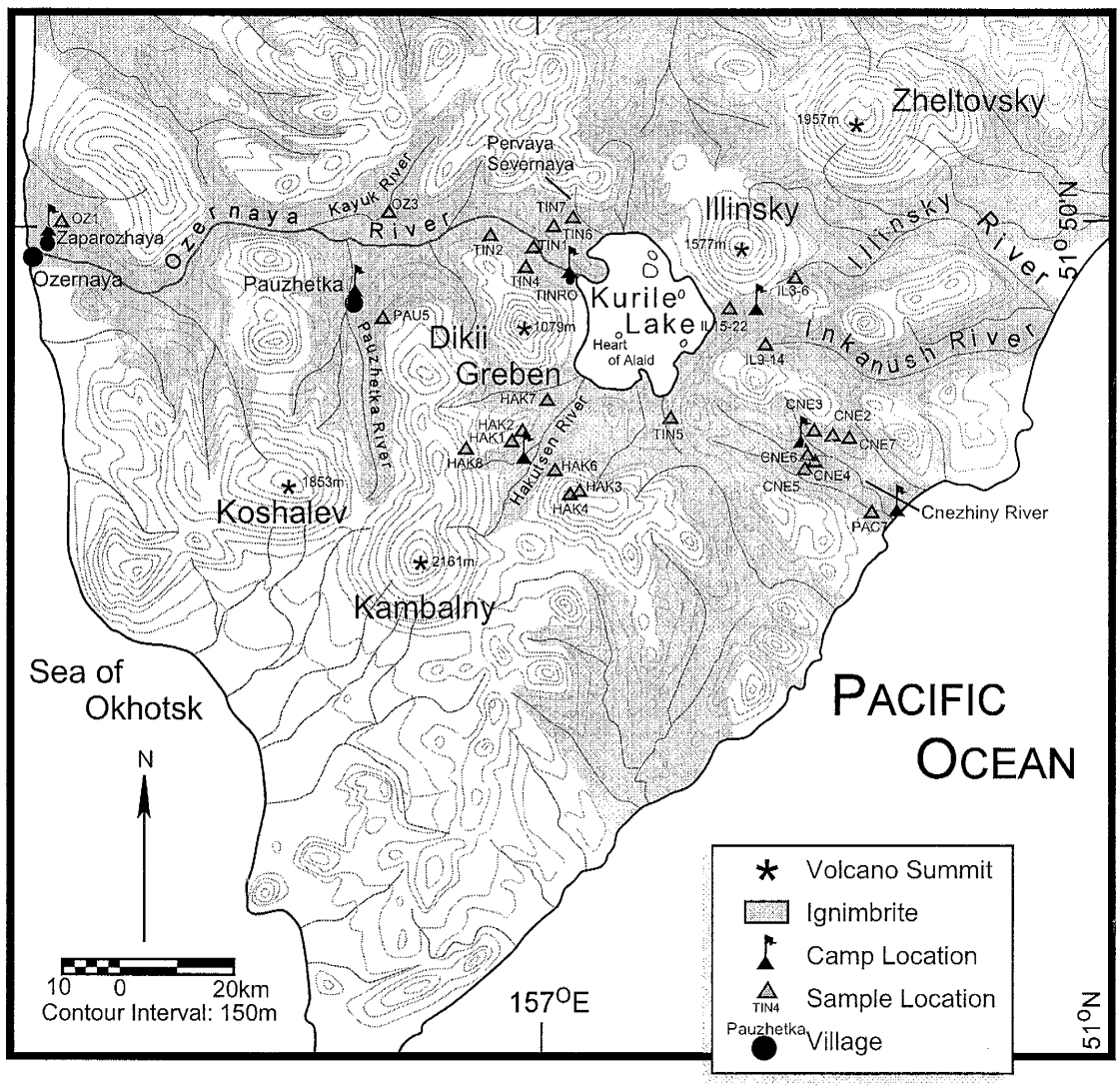

Figure 2.2. Location map of the Southern Kamchatka Volcanic Group and Kurile Lake Ignimbrite. Adapted from Ponomareva, (1998) and 1:100,000 scale topographic map. Ignimbrite cover was determined from an unpublished map by Melekestev (1998).

Tectonic Associations

The Kamchatka Peninsula is a collection of Late Cretaceous to Cenozoic accretionary complexes of Pacific affinity (Fujita et al., 1997) in an accretionary zone between the stable platforms of the North American, Okhotsk and Eurasian plate. Subduction of the Pacific plate under the Okhotsk plate has produced a deep trench and an accompanying volcanic front extending from Shiveluch in the north, to Hokkaido, Japan. The Eastern Volcanic Front (EVF) lies inboard of the Kurile-Kamchatka trench approximately 150km to the west and 100 km above the Wadti-Benioff zone (Gorbatov et al., 1997). Subduction along this margin takes place at 9cm/yr (Lees and Davaille, 1998) (Fig. 2.1). The plate motion changes from subduction along the Kurile-Kamchatka arc to strike-slip motion along the Aleutian arc at the junction of the Kurile-Kamchatka and Aleutian trenches. The Pacific plate subducts at an angle of 55° south of 55°N. There are two submarine structures complicating the subduction of the Pacific plate: the Kruzenstern fracture zone and the Meiji seamounts, which are the northernmost features of the Emperor Seamount chain. According to Gorbatov et al., (1997) the subduction of the Meiji Seamounts and Kruzenstern Fracture Zone above 54°N causes the angle of the subducting Pacific plate to change to 35° north of 55°N. The effect of this shoaling of the subducting plate shifts the depth of seismicity from 500km south of 50°N to 300km north of 55°N. Another effect of the reduction of subduction angle is that north of 55°N volcanism shifts landward to the Central Kamchatka Depression (CKD) (Gorbatov et al., 1997). The shoaling of subduction may account for the unique volcanic nature of the CKD.

Local Geology

The Southern Kamchatka volcanic group includes Zheltovsky, Koshalev, Kambalny, Illinsky and Dikii Greben (Fig. 2.3), which are considered active due to current fumerolic activity or eruptive history (Zonenshain et al., 1980; Erlich and Ghorskov, 1979). Other inactive features are the Pauzhetka volcano-tectonic depression and the Ikranysh caldera. The most recent eruption was at Zheltovsky in 1923, Illinsky erupted in 1901 (Novograblenov, 1932) and Koshalev is thought to have erupted in the 17th century (Litasov, 1991). The Pauzhetka geothermal field is a prominent feature in the region, which produces geothermal power for the towns of Pauzhetka, Zaparozhaya, Ozernaya and small collective farms. Kurile Lake caldera is located roughly in the center of the southern Kamchatka volcanic group (Fig. 2.2).

Basement geology

The basement consists of a slightly deformed and metamorphosed tuffaceous sandstone and siltstone interbedded with andesitic lavas of the Middle-Upper Miocene age Kurile complex. The Kurile complex is overlain by several volcanic suites of Upper Pliocene-Middle Quaternary age. The lowest unit is a lava–pyroclastic suite, 80-150m thick, overlain by tuff and conglomerate containing clasts of silicic tuff, diorite porphyry and andesite. This unit is followed by an ignimbrite horizon 150-190m thick. This horizon is overlain by the terrigenous volcanic rocks of the Pauzhetka suite up to 800m thick (Erlich and Gorshkov, 1979). The Pauzhetka suite is heavily intruded with dikes and sills and changes upward from mafic tuff breccia (lower subunit), to coarse tuff of

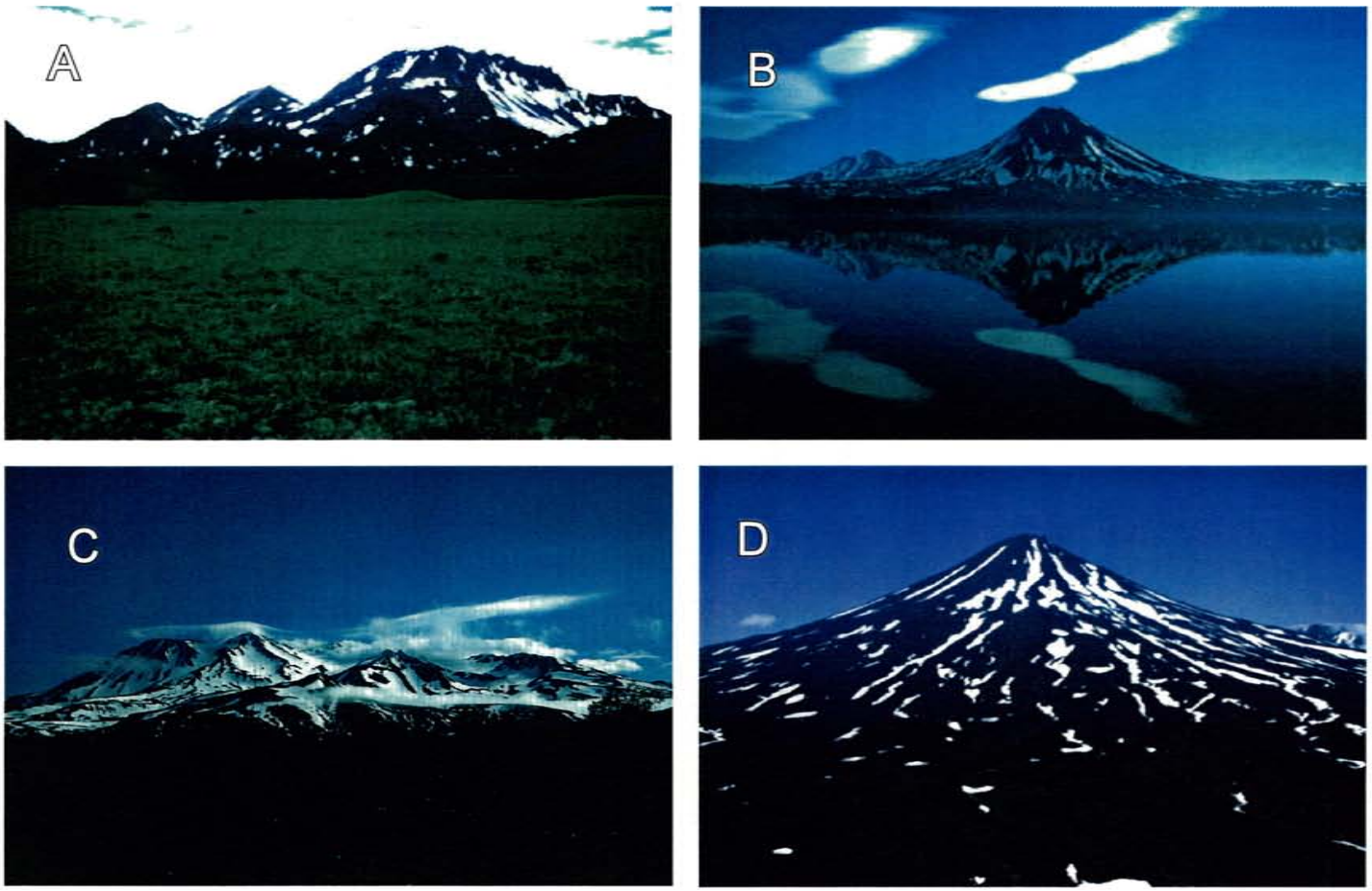

Figure 2.3. Volcanoes of the Southern Kamchatka volcanic group. A) Dikii Greben B) Illinsky with Zheltovsky behind. C) Kambalny D) Koshalev

intermediate to silicic composition (middle subunit), to silicic pumiceous tuff (upper subunit).

Kurile Lake Caldera Structure Associations

The Kurile Lake caldera is a Krakatau-type caldera which formed 7.7ka B.P. (^{14}C) (Braitseva et al., 1995). The caldera is located in the eastern portion of the Pauzhetka depression and is occupied by Kurile Lake (Erlich and Gorshkov, 1979). Melekestev (1974) suggests that the Kurile Lake caldera may be located within a poorly defined Pleistocene caldera. Echo sounder studies by Zubin et al. (1982) divide the lake basin into three parts (Fig. 2.4). The northern portion of the lake is flat-bottomed and 3km across, with a depth of 200m. The southern part is about 10km across, roughly rectangular and characterized by short step-like segments with steep slopes of 60° up to 300m depth. A medial ridge 150m across separates the northern segment and southern segment.

The Kurile Lake caldera represents a gravity and magnetic field minimum within regional low gravity values (Erlich and Gorshkov, 1979; Erlich, 1986). Values are lowest on the rhyolite dome islands in the lake. The low gravity field at Kurile Lake is interpreted to be due to a low-density body, possibly a magma chamber about 10km across and at a depth of 4km. The magnetic field is complex but generally low over the lake. Within the generally low values, the magnetic field is lowest in the northern part of the lake, and in the southern part of the lake. In general, the magnetic field is similar to the bathymetry of the lake bottom.

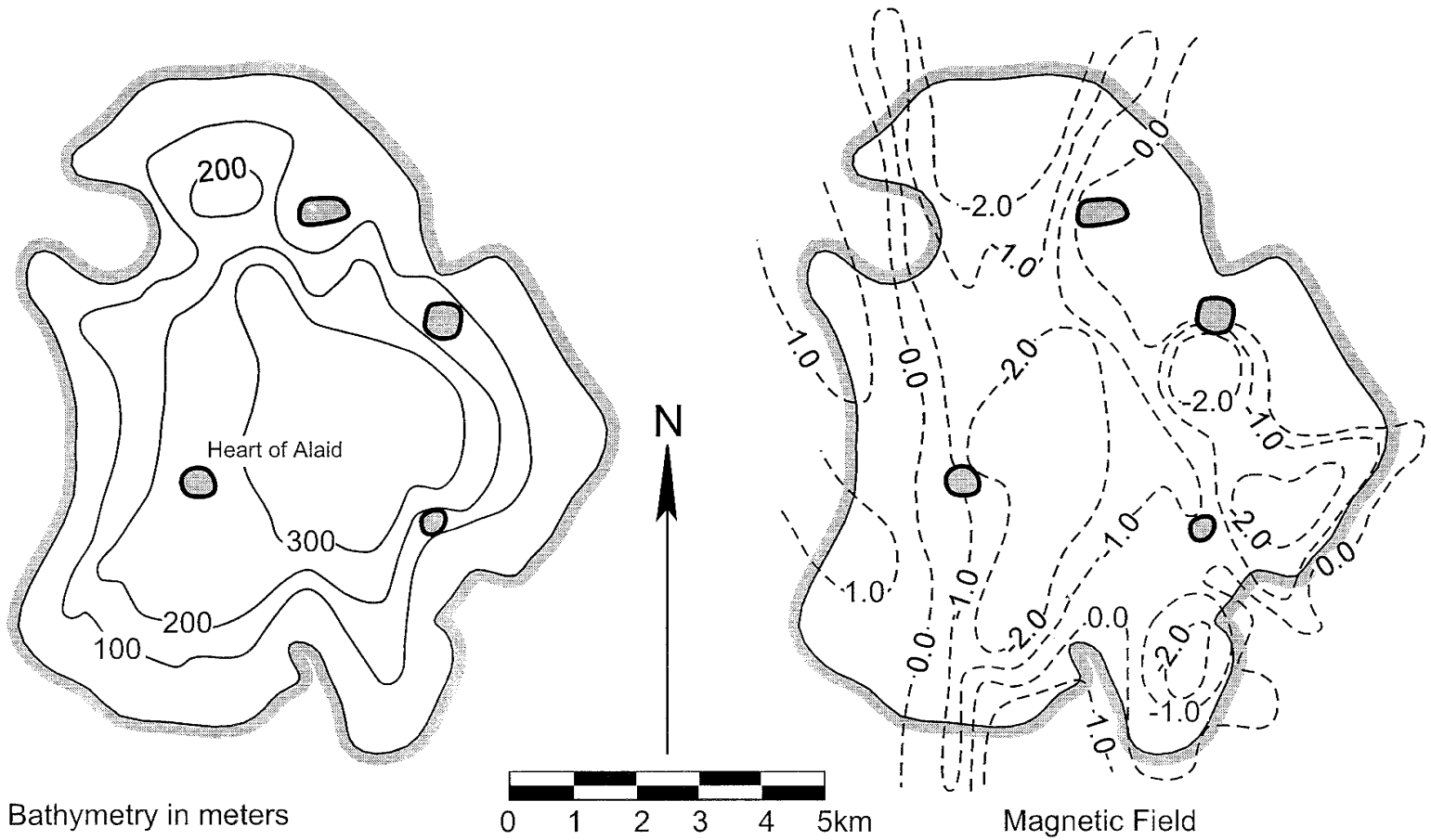

Figure 2.4. Bathymetry and magnetic field data for Kurile Lake as reported in Erlich (1986). Magnetic field data is reported in unspecified units relative to local magnetic field values (also unspecified). (Magnetic data is considered sensitive strategic information by the Russian government and is unavailable.)

Other Associated Volcanoes

Five active volcanic edifices along with the Kurile Lake caldera comprise the southern Kamchatka volcanic group. Of these, Illinsky and Dikii Greben (Fig. 2.3a,b) volcanoes formed after caldera-collapse and are located close to the caldera. Zheltovsky, Kambalny and Koshalev (Fig 2.3b-d) may have started to form in the Pliocene (Fedotov and Mauserenkov, 1991 and references therein) and are still active today.

Illinsky Volcano

Illinsky Volcano (Fig 2.3b), is a 1578m high stratovolcano located on the northeastern shore of Kurile Lake (Kozhemyaka and Vazheyevskaya, 1991). The edifice covers 60km^2 at the base and has a volume of 40km^3. On the northeastern slope a large phreatic crater formed in 1901 and marks the last eruption of the volcano. Two large lava flows are evident on the northern slope of the volcano. The summit crater contains a young nested cone.

Illinsky was formed in three main phases according to Kozhemyaka and Vazheyevskaya (1991). The current edifice is built on the remains of an older (Old Illinsky) edifice (Ponomareva, pers comm 1997). Volcanism began soon after the eruption of Kurile Lake and lasted 1.5ky and produced 11km^3 of andesite to dacite pumice. The last phase was predominantly effusive while becoming more explosive in nature, produced the two lava flows on the northwest slope and several minor effusive and extrusive domes. The formation of a large blast crater on the northeast slope of the volcano marked the last activity of Illinsky in 1901 (Novograblenov, 1932).

Dikii Greben Volcano

Dikii Greben (Fig 2.3a) is a 1500m high series of post-caldera collapse extrusive domes and lava flows located at the southwest shore of Kurile Lake (Bindemann and Bailey, 1994 and references therein). The volcano covers $40km^2$ and exceeds $15km^3$ in volume. Dikii Greben is built on pyroclastic flows of the 7.7ka B.P. Kurile Lake caldera eruption. Initial formation began with the extrusion of three rhyodacite domes from 7.7 to 1.5ka. Dacite and andesite domes and pyroclastics characterize the last 1.5ka of the volcanoes history (Braitseva et al., 1995). Large rockfalls occur annually indicating this dome may have been growing in recent times (Bindeman and Bailey, 1994).

CHAPTER THREE

FIELD INVESTIGATION OF THE KURILE LAKE ERUPTION

Introduction

The 7.7ka B.P. Kurile Lake caldera eruption produced an extensive and voluminous package of fall, surge and pyroclastic flow deposits. The distribution of pyroclastic materials (Fig 2.2) associated with this eruption has been mapped and described during this study and by others (Ponomareva, pers. comm. 1998; Melekestev, unpublished map, 1998). Pyroclastic fall deposits associated with this eruption have been identified 1000km to the west of Kurile Lake near the city of Magadan on the Russian mainland (Melekestev et al., 1991) (Fig. 2.1) and the Komandorsky Islands (Kyle, pers. comm.). Within Kamchatka, the fall deposit serves as a marker volcanic ash layer commonly used in geomorphologic studies. Braitseva et al., (1997) report the combined volume of fall and ignimbrite to total some 120-140km^3, but our field work and air photo interpretations of Melekestev (unpubl. map, Ponomareva, pers. comm. 1998) indicate the deposit may be significantly larger.

An idealized section of the pyroclastic deposits was developed during the 1997 field season and is presented in Fig. 3.1. The eruption commenced with pyroclastic fall and surge deposits, (informally named the Kurile Lake plinian, (KLp)) and ended with the emplacement of a major ignimbrite, informally called the Kurile Lake ignimbrite (KLi). Several individual units are present within each part of the sequence, but no depositional breaks were observed indicating that the eruption and emplacement of the

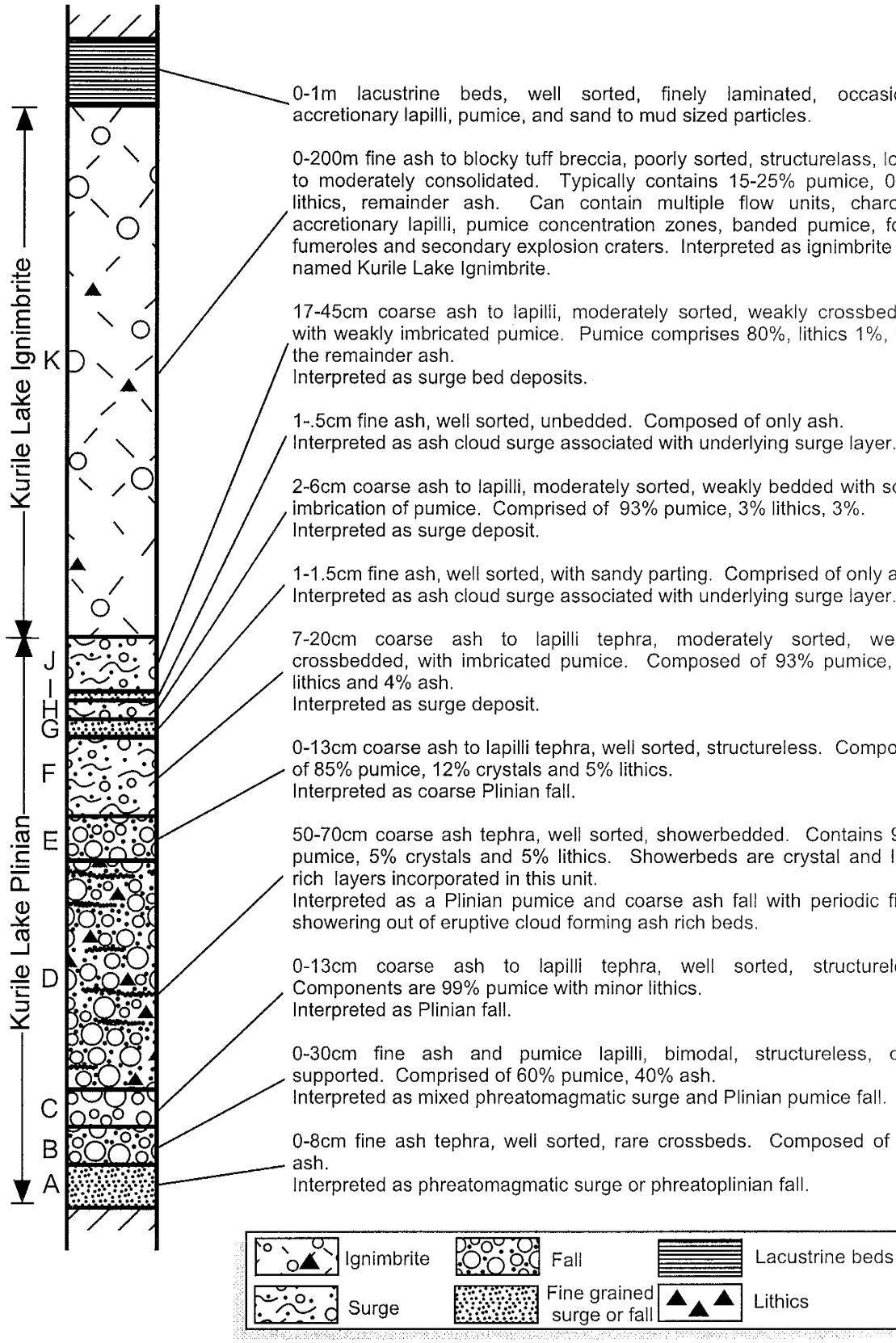

Figure 3.1. Ideal Section of the 7.7ka BP Kurile Lake eruption products

deposits were continuous. The ignimbrite has distinct chemical zonation. Complete descriptions and measured section of KLp and KLi deposits are presented in Appendix E.

Fall and Surge Deposits

Nine individual fall and surge units, (Labeled A-J in Fig. 3.1) have been recognized in the KLp deposits. Measured sections are correlated in Figure 3.2 and show significant local variability in the KLE deposits. Correlations made are based on the transitions from one dominant style of deposition changing to another since few individual units could be reliably traced over large distances. Figure 3.3 shows fall characteristics. Figure 3.4 shows surge characteristics.

Layer A is a grey, fine ash layer, up to 8cm thick, which overlies a paleosol. This has been interpreted as a surge deposit or a phreatoplinian fall deposit based on it's widespread distribution and terrain draping character. In the Pauzhetka area, exposures of fall deposits have a grey, clast supported, bimodal lapilli pumice and fine ash bed (layer B), up to 30cm thick, which overlie the initial fine ash layer. Pumices are white, angular, up to 7cm and easily crushed possibly due to hydrothermal alteration. The bimodality of this layer suggests the mixing of fall derived pumice with phreatomagmatic derived ash. Following the bi-modal layer B is a 50-70cm well sorted, shower-bedded Plinian fall pumice layer (layer C). Pumice in this unit are white, up to 2cm, subangular, and contain plagioclase, hornblende, pyroxene and opaque oxides. Crystal, lithic and vitric ash comprises about 10% of this unit and is concentrated in shower beds up to 2cm thick throughout this layer. It grades normally or reversely at different locations. A sharp contact follows, and is overlain by up to 13cm of well-sorted, shower bedded fall

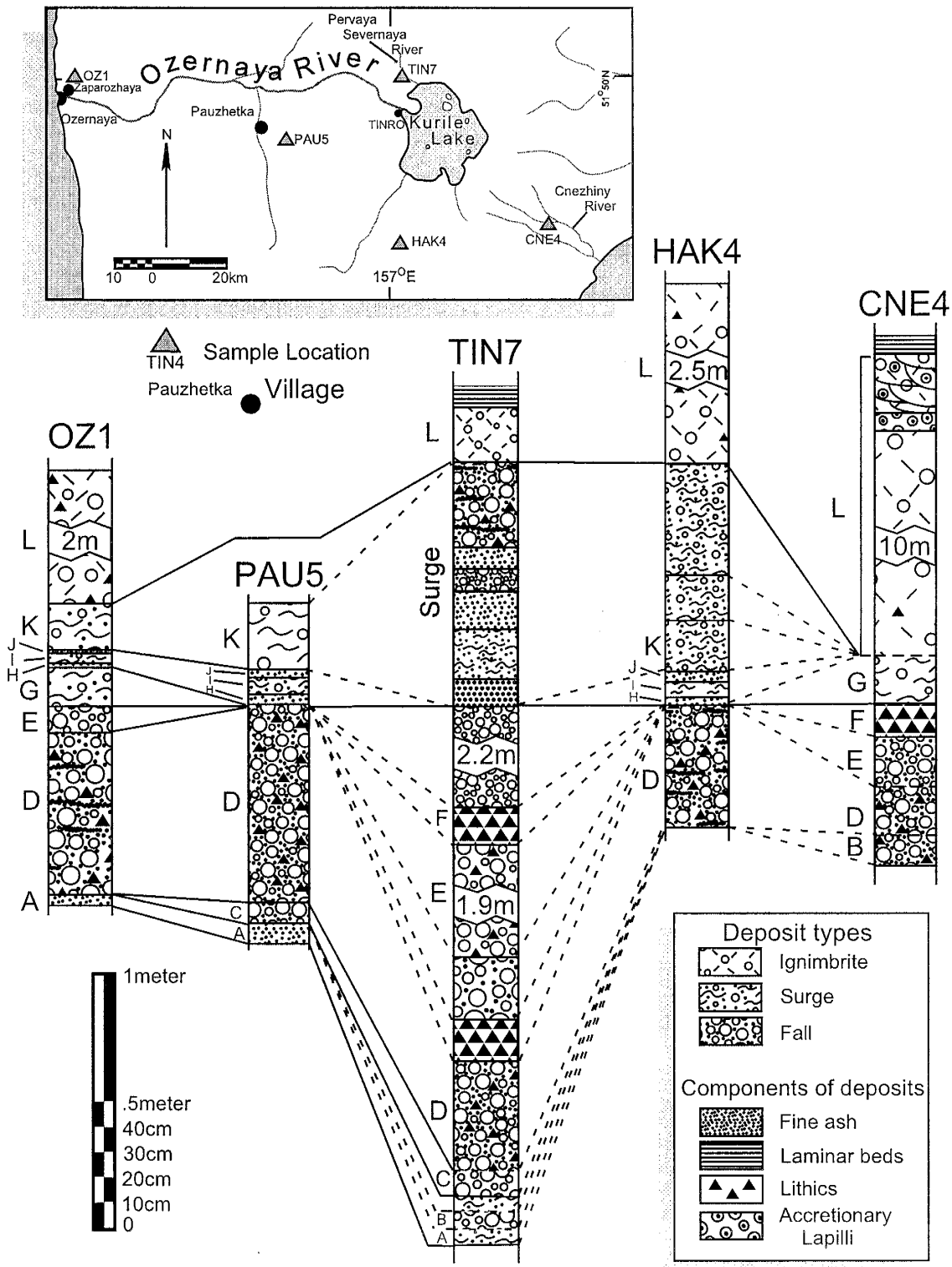

Figure 3.2. Correlated measured fall (KLp) sections. Columns are simplified for clarity. Letters correspond to Figure 3.1 Complete descriptions are given in Appendix E.

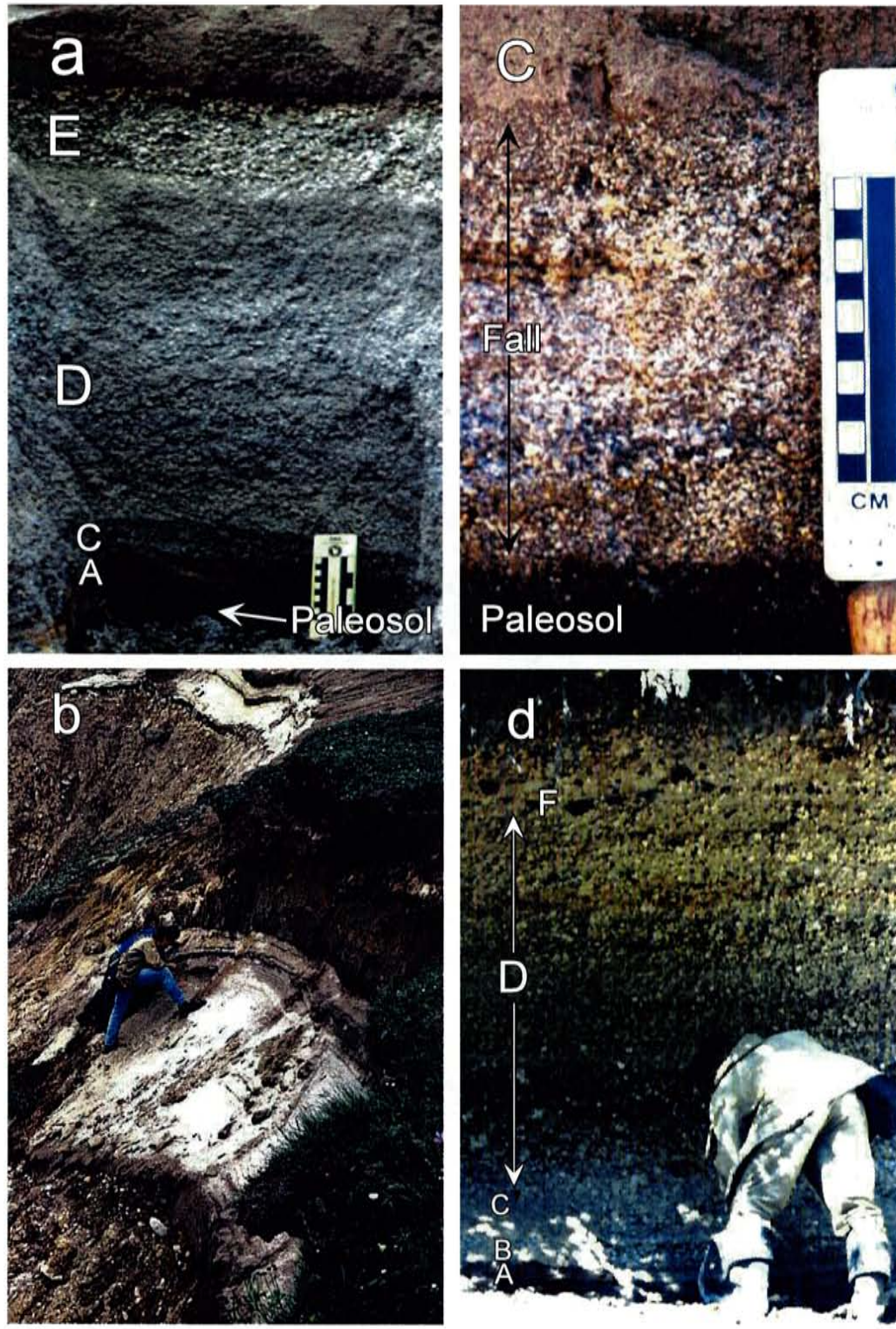

Figure 3.3. Fall deposit features. a) OZ1: Distal fall exposure at Ozernaya, west of Kurile Lake. This exposure is near the fall axis. Letters correspond to those used in Figure 3.1. Scale bar on card equals 10cm. b) Fall exposure south of Ozernaya draping topography. c) Fall exposure at Galiginy River, north of Kurile Lake. Note the thickness and grain size difference with A. d) TIN7b: Pervaya Severdnaya River proximal fall exposure. This exposure is thicker, more complex and contains larger clasts due to close proximity to the vent.

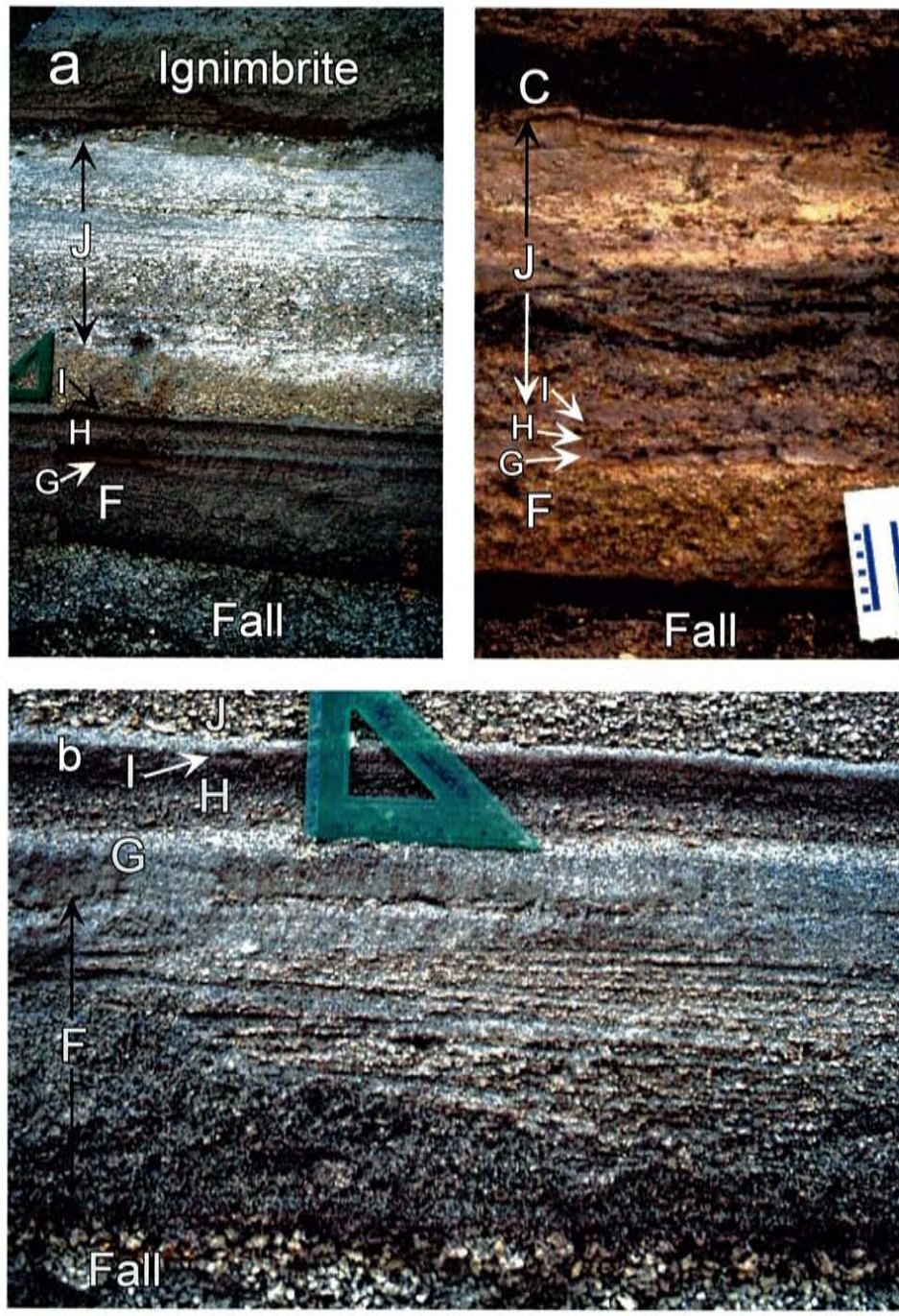

Figure 3.4. Surge deposit features. Letters correspond to Figure 3.1. a) OZ1: Distal surge exposure at Ozernaya, west of Kurile Lake. Bedding is weakly crossbedded to laminar. Green triangle is 12 cm long. b) Close-up of ash beds in surge at OZ1. c) HAK4: Surge beds in thin fall exposure south of Kurile Lake.

deposits (layer D). Pumice in this layer are coarser, up to 6cm and similar to the previous layer in roundedness and crystallinity. Layer E, 0-13cm thick, is the last fall bed in this sequence. It is composed of well-sorted coarse lapilli pumice with rare lithics and crystal ash.

The coarse fall unit (layer E) is followed by 0-20cm lithic layer in some exposures (layer F). This layer contains angular, red and black lithics up to 15cm in diameter. This layer is followed by 7-20 cm of moderately sorted, laminar bedded, coarse ash to lapilli (layer G). As will be discussed later, pumices are similar to layers B-E in composition, but are platy and slightly imbricated. More crystal, lithic and vitric ash is present in layer G. Bedding in this layer can be over a meter long, 1-5cm thick and weakly crossbedded. A 1-1.5cm, brown coarse ash bed (layer H) with a sandy parting overlies layer G, and is always seen in sections of the KLp which are complete. No pumice is present in layer H which is dominated by ash with rare lithic fragments. Layer H is overlain by 2-6cm moderately sorted pumice lapilli (layer I) similar in character to layer G. Overlying layer I is another thinner (0.5-1cm), sandy, brown, fine ash layer (layer I) similar to layer H. Layer I is overlain by a moderately sorted, coarse ash to lapilli, weakly bedded unit, 17-45cm thick (layer K). Pumices are similar in composition to the other parts of the fall and are platy and slightly imbricated. Layers G-K are interpreted to be the result of deposition from pyroclastic surges due to sorting and bedding characteristics. Layers H and J may be the result of a phreatomagmatic surge due to the lack of lithic and crystal ash.

The Pervaya Severnaya River valley, 3km NW of Kurile Lake, has the only known complete proximal fall exposure (TIN7, Appendix E). Correlating this section

with distal fall deposits is impossible due to the complex stratigraphy of this exposure. The overall character of well-sorted fall units followed by moderately sorted and bedded units is seen in here, but the correlation of specific units is not possible.

Ignimbrite Characteristics

The Kurile Lake ignimbrite (KLi) measured sections are presented in Fig. 3.5. Complete descriptions are given in Appendix E. The KLi (Fig. 3.6-3.8) is a widespread and complex deposit. In valleys, ignimbrite deposits form terraces on valley walls, which have been deeply incised by streams and rivers. Ignimbrite exposures around the lake shore to 30km distal are up to 250m thick, thinning to 1-2m at Ozernaya, 70km to the west of Kurile Lake (Fig. 3.7). Meter-thick ignimbrite has also been observed at the Galiginy River, 80km north of Kurile Lake. Ignimbrite over 10m thick was observed on high ridges in the southern part of the field area. In other areas, the ignimbrite left only a thin veneer of ash and small pumices.

Ignimbrite pumice types are generally uniform white, tan or light grey in KLi deposits west and south of Kurile Lake. Ignimbrite extending northwest to east of Kurile Lake contains pumice from basaltic andesite to rhyolite in composition and mixed pumice are common. Typically, a particular pumice variety dominates a region of zoned ignimbrite. In the darker ignimbrite, rhyolitic pumice may be found, but it is extremely rare. Similar pumice population is also noted for the lighter color-index ignimbrites.

KLi is a poorly sorted, structureless deposit containing ash and lapilli to block sized pumice and scoriaceous pumice as well as lithic fragments, accretionary lapilli, pumice concentration zones and carbonized wood (Fig. 3.8). Some ignimbrite exposures

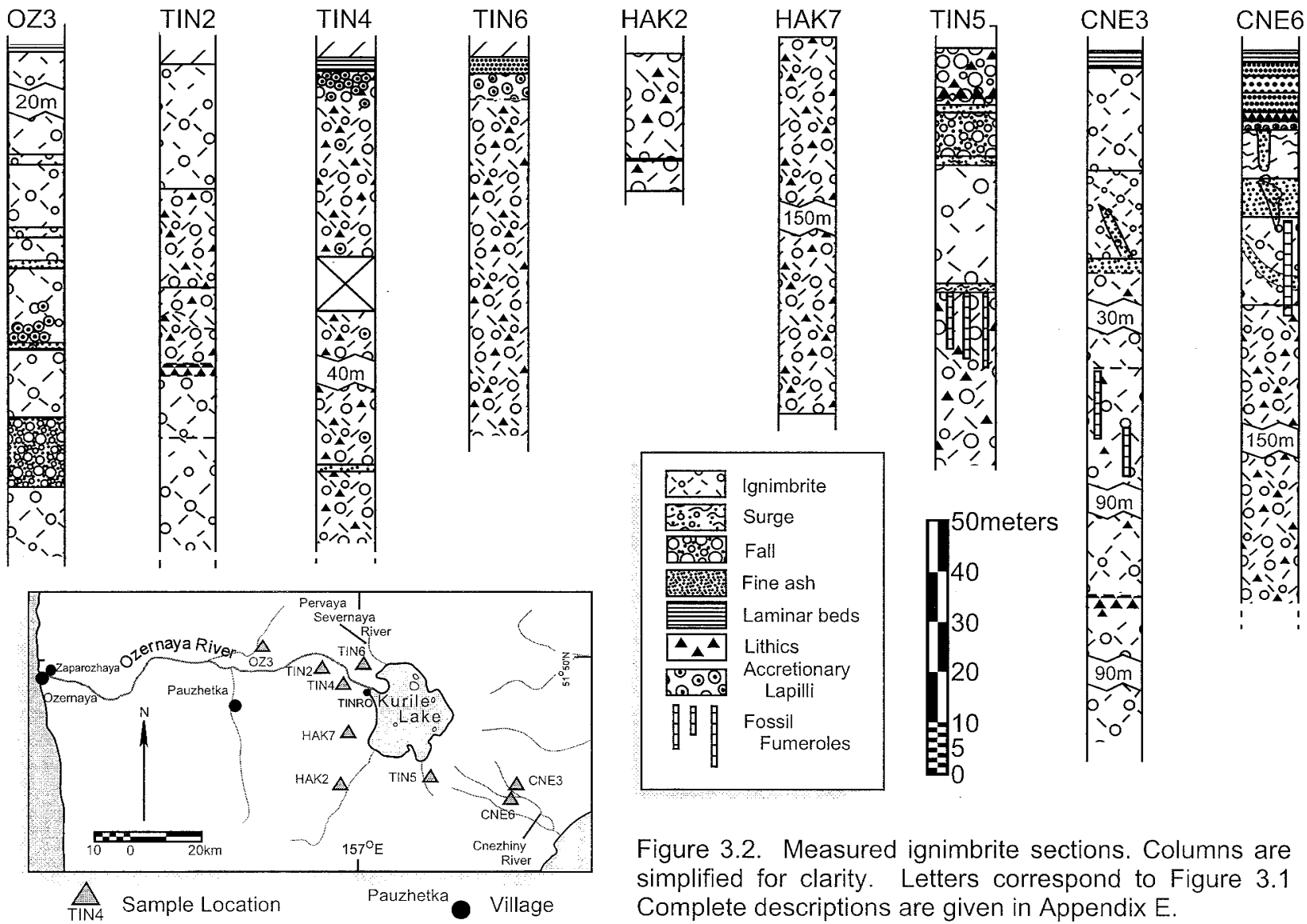

Figure 3.2. Measured ignimbrite sections. Columns are simplified for clarity. Letters correspond to Figure 3.1 Complete descriptions are given in Appendix E.

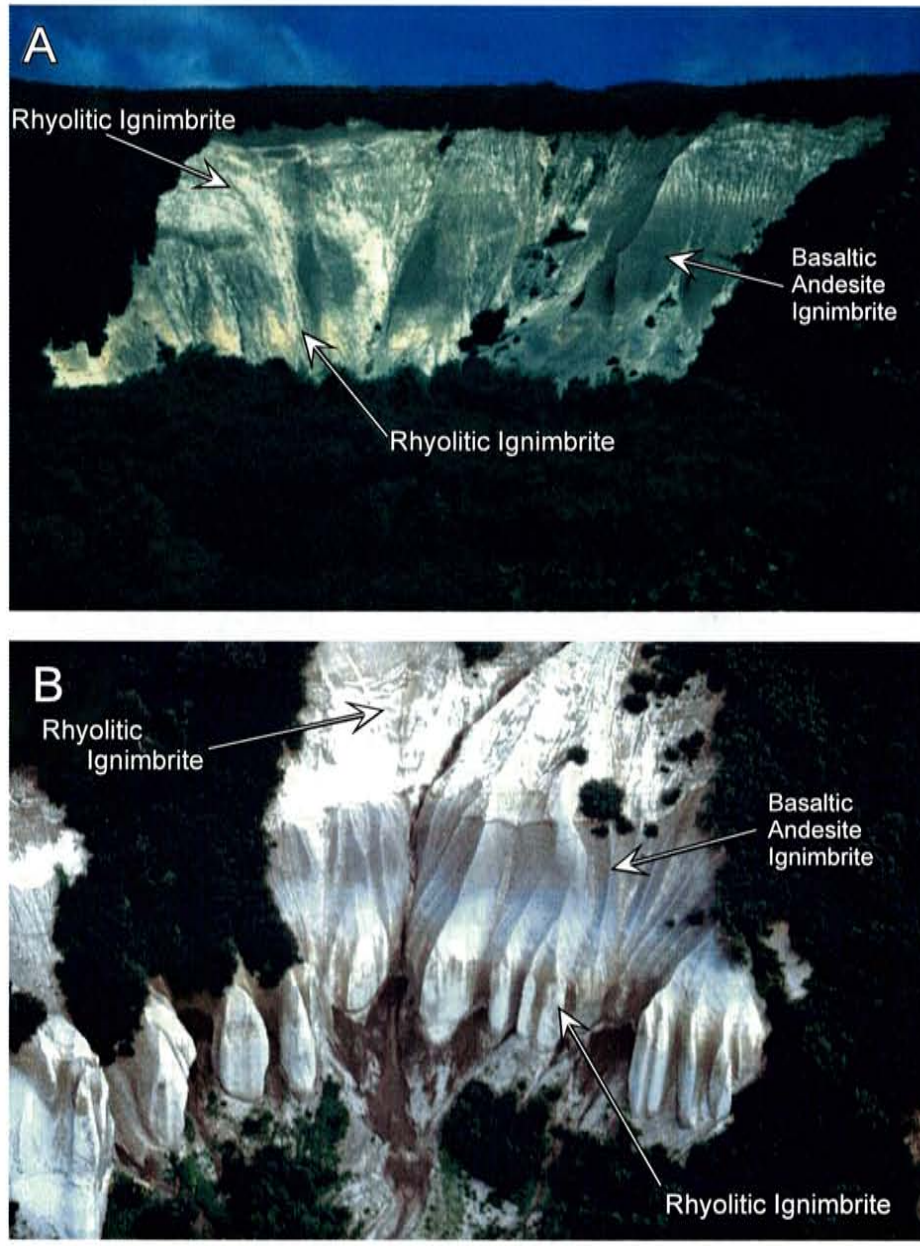

Figure 3.6. Ignimbrite features. A) CNE3: Zoned ignimbrite exposure. Clasts analyzed from the base of this exposure are rhyolites. Analyses from the mid-section are andesites and basaltic andesites. The overlying, lighter ignimbrite is rhyolitic. This exposure is 200m thick with no basal contact. B) Zoned ignimbrite north of Kurile Lake. This exposure exhibits zonation similar to CNE3.

Figure 3.7. Ignimbrite features. A) Typical KLi exposure (CNE6). Note the range in clast size from ash to block-sized pumice. Hammer is 25cm long. B) Wide view of ignimbrite exposure at CNE6. C) Terraces on valley-ponded ignimbrite along the Ozernaya River. D) Fossil fumerole pipe at CNE3. The fumerole pipe is the prominent projection in the slope directly above the figures head.

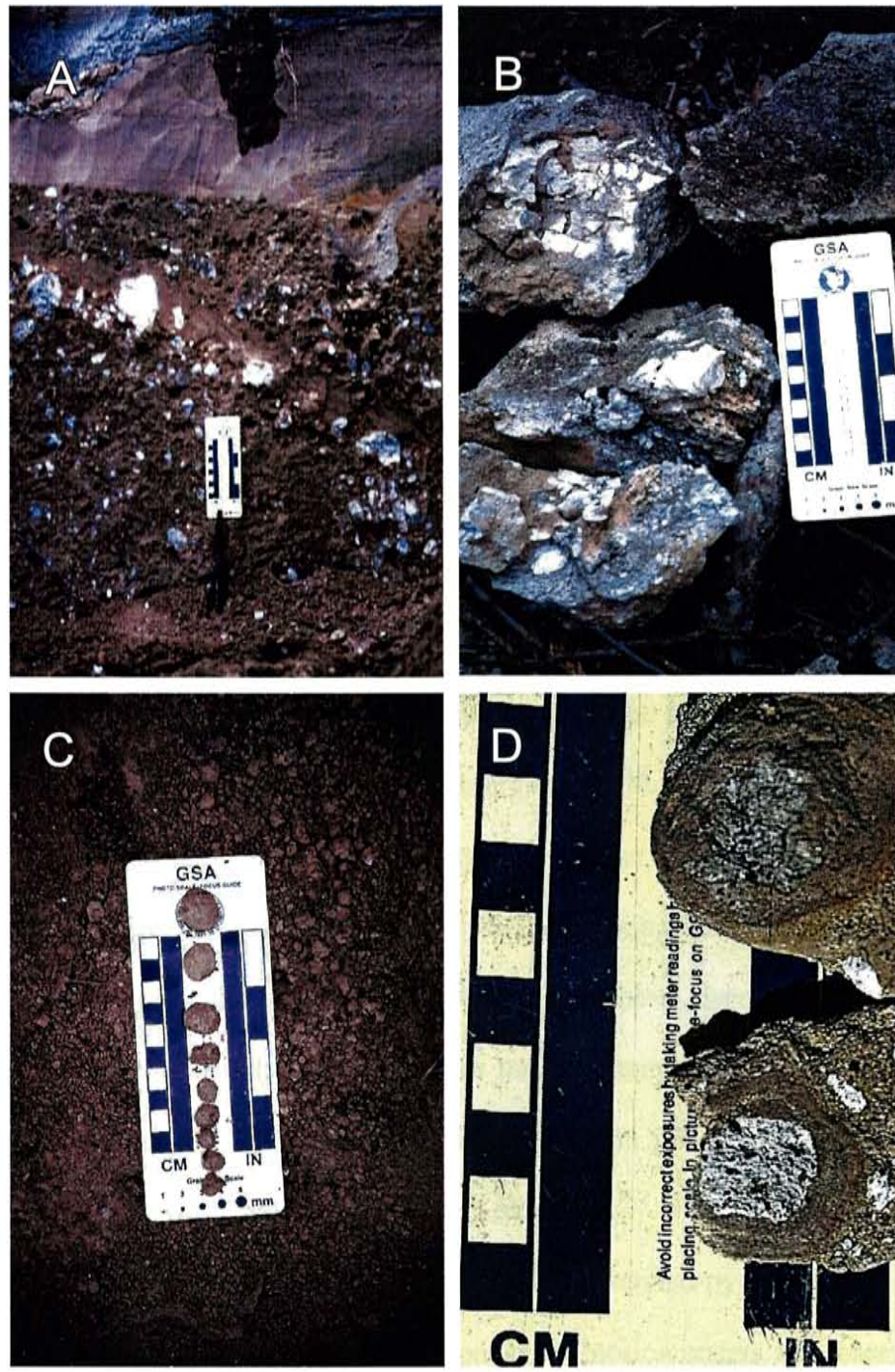

Figure 3.8. Ignimbrite components. A) Secondary explosion crater at the top of CNE6. B) Cored bomb from TIN6. C) Accretionary lapilli from TIN6. D) Coated lapilli from TIN4.

have fossil fumeroles and drape-like erosional character. Several outcrops have reworked upper contacts due to secondary explosions after emplacement or lacustrine deposition. Exposures of ignimbrite observed near the Pacific Ocean are extensively reworked and fines-poor, possibly due to secondary explosions resulting from seawater-pyroclastic flow interaction.

Eruptive Sequence

Distal fall exposures, 30 to 80km from the caldera are generally uniform and follow a recognizable sequence. The eruption began with phreatomagmatic activity, generating phreatomagmatic surge or phreatoplinian fall later followed by a sustained plinian column, generating plinian falls, which may have mixed with phreatomagmatic eruptive products in some localities. Interpretation of the initial fall as phreatoplinian or phreatomagmatic is based only on field observations. More detailed work is required to properly describe this unit. Vent widening or reduction in eruption volume could have resulted in column collapse (e.g. Francis, 1993), depositing bedded, imbricated pyroclasts with a moderate amount of ash. Crossbedding in these layers along with a marked increase in ash and imbrication of pumices indicates emplacement by pyroclastic surge (Fisher and Schminke, 1988). Lithic-rich units seen in fall exposures may result from vent erosion or opening of new vents during eruption.

Following the surge phase of the eruption, sustained pyroclastic flows deposited ignimbrite. Fossil fumerole pipes and secondary explosion craters are observed and may have formed as a result of heating surface and groundwater as was described at Valley of Ten Thousand Smokes (Hildreth, 1983) and Crater Lake by Bacon (1983). These

fumeroles indurated the ignimbrite leaving erosional remnants in the form of hollow, mineralized tubes similar to those found at Crater Lake (Bacon, 1983), Valley of Ten Thousand Smokes (Hildreth, 1983) and in the San Diego Canyon ignimbrite at Valles Caldera (McPhie et al., 1993 p. 135). Vegetation was also incorporated in the flows eventually carbonizing in the hot ignimbrite. This phenomenon was dramatically evident after the 1980 eruption of Mt. St. Helens. As pyroclastic flows traveled down the Ozernaya River and Cneghiny River valleys to the east and west, they entered the ocean. The interaction of cold seawater and hot pyroclasts produced secondary explosions and elutriation of fines as was described at Tambora by Sigurdsson and Carey (1989). Some of the eruption may have occurred through a water column or during a rain event. Accretionary lapilli is a common constituent throughout the ignimbrite showing water was a major part of this eruption (Francis, 1993).

CHAPTER FOUR

GEOCHEMISTRY

Introduction

Major and trace element analyses were made by XRF and INAA. Glass compositions were determined by electron microprobe. Sample preparation and analytical procedures are given in Appendix A-D. Representative whole rock analyses are given in Table 4.1 and a complete table of analyses is given in Appendix C. Representative glass analyses are given in Table 4.2 and a complete table of analyses is given in Appendix D.

Ninety-two pumice and scoria samples were analyzed from fall and ignimbrite sections in the Kurile Lake area. Single clasts (>20g) were analyzed when possible, however, in some samples, a number of clasts were combined to produce enough sample for analyses. Sample locations are shown in Figure 2.2 and are described with an accompanying stratigraphic column in Appendix E. Samples were chosen to represent the variability in clast type within an outcrop. The fall and ignimbrite contain clasts ranging from basaltic andesite to rhyolite using the TAS classification of LeBas et al. (1986) (Fig. 4.1). With the exception of a few basaltic andesites, the KLE rock series represents a calc-alkaline trend using the parameters of Miyashiro (1974) (Fig 4.2).

Pumice from the fall and surge deposits are rhyolitic with minor dacites. In some cases clasts from ignimbrite sections are compositionally uniform throughout the section,

Table 4.1. Representative Whole Rock Analyses

SAMPLE	97KAM29DB	96KAM04	96KAM12	96KAM12L	96KAM3	97KAM32D2
Rock Type	Basaltic Andesite	Basaltic Andesite	Basaltic Andesite	Andesite	Andesite	Dacite
Deposit Type	Ignimbrite	Ignimbrite	Ignimbrite	Ignimbrite	Ignimbrite	Ignimbrite
SiO_2	51.95	53.18	55.05	58.37	60.01	64.35
TiO_2	0.84	0.87	0.71	0.73	0.71	0.55
Al_2O_3	17.99	18.51	19.29	19.50	19.86	17.24
Fe_2O_3*	9.84	9.53	7.36	5.73	5.21	3.90
MnO	0.18	0.18	0.15	0.14	0.13	0.11
MgO	5.02	4.56	3.50	2.01	1.72	1.16
CaO	9.88	9.60	8.85	7.26	6.89	5.06
Na_2O	2.52	2.88	3.29	4.25	4.51	4.62
K_2O	0.45	0.45	0.58	0.73	0.76	1.17
P_2O_5	0.11	0.13	0.13	0.21	0.20	0.14
LOI	0.16	-0.60	0.57	1.02	0.49	2.37
Total	98.94	99.29	99.48	99.95	100.49	100.67
S	288	119	177	119	50	68
Sc	38.40	33.70	25.41	18.02	15.98	
V	326	272	193		80	41
Cr	56	40	27	13	6	5
Ni	12	13	11		3	3
Cu	54	44	28	43	13	10
Zn	70	74	63	65	52	52
Ga	17	18	18		19	16
As	3.9	3.6	4.1	5.1	4.7	
Br		0.37		1.28	0.30	
Rb	7	7	9	11	12	19
Sr	300	335	349	382	393	300
Y	18	18	19		21	26
Zr	49	50	58		74	131
Nb		2	2		2	
Mo	1	1	1		1	2
Sb	0.17	0.13	0.23	0.24	0.22	
Cs	0.42	0.59	0.63	0.68	0.76	
Ba	137	153	178	222	240	334
La	3.37		4.31		5.95	
Ce	8.4	8.4	11.6	13.4	14.2	
Nd	5.5	4.6	5.9	8.1	7.2	
Sm	1.95	2.00	2.33	2.73	2.66	
Eu	0.71	0.79	0.88	1.12	1.13	
Tb	0.38	0.41	0.47	0.48	0.50	
Yb	1.73	1.71	1.79	2.03	1.95	
Lu	0.24	0.24	0.25	0.35	0.27	
Hf	1.55	1.29	1.82	2.17	2.19	
Ta	0.25	0.06	0.11	0.10	0.17	
Pb	6	2	4		6	7
Th	0.51	0.59	0.58	0.82	0.75	
U	0.18		0.30	0.30	0.27	

* Total Fe as Fe_2O_3

A complete listing of whole rock analyses is included in Appendix C

Table 4.1. Representative Whole Rock Analyses

SAMPLE	96KAM18	97KAM17A	97KAM02	97KAM17BS	97KAM32A	96KAM9
Rock Type	Dacite	Rhyolite	Rhyolite	Rhyolite	Rhyolite	Rhyolite
Deposit Type	Ignimbrite	Fall	Fall	Fall	Ignimbrite	Ignimbrite
SiO_2	64.81	68.46	69.52	70.19	70.51	71.46
TiO_2	0.52	0.28	0.29	0.27	0.27	0.29
Al_2O_3	16.24	15.15	14.41	14.56	14.16	14.02
Fe_2O_3*	4.38	1.91	1.89	1.91	1.82	1.91
MnO	0.11	0.07	0.07	0.07	0.07	0.07
MgO	1.57	0.35	0.38	0.36	0.38	0.39
CaO	4.45	2.47	2.54	2.26	2.47	2.42
Na_2O	3.94	4.36	4.53	4.37	4.54	4.51
K_2O	1.45	1.68	1.76	1.79	1.97	1.92
P_2O_5	0.11	0.04	0.06	0.04	0.05	0.05
LOI	2.55	4.48	3.73	4.19	2.77	2.85
Total	100.13	99.25	99.18	100.01	99.01	99.89
S	100	68	61	80	294	75
Sc	13.64	9.83	8.92	8.08	8.49	8.41
V	53	14	12	10	12	17
Cr						8
Ni	5	3	4	3	3	5
Cu	27	9	11	11	10	27
Zn	46	37	39	36	29	39
Ga	15	14	14	13	14	14
As	7.8	11.0	11.6	9.4	12.0	11.9
Br	2.10	4.50	1.70	0.59	1.64	1.14
Rb	26	29	30	30	31	31
Sr	258	175	182	159	173	172
Y	23	32	33	31	33	34
Zr	127	180	172	182	170	172
Nb	2	1	1			3
Mo	2	2	2	2	2	3
Sb	0.47	0.48	0.51	0.48	0.50	0.42
Cs	1.69		1.99	1.99	2.03	2.11
Ba	395	376	422	402	433	423
La	8.42	9.74	10.20	10.26	10.26	10.64
Ce	19.9	23.5	25.3	25.2	25.6	24.9
Nd	9.0	14.2	14.6	11.2	13.3	15.0
Sm	2.84	3.87	3.99	3.74	3.88	3.94
Eu	0.85	1.00	0.98	0.93	0.98	0.94
Tb	0.53	0.72	0.78	0.67	0.73	0.72
Yb	2.43	3.47	3.58	3.56	3.45	3.65
Lu	0.37	0.56	0.55	0.58	0.56	0.54
Hf	3.48	5.13	4.85	5.40	4.90	4.98
Ta	0.15	0.28	0.88	0.30	0.30	0.17
Pb	7	10	9	10	8	9
Th	2.08	2.26	2.19	2.21	2.19	2.16
U	0.83	1.05	0.76	0.81	0.68	0.88

* Total Fe as Fe_2O_3

A complete listing of whole rock analyses is included in Appendix C

Table 4.2. Electron microprobe analyses of glass from homogeneous and banded samples

Homogeneous samples

	K12B-GLS1	K4-AVG	K12L-AVG	K3-AVG	K32D-GLS1	K18-AVG	K32A-AVG	K9-AVG	K2-AVG	K17B-AVG
N	1	7	4	8	1	6	3	2	5	3
Host Lithology	basaltic andesite	basaltic andesite	andesite	andesite	dacite	dacite	rhyolite	rhyolite	rhyolite	rhyolite
SiO_2	61.13	65.60	70.03	74.15	74.06	76.15	76.63	77.41	77.26	77.28
TiO_2	0.69	0.80	0.72	0.40	0.45	0.35	0.28	0.21	0.28	0.17
Al_2O_3	17.72	16.09	14.60	14.61	15.02	13.20	13.78	12.80	13.22	13.36
FeO	5.66	5.21	3.61	1.96	2.43	1.75	1.25	1.43	1.51	1.45
MnO	0.13	0.13	0.10	0.09	0.11	0.06	0.07	0.01	0.07	0.05
MgO	1.85	1.32	0.85	0.43	0.61	0.39	0.25	0.24	0.23	0.25
CaO	5.73	4.53	2.98	2.29	2.56	1.87	1.53	1.41	1.45	1.49
Na_2O	4.73	5.30	5.34	4.22	2.50	4.11	4.07	4.42	3.87	3.88
K_2O	0.81	0.80	1.52	1.75	1.71	2.10	2.14	2.08	2.08	2.03
P_2O_5	0.22	0.22	0.26	0.10	0.09	0.02	0.00	b.d.	0.03	0.03
Total	98.90	100.00	100.00	100.00	99.54	100.00	100.00	100.00	100.00	100.00

Banded clast 96KAM6; clast with basaltic andesite and dacite bands

	K6-GLS15	K6-GLS10	K6-GLS41	K6-GLS40	K6-GLS13	K6-GLS5	K6-GLS22	K6-GLS33	K6-GLS1	K6-GLS39
SiO_2	60.22	63.86	65.11	67.74	69.39	71.81	73.18	74.46	76.27	77.90
TiO_2	0.31	1.15	0.82	0.74	0.69	0.60	0.50	0.33	0.34	0.21
Al_2O_3	22.02	14.07	14.52	16.28	15.35	14.89	13.82	13.26	13.46	13.25
FeO	2.49	7.57	4.29	3.85	2.92	3.14	2.34	1.22	0.90	1.26
MnO	b.d.	0.19	b.d.	0.11	0.13	0.17	0.11	b.d.	b.d.	b.d.
MgO	0.29	2.40	1.03	0.77	0.62	0.81	0.51	0.09	0.11	0.18
CaO	7.47	3.36	3.14	3.33	3.09	2.61	1.81	0.86	1.36	1.16
Na_2O	5.41	3.58	5.63	6.20	5.30	4.60	4.10	3.27	3.71	3.90
K_2O	0.50	2.37	5.98	0.17	1.34	2.13	2.26	5.99	2.31	2.12
P_2O_5	0.09	0.23	0.32	0.33	0.17	0.13	0.12	b.d.	0.08	0.01
Total	98.89	99.15	100.84	99.51	100.25	101.01	98.92	99.48	98.78	99.98

Banded clast 96KAM14; clast with basaltic andesite and andesite bands

	K14-GLS1	K14-GLS11	K14-GLS13	K14-GLS15	K14-GLS22	K14-GLS21	K14-GLS20	K14-GLS4	K14-GLS3	K14-GLS23
SiO_2	62.39	63.97	64.88	65.52	66.04	67.25	68.21	69.73	70.27	71.58
TiO_2	0.79	0.75	0.97	0.70	0.47	0.75	0.64	0.66	0.69	0.56
Al_2O_3	17.59	16.81	14.89	15.50	19.02	15.53	15.53	15.72	15.70	14.82
FeO	4.95	4.81	6.46	4.83	2.51	4.69	3.87	3.44	3.33	3.37
MnO	0.13	0.15	0.16	0.16	0.03	0.13	0.11	0.14	0.14	0.16
MgO	1.23	1.28	1.61	1.35	0.68	1.25	1.06	1.02	0.94	0.85
CaO	5.54	4.46	4.10	3.79	5.11	3.56	2.52	3.11	2.96	2.76
Na_2O	5.26	5.73	5.09	6.01	5.36	5.73	4.39	4.72	4.48	4.85
K_2O	0.68	0.76	0.85	0.53	1.18	0.88	3.25	1.84	1.91	1.89
P_2O_5	0.30	0.23	0.19	0.28	0.21	0.26	0.28	0.23	0.16	0.20
Total	99.00	99.09	99.33	98.85	100.69	100.10	99.99	100.72	100.77	101.13

Individual glass analyses from homogeneous samples are averaged where multiple determinations are available.
Where only one analyses was obtained for a sample, the analytical data is presented.
Data from banded lithologies are not averaged to show continuity between individual analyses.
b.d. indicates below detection limits
N= number of analyses

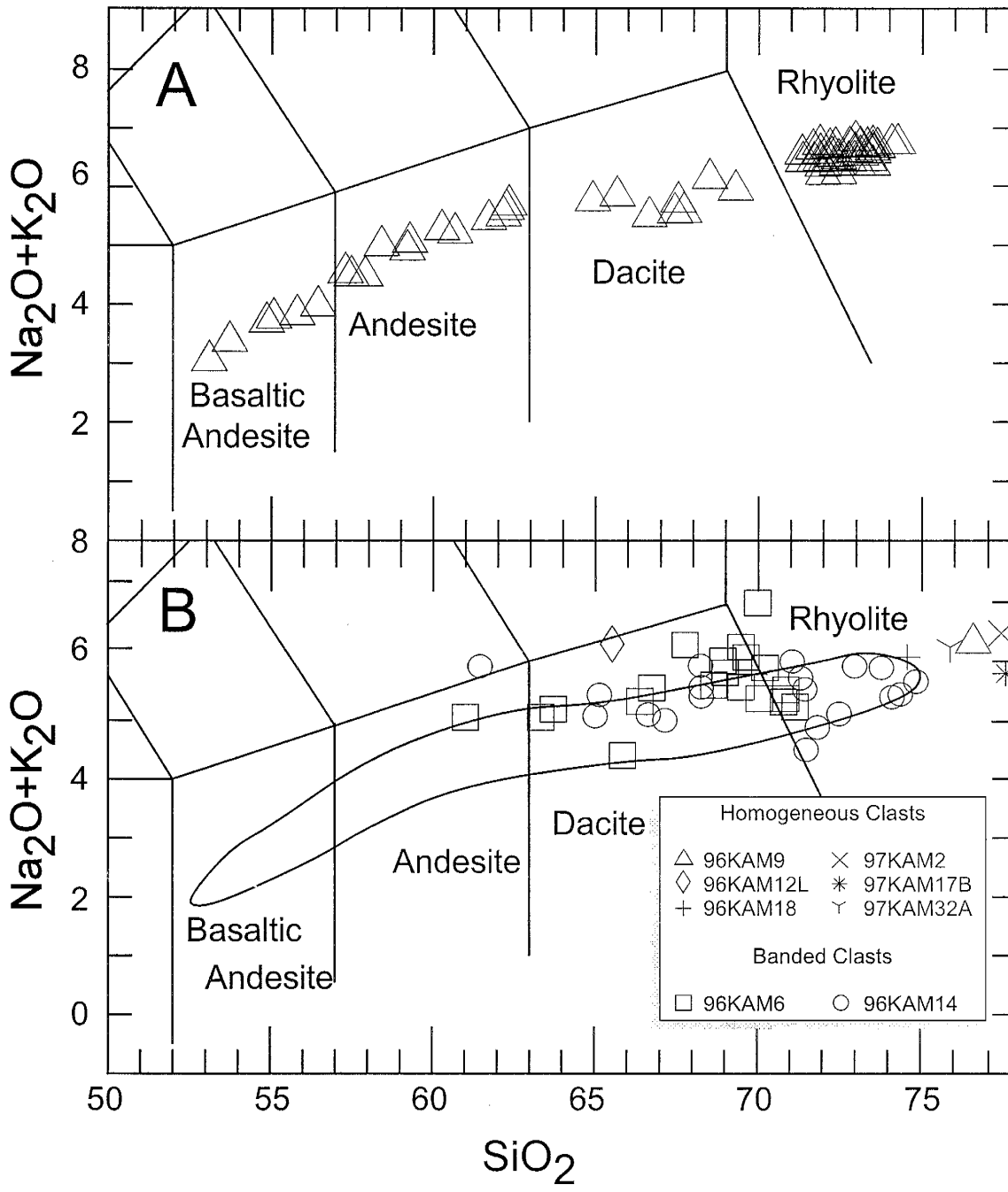

Figure 4.1. Whole rock (A) and glass analysis (B) plotted on the total alkali/silica (TAS) diagram of LeBas et al., (1986). Kurile Lake pumice and scoria range from basaltic andesite to rhyolite. Small compositional gaps can be seen at 63-64% and 70-72% SiO_2. All analyses normalized to 100% on a volatile free basis. Whole rock analyses are given in Appendix C. Glass analyses are given in Appendix D.

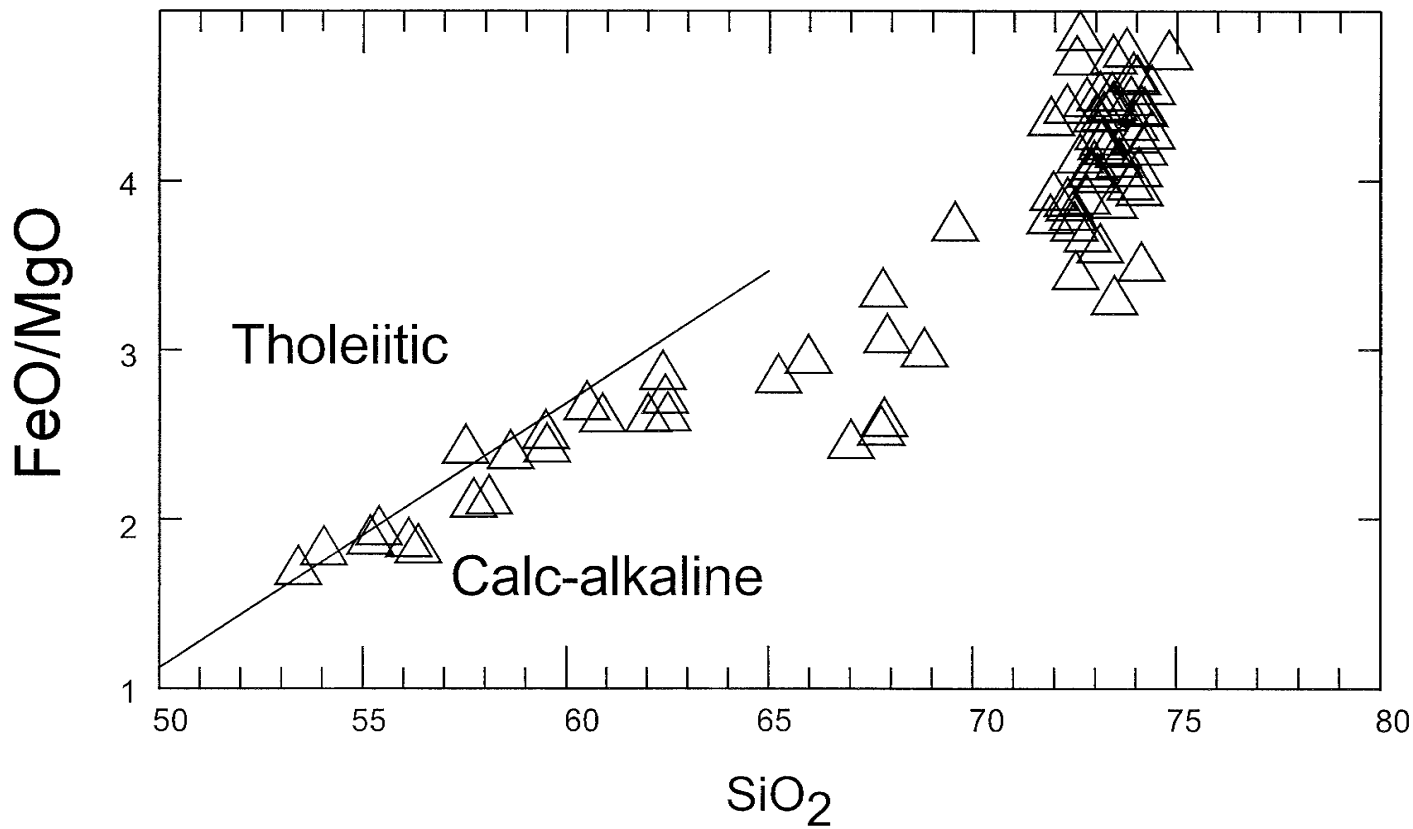

Figure 4.2. Whole rock analyses plotted on the tholeiitic /calc-alkaline diagram of Miyashiro, (1974). Kurile Lake pumices and scoria are calc-alkaline. All analyses normalized to 100% on a volatile free basis. Whole rock analyses are given in Appendix C.

but in others, a range of compositions is observed. When the clasts are uniform in composition they are either rhyolite or dacite. Where the clasts are compositionally diverse, rhyolite and dacite occur low in the section. Up section, andesitic and basaltic andesite scoria become more common until the clasts are exclusively basaltic andesite and andesite. The basaltic andesite and andesite clasts then grade back to rhyolite and dacite clasts up section to the top of the exposure. The strongly zoned ignimbrite only occurs to the north and east of the caldera.

Whole-Rock Analyses

Major Elements

Major element variation diagrams of clasts from the KLE form smooth, continuous trends for all major elements (Fig. 4.3). Although the dacites generally plot along the same trend as the other lithologies, they show a greater scatter in Al_2O_3, MnO, MgO and especially Na_2O. There are small gaps in SiO_2 at 70% and 63%, which may be real compositional gaps or represent a sampling bias. TiO_2, MgO, CaO, FeO^t, and MnO all decrease with increasing SiO_2, whereas K_2O increases. Each of these plots shows a general curvilinear trend. In some plots (TiO, FeO^t, MgO, MnO, CaO and K_2O), a straight line can be fitted to the data from the basaltic andesite samples through andesite (53-63wt.% SiO_2). Al_2O_3, Na_2O, and P_2O_5 show more scatter and less regular trends. The trends represented by these oxides have inflection points around 60% SiO_2. Al_2O_3 and P_2O_5 increase with SiO_2 as does Na_2O for rock compositions containing <60% SiO_2, but Na_2O remains constant as silica increases from 60-73%. Al_2O_3 and P_2O_5 both

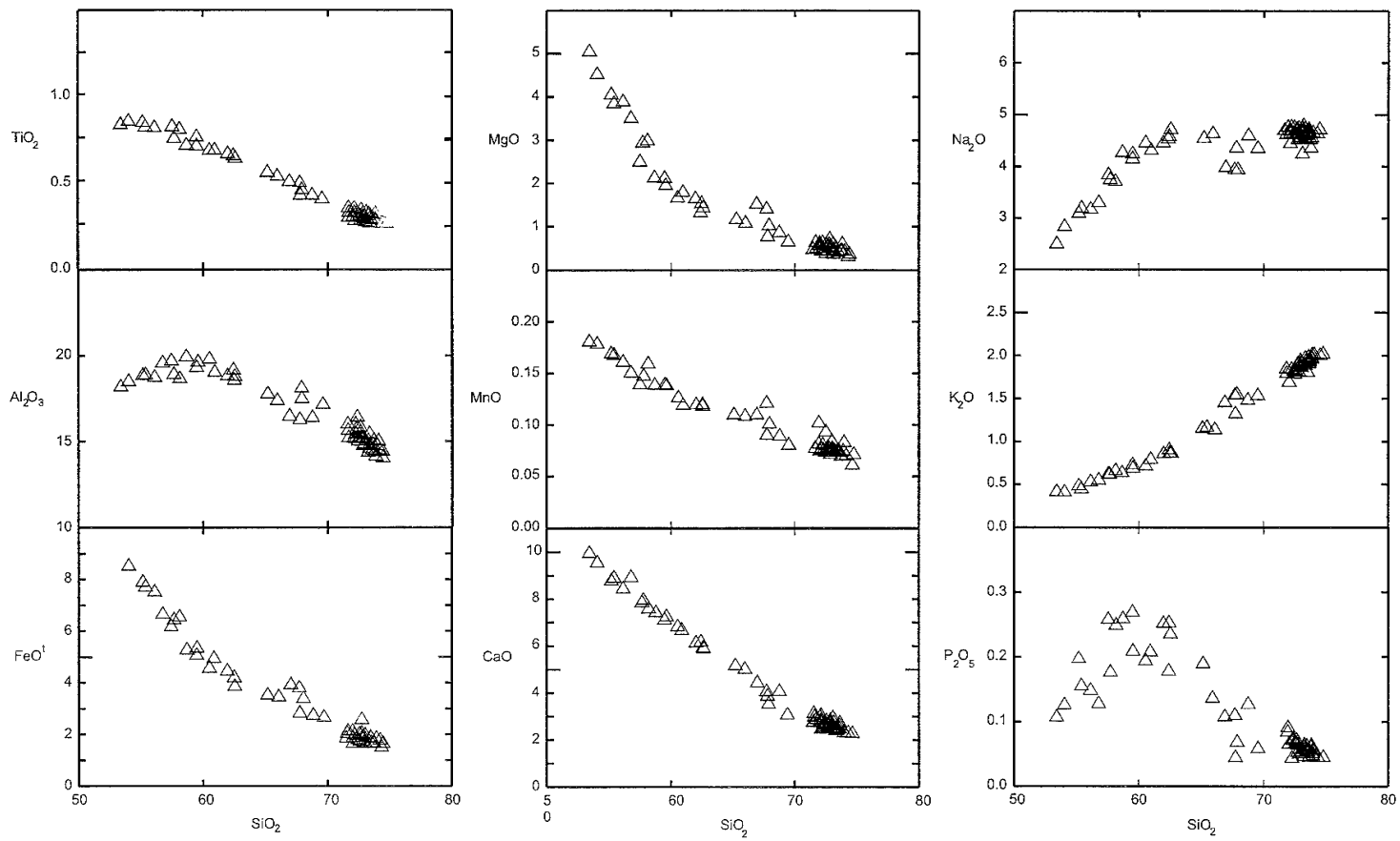

Figure 4.3. Major element silica variation diagrams for whole-rock and glass analyses. All analyses are normalized to 100% on a volatile free basis. Representative whole rock analyses are listed in Table 4.1. All data are given in Appendix D.

decrease sharply over this range. It should be noted that the trends for other oxides vs. SiO_2 have a small, but noticeable deflection near 60% SiO_2, but these trend inflections are at different points along the SiO_2 axis.

Trace elements

Trace elements are plotted against SiO_2 as an index of differentiation to display evolution trends (Fig 4.4a-b). The trace elements show trends which resemble the major element trends. Cs, Rb, Ba, La, Lu, As, Sb, Hf, Zr, Ta, U and Th increase with increasing SiO_2. They show slightly curved or straight trends. Sr and Eu increase to 60% SiO_2 then sharply decrease thereafter. Eu is scattered in dacite compositions and any trend to the rhyolite clump is inferred as a continuum. The dacites in the Eu plot may represent mixing of rhyolite and andesite, which may account for their scatter and plotting off the main trend. Ni, V, Zn and Cr, display non-linear trends with increasing SiO_2. Cr and Ni are almost flat after 60% to 73% SiO_2, while V has a gradual decrease in concentration.

Rare Earth Elements

Normalized REE plots (Fig 4.5) are relatively flat for the Kurile Lake clasts. With increase in SiO_2, La/Yb increases, as well as the overall REE content. Basaltic andesites and andesites have a slight positive Eu anomaly, whereas dacites and rhyolites have a negative Eu anomaly. It should be noted that the rock/chondrite axis is logrythmic and relative change in REE with rock type is very small.

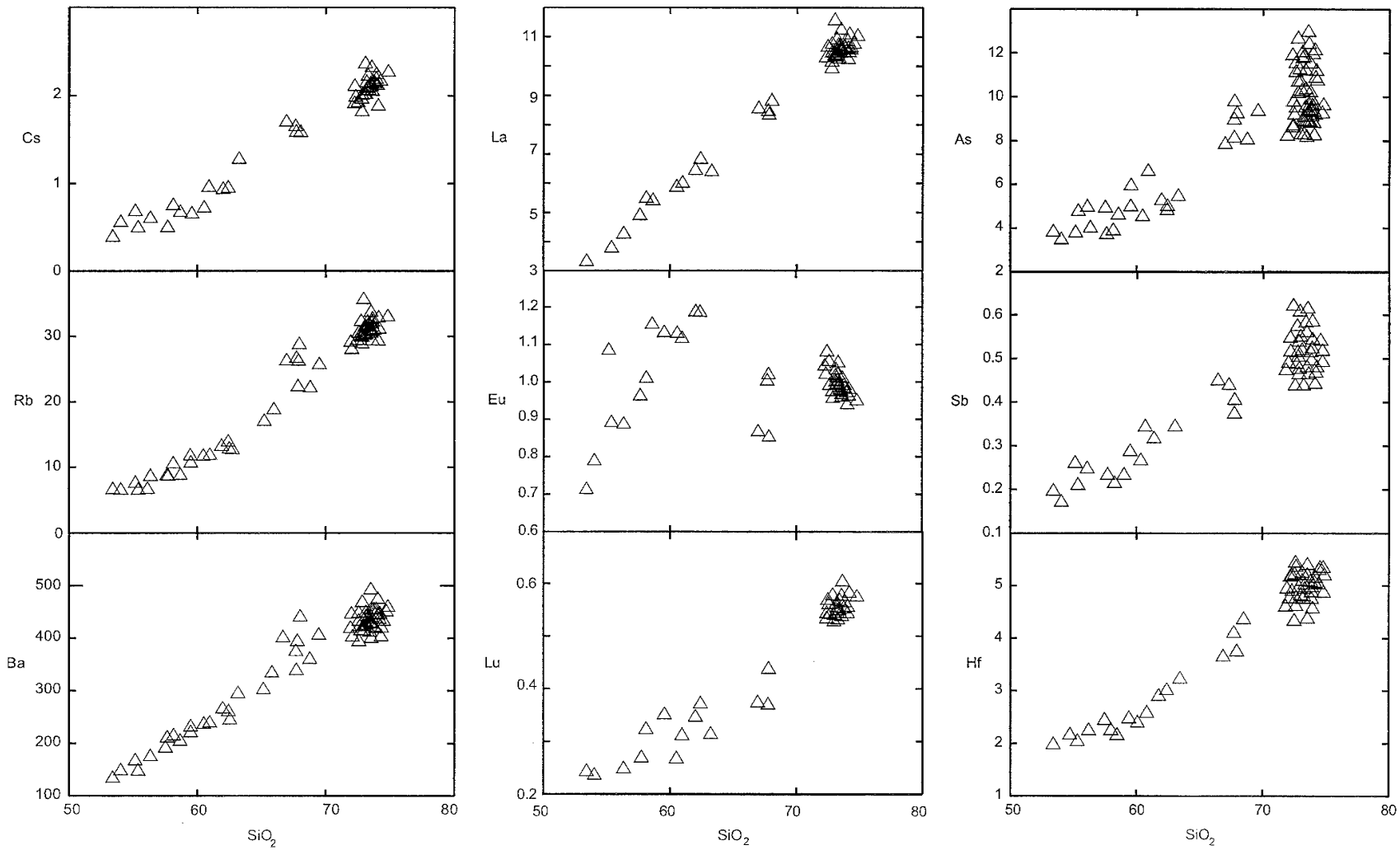

Figure 4.4a. Selected trace element (in ppm) vs. SiO_2 variation diagrams. Data are given in Appendix D. Representative whole rock analyses are listed in Table 4.1.

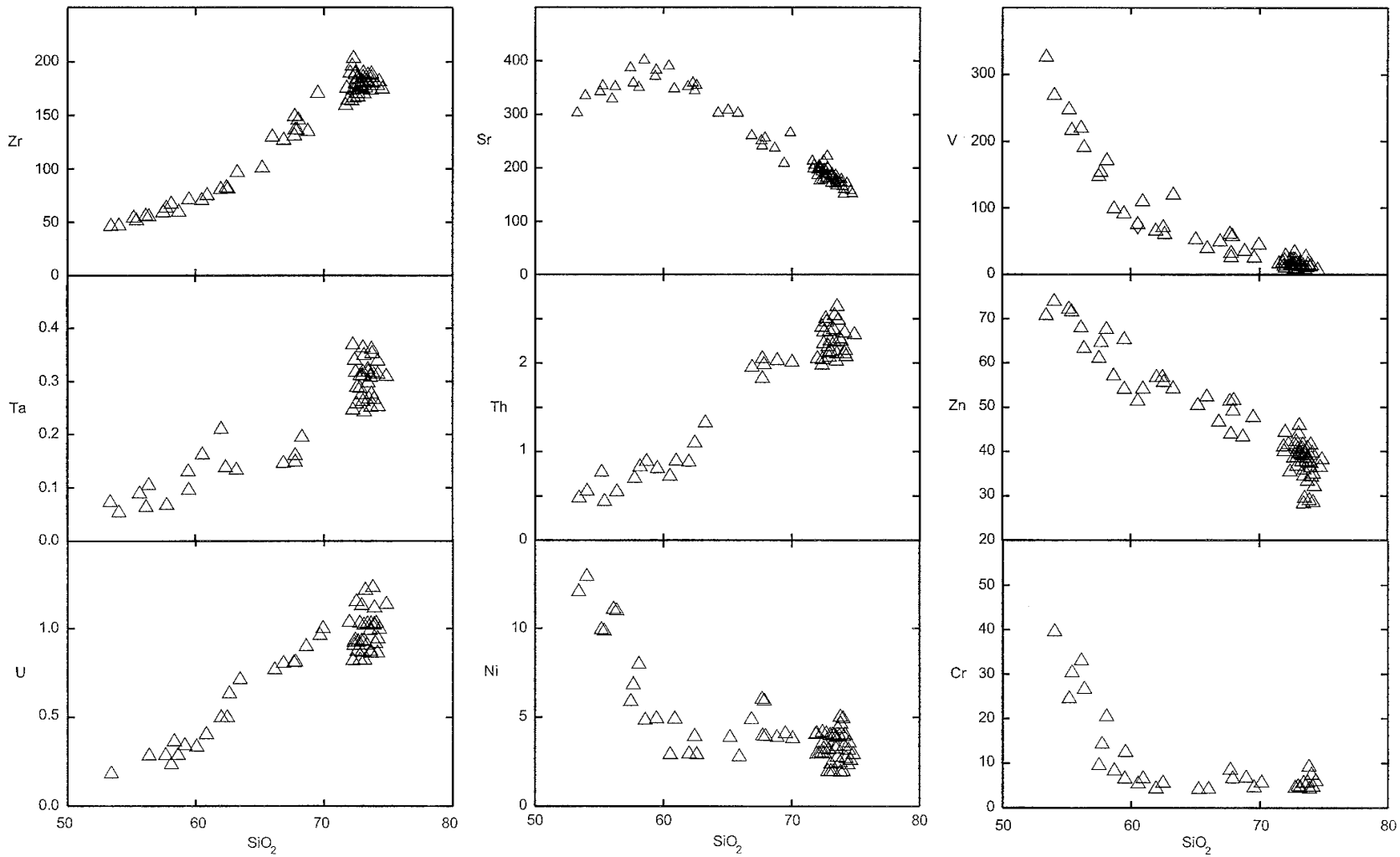

Figure 4.4b. Selected trace element (in ppm) vs. SiO_2 variation diagrams. Data are given in Appendix D. Representative whole rock analyses are listed in Table 4.1.

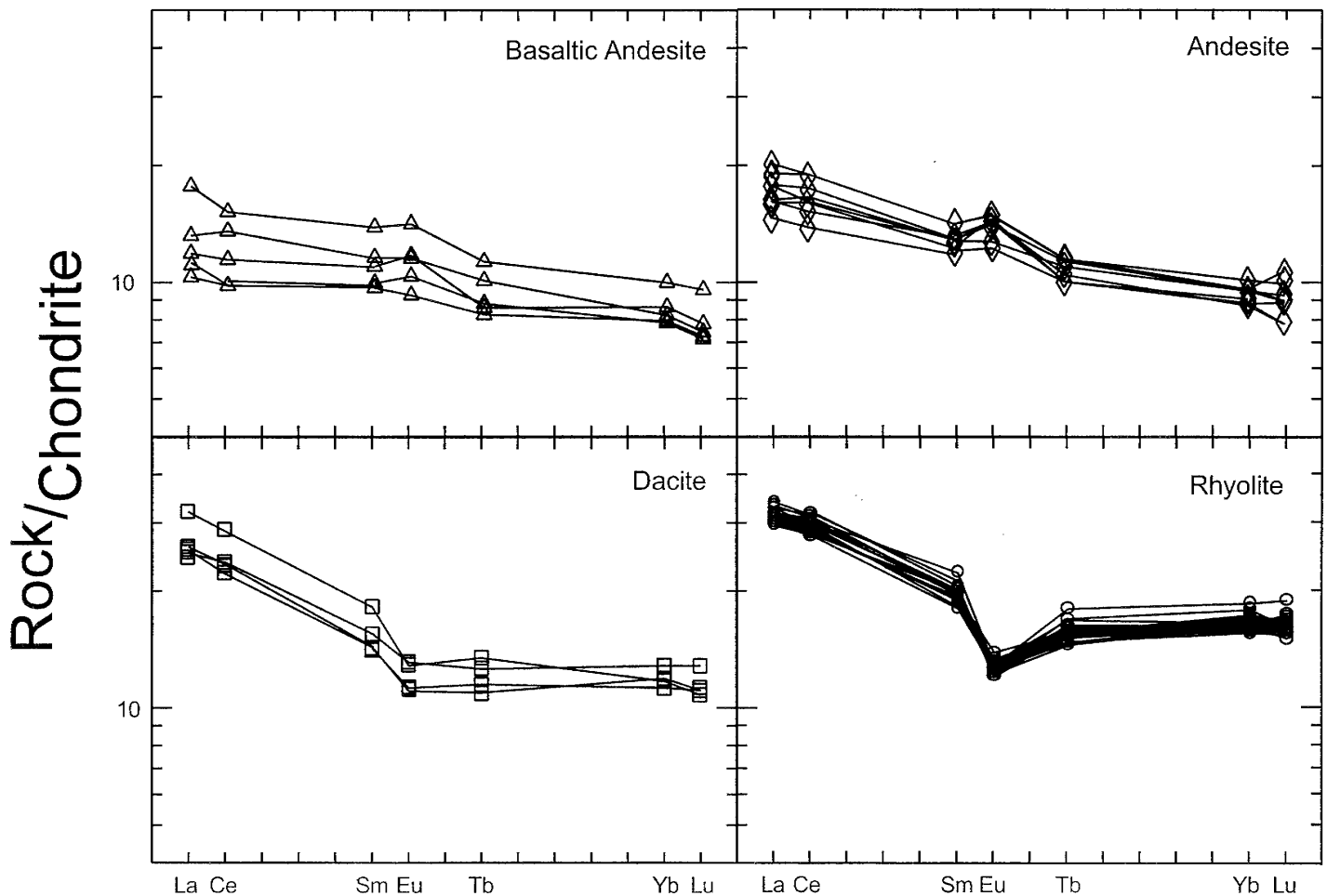

Figure 4.5. Normalized rare earth element plots for Kurile Lake eruptive products. Normalization follows that of Nakamura, (1974). Note the Y axis is very expanded. Rhyolites are slightly enriched in REE relative to the other litholigies. Basaltic andesite and andesite have a positive Eu anomaly. Dacite has no Eu anomaly, while rhyolite has a negative Eu anomaly. Whole rock analyses are given in Appendix C.

Glass Chemistry

Broad-beam (5-25μm) electron microprobe analyses of glass show a range in SiO_2 from 62-78% (Appendix D, Table 4.6). The glass ranges in composition from andesite to rhyolite (Fig. 4.1).

As with the whole rock major element analyses, most major elements decrease with increasing SiO_2 (Fig. 4.6). The exceptions are K_2O, which increases, and Na_2O which may either decrease over the range in SiO_2 or show an inflection at ~70% SiO_2. All trends seem to be linear or slightly curved, but some elements have a wide scatter in data. Some of the spread in Na_2O is likely to be due to volatilization during analysis. Sodium loss also has the effect of increasing the abundances of the other elements.

Glass compositions plot higher in SiO_2 than their host whole rock analyses. In general, glass compositions plot with more silicic whole rock samples. For example, basaltic andesite host glass plots with andesite and dacite whole rock analyses, andesite host glass plots with dacite and rhyolite. In most samples, glass analyses are 5-6% SiO_2 higher than the host whole rock values and define a specific range of composition. Andesite glass plots in two distinct ranges, which may be due to differing crystal content in each of the host whole rock samples.

Glass compositions may define a liquid line of descent from the parent magma to daughter. As crystals grow in a magma, the residual liquid is the material which will be extracted to give the next daughter product. In the Kurile Lake rocks, basalt andesite is producing melt of similar composition in terms of most major elements (e.g. Al_2O_3, FeO,

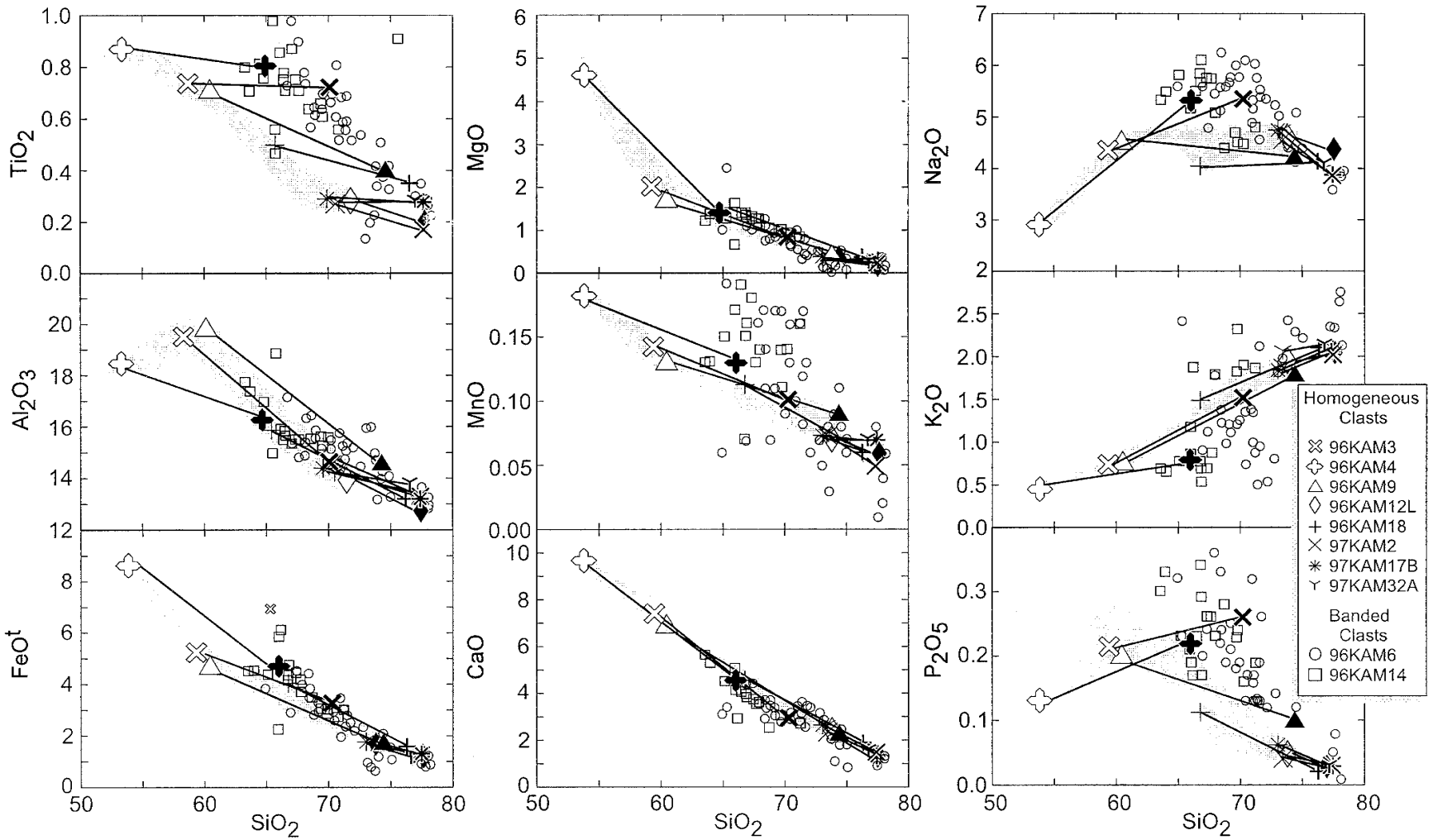

Figure 4.6. Major element vs. SiO_2 variation diagrams for glass. All analyses are normalized to 100% on a volatile free basis. Glass analyses from homogeneous samples are averaged and connected by tie-lines to the host lithology composition. Grey filled symbols are averaged glass values. The fields for whole-rock analyses from Figure 4.3 are outlined for reference. All data are given in Appendix D. Representative glass analyses are listed in table 4.2.

MgO, CaO and K_2O) as andesite and dacite whole-rock determinations. The trends of TiO_2 MnO and P_2O_5 are probably a result of analytical error. Na_2O presents a problem in interpretation. The Na_2O plot alludes to various processes which may be ultimately responsible for forming the magma involved in this eruption. Interpretation of these data will be discussed in a later section

Glass analyses in banded clasts do not show a strong compositional difference from rhyolitic and dacitic bands to andesite and basaltic andesite bands. This may be due to a mingling event overprinting a longer time scale mixing event. In backscatter images, however, strong contrasts are clearly evident, showing an overall difference in composition. These contrasts occur over a few microns, and probably represent mingling. Mixing can only be observed by microprobe analyses.

CHAPTER FIVE

PETROLOGY AND MINERAL CHEMISTRY

Introduction

Mineral assemblages in the KLE were determined by optical microscopy and electron microprobe analyses (Table 5.1). Basaltic andesites, andesites and dacites contain augite, enstatite, plagioclase, magnetite, ilmenite and apatite in a glassy groundmass commonly containing pyroxene microlites. Rhyolite contains similar assemblages, but amphibole is found in rhyolite clasts from the fall deposits. When amphibole occurs, augite is absent.

Analyses of mineral phases in the pumices from the Kurile Lake eruption were made by electron microprobe at New Mexico Institute of Mining and Technology. A suite of minerals was analyzed for all the main rock types present. Analyses and analytical procedures are given in Appendix D.

Petrography

Basaltic Andesites

Basaltic andesite is highly prophyritic, containing ~30% phenocrysts. The groundmass is usually glassy, typically black and highly vesiculated, and makes up 40% of the total expanded volume. Vesicles are round and 10-50 microns to 3-10mm. Plagioclase represents 70% of the crystal content, and is usually sieve textured with a

Table 5.1. Occurrence, morphology and relative abundance of constituents in Kurile Lake pumice and scoria

Component	Basaltic Andesite	Andesite	Dacite	Rhyolite
Glass	40%	25%	15%	15%
Vesicles	30%	50%	75%	75%
Size	10-50μm	10-50μm	10μm-1cm	10μm-1cm
Phenocrysts	30%	25%	10%	10%
Phenocryst relative abundance and characteristics				
Pyroxene				
Orthopyroxene	15%	10%	10%	10% / 5%*
Size	10μm-3mm	10μm-1mm	10-500μm	10-100μm
Inclusions	CPX+MT+IL+AP	CPX+MT+IL+AP	CPX+MT+IL+AP	CPX+MT+IL+AP
Clinopyroxene	5%	5%	5%	5%*
Size	10μm-1mm	10-50μm	10-100μm	10-50μm
Inclusions	OPX+MT+IL+AP	OPX+MT+IL+AP	OPX+MT+IL+AP	OPX+MT+IL+AP
Plagioclase				
sieve	69%	65%	-	-
euhedral				
zoned	1%	4%	50%	40%
unzoned	-	1%	30%	40%
Size	100μm-1mm	100μm-3mm	100μm-3mm	100μm-3mm
Inclusions	OPX+CPX+MT+IL+AP	OPX+CPX+MT+IL+AP	OPX+CPX+MT+IL+AP	OPX+CPX+MT+IL+AP
Amphibole	-	-	-	10%*
Size				100μm-1mm
Inclusions				IL+AP
Magnetite	6%	10%	3%	3%
Size	10-50μm	10-50μm	10-50μm	10-50μm
Inclusions	OPX+CPX+IL+AP	OPX+CPX+IL+AP	OPX+CPX+IL+AP	OPX+CPX+IL+AP
Ilmenite	3%	4%	1%	1%
Size	10-30μm	10-30μm	10-30μm	10-20μm
Inclusions	OPX+CPX+AP	OPX+CPX+AP	OPX+CPX+AP	OPX+CPX+AP
Apatite	1%	1%	1%	1%
Size	10-20μm	10-20μm	10-20μm	10-20μm
Inclusions	none	none	none	none

*In fall derived rhyolite clasts, amphibole replaces clinopyroxene.
-, absent

anhedral, ragged shape, (Fig 5.1a-c) and ranges in size from 100μm to 1cm. About 30% of sieve plagioclase are euhedral shaped and have a solid rim. Rare euhedral plagioclase (Fig 5.1 d-f) are also present. Inclusions of small orthopyroxene, clinopyroxene, magnetite, ilmenite and apatite commonly occur in plagioclase. Clinopyroxene and orthopyroxene (Fig 5.2) each represent 10% of the phenocryst content. Clinopyroxene is generally euhedral and up to 1mm in size. Orthopyroxene is usually subhedral to anhedral and up to 3mm. Orthopyroxene usually has clinopyroxene, magnetite, ilmenite and apatite inclusions. Magnetite (Fig 5.2, 5.3) represents about 5% of phenocrysts, is anhedral to euhedral and may have orthopyroxene, clinopyroxene and apatite inclusions. Ilmenite (Fig 5.2, Fig 5.3) is generally smaller than magnetite and is less abundant (3%), anhedral to euhedral and also may have orthopyroxene, clinopyroxene and apatite inclusions. Magnetite and ilmenite can be found as coexisting pairs. Apatite (Fig 5.3d) makes up 1% of crystal content, and is usually lath shaped. Glomerocrystic clumps (Fig 5.3C) are common and contain mostly clinopyroxene and orthopyroxene with minor amounts of plagioclase magnetite, ilmenite and apatite.

Andesite

Andesites are porphyritic and contain ~25% phenocrysts, ~25% glassy groundmass and ~50% round vesicles. Plagioclase (Fig 5.1) makes up 70% of the phenocrysts and is sieve textured or less commonly un-resorbed. Most sieve plagioclase cores are euhedral with solid overgrowth rims. Some sieve plagioclase are ragged and anhedral. Pristine, non-sieve textured plagioclase commonly exhibit oscillatory zonation and have un-zoned cores. Plagioclase can be up to 3mm and commonly has

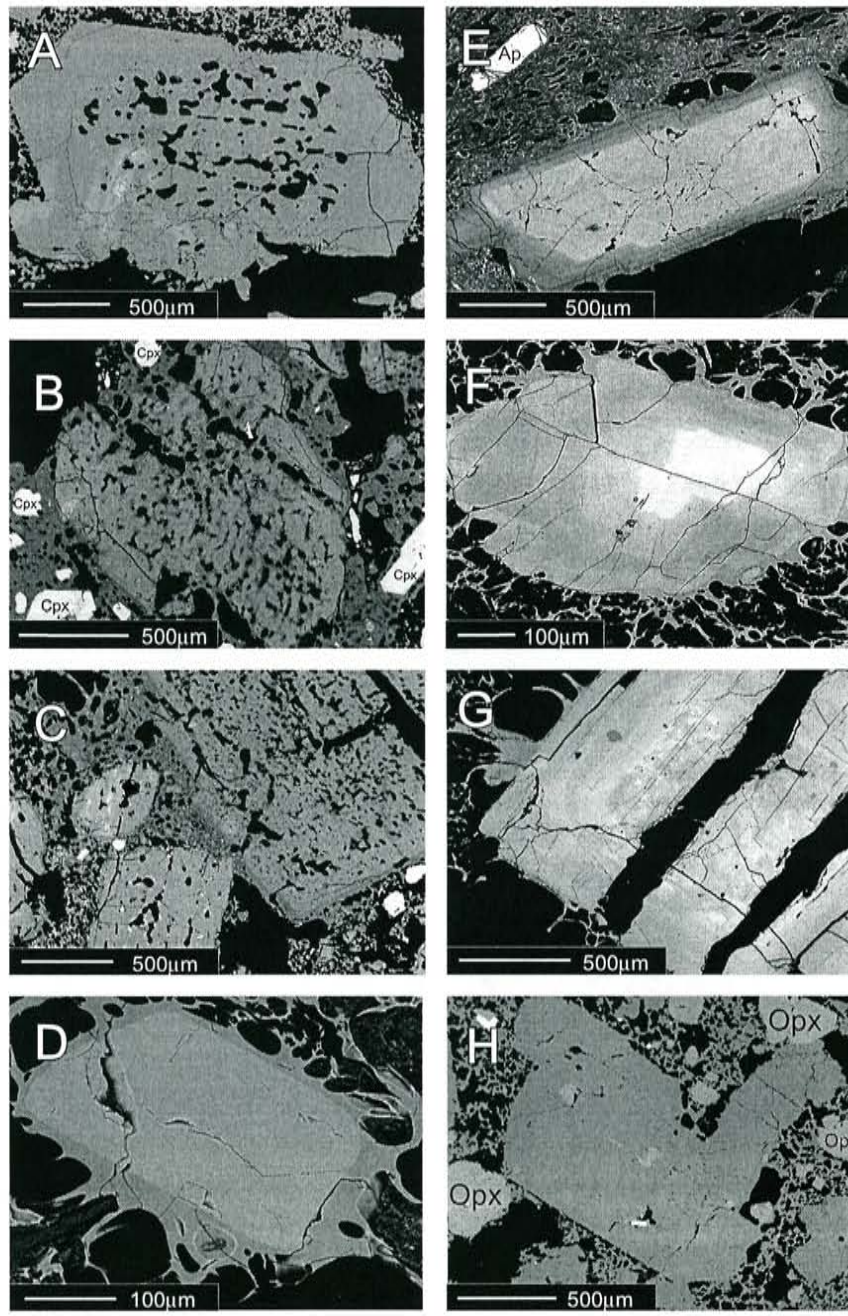

Figure 5.1. Plagioclase phenocryst morphologies from electron microprobe backscatter images. A) Sieve textured plagioclase with a rim overgrowth of the same composition from 96KAM3. B) Sieve textured plagioclase with no rim. C) Sieve plagioclase phenocrysts from 96KAM12I. The lighter phase is An_{85}; the darker is An_{76}. D) Unzoned, euhedral plagioclase from 97KAM2. E) Oscillatory zoned plagioclase from 96KAM6 basaltic andesite glass. F) Oscillatory zoned plagioclase from 96KAM18. G) Splotchy-cored euhedral plagioclase with oscillatory zoning from 97KAM2. H) Euhedral, unzoned plagioclase from 96KAM3. Cpx=clinopyroxene, Opx=orthopyroxene, Ap=apatite

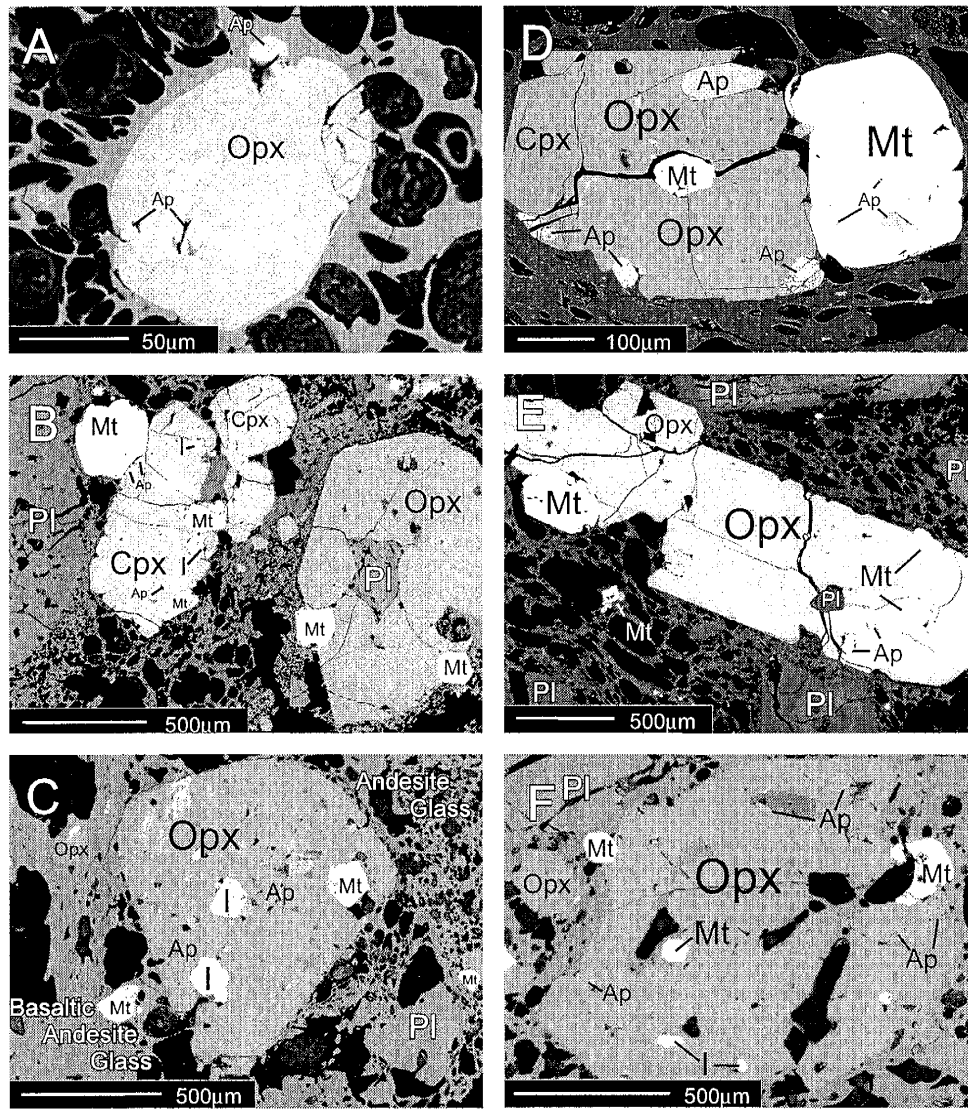

Figure 5.2. Electron microprobe backscatter images of pyroxene and associated phases. A) Subhedral orthopyroxene phenocryst with apatite inclusions from 97KAM2. B) Euhedral clinopyroxene and anhedral orthopyroxene with sieve plagioclase, magnetite, ilmenite and apatite from 96KAM6. C) Euhedral orthopyroxene with magnetite, ilmenite and apatite inclusions from 96KAM14. D) Subhedral orthopyroxene and magnetite with magnetite and apatite inclusions from 96KAM9. E) Tabular orthopyroxene and zoned plagioclase phenocrysts with magnetite inclusions from 96KAM6. F) Euhedral clinopyroxene and plagioclase with magnetite, ilmenite and apatite inclusions from 96KAM9. Opx=orthopyroxene, Cpx=clinopyroxene, Pl=plagioclase, Mt=magnetite, I=ilmenite, Ap=apatite

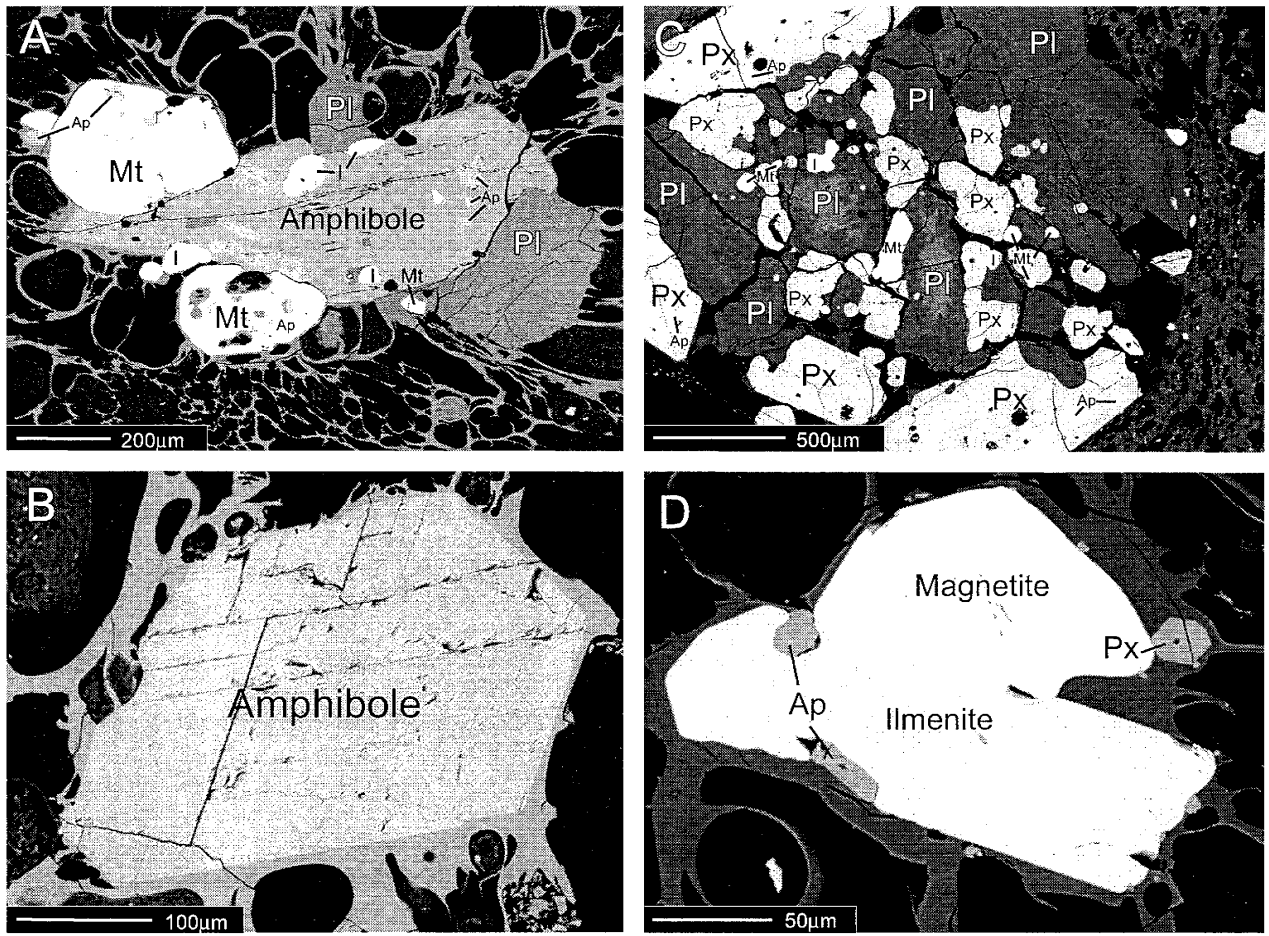

Figure 5.3. Amphibole, glomerocryst, ilmenite and magnetite electron microprobe backscatter images. A) Amphibole, plagioclase magnetite, ilmenite and apatite phenocrysts from 97KAM17b. B) Amphibole phenocryst from 97KAM2. C) Glomerocryst containing plagioclase, pyroxene, magnetite, ilmenite and apatite from 96KAM6. D) Co-existing magnetite and ilmenite pair with small pyroxene and apatite phenocrysts from 97KAM2. Pl=plagioclase, Px=pyroxene, Amp=amphibole, Mt=magnetite, I=ilmenite, Ap=apatite

orthopyroxene, clinopyroxene, magnetite, ilmenite and apatite inclusions. Orthopyroxene (Fig 5.2) represents 10% of phenocrysts and is euhedral to anhedral. Orthopyroxene can be up to 3mm and is typically included by clinopyroxene, magnetite, ilmenite and apatite. Clinopyroxene (Fig 5.3) represents 5% of crystals and is commonly euhedral and rarely anhedral. Orthopyroxene can be up to 50μm and may be included by clinopyroxene, magnetite, ilmenite and apatite. Magnetite and ilmenite (Fig 5.2, 5.3) represents 10% and 4% of phenocrysts, respectively and are anhedral to euhedral. Magnetite is included in all phases except plagioclase. Ilmenite is included in magnetite and all other phases except plagioclase. Apatite (Fig 5.1e) is rare (1%) and is commonly euhedral. As with basaltic andesite, glomerocrysts (Fig. 5.3c) of orthopyroxene and clinopyroxene with lesser amounts of plagioclase, ilmenite, magnetite and apatite are present, but less common than in the basaltic andesites.

Dacite

Dacite clasts are porphyritic with a glassy groundmass, (85%) and contain about 15% phenocrysts. Phenocryst content is predominantly plagioclase (80%), which are euhedral to anhedral and up to 3mm. Plagioclase commonly exhibits oscillatory zonation (Fig 5.1d-h) with uniform cores. About 30% of plagioclase is unzoned. Plagioclase is included by the other phases. Orthopyroxene (Fig 5.2) makes up 10% of the phenocrysts, is up to 500μm in size, and euhedral to anhedral. Orthopyroxene is included with all phases except plagioclase. Clinopyroxene (Fig 5.2) makes up 5% of the phenocryst content, is 100μm in size, and usually euhedral but can be anhedral. Clinopyroxene is included by orthopyroxene, magnetite, ilmenite and apatite. Magnetite and ilmenite (Fig

5.2, Fig 5.3) make up 3% and 1% of the crystal content, respectively and are anhedral to euhedral. Magnetite is up to 50μm in size; ilmenite is up to 30μm. Both oxides are included by all other phases except plagioclase. Apatite (1%) is small (10-20μm in size), usually lath shaped and included by the other mineral phases except plagioclase. As with andesites and basaltic andesites, glomerocrystic clumps are present but rare.

Rhyolite

Rhyolite clasts are crystal-poor (10%) and pumiceous. Glass composes 15% of samples and contains elongated vesicles up to 3cm long and 1cm wide. Plagioclase (Fig. 5.1) represents 70 % of phenocrysts, is usually euhedral, and commonly exhibits oscillatory zonation, but may be unzoned. Cores are unzoned. Plagioclase can be up to 2mm in size and is rarely included by other phases. Orthopyroxene (Fig. 5.2) represents 10% of phenocrysts and is euhedral to anhedral and up to 200μm in size. Clinopyroxene represents 10 % of phenocrysts, is up to 200μm in size and is rarely included by magnetite, ilmenite and apatite. Amphibole is present in rhyolitic pumice from the KLp fall deposits. Amphibole (Fig 5.3) in these samples makes up 10% of phenocrysts, is euhedral, up to 200μm in size and is included by other mineral phases except plagioclase. When clinopyroxene (Fig 5.2) is present, no amphibole is observed. Clinopyroxene-bearing rhyolites are only found in the ignimbrite. Clinopyroxene represents 10 % of phenocrysts, is anhedral to euhedral and is up to 50μm in size. Clinopyroxene may be included by apatite, magnetite, ilmenite and orthopyroxene. Magnetite represents 5% of phenocrysts, is euhedral to anhedral, up to 50μm in size and is rarely included by orthopyroxene, clinopyroxene or apatite. Ilmenite (2%) is similar, but smaller (20μm)

and is very rarely included by other minerals. Apatite is rare (2%) and occurs as small (5-15μm) laths.

Banded Clasts

Banded clasts are common in KLE exposures north and west of Kurile Lake. Figure 5.4 is a set of six backscatter images of banded clasts. Banded clasts may contain all lithologies, but typically are a combination of two compositions. Bands can be over 5cm thick to less than 50μm thick strands visible in thin section. Sometimes phenocrysts are mixed into another lithology while retaining a glass jacket of the host lithology. However, some phenocrysts loose the glass coating causing the mis-assignment of phenocrysts to the improper source lithology. This can only be observed indirectly by comparing the phenocryst end-member composition from banded clasts to end-member compositions from homogeneous clasts. Banding in clasts seems to be mingling as no mixing has been observed in thin section by petrographic microscopy or in hand sample.

Mineralogy

Pyroxene

Pyroxene is ubiquitous as phenocryst or groundmass phases in all rock types. Usually clinopyroxene (augite) and orthopyroxene (enstatite) occur, but rhyolite pumice clasts in the KLp deposits only contain enstatite. Abundances of augite and enstatite decrease with increasing silica content of the rock; augite more rapidly than enstatite.

Microprobe analyses of FeO^T in pyroxenes was partitioned between Fe_2O_3 and FeO using the charge-balancing scheme of Yoder and Tilley (1962). This method

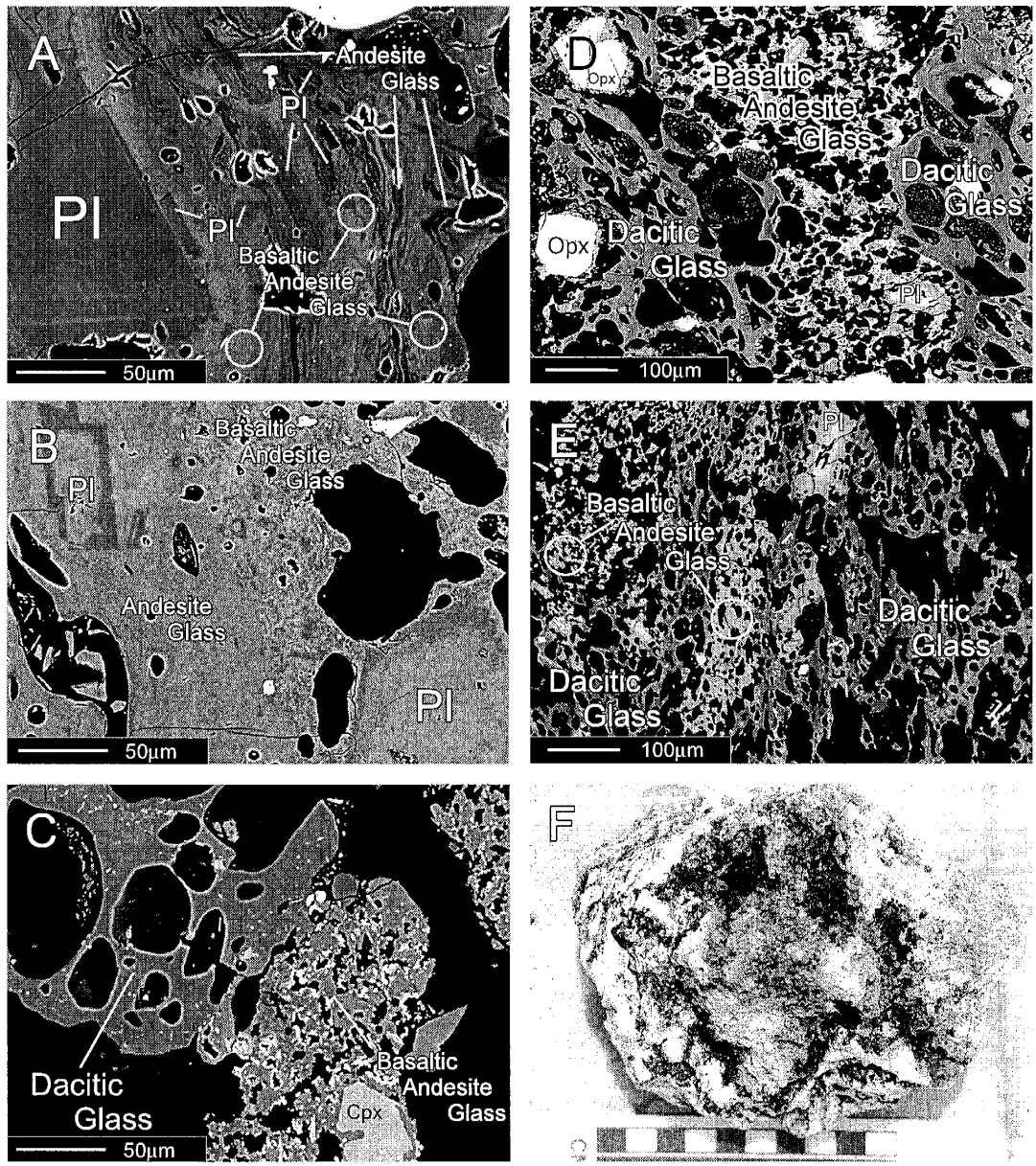

Figure 5.4. Electron microprobe backscatter images of glass from mixed clasts. A) Aphyric mixed glass of basaltic andesite and andesite compoistions in 96KAM14. B) Aphyric andesitic and phyric basaltic andesite glass from 96KAM14. C) Aphyric dacitic glass and phyric basaltic andesite glass from 96KAM6. D) Aphyric dacitic and basaltic andesite glass from 96KAM15. E) Aphyric basaltic andesite and dacitic glass from 96KAM6. F) Typical banded clast hand sample. This clast was collected from the zoned CNE3 section shown in Fig. 3.6 (scale bar is in centimeters).

normalizes the pyroxene formula to 6 oxygens and recalculates to four cations. Cations were assigned to each site according to IMA guidelines (Morimito, 1988). The end-members were calculated using the method of Cawthorn and Collerson (1974). Pyroxene analyses (Table 5.2) are plotted in Figure 5.5a-b.

Augite mainly occurs as small, unzoned microphenocrysts and phenocrysts. It is usually euhedral, but can be sub- to anhedral. In basaltic andesite and andesite, augite occurs as phenocryst, glomerophyric clumps, and in the groundmass. In dacite, augite occurs as phenocryst and in the groundmass. Augite is absent in rhyolites from fall deposits but is present in ignimbrite rhyolite pumices.

Augite compositions show little variation in all rock types (Fig. 5.5). Average compositions are Wo_{44-42}, En_{44-41}, Fs_{16-13} for basaltic andesites, Wo_{44-42}, En_{44-41}, Fs_{17-15} for andesites and Wo_{44-42}, En_{41-39}, Fs_{18-16} for dacites and rhyolites.

Unzoned enstatite occurs in all samples and has the same morphology as augite. Enstatite has a range of compositions depending on rock type (Fig. 5.5). In basaltic andesite enstatite is Wo_{4-0}, En_{72-68}, Fs_{16-13}, in andesites; Wo_{3-2}, En_{66-61}, Fs_{17-14}, dacite; Wo_{3-2}, En_{65-55}, Fs_{42-31} and rhyolites; Wo_{3-2}, En_{63-52}, Fs_{46-34}.

Ti and Al (in atoms per formula unit (O=6)) are plotted against Mg index (Mg#) ($Mg/(Mg+Fe^{2+}+Mn)$ (Fig 5.6). Ti varies from 0.001 to 0.008. Pyroxene phenocrysts in mixed pumices have some higher Ti and Al contents, but most are similar to pyroxene in homogeneous clast samples. Most of the Ti variation is in the basaltic andesites, andesites and dacites. Pyroxenes in rhyolites have low Ti and Al and little variation in Figure 5.6.

Table 5.2. Representative Pyroxene Analyses

	K4-PYX13	K4-PYX15	K12B-PYX3	K12B-PYX8	K3-PYX52	K3-PYX1	K12L-PYX2	K12L-PYX3	K18-PYX14	K18-PYX15	K32D-PYX18	K32D-PYX19	K9-PYX5
Analysis	euhedral	euhedral	anhedral	euhedral	glomerocryst	glomerocryst	microphenocryst	microphenocryst	euhedral	euhedral	euhedral	euhedral	euhedral
Rock Type	basaltic andesite	basaltic andesite	basaltic andesite	basaltic andesite	andesite	andesite	andesite	andesite	dacite	dacite	dacite	dacite	rhyolite
SiO_2	51.29	53.54	51.49	53.64	52.73	52.42	53.37	51.02	52.66	52.86	52.19	53.09	51.60
TiO_2	0.39	0.23	0.41	0.21	0.07	0.17	0.17	0.49	0.24	0.12	0.38	0.21	0.10
Al_2O_3	1.98	1.17	2.15	1.54	0.35	0.94	0.84	2.91	1.35	0.45	1.34	0.78	0.40
FeO	7.58	16.92	7.92	17.70	20.07	8.55	19.04	8.49	9.68	22.87	9.72	20.74	25.81
MnO	0.27	0.58	0.31	0.46	1.24	0.49	0.92	0.26	0.52	1.21	0.63	0.85	1.78
MgO	15.13	25.47	15.43	25.94	23.09	14.39	24.03	14.88	14.52	22.01	14.68	23.61	18.88
CaO	20.63	1.31	21.54	1.41	1.01	21.48	1.23	21.17	21.50	0.95	21.05	1.31	1.01
Na_2O	0.32	0.02	0.26	0.02	0.02	0.29	0.03	0.27	0.31	0.02	0.32	0.01	0.04
K_2O	0.01	0.01	0.00	0.00	0.01	0.00	0.02	0.02	0.00	0.00	0.00	0.00	0.01
Total	97.60	99.25	99.51	100.92	98.59	98.73	99.65	99.51	100.78	100.49	100.31	100.60	99.63
FeO(calculated)	6.39	16.30	5.23	17.67	19.68	7.75	18.34	6.13	7.71	21.41	7.42	18.85	24.70
Fe_2O_3(calculated)	2.30	1.05	2.82	0.00	0.46	1.55	0.68	2.46	2.06	0.96	2.30	1.36	0.83
Total	98.71	99.68	99.64	100.89	98.66	99.47	99.63	99.61	100.87	99.99	100.31	100.07	99.35
M1Al	0.011	0.005	0.002	0.022	0.000	0.004	0.006	0.025	0.005	0.000	0.000	0.000	0.000
M1Ti	0.011	0.006	0.011	0.006	0.002	0.005	0.005	0.014	0.007	0.003	0.011	0.006	0.003
M1Fe^{3+}	0.066	0.029	0.081	0.011	0.013	0.044	0.019	0.070	0.058	0.027	0.065	0.038	0.024
M1Fe^{2+}	0.065	0.000	0.048	0.000	0.000	0.143	0.000	0.066	0.131	0.000	0.113	0.000	0.000
M1Mg	0.846	0.959	0.853	0.961	0.985	0.803	0.971	0.825	0.800	0.968	0.812	0.956	0.974
M2Mg	0.000	0.427	0.000	0.450	0.299	0.000	0.351	0.000	0.000	0.252	0.000	0.337	0.103
M2Fe^{2+}	0.139	0.502	0.116	0.480	0.619	0.102	0.569	0.128	0.110	0.670	0.120	0.584	0.794
M2Mn	0.009	0.018	0.010	0.014	0.039	0.016	0.029	0.008	0.016	0.038	0.020	0.026	0.058
M2Ca	0.829	0.051	0.855	0.055	0.040	0.862	0.049	0.844	0.851	0.038	0.837	0.052	0.041
M2Na	0.023	0.001	0.019	0.001	0.001	0.021	0.002	0.019	0.022	0.001	0.023	0.001	0.003
Sum Cations	4.00	4.00	4.00	4.00	4.00	4.00	4.00	4.00	4.00	4.00	4.00	4.00	4.00
Wo	42.43	2.58	43.57	2.80	2.00	43.74	2.45	43.47	43.29	1.89	42.47	2.57	2.07
En	43.29	69.77	43.43	71.57	63.75	40.77	66.53	42.51	40.68	60.78	41.21	64.39	53.80
Fs	14.28	27.66	13.00	25.64	34.25	15.49	31.02	14.03	16.04	37.33	16.31	33.05	44.14
Wo+En+Fs	97.59	99.86	98.05	99.86	99.85	97.86	99.78	97.96	97.73	99.85	97.64	99.93	99.70
Jd	0.35	0.02	0.06	0.10	0.00	0.18	0.05	0.54	0.17	0.00	0.00	0.00	0.00
Ae	2.06	0.12	1.89	0.05	0.15	1.96	0.17	1.50	2.11	0.15	2.37	0.07	0.30

Wo - Wollastonite; En - Enstatite; Fs - Ferrosillite; Jd - Jadeite; Ae - Aegirine

A complete listing of pyroxene analyses is given in Appendix D.

Table 5.2. (continued) Representative Pyroxene Analyses

	K9-PYX11	K2-PYX7	K17B-PYX5	K32A-PYX9	K32A-PYX10	K6-PYX11	K6-PYX13	K6-PYX22	K6-PYX55	K14-PYX11	K14-PYX13	K14-PYX14	K14-PYX18
Analysis	euhedral	euhedral	euhedral	microphenocryst	euhedral	euhedral	euhedral	anhedral	anhedral	euhedral	euhedral	euhedral	euhedral
Rock Type	rhyolite	rhyolite	rhyolite	rhyolite	rhyolite	mixed dacite	mixed dacite	mixed bas. and.	mixed bas. and.	mixed andesite	mixed andesite	mixed bas. and.	mixed bas. and.
SiO_2	51.14	52.14	51.09	52.15	51.52	52.33	54.27	53.84	51.00	50.90	53.20	52.95	51.42
TiO_2	0.12	0.10	0.11	0.10	0.25	0.25	0.19	0.19	0.51	0.45	0.26	0.18	0.48
Al_2O_3	0.36	0.35	0.39	0.32	1.14	1.10	1.02	1.02	3.19	2.77	1.11	1.30	2.39
FeO	26.41	25.64	26.02	24.64	9.90	9.90	16.34	17.13	7.77	9.19	19.12	16.64	9.06
MnO	1.82	1.77	1.87	1.62	0.66	0.59	0.45	0.80	0.24	0.40	0.78	0.52	0.41
MgO	18.63	19.44	18.73	20.03	13.87	13.88	26.24	25.49	15.14	15.28	24.82	26.57	15.15
CaO	0.96	0.98	1.00	1.14	21.55	20.76	1.36	1.05	21.15	20.21	1.25	1.46	20.52
Na_2O	0.01	0.06	0.01	0.04	0.19	0.32	0.03	0.02	0.24	0.31	0.03	0.01	0.29
K_2O	0.01	0.00	0.01	0.02	0.01	0.00	0.01	0.01	b.d.	0.02	0.00	0.03	0.00
Total	99.46	100.48	99.23	100.06	99.09	99.13	99.91	99.55	99.24	99.53	100.57	99.66	99.72
FeO(calculated)	24.750	24.330	24.410	4.370	7.84	9.33	15.840	16.750	5.910	6.120	16.930	13.140	6.750
FE_2O_3(calculated)	1.030	0.910	1.030	4.360	1.95	0.56	0.470	0.330	1.930	3.230	1.770	2.530	2.390
Total	98.83	100.08	98.65	84.15	98.98	99.12	99.88	99.50	99.31	99.69	100.15	98.69	99.80
M1Al	0.000	0.000	0.000	0.000	0.000	0.021	0.012	0.013	0.037	0.013	0.000	0.000	0.015
M1Ti	0.003	0.003	0.003	0.003	0.007	0.007	0.005	0.005	0.014	0.013	0.007	0.005	0.013
M1Fe^{3+}	0.030	0.026	0.030	0.026	0.056	0.016	0.013	0.009	0.055	0.092	0.049	0.070	0.068
M1Fe^{2+}	0.000	0.000	0.000	0.000	0.156	0.176	0.000	0.000	0.055	0.035	0.000	0.000	0.064
M1Mg	0.967	0.971	0.966	0.971	0.780	0.780	0.971	0.973	0.840	0.847	0.944	0.925	0.839
M2Mg	0.100	0.125	0.107	0.158	0.000	0.000	0.448	0.417	0.000	0.000	0.404	0.513	0.000
M2Fe^{2+}	0.800	0.774	0.789	0.740	0.094	0.120	0.483	0.515	0.132	0.159	0.521	0.412	0.149
M2Mn	0.059	0.057	0.061	0.052	0.021	0.019	0.014	0.025	0.008	0.013	0.024	0.016	0.013
M2Ca	0.040	0.040	0.041	0.046	0.871	0.838	0.053	0.041	0.843	0.805	0.049	0.057	0.817
M2Na	0.001	0.004	0.001	0.003	0.014	0.023	0.002	0.001	0.017	0.022	0.002	0.001	0.021
Sum Cations	4.00	4.00	4.00	4.00	4.00	4.00	4.00	4.00	4.00	4.00	4.00	4.00	4.00
Wo	1.96	1.98	2.05	2.30	43.89	43.01	2.67	2.08	43.64	41.28	2.44	2.82	41.88
En	52.97	54.71	53.35	56.28	39.31	40.01	71.62	70.20	43.46	43.42	67.29	71.33	43.02
Fs	45.07	43.31	44.60	41.42	16.80	16.98	25.72	27.72	12.90	15.30	30.28	25.85	15.10
Wo+En+Fs	99.92	99.55	99.92	99.70	98.57	97.64	99.79	99.86	98.19	97.65	99.78	99.93	97.83
Jd	0.00	0.00	0.00	0.00	0.00	1.32	0.10	0.09	0.73	0.30	0.00	0.00	0.39
Ae	0.08	0.45	0.08	0.30	1.43	1.04	0.11	0.06	1.08	2.05	0.22	0.07	1.78

Wo - Wollastonite; En - Enstatite; Fs - Ferrosillite; Jd - Jadeite; Ae - Aegirine

A complete listing of pyroxene analyses is given in Appendix D.

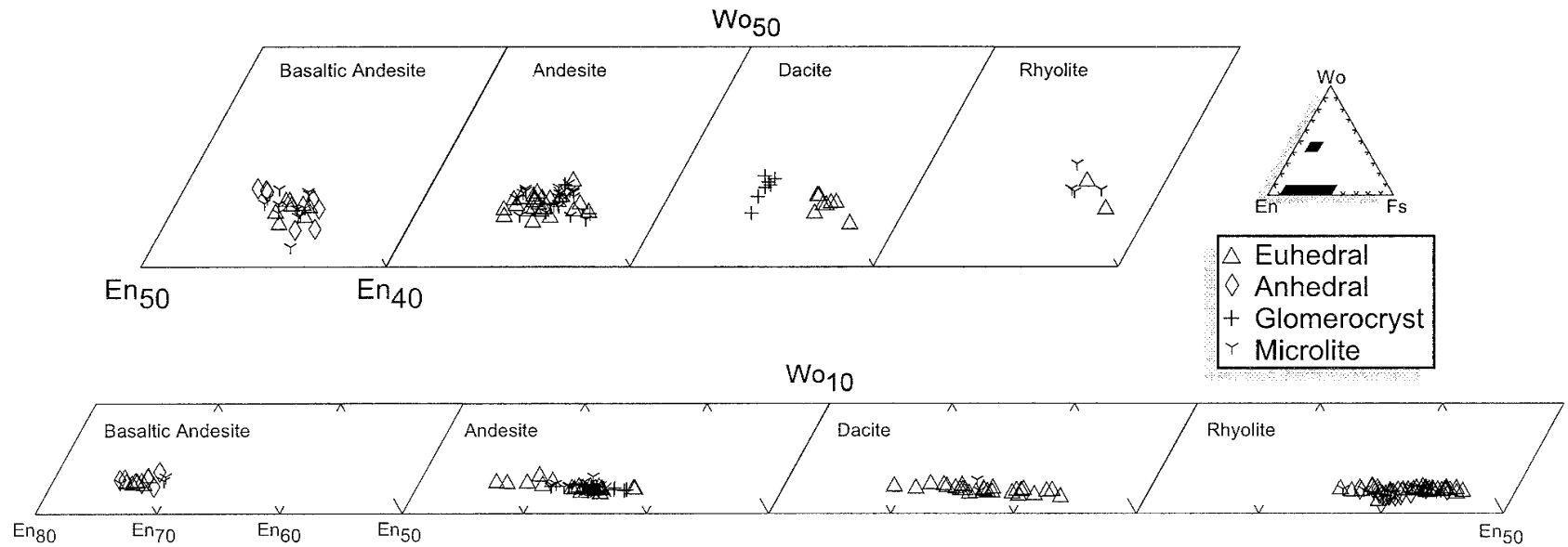

Figure 5.5a. Composition of pyroxene in homogeneous clasts. Pyroxene are plotted in the Wo-En-Fs end-member system. Regions within the triangle are enlarged for clarity and correlate to the dark boxes on the small triangles. Euhedral, anhedral, glomerocrystic and microlites are plotted. Analyses from each lithology are plotted seperately for clarity. Pyroxene analyses are given in Appendix D.

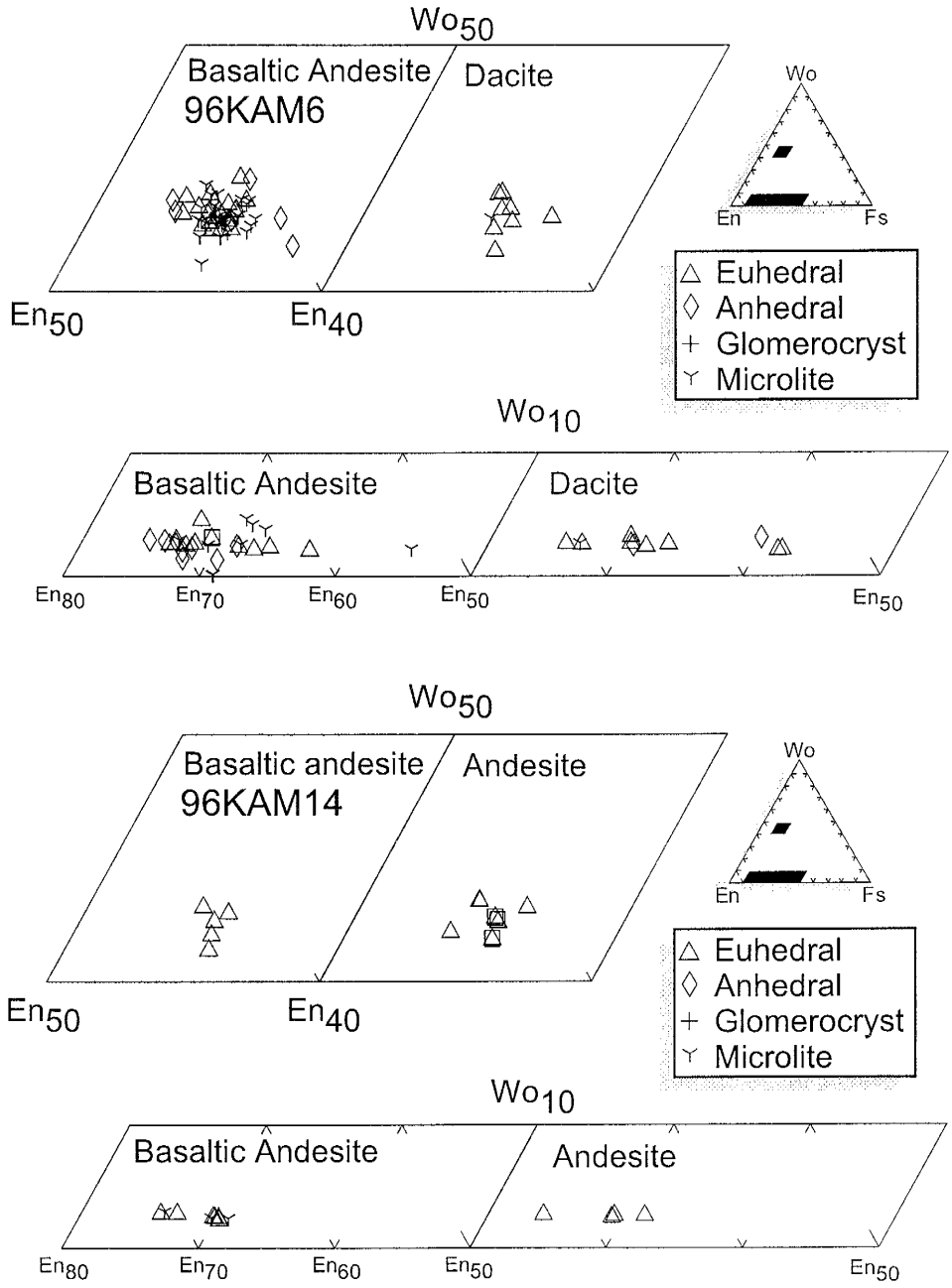

Figure 5.5b. Pyroxene from mixed clasts. Pyroxene are plotted in the Wo-En-Fs end-member system. Regions within the triangle are enlarged for clarity and correlate to the indicated boxes on the small triangles. Euhedral, anhedral, glomerocrystic and microlites are plotted. Analyses from each lithology contained in each sample are plotted seperately for clarity. Pyroxene analyses are given in Appendix D.

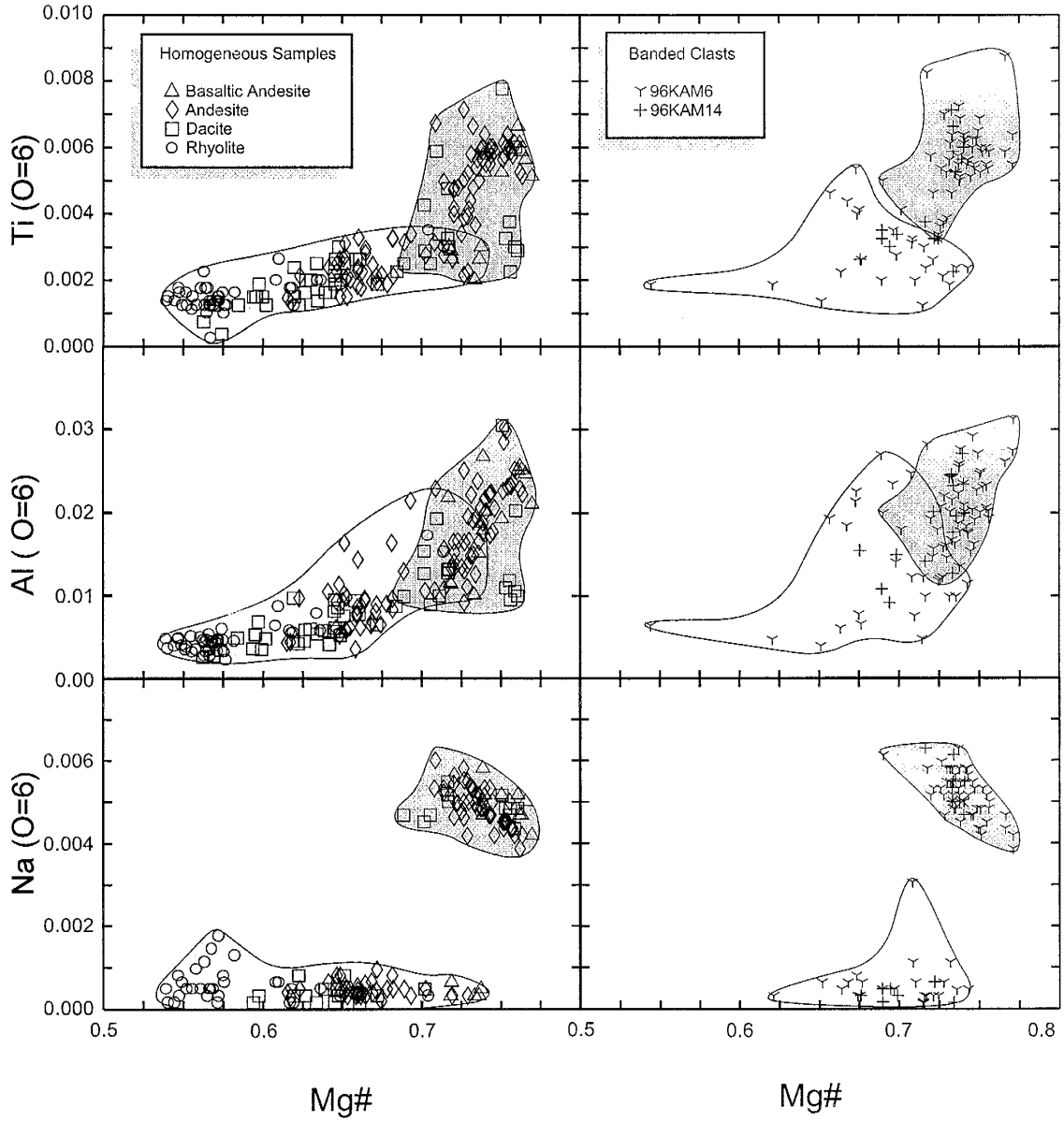

Figure 5.6. Ti, Al and Na (atoms per formula unit (O=6)) vs Mg# [Mg/(Mg+Fe^{2+}+Mn)] for pyroxenes. Orthopyroxene are within the light grey field. Clinopyroxene are in the dark grey field. Analyses from mingled clasts are plotted separately from homogeneous clasts for clarity and designated by host lithology such as dacite or basaltic andesite and the specific sample name. Pyroxene analyses are given in Appendix D.

All pyroxenes have low Na contents and K is usually below detection limits. Na is only slightly higher in clinopyroxene than orthopyroxene when plotted against Mg#. Na plots in two groups These groups are clinopyroxene and orthopyroxene. Clinopyroxene has higher Na contents but varies little over the range of Mg#, as does orthopyroxene.

Augite shows little compositional variation in Kurile Lake samples. A slight increase in Fs content is observed as the host rock composition progresses from basaltic andesite to rhyolite. Enstatite also shifts toward higher Fs values from basaltic andesite to rhyolite. This corresponds to the removal of Mg from the melt during fractionation. The low alkalis, Ti and Al contents indicate that these elements were either involved in other processes or generally incompatible at the conditions present in the melt at the time of formation. Ti and Al could be involved in magnetite and ilmenite fractionation. Partition coefficients for Ti are one or two orders of magnitude greater for magnetite and ilmenite (Rollinson, 1993 and references therein). Al could have been involved in plagioclase fractionation as well as Na and K. Amphibole and enstatite occurrence indicates a high P_{H2O} in the parent magma for rhyolites. The slight deflection toward En for enstatites in amphibole-bearing rocks indicates Mg was being preferentially fractionated into amphibole. Experiments using Mt. St. Helens cummingtonite-bearing Yn tephra (Gerschwind and Rutherford, 1992) show hornblende and orthopyroxene to be stable at ~1.2-2 P_{H2O} (kbar) over a temperature range of 790-910°C. Over this temperature range and below this pressure, orthopyroxene and clinopyroxene are stable, indicating P_{H2O} is critical in the stability of hornblende.

Feldspar

Plagioclase is the only feldspar phase present in KLE clasts. It is ubiquitous and is the most abundant phenocryst phase. Plagioclase ranges in size from 50μm to 3mm and shows a wide range of morphology from euhedral to anhedral and is often sieve textured. Few, if any, plagioclase microlites are present, although 10-50μm fragments of larger phenocrysts are common. Sieve textured plagioclases are most common in basaltic andesites and decrease in frequency from basaltic andesite to andesite. Rhyolite and dacite contains no sieve textured plagioclase phenocrysts. Some sieve textured plagioclase phenocrysts can be euhedral with solid rims or anhedral and ragged. Euhedral to anhedral plagioclase phenocrysts are most common in rhyolites and decrease in frequency from dacite to basaltic andesite. Euhedral-anhedral plagioclase phenocrysts may be oscillatory zoned or unzoned.

Figure 5.7a-b are ternary plots of all plagioclase phenocryst analysis (Table 5.3) by rock type, morphology and location. Feldspar end members were calculated using the method of Deer et al., (1966). Sieve textured plagioclase phenocrysts range continuously in basaltic andesites from An_{89-81} (core) to An_{92-84} (rim); andesite ranges from An_{56-43} (core), An_{83-40} (middle) to An_{52-56} (rim); dacites range from An_{86-60} (core) to An_{86-60} (rim). Euhedral plagioclase phenocryst compositions range in basaltic andesites from An_{94-68} (core) to An_{89-69} (rim); andesites range from An_{58-42} (core), An_{82-43} (middle) to An_{62-50} (rim); dacites range from An_{84-45} (core), An_{74-60} (middle) to An_{52-41} (rim); rhyolites range from An_{87-33} (core) to An_{87-31} (rim). Some of the more An rich plagioclase phenocrysts may be inherited. Plagioclase range in Or content from Or_0 to Or_2. The presence of sieve

Table 5.3. Representative Feldspar Analyses

	K4-FSP6	K4-FSP31	K4-FSP25	K3-FSP17	K3-FSP23	K12L-FSP3	K12L-FSP16	K18-FSP1	K18-FSP9	K32D-FSP10
Type	euhedral	sieve	euhedral	sieve	sieve	euhedral	euhedral	euhedral	euhedral	microphenocryst
Rock Type	basaltic andesite	basaltic andesite	basaltic andesite	andesite	andesite	andesite	andesite	dacite	dacite	dacite
SiO_2	44.21	46.47	50.60	53.89	53.51	46.67	51.51	47.26	56.35	59.91
Al_2O_3	35.67	34.16	31.45	29.32	29.56	32.77	29.67	32.68	26.78	26.31
Fe_2O_3	0.60	0.57	0.69	0.39	0.36	0.57	0.68	0.42	0.33	0.30
CaO	18.72	16.93	13.89	11.27	11.31	16.54	12.91	16.22	9.20	7.46
Na_2O	0.79	1.87	3.56	5.16	5.18	1.95	3.93	2.10	6.14	5.96
K_2O	0.00	0.03	0.05	0.09	0.10	0.01	0.07	0.01	0.16	0.22
Total	99.99	100.02	100.23	100.12	100.03	98.51	98.76	98.69	98.96	100.16
Si	8.177	8.549	9.203	9.732	9.679	8.706	9.476	8.782	10.226	10.616
Al	7.771	7.400	6.735	6.236	6.297	7.198	6.428	7.152	5.723	5.490
Fe^3	0.083	0.078	0.095	0.053	0.049	0.080	0.094	0.059	0.045	0.040
Ca	3.710	3.337	2.707	2.180	2.193	3.306	2.545	3.229	1.789	1.417
Na	0.284	0.665	1.254	1.808	1.818	0.706	1.403	0.757	2.160	2.046
K	0.001	0.006	0.010	0.022	0.024	0.002	0.016	0.002	0.037	0.051
Sum Cations	20.026	20.035	20.004	20.031	20.060	19.998	19.962	19.981	19.980	19.660
Ab	7.10	16.60	31.60	45.10	45.10	17.60	35.40	19.00	54.20	58.20
An	92.90	83.30	68.20	54.40	54.30	82.40	64.20	81.00	44.90	40.30
Or	0.00	0.10	0.30	0.50	0.60	0.00	0.40	0.10	0.90	1.50

Sample	K32D-FSP11	K9-FSP12	K9-FSP4	K17B-FSP16	K17B-FSP5	K2-FSP6	K2-FSP25	K14-FSP18	K14-FSP20	K14-FSP19
Type	euhedral	euhedral	euhedral	euhedral	euhedral	euhedral	euhedral	sieve	sieve	sieve
Rock Type	dacite	rhyolite	rhyolite	rhyolite	rhyolite	rhyolite	rhyolite	mixed bas. and.	mixed bas. and.	mixed bas. and.
SiO_2	47.10	55.96	57.65	48.29	59.37	53.51	60.52	45.72	55.29	50.20
Al_2O_3	34.56	27.76	27.29	33.45	25.93	29.71	25.55	34.05	28.00	31.57
Fe_2O_3	0.41	0.31	0.35	0.38	0.28	0.43	0.24	0.60	0.53	0.56
CaO	16.79	9.35	8.35	15.92	7.22	11.75	6.64	17.25	10.60	14.34
Na_2O	2.10	6.44	6.91	3.10	7.32	4.90	7.75	1.51	5.49	3.15
K_2O	0.03	0.13	0.19	0.05	0.20	0.11	0.25	0.02	0.09	0.03
Total	101.00	99.95	100.73	101.19	100.32	100.41	100.94	99.15	100.00	99.85
Si	8.572	10.077	10.266	8.767	10.563	9.649	10.684	8.492	9.972	9.164
Al	7.407	5.887	5.722	7.152	5.432	6.310	5.311	7.448	5.947	6.787
Fe^3	0.056	0.041	0.047	0.052	0.038	0.059	0.032	0.084	0.072	0.077
Ca	3.275	1.803	1.593	3.097	1.377	2.270	1.256	3.433	2.048	2.805
Na	0.740	2.249	2.385	1.092	2.525	1.713	2.651	0.544	1.920	1.115
K	0.007	0.031	0.043	0.012	0.044	0.026	0.055	0.005	0.021	0.007
Sum Cations	20.057	20.088	20.056	20.172	19.979	20.027	19.989	20.006	19.980	19.955
Ab	18.40	55.10	59.30	26.00	64.00	42.70	66.90	13.70	48.10	28.40
An	81.40	44.20	39.60	73.70	34.90	56.60	31.70	86.20	51.30	71.40
Or	0.20	0.80	1.10	0.30	1.10	0.60	1.40	0.10	0.50	0.20

Sample	K14-FSP16	K14-FSP17	K14-FSP3	K14-FSP6	K6-FSP130	K6-FSP140	K6-FSP132	K6-FSP133	K6-FSP138	K6-FSP139
Type	euhedral	euhedral	euhedral	euhedral	euhedral	euhedral	sieve	sieve	euhedral	euhedral
Rock Type	mixed bas. and.	mixed bas. and.	mixed andesite	mixed andesite	mixed dacite	mixed dacite	mixed bas. and.	mixed bas. and.	mixed bas. and.	mixed bas. and.
SiO_2	52.11	54.44	47.19	50.34	56.65	56.61	47.21	48.59	54.70	56.17
Al_2O_3	29.79	28.14	33.40	30.83	26.61	26.86	33.01	32.04	28.13	27.01
Fe_2O_3	0.42	0.56	0.45	0.53	0.35	0.28	0.59	0.59	0.38	0.36
CaO	12.14	10.67	16.44	13.52	8.62	8.61	15.81	14.90	10.03	8.82
Na_2O	4.44	5.38	2.04	3.49	6.31	6.39	2.41	3.01	5.67	6.21
K_2O	0.06	0.07	0.03	0.05	0.18	0.17	0.04	0.03	0.13	0.16
Total	98.96	99.26	99.55	98.76	98.73	98.91	99.07	99.16	99.04	98.72
Si	9.544	9.900	8.701	9.274	10.287	10.261	8.745	8.967	9.951	10.209
Al	6.425	6.027	7.252	6.689	5.691	5.733	7.200	6.964	6.028	5.781
Fe^3	0.058	0.077	0.062	0.073	0.048	0.039	0.082	0.082	0.052	0.049
Ca	2.382	2.079	3.248	2.669	1.678	1.672	3.138	2.945	1.954	1.717
Na	1.577	1.897	0.729	1.247	2.221	2.244	0.867	1.077	2.000	2.188
K	0.014	0.016	0.007	0.012	0.042	0.038	0.009	0.007	0.029	0.037
Sum Cations	20.000	19.996	19.999	19.964	19.967	19.987	20.041	20.042	20.014	19.981
Ab	39.70	47.50	18.30	31.70	56.4	56.8	21.6	26.7	50.2	55.5
An	60.00	52.10	81.50	67.90	42.6	42.3	78.2	73.1	49.1	43.6
Or	0.40	0.40	0.20	0.30	1.1	1.0	0.2	0.2	0.7	0.9

A complete list of feldspar analyses is given in Appendix D.

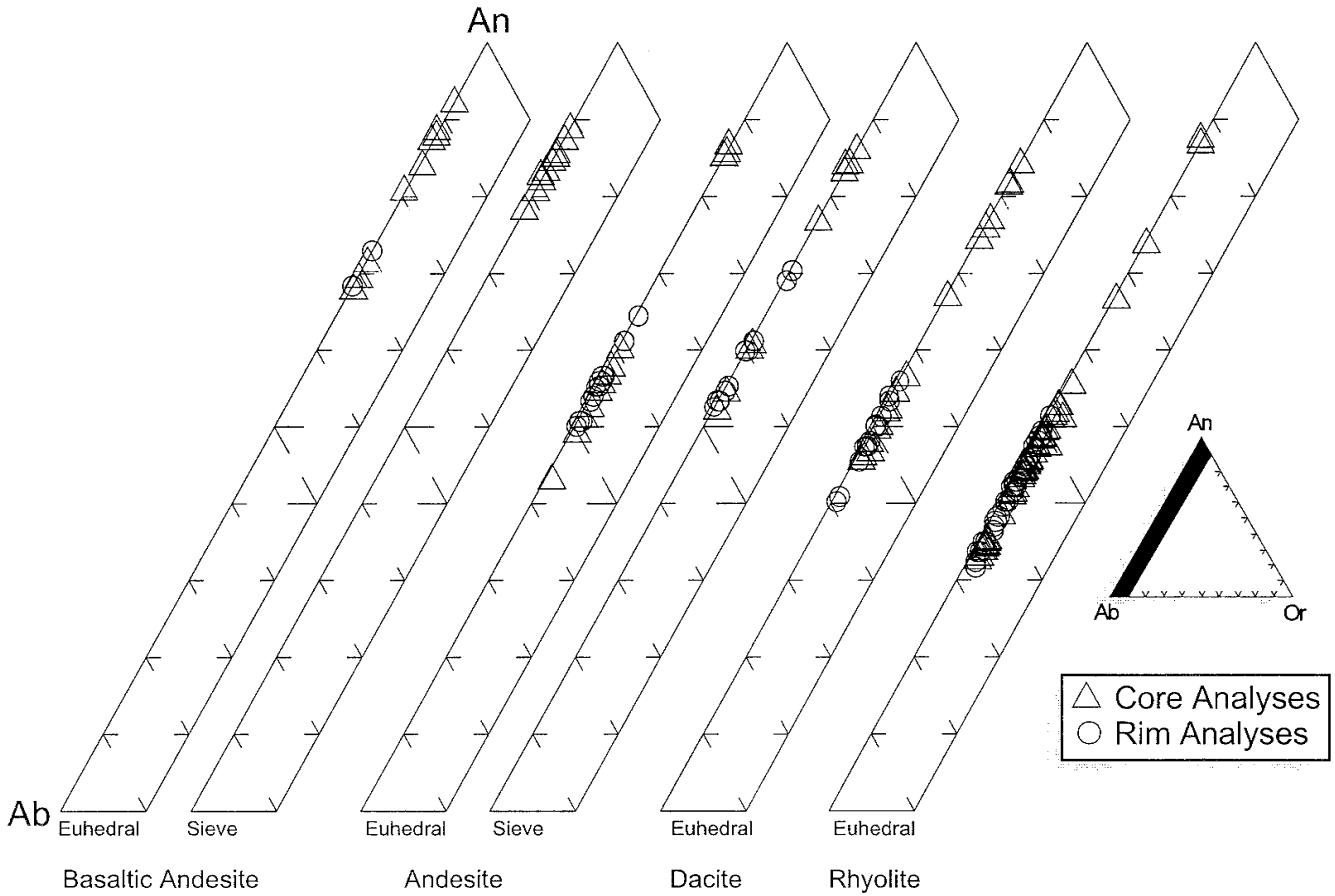

Figure 5.7a. Feldspars from homogeneous samples. Only the extreme left edge of the An-Ab-Or ternary diagram between An and Ab is presented here due to the very low Or content in Kurile Lake feldspars. Feldspar analyses from each lithology are plotted separately for clarity. Sieve textured feldspars are given their own plot to clearly show the differences between the sieve and euhedral feldspars. A complete listing of feldspar analyses is given in Appendix D.

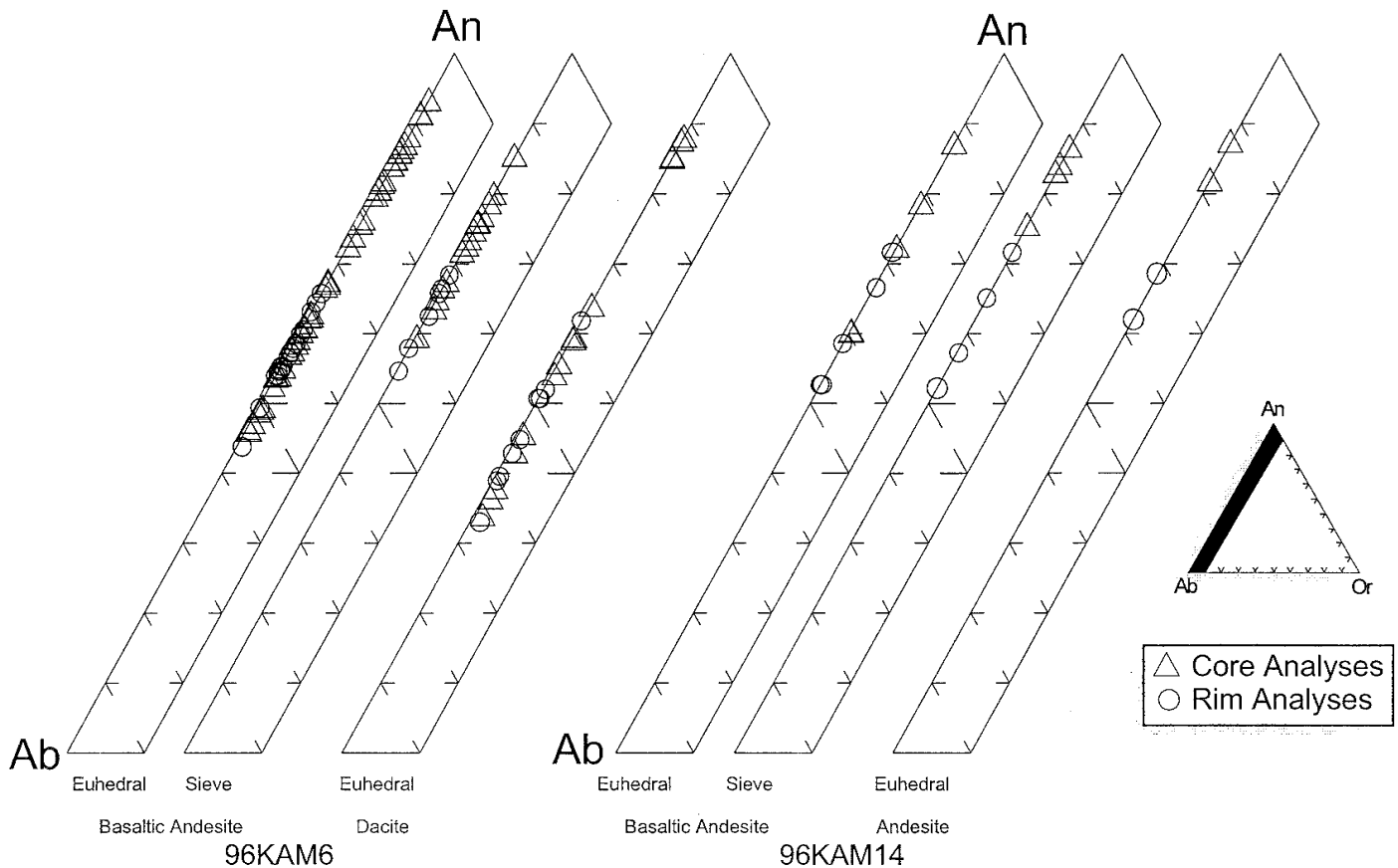

Figure 5.7b. Feldspar from mixed clasts 96KAM6 and 96KAM14. Only the extreme left edge of the An-Ab-Or ternary diagram between An and Ab is presented here due to the very low Or content in Kurile Lake feldspars. Each mixed sample is separated into discrete plots for the various lithologies contained in each sample. As with figure 5.7a, sieve textured feldspars are also given their own plot to clearly show the differences between the sieve and euhedral feldspars. Feldspar analyses are given in Appendix D.

textured cores, oscillatory zoned, and non-zoned, euhedral plagioclase phenocrysts in clasts, indicates a combination of process may have been present to produce these morphologies.

An-rich feldspar phenocryst cores have been observed in arc lavas. Several authors have described high An core feldspar phenocrysts with oscillatory zoned overgrowths from basalt to dacite at Adak volcano, Alaska (Ronnick et al., 1992); at St Martin, Lesser Antilles (Davidson et al., 1993); northern Marianas (Dixon and Bratiza, 1979); at Usu volcano, Japan (Tomiya and Takashi, 1995); and at Sequam volcano, Alaska (Singer et al., 1993) as examples. These authors explain the high-An cores are a result of rapid growth at high P_{H2O}. Other studies conducted by Nixon and Pearce (1987), Tsuchiyama (1985a) and Castellena (1998) suggest high-An cores and oscillatory zoned overgrowths represent magma mixing and recycling of plagioclase phenocrysts. Similarly, Lofgren and Norris, (1981) explain sieve textured growth to be a result of intorduction of foreign plagioclase into a basaltic liquid. But their investigation used plagioclase of a lower An content than is observed in KLE clast sieve-textured plagioclases. Loomis (1982) suggests these textures result from of rapid growth due to undercooling in equilibrium crystallization conditions.

High P_{H2O} can lower the liquidus for plagioclase (Green, 1982; Baker and Eggler, 1987) by suppressing the formation of bridging oxygen sites (Burnham, 1979). Loss of volatiles during eruption would cause fractionation of plagioclase microlites due to water-loss during eruption. An alternate explanation for the sieve-textured cores is similar to that of Bacon (1983) at Crater Lake. During the final stages of eruption of Mt. Mazama, a residual crystal-rich cumulate was erupted. It is conceivable that such a

cumulate was left behind in a cooling remnant chamber in the aftermath of previous volcanic eruptions. Many calderas experience repeated episodes of eruption and repose such as Yellowstone caldera (Christiansen, 1979), Mono-Inyo caldera (Bailey et al., 1976) and Valles caldera (Smith, 1979). Injections of new magma would serve to re-heat and recharge a cooling chamber as well as influence crystal growth. Plagioclase from cumulate leftover would seem like a restite, but would originate in the chamber itself.

No eruptions are known from this caldera before the 7.7Ka eruption, but periodic venting of volatiles during chamber formation could explain the oscillations. Mixing of magma added to the chamber seems a likely process by which convection, variance in heat, pressure and melt composition would be affected. Sieve-textured plagioclase is often used as criteria for identifying mixing in magmas (Lofgren and Norris, 1981). Banded pumice indicates mixing was occurring during eruption and may have occurred many times in the past. Fresh pulses of magma would be hotter, more water-rich and calcic than the evolving magma already present in the chamber. Zoning in feldspars consistently begins with An-rich plagioclase and gradually becomes more Ab-rich. Each pulse of magma is recorded in a new zone.

Unzoned feldspars may have formed in a region of the chamber where magma conditions were uniform over long periods of time. This may have occurred in an area separated from the more dynamic regions by a density contrast as explained by Hildreth (1981), or these phenocrysts may have formed along the walls of the chamber in a crystallizing zone.

All samples contain high-An cored feldspars. Certainly the rhyolites would not host high-An plagioclase except as xenocrysts or restitic material. Dacites also have such

plagioclases. Rhyolites and dacites, however, contain no sieve-textured plagioclases suggesting the cores were in equilibrium with the melt or were armored with plagioclase overgrowths preventing resorption. Sieve feldspars are only found in andesites and basaltic andesites suggesting crystal settling or introduction of plagioclase phenocrysts as restite in melt batches. Quench crystallization or rapid crystal growth could also be an explanation for sieve-textures. As shown below, dramatic changes would have to occur in the magma chamber the affect resorption. Rapid crystal growth can result from undercooling due to eruption or loss of pressure due to outgassing.

Sieve core plagioclase have been experimentally explained by Tsuchiyama (1985b) as the result of plagioclase composition in a melt being less An-rich than the equilibrium composition. The interface of the crystal and melt becomes rough and sieve like structures develop on the scale of a few micrometers. This behavior, called partial dissolution is similar to incongruent melting (Tsuchiyama and Takahashi 1983). As the low-temperature melting Ab content dissolves preferentially, a more An rich core remains. This core maintains its original shape providing the temperature of the melt is below the liquidus of the remaining plagioclase. Another explanation of sieve textured plagioclase is from rapid growth due to quench crystallization (Lofgren, 1981)

Most interpretations of zoning in igneous feldspars assume that chemical zones are growth zones. In KLE clasts, plagioclase zonation is considered normal zoning since An decreases outward from the center of the crystal. The zoning is also oscillatory since many zones are present. No laboratory studies have successfully produced oscillatory-zoned feldspars, so determining the origin of this texture is difficult. Several authors, undaunted, have put forward ideas on the topic.

Pressure raises the melting temperature of albite by 8°K/100MPa (Boyd and England, 1961). Plagioclase is less affected as it only experiences +2°K/100MPa up to 0.9GPa (Goldsmith, 1980). Water lowers the melting temperature of anorthite by depolymerizing the melt. The affect of water pressure is –65°K/100MPa (Yoder et al., 1957, Smith, 1984) so that the correction for the affect of pressure alone is negligible. Undercooling has been presented as another solution to explain zoning in feldspar. Growth can only be initiated and continued at a finite undercooling since the growth rate of a solid at its liquidus is zero (Smith and Brown, 1988). Undercooling is achieved in the following ways: (1) by raising pressure, (2) by lowering temperature, (3) by increasing the supersaturation by a change in melt composition, or (4) by some combination of the preceding. Isothermal compression increases the degree of supersaturation more efficiently than adiabatic compression. Supersaturation may also be chemically increased by increasing the An/(Ab + An) ratio of the melt or by removing a stabilizing component from the melt such as H_2O. According to these ideas for zoning, repeated changes in the magmatic conditions would have to take place to produce oscillatory zones in feldspars.

Magnetite and Ilmenite

Magnetite and ilmenite are found in all rock types. Microprobe analyses were recalculated and total Fe was partitioned between Fe^{3+} and Fe^{2+} assuming stoichometery (Anderson and Lindsley, 1988). Molecular proportions of ulvospinel (Usp), magnetite (Mt), hematite (Hem), ilmenite (Il) were calculated using the same method. Magnetite analyses are presented in Table 5.4, ilmenite in Table 5.5.

Table 5.4. Representative Magnetite Analyses

Sample	K4-MAG2	K4-MAG8	K3-MAG3	K3-MAG11	K18-MAG4	K18-MAG8	K32D-MAG5	K32D-MAG11
Host Lithology	basaltic andesite	basaltic andesite	andesite	andesite	dacite	dacite	dacite	rhyolite
TiO_2	9.41	11.66	9.94	10.00	8.65	8.30	8.99	10.92
Al_2O_3	3.83	2.95	2.00	1.86	2.33	1.96	1.56	2.47
Cr_2O_3	0.31	0.03	b.d.	0.06	0.09	0.11	0.05	b.d.
Fe_2O_3	46.75	43.49	48.33	48.53	48.51	49.76	50.06	46.16
FeO	34.97	37.42	36.58	36.21	38.67	38.27	37.48	38.22
MnO	0.39	0.60	0.56	0.55	0.39	0.47	0.56	0.56
MgO	2.94	2.46	1.40	1.72	n.a	n.a	0.99	1.89
CaO	b.d.	b.d.	b.d.	0.03	b.d.	0.05	b.d.	b.d.
Total	98.61	98.63	98.83	98.95	98.64	98.93	99.69	100.23
Usp	0.28	0.34	0.29	0.29	0.26	0.24	0.26	0.32

Sample	K2-MAG2	K2-MAG3	K9-MAG1	K9-MAG9	K17B-MAG1	K17B-MAG2	K32A-MAG1	K32A-MAG4
Host Lithology	rhyolite	rhyolite	rhyolite	rhyolite	rhyolite	rhyolite	rhyolite	rhyolite
TiO_2	9.14	9.11	9.21	8.31	8.05	9.42	8.70	9.12
Al_2O_3	1.60	1.59	1.99	1.69	2.20	1.60	1.60	1.75
Cr_2O_3	b.d.	b.d.	0.05	0.05	0.18	b.d.	b.d.	b.d.
Fe_2O_3	49.13	49.69	48.66	50.65	51.77	48.99	51.34	50.21
FeO	37.31	37.49	36.96	36.41	36.05	37.63	37.26	37.60
MnO	0.58	0.57	0.49	0.57	0.56	0.61	0.72	0.63
MgO	1.00	1.01	1.37	1.10	1.56	1.05	1.05	1.12
CaO	b.d.	b.d.	0.03	0.04	0.09	b.d.	b.d.	b.d.
Total	98.77	99.48	98.76	98.82	100.46	99.30	100.67	100.43
Usp	0.26	0.26	0.27	0.24	0.23	0.27	0.24	0.26

Sample	K6-MAG7	K6-MAG42	K6-MAG12	K6-MAG41	K14-MAG5	K14-MAG6	K14-MAG9	K14-MAG10
Host Lithology	basaltic andesite	basaltic andesite	dacite	dacite	basaltic andesite	basaltic andesite	andesite	andesite
TiO_2	8.48	9.05	8.98	11.18	11.14	11.24	11.01	10.10
Al_2O_3	4.61	1.61	4.18	2.78	3.04	2.94	2.75	2.88
Cr_2O_3	0.10	0.07	0.14	0.06	b.d.	0.05	0.05	0.05
Fe_2O_3	49.15	49.93	47.21	45.45	45.89	45.76	42.52	43.07
FeO	34.97	37.32	35.68	38.09	37.67	37.69	42.68	40.07
MnO	0.30	0.65	0.35	0.45	0.42	0.46	0.49	0.46
MgO	3.02	1.09	2.44	2.24	2.65	2.67	2.23	2.20
CaO	b.d.	0.09	b.d.	b.d.	0.04	0.04	b.d.	0.03
Total	100.64	99.81	98.99	100.26	100.86	100.84	101.72	98.84
Usp	0.25	0.31	0.27	0.33	0.27	0.32	0.34	0.31

A complete listing of magnetite analyses is given in Appendix D

Table 5.5. Representative Ilmenite Analyses

Sample	K4-ILM2	K4-ILM3	K3-ILM11	K3-ILM16	K18-ILM1	K18-ILM4	K32D-ILM1	K32D-ILM4
Host Lithology	basaltic andesite	basaltic andesite	andesite	andesite	dacite	dacite	dacite	dacite
TiO_2	42.87	43.38	43.17	43.79	38.37	40.02	42.91	44.45
Al_2O_3	0.37	0.39	n.a.	n.a.	0.46	0.23	0.31	0.13
Cr_2O_3	b.d.	b.d.	b.d.	b.d.	b.d.	b.d.	b.d.	b.d.
Fe_2O_3	18.96	18.31	19.44	18.18	25.83	24.39	20.94	16.19
FeO	32.20	32.60	33.26	33.90	30.18	31.54	31.83	35.61
MnO	0.57	0.72	0.59	0.67	0.66	0.52	0.61	0.94
MgO	3.46	3.31	2.79	2.70	2.20	2.29	3.57	1.97
CaO	0.12	0.13	b.d.	b.d.	0.86	0.31	b.d.	0.06
Total	98.55	98.84	99.29	99.25	98.55	99.31	100.18	99.37
Ilm	0.79	0.80	0.79	0.81	0.72	0.74	0.77	0.83

Sample	K2-ILM2	K2-ILM3	K9-ILM7	K9-ILM5	K17B-ILM5	K17B-ILM6	K32A-ILM3	K32A-ILM4
Host Lithology	rhyolite	rhyolite	rhyolite	rhyolite	rhyolite	rhyolite	rhyolite	rhyolite
TiO_2	44.51	44.70	42.81	44.83	44.94	45.03	45.25	45.02
Al_2O_3	0.14	0.15	0.26	0.16	0.14	0.16	0.14	0.32
Cr_2O_3	b.d.	b.d.	b.d.	b.d.	b.d.	b.d.	b.d.	b.d.
Fe_2O_3	15.98	15.43	19.71	14.71	15.86	15.00	16.12	16.23
FeO	35.54	35.78	33.14	36.30	35.83	36.06	35.96	35.88
MnO	0.91	0.98	0.73	0.96	1.01	0.99	1.01	0.97
MgO	2.06	1.99	2.70	1.77	2.05	1.99	2.14	2.16
CaO	b.d.	0.06	0.04	0.03	b.d.	0.11	0.04	b.d.
Total	99.19	99.13	99.42	98.78	99.84	99.34	100.67	100.61
Ilm	0.83	0.84	0.79	0.85	0.83	0.84	0.77	0.83

Sample	K6-ILM20	K6-ILM9	K6-ILM16	K6-ILM11	K14-ILM9	K14-ILM10	K14-ILM3	K14-ILM14
Host Lithology	basaltic andesite	basaltic andesite	dacite	dacite	basaltic andesite	basaltic andesite	andesite	andesite
TiO_2	42.53	43.28	41.85	43.29	41.47	41.63	43.32	43.03
Al_2O_3	0.37	0.29	0.39	n.a.	0.29	0.35	0.37	0.36
Cr_2O_3	b.d.	b.d.	0.08	b.d.	b.d.	b.d.	b.d.	b.d.
Fe_2O_3	22.23	18.21	21.82	18.70	23.06	21.82	20.67	19.23
FeO	31.77	32.50	31.55	33.46	31.93	30.67	32.26	31.96
MnO	0.53	0.82	0.48	0.71	0.53	0.52	0.54	0.48
MgO	3.48	3.31	3.31	2.66	2.83	3.65	3.60	3.65
CaO	0.09	0.14	0.10	b.d.	0.14	b.d.	0.05	0.03
Total	101.00	98.55	99.59	55.54	100.25	57.00	100.81	98.73
Ilm	0.76	0.80	0.76	0.80	0.75	0.76	0.77	0.78

A complete listing of ilmenite analyses is given in Appendix D
b.d. below detection limits
n.a. not analyzed

Magnetite is commonly subhedral, and rarely euhedral. Ilmenite has similar morphology to magnetite but is less common. Some samples provided co-existing magnetite and ilmenite phenocrysts but more commonly magnetite was a separate phase from ilmenite. Magnetites range in size from 50 to 1μm. Ilmenite is usually smaller, 20-1μm. Some magnetite occurs as symplectic intergrowths in pyroxene.

The Ti content of magnetite shows little variation for TiO_2 (Figure 5.8). FeO, Al_2O_3, Cr_2O_3, and MgO increase with increased magmatic evolution. Fe_2O_3 decreases by ~10wt.% over ~5wt.% TiO_2. MnO is uniform throughout the range of TiO_2. CaO shows no relation with magma composition. Ilmenite composition varies for most elements except Cr_2O_3 and CaO (Figure 5.8). MnO and FeO increase with increased differentiation while Fe_2O_3 Al_2O_3 and MgO decrease with increasing TiO_2. In basaltic andesites, magnetite and ilmenite are Usp_{32-33} and Ilm_{80} respectively; from Usp_{32-29} and Ilm_{80-75} in andesites; Usp_{30-26} and Ilm_{23-17} in dacites; and from Usp_{85-81} and Ilm_{27-23} in rhyolites.

Amphibole

Cummingtonite amphibole occurs in rhyolite pumices from the KLp deposits (Table 5.6 and Fig 5.9). It occurs as brownish-green, large 100-20μm, unzoned, euhedral phenocrysts. Classification as cummingtonite is based on low Ca, Na and K contents (Deer et al., 1992). Cummingtonite-bearing rhyolites contain enstatite, but not augite, which occurs in all other rock types. Amphibole analyses were recalculated using MinPet2.02, which employs the method of Richard and Clarke (1990). This method recalculates mineral formula from the weight percent oxides based on an anhydrous basis

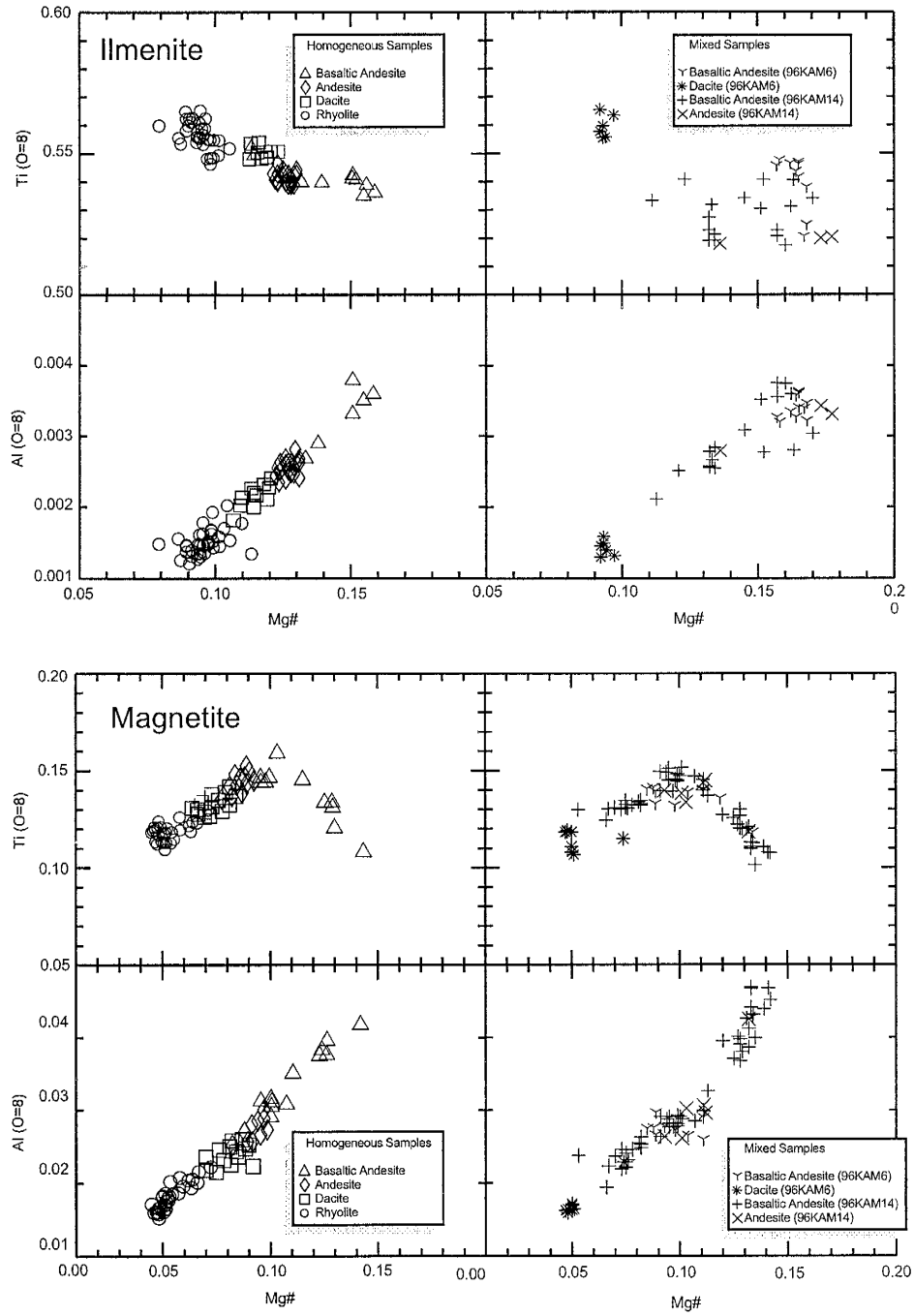

Figure 5.8. Ti and Al (atoms per formula unit (O=8)) vs Mg# [Mg/Mg+Fe^{2+}+Mn)] in ilmenite and magnetite from homogeneous and mixed clasts. Analyses from homogeneous samples are plotted separately from mixed samples for clarity. Ilmenite and magnetite analyses are given in Appendix D.

Table 5.6. Representative Amphibole Analyses

	K2-AMP2	K2-AMP8	K2-AMP7	K17B-AMP5	K17B-AMP1	K17B-AMP-4	K32A-AMP2	K32A-AMP3	K32A-AMP6	K32A-AMP5
SiO_2	48.12	47.64	46.27	48.98	47.10	46.23	48.04	47.61	46.26	45.37
TiO_2	1.44	1.55	1.84	1.34	1.73	1.77	1.46	1.66	1.71	1.74
Al_2O_3	6.37	6.42	7.83	5.52	6.84	7.23	6.19	6.86	6.84	7.18
FeO	14.24	14.85	14.84	14.30	14.28	14.61	14.33	14.41	14.45	14.62
MnO	0.51	0.48	0.45	0.53	0.49	0.45	0.46	0.50	0.48	0.49
MgO	14.82	14.22	13.90	15.01	14.59	14.04	14.07	14.53	14.40	14.16
CaO	10.80	10.88	10.97	10.92	10.96	11.06	11.10	11.10	11.19	11.14
Na_2O	1.50	1.52	1.81	1.47	1.87	1.75	1.53	1.68	1.65	1.88
K_2O	0.19	0.19	0.24	0.19	0.19	0.24	0.18	0.19	0.22	0.17
H_2O*	1.93	1.88	1.89	1.90	1.87	1.87	1.90	1.94	1.85	1.84
F	0.25	0.33	0.31	0.33	0.36	0.31	0.29	0.24	0.37	0.35
Total	100.18	99.96	100.35	100.48	100.28	99.55	99.54	100.73	99.39	98.93
T Al	1.328	1.267	1.529	1.073	1.357	1.427	1.200	1.292	1.382	1.456
TFe	1.876	2.081	2.058	1.976	2.014	2.048	1.972	1.928	2.073	2.106
TMn	0.068	0.069	0.064	0.074	0.070	0.064	0.065	0.068	0.070	0.072
TMg	3.541	3.553	3.437	3.695	3.669	3.507	3.452	3.463	3.684	3.638
TCa	1.904	1.955	1.949	1.932	1.980	1.985	1.957	1.902	2.058	2.056
Pressure calculations(kbar)										
Johnson	2.16	1.90	3.01	1.08	2.28	2.58	1.62	2.01	2.39	2.70
Hammarstrom	2.76	2.45	3.77	1.48	2.91	3.26	2.12	2.58	3.03	3.40
Hollister	2.73	2.39	3.86	1.29	2.89	3.29	2.01	2.53	3.03	3.45

A complete listing of amphibole analyses is given in Appendix D.

* H_2O reported is theoretical and based from the amphibole structural formula.

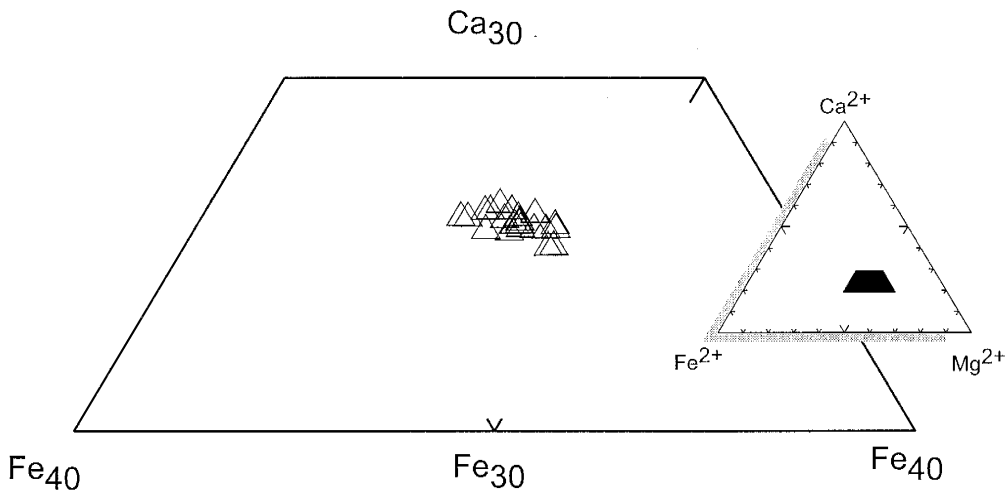

Figure 5.9. Ternary plot of Ca, Fe and Mg (based on O=23) for amphiboles in rhyolite clasts. Amphibole plots within a small range similar to augite in Figure 5.1. Amphibole analyses are given in Appendix D.

and 23 oxygens. All iron was set to Fe^{2+} and recalculated using 23 oxygens. Cations are assigned to each site according to IMA guidelines (Robinson et al., 1981).

Amphibole shows little variation in composition. Silica varies slightly from 49 to 46.3wt.%. As SiO_2 increases, TiO_2, Al_2O_3, FeO and Na_2O decrease, MgO and H_2O (from stoichometery) both increase and CaO, MnO and F content have no correlation. Figure 5.9 is a ternary plot of total Ca, Fe and Mg. All hornblende analyses plot in the same position with a slight linear trend.

The presence of amphibole in the earliest eruptive products suggests higher P_{H2O} in the magma chamber where the eruption originated than in other regions of the chamber. High P_{H2O} in this part of the magma chamber may have influenced growth of amphibole instead of augite, which was in equilibrium at lower P_{H2O}.

Apatite

Apatite is found in all samples, and is commonly associated with pyroxenes and Fe-Ti oxides. Apatite is euhedral to anhedral and occurs as a phenocryst and microphenocryst phase. Representative apatite analyses are reported in Table 5.7. F is relatively high in apatite, averaging at 2.6wt%. Other constituents are relatively constant.

Intensive Variables

Temperature and fO_2

Magnetite and ilmenite pairs and co-existing augite and enstatite, when available, were used to determine temperature and fO_2 of the magma at the time of eruption using

Table 5.7. Representative Apatite Analyses

	K4-APT1	K3-APT2	K3-APT3	K12L-APT6	K12L-APT1	K9-APT4
Lithology	basaltic andesite	andesite	andesite	andesite	andesite	rhyolite
FeO	1.64	0.58	0.72	0.36	0.36	0.29
MnO	b.d.	0.12	0.17	b.d.	b.d.	0.13
CaO	53.82	54.34	54.30	54.51	54.44	53.55
P_2O_5	41.79	42.31	41.96	41.40	42.59	43.04
F	2.29	2.42	2.81	2.47	0.66	3.30
Cl	0.52	0.72	0.71	0.50	0.51	0.58
Total	100.61	100.94	100.92	99.70	99.90	100.88

	K9-APT8	K32A-APT1	K6-APT2	K6-APT4	K14-APT1	K14-APT2
Lithology	rhyolite	rhyolite	mixed bas. and.	mixed dacite	mixed andesite	mixed bas. and.
FeO	0.80	0.53	0.62	1.10	0.44	0.71
MnO	b.d.	b.d.	0.17	0.19	b.d.	b.d.
CaO	53.69	54.37	53.53	52.86	54.40	53.86
P_2O_5	41.41	41.77	42.35	42.47	42.21	42.45
F	2.29	3.05	3.55	1.85	2.22	2.59
Cl	0.86	0.96	0.75	0.72	0.50	0.55
Total	99.50	100.75	100.97	98.75	100.37	100.57

A complete listing of apatite analyses is given in Appendix D

the QUILF program of Anderson and Lindsley, (1988). Temperature and fO_2 are plotted in Figure 5.10.

The temperatures range from 870° to 770°C and log fO_2 ranges from –11.5 to –13.2 and show a progression toward lower T and fO_2 with increasing SiO_2 content. In general, rhyolites tend to clump at the cooler end of this spectrum from 780-820°C, fO_2 of –13.3 to –12.4. Dacite temperature (810°-840°C) and log fO_2 (-12.5 to -12.0) overlap the rhyolite range as well as the basaltic andesite range (820°-870°C, log fO_2 of –12.1 to –11.5). Andesite temperatures (830°-850°C) and log fO_2 (-12.1 to – 11.7) are within the temperature range of basaltic andesite.

Pressure

The amphibole geobarometer of Johnson and Rutherford (1989) was used to determine the pressure of crystallization of hornblende. This geobarometer uses the total Al of hornblende to determine the pressure by the equation:

$$P\ (\pm 0.5\ kbar) = 3 - 3.46(\pm 0.24) + 4.23(\pm 0.13)(Al^t)$$

where P is pressure in kbar, and Al^t is total Al from the Al^{IV} and Al^{VI} sites in the amphibole structural formula. Alternative geobarometers of Hammarstrom and Zen (1986) and Hollister et al., (1987) are presented for comparison to that of Johnson and Rutherford (1989). The geobarometer of Hammarstrom and Zen (1986) uses the following equation:

$$P\ (\pm 3kbar) = -3.92 + 5.03(Al^t)$$

The geobarometer of Hollister et al., (1987) uses the following equation:

$$P\ (\pm 1kbar) = -4.76 + 5.64(Al^t)$$

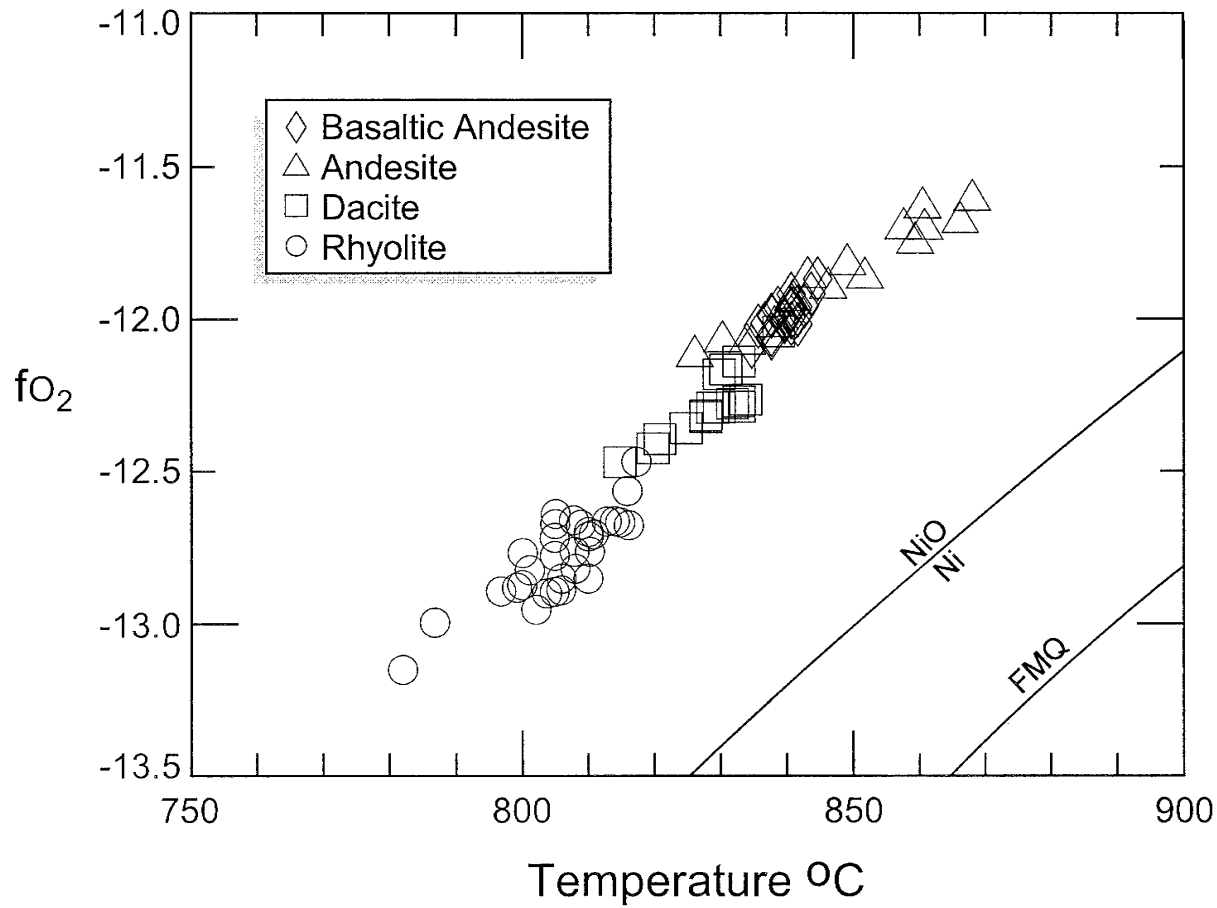

Figure 5.10. Temperature and fO_2. Temperatures and fO_2 are calculated by the method of Anderson et al. (1988) from co-existing magnetite and ilmenite phenocrysts. Buffer trends are from Lindsley (1991) and references therein.

The results of these geobarometers can be found in Appendix D and in Figure 5.11.

An average of 2.22kbar with a standard deviation of 0.43 is calculated by the method of Johnson and Rutherford (1989). The equation of Hammarstrom and Zen (1986) calculates 2.84kbar with a standard deviation of 0.53. Pressure of 2.82kbar with a standard deviation of 0.6 is calculated using the geobarometer of Hollister (1987). Pressures calculated by these methods are in general agreement within the error stated in each equation.

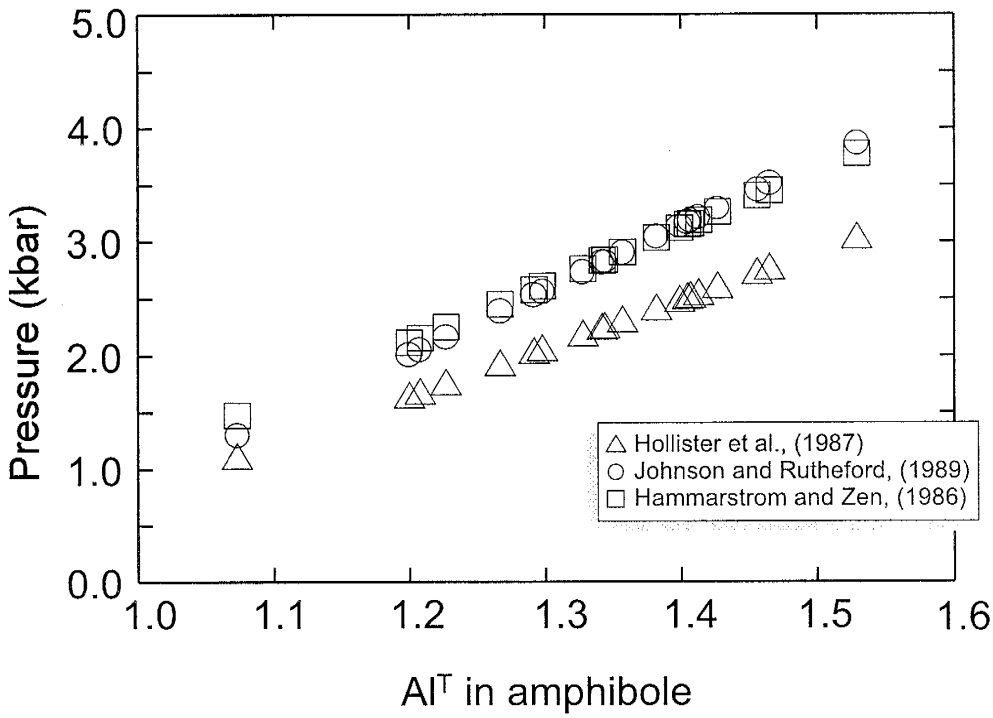

Figure 5.11. Pressure vs. Al^T in amphibole. Pressures calculated using the method of Hollister et al. (1987), Johnson and Rutheford (1989) and Hammarstrom and Zen (1986). Total aluminum determined from microprobe analyses. Average pressure calculated with these methods is 2.22-2.84kbar. Pressure calculations are given in Appendix D.

CHAPTER SIX

DISCUSSION

Introduction

Strong compositional contrasts in individual clasts are common in the ignimbrite cropping out to the east and north of Kurile Lake. In some clasts, basaltic andesite scoria is in contact with dacitic or rhyolitic pumice bands. Determining whether mixing or comingling of magma types during or just before eruption is a key problem in describing this eruption. Another issue is determining if magma was mixing or comingling within the chamber from a single, fractionated parent, or magma from separate chambers, sources, or processes was interacting to produce these banded clasts and the wide range in compositions present in the KLE deposit.

Geochemical Characteristics

The KLE exhibits a wide compositional range of erupted magma types, ranging from basaltic andesite to rhyolite. Strong correlations are observed between SiO_2 and many major and trace elements, suggesting that most of the magma types observed are genetically related. Dacites show a wider scatter and seem to plot off the main trend, which may indicate this lithology may not be genetically related to the other KLE lithologies. Correlations between SiO_2 and Al_2O_3, Na_2O, P_2O_5, Sr and Eu change from positive correlations within rock types with less than ~60% SiO_2 to negative correlations in more differentiated rocks. These trends could suggest fractionation of plagioclase and

apatite indicating the magmatic evolution is at least partialy controlled by fractional crystallization. However, the role of magma mixing must be considered as a possible mechanism of magmatic differentiation. One possible means for distinguishing between these two processes is that differentiation trends produced by fractional crystallization are typically curved, whereas those produced by magma mixing are linear (Rollinson, 1993).

Trace elements mimic the curvilinear trends displayed by some major element trends. As for some major elements, straight lines can be fit to the rock series from basaltic andesite to andesite, suggesting mixing may have been responsible for the petrogenesis of these lithologies. Notably Sr and Eu show similar trend reversals near 60% SiO_2 like Al_2O_3 and Na_2O, indicating plagioclase fractionation begins near 60% SiO_2. Furthermore, the switch from positive Eu anomalies in basaltic andesites and andesites to negative anomalies in dacites and rhyolites suggests plagioclase fractionation from dacitic and rhyolitic host magma. Basaltic andesite and andesite Eu anomalies may reflect an inherited, source signature instead of indicating plagioclase resorption in these compositions. Indeed, sieve textured plagioclase are probably the result of quench crystallization instead of resorption.

Rhyolite and dacite magmas may have formed separately from andesite and basaltic andesite. The spread in dacite compositions in the Na_2O and Eu trend (Fig. 4.3, 4.4b and 4.6) may indicate dacite magma formed separately from the main suite of KLE magma. Close examination of the Na_2O plot (Fig. 4.6) shows glass compositions plotting up to 1.5wt.% over the whole rock trend. In the other plots, the spread in glass analyses can be easily attributed to analytical error, but not with Na_2O. Indeed, due to the method of analyses, these values should be treated as minimums due to sodium loss during

analyses. It can be argued that the basaltic andesite and andesites are fractionated up to ~60wt% SiO_2. After this interval, the whole rock trend increases in SiO_2, but Na_2O remains constant. This may be due to increased fractionation of more albitic plagioclase, or possibly mixing between andesite and rhyolite. The glass evolved from basaltic andesite, if it were a true liquid line of descent would be parental material for andesite and dacite. If this were the case, dacite compositions would be higher in Na_2O than they are. Since they are not, this indicates dacites form by mixture of a rhyolite melt and the residual liquid from basaltic andesite and andesite formation. This may account for the small compositional gaps in the whole rock trend, as well as the separation of rhyolites from the main trend in REE/SiO_2 variation diagrams. This begs the question of the source of rhyolite.

Rhyolite may be formed by partial melting of country rock. In a large, long-lived magmatic system it would be unlikely that no country rock would be partially melted. This partial melt would be rhyolitic or dacitic in composition. If rhyolite was a partial melt of pre-existing country rock, there should be some difference in mineralogy and radiogenic isotopes. There is amphibole substituting clinopyroxene in some rhyolites, but there is no real variance in isotope values as will be shown in the next section. So the source of rhyolite is somewhat enigmatic, leaving the process of dacite formation in question.

Analyses of pumiceous samples presents a problem. Due to the highly expanded nature of pumice, there is a large volume but a very small sample mass. Even though most samples were prepared from large, single clasts, some samples are a combination of 2 or more small clasts. It is also possible that the analses of a sample may be skewed due

to the addition or loss of a phenocryst since the ratio of glass to phenocrysts can be high. Addition of a large pyroxene phenocryst to an ash or small lapilli sized pumice may cause the analysis of the sample to appear more mafic, for example, than a larger pumice block with the addition of an extra phenocryst.

As mentioned before, the whole-rock trend for Na_2O does not follow a possible liquid line of descent. An alternate explanation for this phenomena only occurring in Na_2O and not the other major element plots may be the result of fractionation of plagioclase. As the initial parental melt fractionates, calcic plagioclase and pyroxene are fractionated producing a residual melt high in Na. Subsequent melt compositions are derived from this residual liquid and should be high in Na, but are not. This may be the result of inherited, low Na plagioclase or pyroxenes. The parental liquid would form higher Ab plagioclase, but the low Na plagioclase are still present in the whole-rock, making the whole rock seem lower in Na than the parental melt. As fractionation progresses, more Na is removed from the residual liquid to form plagioclase, since there is less Ca to fractionate into plagioclase and pyroxene fractionation is still occurring. This causes the total Na content to decrease in the whole rock as well as the residual liquid. So, the glass does reflect a liquid line of descent, but the whole rock trend is pulled down due to inherited phenocrysts.

Radiogenic Isotopes

Preliminary radiogenic isotope determinations have been undertaken by Chang-Hwa Chen (personal communication to P. R. Kyle, 1999) on three KLE samples. In all, a rhyolite, andesite, basaltic andesite from the KLE, and one dacite sample from a post-

caldera extrusive dome was analyzed. $^{87}Sr/^{86}Sr$ and $^{143}Nd/^{144}Nd$ values, presented in Table 6.1 show little variation from basaltic andesite to andesite.

Relative to p-MORB, $^{87}Sr/^{86}Sr$ values are slightly more radiogenic, while $^{143}Nd/^{144}Nd$ are identical (Table 6.1). These show assimilation of older rocks may have occurred during petrogenesis, but the low values show the magma was generated from a homogeneous depleted mantle source.

Table 6.1. Preliminary $^{87}Sr/^{86}Sr$ and $^{143}Nd/^{144}Nd$ determinations for Kurile Lake, Illinsky and Dikii Greben

Sample	Description	SiO_2 wt%	$^{87}Sr/^{86}Sr$*	$^{143}Nd/^{144}Nd$*	εNd
1351-1	Pumice from fall	72.50	0.703257±16	0.513108±14	9.07
1316a/2	Scoria from ignimbrite	53.27	0.703295±13	0.513100±20	8.91
1370-1	Scoria from ignimbrite	57.51	0.703292±15	0.513145±16	9.79
86680	Heart of Alaid, post-caldera extrusive dome	64.65	0.703180±14	0.513116±19	9.23
p-MORB (Rollinson, 1983)			0.70240-0.70256	0.5130-0.5133	

Data from Chen (personal communication to P.R. Kyle, 1999).
Samples are from Ponomareva (unpubl. data).
*Normalized to $^{86}Sr/^{88}Sr=0.1194$; reproducibility (2σ)=±0.00002; NBS987 $^{87}Sr/^{86}Sr=0.710226$
*Normalized to $^{146}Nd/^{144}Nd=0.7219$; $\varepsilon Nd=[(^{143}Nd/^{144}Nd)/0.51264-1] \times 10^4$;
reproducibility (2σ)=±0.3 εNd; UCSD $^{143}Nd/^{144}Nd=0.511845$

KLE rocks have similar Sr and Nd values to Illinsky and Dikii Greben (Fig 6.1). Very little deviation from the mantle array towards sedimentary values is evident.

KLE isotopic composition is similar to that from other island arcs like the Marianas and Rabaul. Crater Lake, Taupo and Pinatubo have significant continental crust influence as do some Kamchatkan arc volcanoes. As such, the KLE is more ocean island arc-like than continental arc in character.

The Sr and Nd isotopic systems appear to be decoupled. Radiogenic isotope values ($^{87}Sr/^{86}Sr$= 0.703180-0703295±16; $^{143}Nd/^{144}Nd$=0.513100-0.513145±20) indicate

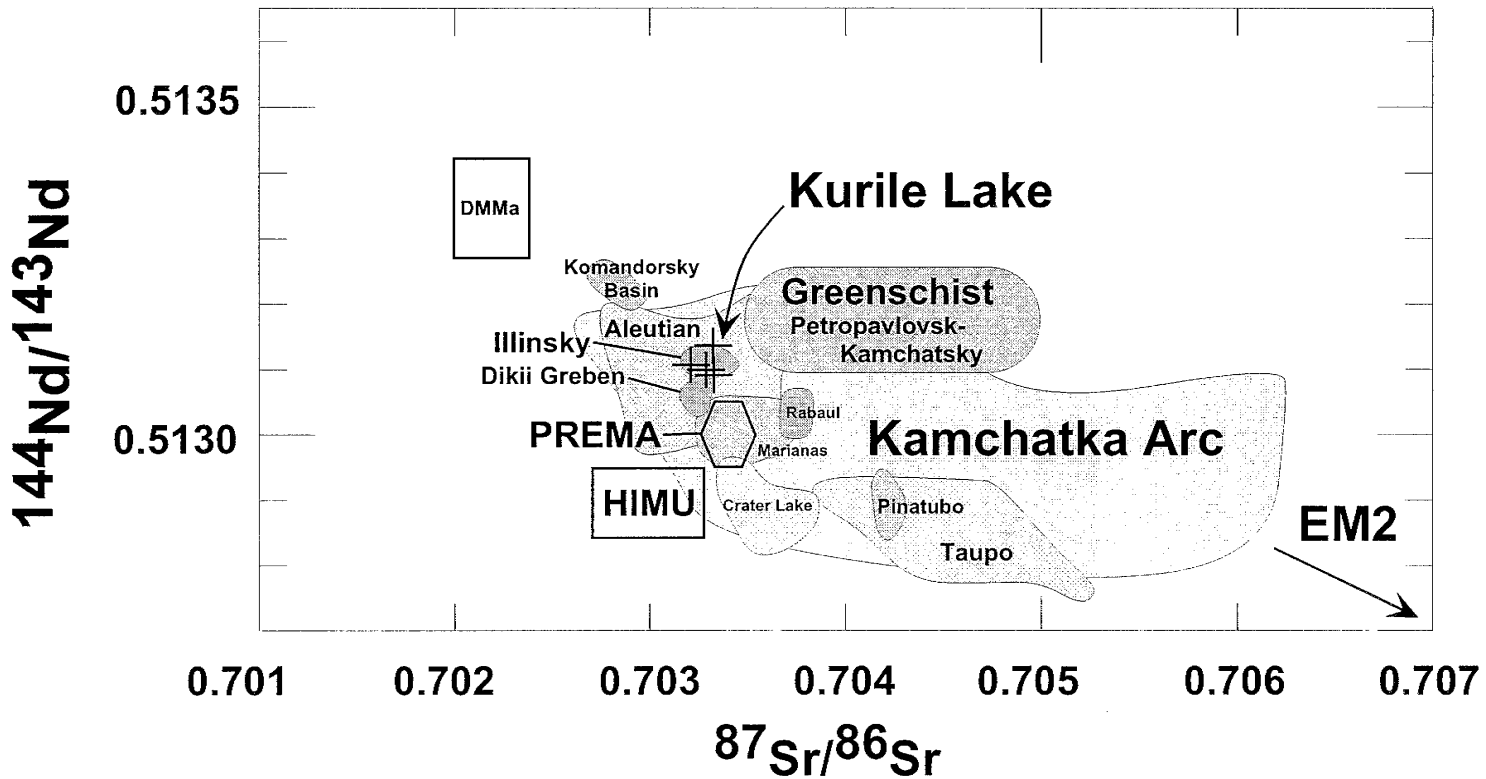

Figure 6.1. Kurile Lake eruption clasts are plotted with other arc volcanoes Sr and Nd for comparison. Illinsky and Dikii Greben volcanoes have similar ranges as Kurile Lake and show little influence of evolved component. Kurile Lake, Illinsky and Dikii greben values are from Chen, (personal communication to P.R. Kyle 1999), Greenschist values are from Castellena (1998). Kamchatka Arc and Kommandorsky basin data: Kepezhinskas et al. (1997), Kersting and Arculus (1995) and Tatsumi et al. (1995). Taupo: Gamble et al. (1993), Pinatubo: Bernard et al. (1995), Aleutians: Kay et al. (1986), Crater Lake: Bacon et al. (1994), Marianas and Rabaul: Rollinson (1993).

KLE magma was derived from a depleted mantle source (p-MORB: $^{87}Sr/^{86}Sr$=0.70240-0.70256; $^{143}Nd/^{144}Nd$=0.5130-0.5133) (Rollinson, 1993) and experienced minor crustal contamination during ascent and storage. Nd isotope values overlap with Pacific MORB Nd isotope values, but Sr is shifted to slightly more radiogenic values. The small variation in Sr and Nd isotopic compositions is similar to values found at Klyuchevskoy volcano in northern Kamchatka by Kersting and Arculus (1995), who interpreted these values to reflect tapping of an isotopically homogeneous reservoir. These data show the KLE magma was derived from slightly modified primary melts generated above the subducting slab, most likely by melting of the fluid-fluxed mantle wedge.

Fractionation sequence

Quantitative crystal fractionation models to explain the evolution of KLE pumices were made by least-squares mass balance methods using major elements. Calculations were carried out using the least-squares mass-balance method of Bryan et al. (1969). This method back-calculates parental compositions by adding minerals to the daughter using a least-squares method. Calculated totals are compared to observed compositions to determine the success of the model. Microprobe analyses of phenocrysts from the samples were used in model calculations. Geologically and mineralogically reasonable models with sums of squares differences of <0.05 were accepted. Only the three best models are shown. Phenocryst proportions as well as the weight fraction of the daughter composition are reported. Trace element partition coefficients (Table 6.2) of Carr et al. (1990) were used to determine the fit of predicted trace elements to observed values. The

Table 6.2. Partition coefficents used in calculating least-squares mass-balance models.

	Plagioclase	Clinopyroxene	Orthopyroxene	Magnetite	Ilmenite
Sc	0	3	3	2	2
V	0	1.1	1.1	20	30
Ni	0.01	3.5	8	5	10
Cu	0	0	0	2	2
Rb	0.07	0.03	0.02	0	0.01
Sr	1.8	0.12	0.02	0	0.01
Y	0.05	0.33	0.025	0.003	0.001
Zr	0.01	0.2	0.08	0.2	0.4
Ba	0.16 (15.63*)	0.02	0.02	0	0.01
La	0.2	0.1	0.003	0.003	0.001
Ce	0.18	0.15	0.006	0.003	0.001
Nd	0.14	0.2	0.01	0.003	0.001
Sm	0.11	0.25	0.012	0.003	0.001
Eu	0.1	0.27	0.015	0.003	0.001
Yb	0.03	0.35	0.05	0.003	0.001

from Carr, M.J., Feigenson, M.D., and Bennett, E.A., (1990)

* from Mahood, G., and Hildreth, W. 1983, used in dacite to rhyolite model

plagioclase Ba partition coefficient of Mahood and Hildreth (1983) was used for the dacite to rhyolite step.

Fractionation was modeled in three steps from basaltic andesite (97KAM29DB) to andesite (96KAM3); andesite to dacite (96KAM18); and finally dacite to rhyolite (97KAM17A) (Table 6.3). A single step fractionation from basaltic andesite (97KAM29DB) to rhyolite (97KAM17A) was also modeled. In all fractionation models, orthopyroxene, clinopyroxene, magnetite, ilmenite and plagioclase were used. Apatite was used in models from andesite to rhyolite. Amphibole was not used in the modeling due to its rarity at Kurile Lake and its absence from all but fall rhyolite. Weight fractions of daughter material and mineral phases can be found in Table 6.3. Evolution of andesite from basaltic andesite gave three acceptable solutions (Table 6.3a). The main phenocryst phases present in KLE clasts were fractionated in these models. Phenocryst analyses from basaltic andesite were used in model calculations preferentially over those from other lithologies due to model results. Model 1 has predicted trace element concentrations most similar to those observed in basaltic andesite (96KAM29DB) with the exception of V and Sc and Y. This may be due to uncertainties in partition coefficients for these elements. Predicted trace element concentrations in models 2 and 3 are less similar, suggesting these models are less likely

The three models presented in Table 6.3b for the andesite to dacite step are almost identical. Predicted V and Sr are significantly lower than the observed values suggesting problems with the partition coefficients for these elements. The dacite to rhyolite step (Table 6.3c) also has three practically identical models. Ba, Sr, V and Zr predicted

Table 6.3a. Least-squares mass-balance models for derivation of andesite (96KAM3) from basaltic andesite (97KAM29DB)

	Observed basaltic andesite	Estimated basaltic andesite 1		2		3
SiO_2	53.12	53.08		53.03		53.01
TiO_2	0.86	0.86		0.86		0.86
Al_2O_3	18.4	18.42		18.42		18.43
FeO*	9.05	9.05		9.05		9.05
MnO	0.18	0.26		0.26		0.27
MgO	5.13	5.15		5.17		5.17
CaO	10.1	10.11		10.11		10.12
Na_2O	2.58	2.65		2.73		2.75
K_2O	0.46	0.42		0.37		0.38
P_2O_5	0.11	0.11		0.1		0.1
Wt. Fraction andesite		0.54		0.484		0.491
Clinopyroxene	Wo_{43}-En_{41}-Fs_{16}	0.107	Wo_{43}-En_{42}-Fs_{15}	0.115	Wo_{43}-En_{41}-Fs_{16}	0.121
Orthopyroxene	Wo_2-En_{62}-Fs_{36}	0.122	Wo_2-En_{62}-Fs_{36}	0.114	Wo_2-En_{63}-Fs_{35}	0.109
Magnetite	$Usp_{0.23}$	0.033	$Usp_{0.23}$	0.034	$Usp_{0.23}$	0.035
Ilmneite	$Ilm_{0.72}$	0.003	$Ilm_{0.72}$	0.004	$Ilm_{0.72}$	0.003
Feldspar	An_7-Ab_{93}-Or_0	0.198	An_{18}-Ab_{83}-Or_0	0.25	An_{18}-Ab_{83}-Or_0	0.242
Sum		1.003		1.001		1.001
Sum R^2*		0.012		0.041		0.05

Trace element abundances (ppm) in basaltic andesite

	Observed			Calculated
Rb	7	7	6	6
Ba	140	137	124	126
Sr	307	351	368	365
V	333	162	171	169
Ni	12	12	12	12
Zr	50	43	38	39
Sc	39	24	23	23
La	3.5	3.5	3.2	3.2
Ce	8.6	8.3	7.6	7.7
Nd	5.6	4.2	3.8	3.9
Sm	2.0	1.6	1.4	1.4
Eu	0.7	0.7	0.6	0.6
Yb	1.8	1.1	1.0	1.0
Y	18.4	11.9	10.8	10.9

*R^2 is the square of the residuals.

Table 6.3b. Least-squares mass-balance models for derivation of dacite (96KAM18) from andesite (96KAM3)

	Observed andesite	Estimated andesite 1		2		3
SiO_2	60.32	60.3		60.3		60.3
TiO_2	0.71	0.72		0.72		0.72
Al_2O_3	19.96	20.07		20.08		20.08
FeO*	4.71	4.71		4.71		4.71
MnO	0.13	0.13		0.11		0.1
MgO	1.73	1.74		1.74		1.74
CaO	6.93	6.93		6.93		6.93
Na_2O	4.53	4.43		4.43		4.42
K_2O	0.76	0.91		0.91		0.91
P_2O_5	0.2	0.2		0.2		0.2
Wt. Fraction dacite		0.578		0.58		0.584
Clinopyroxene		0.019	Wo_{43}-En_{42}-Fs_{15}	0.018	Wo_{43}-En_{41}-Fs_{16}	0.018
Orthopyroxene		0.021	Wo_2-En_{63}-Fs_{35}	0.021	Wo_5-En_{64}-Fs_{31}	0.02
Magnetite		0.018	$Usp_{0.34}$	0.015	$Usp_{0.23}$	0.016
Ilmneite		0.004	$Ilm_{0.78}$	0.007	$Ilm_{0.72}$	0.006
Feldspar		0.359	An_{55}-Ab_{44}-Or_1	0.357	An_{55}-Ab_{44}-Or_1	0.353
Apatite		0.003	K9-APT2	0.003	K9-APT4	0.003	K3-APT10	0.003
Sum		1.002		1.001		1
Sum R^2*		0.035		0.037		0.041

Trace element abundances (ppm) in andesite

	Observed			Calculated
Rb	12	16	16	16
Ba	241	253	254	256
Sr	395	356	355	353
V	80	61	64	65
Ni	3	5	5	5
Zr	74	77	77	78
Sc	16	10	10	10
Cu	12.6	17.0	17.1	17.2
La	6.0	5.5	5.5	5.6
Ce	14.3	12.9	13.0	13.0
Nd	7.2	5.8	5.8	5.8
Sm	2.8	1.8	1.8	1.8
Eu	1.1	0.5	0.5	0.5
Yb	2.0	1.5	1.5	1.5
Y	20.6	14.1	14.2	14.3

*R^2 is the square of the residuals.

Table 6.3c. Least-squares mass-balance models for derivation of rhyolite (97KAM17A) from dacite (96KAM18)

	Observed dacite		Estimated dacite 1		2		3
SiO_2	66.72		66.7		66.7		66.7
TiO_2	0.54		0.53		0.53		0.53
Al_2O_3	16.72		16.63		16.62		16.62
FeO*	4.06		4.06		4.06		4.06
MnO	0.11		0.1		0.12		0.13
MgO	1.62		1.62		1.62		1.62
CaO	4.58		4.58		4.58		4.58
Na_2O	4.06		4.23		4.23		4.24
K_2O	1.49		1.38		1.37		1.37
P_2O_5	0.11		0.11		0.11		0.11
Wt. Fraction rhyolite			0.77		0.767		0.765
Clinopyroxene		Wo_{43}-En_{41}-Fs_{16}	0.034	Wo_{43}-En_{41}-Fs_{16}	0.035	Wo_{43}-En_{42}-Fs_{15}	0.033
Orthopyroxene		Wo_5-En_{64}-Fs_{31}	0.034	Wo_2-En_{63}-Fs_{35}	0.035	Wo_2-En_{63}-Fs_{35}	0.035
Magnetite		$Usp_{0.23}$	0.017	$Usp_{0.23}$	0.016	$Usp_{0.23}$	0.016
Ilmneite		$Ilm_{0.72}$	0.003	$Ilm_{0.72}$	0.004	$Ilm_{0.72}$	0.004
Feldspar		An_{42}-Ab_{58}-Or_1	0.138	An_{42}-Ab_{58}-Or_1	0.142	An_{42}-Ab_{58}-Or_1	0.144
Apatite		K3-APT10	0.002	K3-APT10	0.002	K3-APT10	0.002
Sum			0.998		1.001		0.999
Sum R^2*			0.046		0.048		0.05

Trace element abundances (ppm) in dacite

	Observed			Calculated
Rb	27	24	24	24
Ba	406	391	392	392
Sr	266	190	191	192
V	55	21	20	20
Ni	5	4	4	4
Zr	131	150	149	149
Sc	14	11	11	11
La	8.7	8.2	8.2	8.2
Ce	20.5	19.8	19.7	19.7
Nd	9.3	11.9	11.9	11.9
Sm	2.9	3.2	3.2	3.2
Eu	0.9	0.8	0.8	0.8
Yb	2.5	2.9	2.9	2.9
Y	23.7	26.9	26.8	26.7

*R^2 is the square of the residuals.

values are significantly lower than observed values, while other elements show close agreement.

A fourth model (Fig. 6.3d) was attempted to see whether a complete one-step fractionation model could be found from basaltic andesite to rhyolite. While the R^2 value was higher than the other models, single-step fractionation was modeled. Calculated Sr, V, Ni, Sc and Cu vary widely from observed values, suggesting partition coefficients for such a wide fractionation may not be adequate.

Least squares modeling demonstrates that the range of KLE magma could have been produced exclusively by fractional crystallization. Based on trace element data, model one is preferred in each model. Andesite is a 54% residual liquid of basaltic andesite. Dacite is a 58% residual liquid of andesite. Rhyolite is a 77% residual liquid of dacite. These models indicate the erupted materials may only represent 24% of the entire amount of magma needed to produce compositions present. The basaltic andesite to rhyolite model predicts rhyolite is a 31% residual liquid of basaltic andesite. Both the multiple step and single step models imply three times the erupted material remains in the magma chamber. The multiple step models show the diminishing amount of pyroxene, magnetite, ilmenite and apatite fractionation while showing the increasing fractionation of plagioclase with each step. Models involving amphibole were attempted but no reasonable solutions were found. This is consistent with the lack of amphibole in all but the KLp rhyolite. Phenocryst abundances calculated by the models are much higher then the estimated phenocryst totals presented in Table 5.1. This is most likely due to inaccuracies in evaluating the phenocryst abundances in hand specimen since no rigorous

Table 6.3d. Least-squares mass-balance models for derivation of rhyolite (97KAM17A) from basaltic andesite (97KAM29DB)

	Observed basaltic andesite	Estimated basaltic andesite 1		2		3
SiO_2	53.12	53.26		53.28		52.97
TiO_2	0.86	0.86		0.86		0.85
Al_2O_3	18.4	18.38		18.37		18.12
FeO*	9.05	9.06		9.06		9.06
MnO	0.18	0.19		0.25		0.19
MgO	5.13	5.08		5.07		5.19
CaO	10.1	10.09		10.09		10.12
Na_2O	2.58	2021		2.18		3.22
K_2O	0.46	0.54		0.52		0.35
P_2O_5	0.11	0.13		0.13		0.09
Wt. Fraction rhyolite		0.307		0.293		0.169
Clinopyroxene		Wo_{43}-En_{41}-Fs_{16}	0.116	Wo_{43}-En_{42}-Fs_{15}	0.11	Wo_{43}-En_{41}-Fs_{16}	0.159
Orthopyroxene		Wo_5-En_{64}-Fs_{31}	0.137	Wo_2-En_{62}-Fs_{36}	0.143	Wo_5-En_{64}-Fs_{31}	0.117
Magnetite		$Usp_{0.23}$	0.051	$Usp_{0.32}$	0.046	$Usp_{0.23}$	0.054
Ilmneite		$Ilm_{0.72}$	0.005	$Ilm_{0.72}$	0.006	$Ilm_{0.72}$	0.005
Feldspar		An_{18}-Ab_{83}-Or_0	0.379	An_{18}-Ab_{83}-Or_0	0.397	An_{42}-Ab_{58}-Or_1	0.495
Apatite		K3-APT10	0.003	K3-APT10	0.003	K3-APT10	0.002
Sum		0.998		0.998		1.001
Sum R^2*		0.145		0.175		0.451

Trace element abundances (ppm) in basaltic andesite

	Observed			Calculated
Rb	7	10	9	6
Ba	140	136	131	81
Sr	307	187	193	220
V	222	55	48	66
Ni	12	22	22	26
Zr	50	64	61	37
Sc	39	14	14	13
Cu	55.2	3.5	3.3	2.1
La	3.5	3.7	3.5	2.2
Ce	8.6	8.8	8.5	5.4
Nd	5.6	5.3	5.1	3.2
Sm	2.0	1.4	1.4	0.9
Eu	0.7	0.4	0.4	0.2
Yb	1.8	1.2	1.2	0.7
Y	18.4	11.6	11.1	6.9

*R^2 is the square of the residuals.

point-counting was undertaken. Estimation of modal abundance was difficult due to the highly expanded nature of the samples.

Mixing vs. Fractional Crystallization

Straight-line correlations can be fit to segments of any element vs. SiO_2. This could indicate mixing of various compositions to produce the range of compositions observed in the KLE deposits. Dacite samples plot slightly lower than the main trends, and are positioned between the andesite and rhyolite trends in Eu. Dacite may define a mixed composition of rhyolite and andesite magma. It should be noted that the inflections in whole-rock trends are located at different SiO_2 concentrations for each element. Whereas the inflection point in Al_2O_3 is at 60% SiO_2, the inflection for Na_2O is higher at 64% which may be an indicator of plagioclase fractionation becoming more albite rich. If mixing were solely responsible for the range of compositions, inflection points should all be at the same SiO_2 concentration for all elements.

Banded pumice is common in eastern and northern exposures of KLi. This texture is interpreted to be the result of syneruptive mingling during drawup into the conduit. Backscatter images show the interface of differing glasses is sharp in each banded sample, indicating mixing has not occurred across bands, suggesting mingling took place over a short interval. In contradiction to this observation, microprobe analyses of glass from banded samples plot along a continuum, suggesting mixing was taking place. These observations may be the result of either mixing of magma types within the sample, or the textures observed result from a mingling event overprinting another mixing event.

The range in temperatures determined for the KLE have a continuous trend with significant overlap of host lithology. If magma from a hotter source was mixing in the chamber during eruption, temperature ranges should be separated into bimodal ranges. Hildreth (1983) noted similar continuous temperature characteristics in magnetite-ilmenite temperatures in the Valley of Ten Thousand Smokes ignimbrite. He attributed a continuum of temperatures to reflect physical continuity in the magma chamber.

Hybridization, fractionation and repeated internal mixing are probably part of the pre-eruptive history of any long-lived intermediate magmatic system (Hildreth, 1981; Sakuyama, 1981; DePaolo, 1981), but the superficial syn-eruptive mingling textures evident in KLE pyroclasts is not responsible for the compositional gradients. The KLE tapped a well-established, compositionally stratified magma chamber. Mixing between a partial melt derived rhyolite magma and andesite melt may have produced dacite compositions.

Eruption Sequence

The axis of this eruption has been determined to be NNW (Braitseva et al., 1996). This was determined by thickness measurements of KLE deposits at and around Kurile Lake, as well as distal locations. This would imply the eruption began with a single vent eruption. The initial layer of the eruption is a fine ash, which may exhibit bedding. Due to the grain size, this layer is either a result of a phreatoplinian fall or surge. The bimodal ash and lapilli pumice layer found near the town of Pauzhetka may be the result of the mixing of phreatomagmatic surge with pumice from a plinian column. After this layer was deposited, plinian style eruption continued, depositing a thick shower-bedded pumice

layer. Column collapse may be indicated by a layer of block-sized lithic fragments seen in the fall sequence at the Pervaya Severnaya section (TIN 7, Fig 2.2). These lithics may represent the widening of the vent. Vent widening may have caused column collapse, as might have a reduction of the eruption rate. In either scenario, surge formation may have resulted from the collapse of the plinian column. Laminar bedded layers form. After a period of surge deposition, pyroclastic flows issue from new vents presumably opened as a result of chamber collapse. Pyroclastic flow eruption continues until the eruption ceased, depositing a thick and chemically zoned ignimbrite discussed in the following section.

Zonation of the Ignimbrite

The chemical zoning observed in the KLi is not a simple rhyolite to basaltic andesite sequence, as rhyolite clasts overlie a zone of banded clasts. Strong chemical zonation in small ignimbrites is common (Cas and Wright, 1987). The Crater Lake and Valley of Ten Thousand Smokes ignimbrites are zoned from rhyolite at the base, to andesite and basalt higher in the deposit (Bacon, 1983; Hildreth, 1981; 1983). The presence of rhyolite overlying mixed pumices in the KLi is enigmatic in that it is different than the conventional silicic to mafic sequence. Several models have been developed to explain this zoned character and are presented below.

Many magma chambers associated with caldera-forming eruptions are chemically zoned (Fig. 6.2) with less dense siliceous magma at the top of the chamber, and more dense magma at lower depths (e.g. Smith, 1979; Hildreth, 1981). The initial eruptive

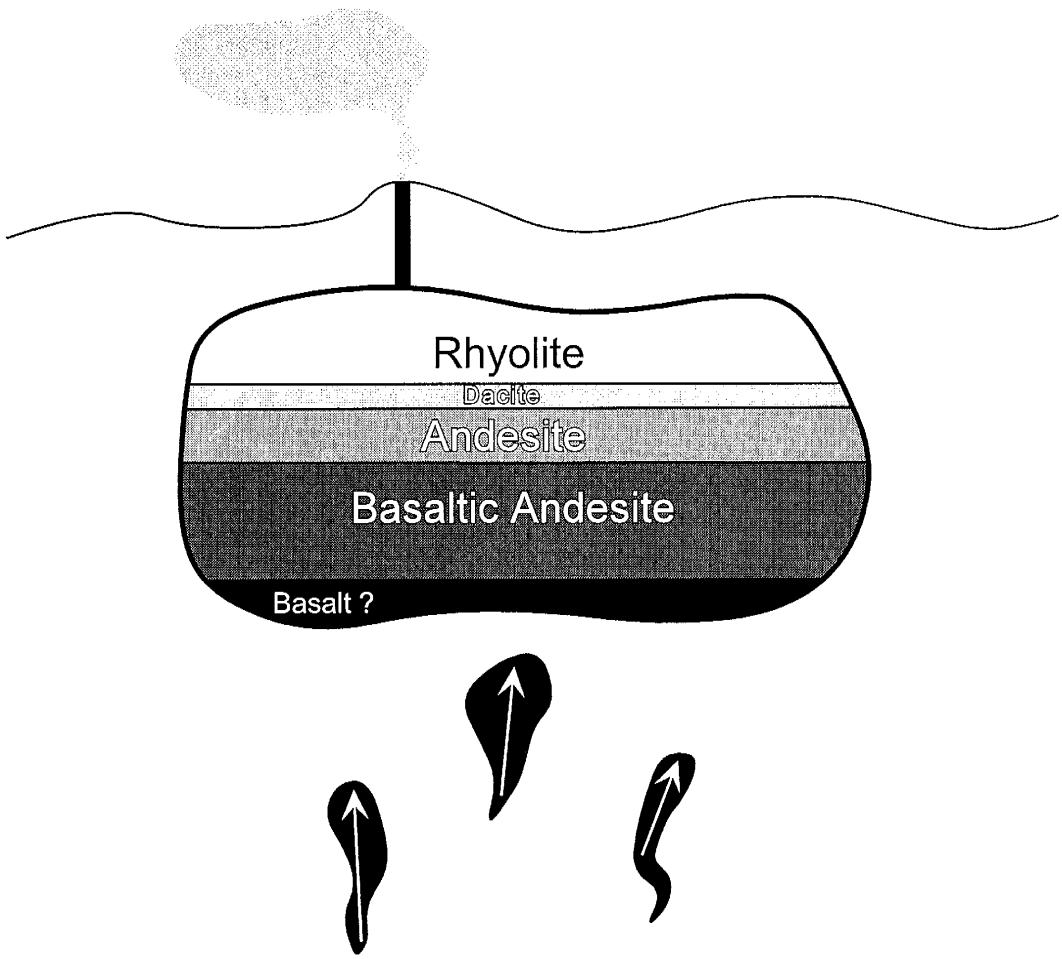

Figure 6.2. Stratified recharged magma chamber. The magma chamber is probably long-lived,periodically recharged, differentiated and stratified. This graphic shows the pre-eruptive zonation of the chamber with the most evolved magma at the top of the magma chamber and the most primitive magma at the bottom. Rising diapirs of mantle-derived basalt arrive at the base of the chamber and add heat and material to the chamber keeping it molten and possibly leading to eruption.

stages from such a chamber are typically rhyolite fall and surge grading into less evolved pyroclastic flows that deposit ignimbrite (Cas and Wright, 1988). The following models address chamber geometry and venting characteristics to account for the zoned ignimbrite observed at Kurile Lake.

The first scenario (Fig 6.3) involves simple drawdown from a zoned chamber. As eruption progresses, the chamber roof collapses, and ring fracture vents open due to collapse. Instead of simple ring fracturing, some fractures along the north and east edge of the caldera tap the chamber at lower levels, thus venting mafic magma while other vents tap silicic magma. Eventually the vents on the east and north cease eruption, and the remaining vents tap the silicic magma. This may account for the silicic-mafic-silicic zoned ignimbrite occurring only to the east and north of Kurile Lake. Ring fracturing is favored over a central vent based on the emplacement of zoned ignimbrite along one sector of the caldera, not the entire deposit.

In a second scenario an odd shaped magma chamber (Fig 6.4) may have a cupola, which during drawdown behaves metastably and remains untapped while deeper, more mafic magma is erupted, eventually a substantial amount of magma empties from the chamber, and the silicic magma cupola flushes and erupts. This scenario was presented by Wilson and Hildreth (1997) to explain the zonation in the Bishop Tuff. This scenario, however, does not account for the zoned ignimbrite occuring along one side of the caldera.

The third scenario involves magma stored in separate but interconnected chambers which acted together in the climactic eruption. This model has been proposed for the 1912 Valley of Ten Thousand Smokes (VTTS) eruption (Hildreth, 1983, and

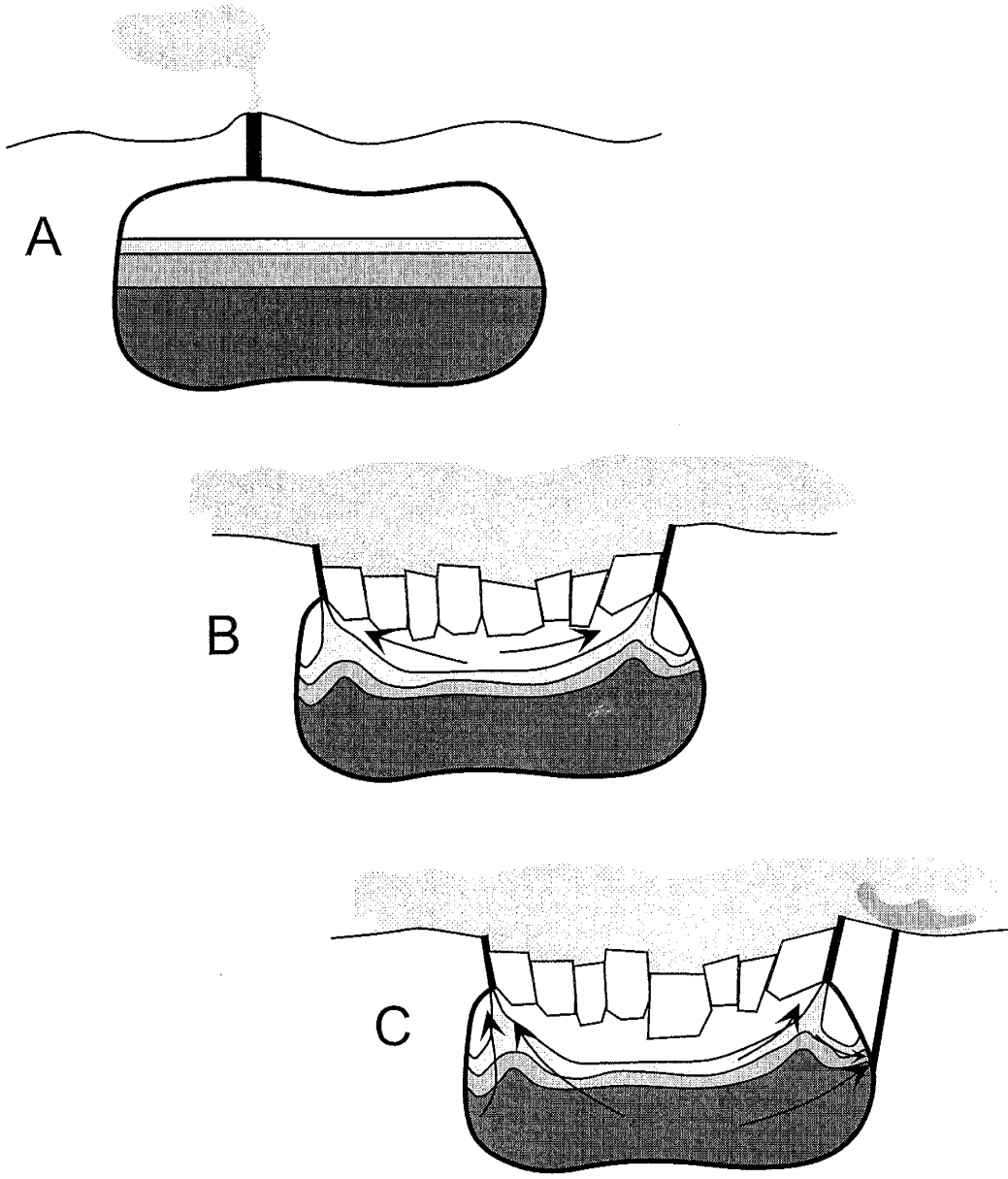

Figure 6.3. Stratified chamber eruption sequence. These diagrams are the most likely scenarios for the eruption. The eruption begins with a central vent eruption (A). Chamber roof collapse occurs (B) and the eruption continues through fractures in the subsiding chamber roof. C shows a vent tapping deeper, mafic magma. Since the ignimbrite is only zoned on the north and east sectors, venting of basaltic andesite could have only occured from vents on on the east and north sides of the caldera. Since the ignimbrite is rhyolitic-dacitic at the top of ignimbrite exposures, it is possible the venting of mafic magma may have stopped and the eruptive style returned to that of B.

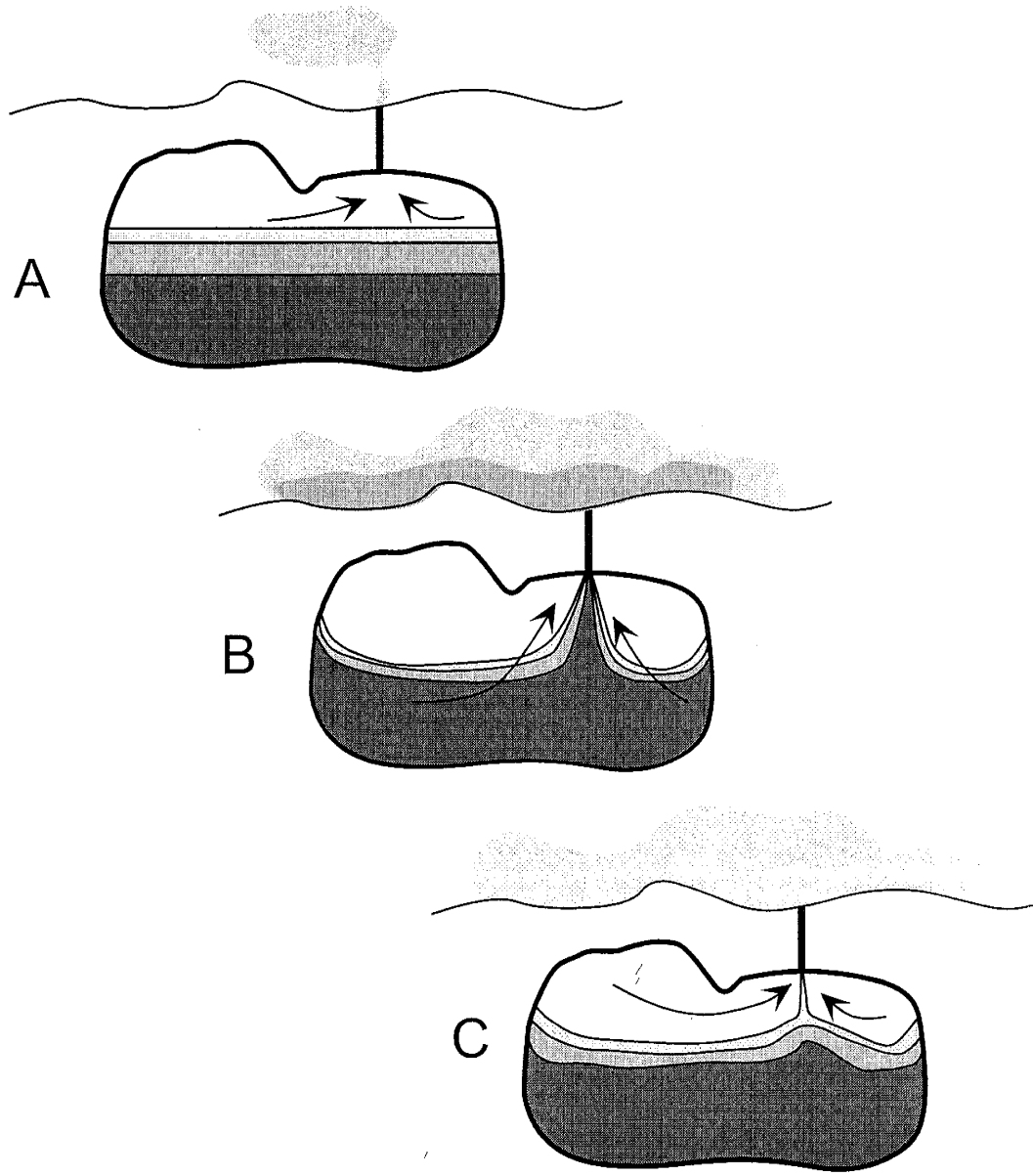

Figure 6.4. Odd-shaped magma chamber. A magma chamber with a irregularly shaped magma chamber may account for the zoned ignimbrite at Kurile Lake, The eruption begins with a central vent (plinian) eruption (A). As the eruption progresses (B), magma is tapped from deeper levels sooner than magma in a cupola can respond to drawdown. Mafic magma is erupted for an interval, then the magma in the cupola responds to drawdown and flushes into the main part of the chamber (C) supplying the vent with silicic magma. This may serve to block the mafic magma from erupting. A similar model was used by Wilson, (1998) to account for zonation in the Bishop Tuff in California.

references therein). This model does not satisfy the temperature data in that there is a continuum of temperatures. At VTTS Hildreth (1983) noted temperature groupings based on lithology. These temperature groups did not overlap like the Kurile Lake data.

The last model involves magma recharge from some depth enters the chamber causing overpressure, superheating and convection. The eruption progresses as per the first scenario, but the erupted materials are discrete blobs and swirls of magma caught on draw-up in the erupting chamber. As stated in model three, temperature calculations rule out this model. Mixing has been cited as an eruption trigger (Sparks and Sigurdsson, 1977), but was not responsible for the Kurile Lake eruption. Overlap in mineral compositions, lack of quench morphologies in mafic clasts, temperature continuity, lack of a significant compositional gap and similarity in radiogenic isotopes indicate the source magma was from a fractionating, compositionally zoned magma chamber.

CHAPTER SEVEN

CONCLUSIONS

The KLE began with a single vent producing a phreatomagmatic surge or phreatoplinian eruption. The eruption column may have encountered a pre-existing lake or intersected the local water table. A plinian-style eruption continued to tap rhyolite and produce extensive pyroclastic fall deposits. Column collapse, due to reduction in eruption volume or widening of the vent produced pyroclastic surges. Removal of sufficient volume of magma caused the chamber roof to collapse, opening fissures which acted as new vents. Pyroclastic flows issued from fissures, emplacing the ignimbrite, which formed thin veneers on ridges and filled in valleys. Compositionally zoned ignimbrite deposited on the north and east sectors of the caldera were the result of collapse fissures venting deeper, more mafic magma. Venting on the west and south sectors only tapped silicic magma. Entrainment of dacitic, andesitic and basaltic andesite melt along with syn-eruptive mixing in collapse fissures produced the banded pumice common in KLi. Eventually vents tapping mafic stopped erupting and only silicic magma erupted.

After the eruption ceased, secondary phreatic craters formed from the interaction of hot pyroclastic material and groundwater, rain and surface water. Fossil fumeroles formed and began to indurate the ignimbrite in various locations. Small ephemeral lakes formed on top of the ignimbrite depositing reworked pyroclastic materials. Eventually these lakes drained and streams re-established former drainages, deeply incising the

ignimbrite deposit. The caldera formed by this eruption began to fill with water while several small extrusive domes formed in the caldera basin.

The KLE tapped a stratified magma chamber. This magma was derived from the fluxed mantle wedge above the subducting Pacific plate. During transport and storage, this magma experienced little contamination. Over time, magma in the main chamber fractionated and formed discrete compositional layers. Geochemical evidence suggests the magma chamber was supplied by a single source based on radiogenic isotopes, major element and trace element data. Least-squares mass balance models show the entire range of compositions found in the KLi deposits may be a result of fractional crystallization. In contrast, some elements indicate fractional crystallization, mixing and assimilation may have produced the KLE magma. Temperature and pressure data shows erupted materals were in thermal equilibrium indicating mixing of hot and cool magma was not occurring during eruption. Microprobe images of glass in banded clasts show no chemical diffusion between compositions. However, individual glass analyses do not demonstrate this and may indicate mixing was occuring on a longer time scale than the mingling process.

In terms of petrological processes, KLE geochemistry presents an example where a large chamber may be formed from a single parent source that underwent fractionation but no contamination from isotopically dissimilar country rock occurs. The country rock in southern Kamchatka is probably of the same source as the KLE magma and may have similar isotopic and elemental values, obscuring assimilation and mixing processes. Other research has indicated this situation for other volcanoes along the EVF (Kersting and Arculus, 1995; Kepezhinskas et al., 1997). Large caldera-forming eruptions are all

variations on the classic caldera eruption model of central vent eruption and eventual chamber collapse leading to venting of pyroclastic flows. The KLE sequence presents another variation to this model.

REFERENCES

Anderson, D.J., Lindsley, D.H., 1988. Internally consistent solution models for Fe-Mg-Mn-Ti oxides: Fe-Ti oxides. American Mineralogist, 73: 714-726.

Bacon, C.R., 1983. Eruptive history of Mount Mazama and Crater Lake caldera, Cascade range, U.S.A. Journal of Volcanology and Geothermal Research, 18: 57-115.

Bacon, C.R., Gunn, S.H., Lanphere, M.A., Wooden, J.L., 1994. Multiple isotopic components in Quaternary volcanic rocks of the Cascade Arc near Crater Lake, Oregon. Journal of Petrology, 35: 1521-1556.

Bailey, R.A., Dalryrmple, G.B., Lanphere, M.A., 1976. Volcanism, structure and geochronology of Long Valley caldera, Mono County, California. Journal of Geophysical Research, 81: 725-744.

Baker, D.R., Eggler, D.H., 1987. Compositions of anhydrous and hydrous melts coexisting with plagioclase, augite and olivine or low-Ca pyroxene from 1 atm to 8 kbar: application to the Aleutian volcanic center of Atka. American Mineralogist, 72: 12-28.

Bernard, A., Knitter, U., Weber, B., Weis, D., Albrecht, A., Hattori, K., Klien, J., Oles, D., 1995. Petrology and geochemistry of the 1991 eruption products of Mount Pinatubo. In: C.G. Newhall and R.S. Pononbayan (Editors), Fire and Mud, Eruptions and Lahars of Mount Pinatubo, Philippines. University of Washington Press. Seattle, WA, pp767-797.

Bindemann, J.N., Bailey, J.C., 1994. A model of reverse differentiation at Dikii Greben' volcano, Kamchatka: progressive basic magma vesiculation in a silicic magma chamber. Contributions to Mineralogy and Petrology, 117: 263-278.

Boyd, F.R., England, J. L., 1961. Melting of silicates at high pressures. Carnegie Institution of Washington, Year Book 59. pp. 113-125.

Braitseva, O.A., Meleketsev, I.V., Ponomareva, V.V., Sulerzhitsky, L.D., 1995. Ages of calderas, large explosive craters and active volcanoes in the Kurile-Kamchatka region, Russia. Bulletin of Volcanology, 57: 383-402.

Braitseva, O.A., Ponomareva, V.V., Sulerzhitsky, L.D., Melekestsev, I.V., Bailey, J., 1997. Holocene key-marker tephra layers in Kamchatka Russia. Quaternary Research, 47: 125-139.

Bryan, W.B., Finger, L.W., Chayes, F., 1969. Estimating proportions in petrographic mixing equations by least-squares approximation. Science, 163: 231-252.

Burnham, C.W., 1979. The importance of volatile constituents. In: Yoder, H.S. (Editor), The Evolution of the Igneous Rocks; Fiftieth Anniversary Perspectives. Princeton University Press, Princeton NJ, pp. 439-482.

Carr, M.J., Feigenson, M.D., Bennett, E.A., 1990. Incompatable element and isotopic evidence for tectonic control of source mixing and melt extraction along the Central American volcanic front. Contributions to Mineralogy and Petrology, 105: 369-380.

Cas, R.A.F., Wright, J.V., 1987. Volcanic Successions. Chapman and Hall, New York, NY.

Castellana, B., 1998. Geology, chemostratigraphy, and petrogenesis of the Avachinsky Volcano, Kamchatka, Russia. Ph.D. Thesis, University of California, Los Angeles.

Cawthorn, R.G., Collerson, K.D., 1974. The recalculation of pyroxene end-member parameters and the estimation of ferrous and ferric iron content from electron microprobe analyses. American Mineralogist, 59: 1203-1208.

Christiansen, R.L., 1979. Cooling units and composite sheets in relation to caldera structure. In: Chapin, C.E. and Elston, W.E. (Editors), Ash Flow Tuffs. Special Paper 180, Geological Society of America, Boulder, CO, pp. 29-42.

Davidson, J.P., Boghossian, N.D., Wilson, M., 1993. The geochemistry of the igneous rock suite of St. Martin, Northern Lesser Antilles. Journal of Petrology, 34: 839-866.

Deer, W.A., Howie, R.A., Zussman, J., 1966. An Introduction to Rock Forming Minerals. Longman Group Ltd., London.

Deer, W.A., Howie, R.A., Zussman, J., 1992. An Introduction to the Rock-Forming Minerals. Longman Asia Ltd., Hong Kong.

DePaolo, D.J., 1981. Trace element and isotopic effects of combined wallrock assimilation and fractional crystallization. Earth and Planetary Science Letters, 53: 189-202.

Didier, J., Barbarin, B., 1991. Enclaves and Granite Petrology. Elsvier, Amsterdam.

Dixon, D.J., Batzia, R., 1979. Petrology and chemistry of recent lavas in the northern Marianas: implications for the origin of island arc magmas. Contributions to Mineralogy and Petrology, 70: 167-181.

Druitt, T.H., Bacon, C.R., 1988. Compositional zonation and cumulus processes in the

Mount Mazama magma chamber, Crater Lake, Oregon. Transactions of the Royal Society of Edinburgh: Earth Sciences, 79: 289-297.

Erlich, E.N., 1986. Geology of the Calderas of Kamchatka and Kurile Islands with comparison to calderas of Japan and the Aleutians, Alaska. United States Geological Survey Open File Report 86-291.

Erlich, E.N., Gorsikov, G.S., 1979. Quaternary volcanism in Kamchatka. Bulletin Volcanologique, 42: 1-298.

Fedotov, S.A., Mauserenkov, Yu.P., 1991. Active Volcanoes of Kamchatka. Vol. 2, Nauka Publishers, Moscow.

Fisher, R.V., Schmincke, H-U., 1984 Pyroclastic Rocks. Springer-Verlag, New York.

Francis, P., 1993. Volcanoes. Oxford University Press, Oxford.

Fujita, K., Stone, D.B., Layer, P. W., Parfenov, L. M., Koz'min, B. M., 1997. Cooperative program helps decipher tectonics of northeastern Russia. EOS, Transactions American Geophysical Union, 78: 252-253.

Gamble, J.A., Smith, I.E.M., McCulloch, M.T., Graham, I.J., Kokelaar, B.R., 1993. The geochemistry and petrogenesis of basalts from the Taupo Volcanic Zone and Kermadec Island Arc, S.W. Pacific. Journal of Volcanology and Geothermal Research, 54: 256-290.

Gerschwind, C.H., Rutherford, M.J., 1992. Cummingtonite and the evolution of the Mount St. Helens (Washington) magma system: an experimental study. Geology, 20: 961-1056.

Goldsmith, J.R., 1980. The melting and breakdown reactions of anorthite at high pressures and temperatures. American Mineralogist, 65: 272-284.

Gorbatov, A., Kostoglodov, V., Suarez, G., Gordeev, E., 1997. Seismicity and structure of the Kamchatka subduction zone. Journal of Geophysical Research, 102: 17,883-17,898.

Gordeev, E.I., Ivanov, B.V., Vikulin, A.V., 1998. Kronotskoye earthquake of December 5, 1997 on Kamchatka. Precursors, properties, and effects. Kamchatkan State Academy of Fishing Marine, Petropavlovsk-Kamchatsky (in Russian)

Green, T.H., 1982. Anatexis of mafic crust and high pressure crystallization of andesite. In: Thorpe, R.S. (Editor), Andesites; Orogenic Andesites and Related Rocks. Wiley. New York.

Hallett, R.B., Kyle, P.R., 1993. XRF and INAA determinations of major and trace elements in Geological Survey of Japan igneous and sedimentary rock standards. Geostandards Newsletter, 17: 127-133.

Hammarstrom, J.M., Zen, E-an., 1986. Aluminum in hornblende: an empirical igneous geobarometer. American Mineralogist, 71: 1297-1313.

Hess, P.C., 1989. Origins of Igneous Rocks. Harvard Press. Cambridge.

Hildreth, W., 1981. Gradients in silicic magma chambers: implications for lithospheric magmatism. Journal of Geophysical Research, 86: 10,153-10,192.

Hildreth, W., 1983. The compositionally zoned eruption of 1912 in the Valley of Ten Thousand Smokes, Katmai National Park, Alaska. Journal of Volcanology and Geothermal Research, 18: 1-56.

Hildreth, W., Moorbath, S., 1988. Crustal contributions to arc magmatism in the Andes of Central Chile. Contributions to Mineralogy and Petrology, 98: 455-489.

Hollister, L.S., Grissom, G.C., Peters, E.K., Stowell, H.H., Sisson, V.B., 1987. Confirmation of the empirical correlation of Al in hornblende with pressure of solidification of calc-alkaline plutons. American Mineralogist, 72: 231-239.

Jarosewich, E., Nelen, J.A., Norberg, J.A., 1980. Reference samples for electron microprobe analyses. Geostandards Newsletter, 4: 43-47.

Johnson, M.C., Rutherford, M.J., 1989. Experimental calibration of the aluminum-in-hornblende geobarometer with application to Long Valley caldera (California) volcanic rocks. Geology, 17: 837-841.

Kay, R.W., Rubenstone, J.L., Kay, S.M., 1986. Aleutian terranes from Nd isotopes. Nature, 322: 605-607.

Kepezhinskas, P., Mc Dermott, F., Defant, M.J., Hochstaedter, A., Drummond, M.S., Hakesworth, C.J., Koloskov, A., Mauray, R.C., Bellon, H., 1997. Trace element and Sr-Nd-Pb isotopic constraints on a three component model of Kamchatka Arc petrogenesis. Geochimica et Cosmochimica Acta, 61: 577-600.

Kersting, A. B., Arculus, R. J., 1995. Pb isotope composition of Kluchevskoy volcano, and north Pacific sediments; implications for magma genesis and crustal recycling in the Kamchatkan arc. Earth and Planetary Science Letters, 136: 133-148.

Kozhemyaka, N.N., Vazheyevskaya, A.A., 1991. Illinsky volcano. In: S.A. Fedotov and Yu.P. Mauserenkov (Editors), Active Volcanoes of Kamchatka. Vol. 2, Nayuka Publishers, Moscow. pp. 364-381.

LeBas, M.J., LeMatrie, R.W., Streckeisen, A., Zanettin, B., 1986. A chemical classification of volcanic rocks based on the total alkali silica diagram. Journal of Petrology, 27: 745-750.

Lees, J.M., Davaille, A., 1998. Heat transport in the torn edge of the Pacific slab in Kamchatka (abstract). International Seismic Volcanic Workshop on Kamchatkan-Aleutian Subduction Processes. Petropavlovsk-Kamchatsky, Russia. pp65-66.

Lindstrom, D.J., Korotev, R.L., 1982. TEABAGS: computer programs for instrumental neutron activation analysis. Radioanalytical Chemistry, 70: 439-458.

Litasov, N.Ye., 1991. Koshalev volcano. In: S.A Fedotov and Yu.P. Mauserenkov (Editors), Active Volcanoes of Kamchatka. Vol 2, Nauka Publishers, Moscow. pp. 382-393.

Lofgren, G.E., Norris, P.N., 1981. Experimental duplication of plagioclase sieve and overgrowth textures. Abstracts with Programs, Geological Society of America, 13: 498.

Loomis, T.P., 1982. Numerical simulations of crystallization process of plagioclase in complex melts: the origin of major and oscillatory zoning in plagioclase. Contributions to Mineralogy and Petrology, 81: 219-229.

Mahood, G., Hildreth, W., 1983. Large partition coefficients for trace elements in high-silica rhyolites. Geochimica et Cosmochimica Acta, 47: 11-30.

McPhie, J., Doyle, M., Allen, R., 1993. Volcanic Textures. Tasmanian Government Publishing Office.

Melekestev, I.V., 1974. Yuzhnaya Kamchatsky. In; Luchitsky I.V. (Editor), Istoria razvitiya reliefa Sibiri i Dal'nego Vostoka. Kamchatka, Kurile and Komandor Islands. Nauka Press, Moscow. pp.198-213 (in Russian).

Melekestev, I.V., Glushkova, O. Yu., Kirianov, V.Yu., Lozhkin, A.V., Sulerzhitsky, L. D., 1991. The origin and age of the Magadan volcanic ashes. Transactions of the USSR Academy of Sciences, 317: 1187-1192. (in Russian).

Miyashiro, A., 1974. Volcanic rock series in island arcs and active continental margins. American Journal of Science, 274: 321-355.

Morimito, N., 1988. Nomenclature of pyroxenes. American Mineralogist, 73: 1123-1133.

Nakamura, M., 1995. Continuous mixing of crystal mush and replenished magma in the ongoing Unzen eruption. Geology, 23; 807-810.

Nakamura, N., 1974. Determination of REE, Ba, Fe, Mg, Na and K in carbonaceous and ordinary chondrites. Geochimica et Cosmochimica Acta, 38: 757-775.

Nixon, G.T., Pearce, T. H., 1987. Laser-interferometery study of oscillatory zoning in plagioclase: the record of mixing and phenocryst recycling in calc-alkaline magma chambers, Iztaccihuatl volcano, Mexico. American Mineralogist, 72: 1144-1162.

Novograblenov, P.T., 1932. Catalogue of Kamchatka Volcanoes. Izvestia Geographicheskogo Obschestva, Moscow. (in Russian).

Reay, A., Johnstone, R.D., Kawachi, Y., 1989. Kaersutite, a possible international microprobe standard. Geostandards Newsletter, 13: 187-190.

Richard, L.R., Clarke, D.B., 1990. AMPHIBOL: a program for calculating structural formulae and for classifying and plotting analyses of amphiboles. American Mineralogist, 75: 421-423.

Robinson, P., Spear, F.S., Schumacher, J.C., Laird, J., Klein, C., Evans, B.W., Doolan, B.L., 1981. Phase relations of metamorphic amphiboles: natural occurrence and theory. In: D.R. Verleben and P.H. Ribbe (Editors), Amphiboles: Petrology and Experimental Phase Relations. Mineralogical Society of America Reviews in Mineralogy 9B. Washington D.C., pp. 1-228.

Rollinson, H.R., 1993. Using Geochemical Data. Longman Singapore Publishers (Pte) Ltd., Singapore.

Ronnick, J.D., Kay, S. M., Kay, R.W., 1992. The influence of amphibole fractionation on the evolution of calc-alkaline andesite and dacite tephra from the central Aleutians, Alaska. Contributions to Mineralogy and Petrology, 112: 101-108.

Sakuyama, M., 1981. Petrological study of the Myoko and Kurohime volcanoes, Japan: crystallization sequence and evidence for magma mixing. Journal of Petrology, 22: 553-583.

Sigurdsson, H., Carey, S., 1989. Plinian and co-ignimbrite tephra fall from the 1815 eruption of Tambora volcano. Bulletin of Volcanology, 51: 243-270.

Singer, B.S., Pearce, T.H., Kolisnik, A.M., Meyer, J., Meyer., 1993 Plagioclase zoning in mid-Pleistocene lavas from the Sequam volcanic center, central Aleutian arc, Alaska. American Mineralogist, 78: 143-157.

Smith, J.V., 1984. Phase relations of plagioclase feldspars. In: W.L. Brown (Editor), Proceedings of the NATO Study Institute on Feldspars and Feldspathoids. NATO ASI, Vol. #C 137. Rennes, France. pp. 55-94.

Smith, J.V., Brown, W.L., 1988. Feldspar Minerals. Springer-Verlag, New York.

Smith, R.L., 1979. Ash-flow magmatism. In: C.E. Chapin and W.E. Elston, (Editors), Ash Flow Tuffs. Special Paper 180, Geological Society of America. Boulder, CO. pp. 5-25.

Sparks, R.J.S., Sigurdsson, H., 1977. Magma mixing, a mechanism for triggering acid explosive eruptions. Nature, 267: 315-318.

Tatsumi, Y., Kosigo, T., Nhoda, S., 1995. Formation of a third volcanic chain in Kamchatka: generation of unusual subduction-related magmas. Contributions to Mineralogy and Petrology, 120: 120-128.

Tomiya A., Takahashi, E., 1985. Reconstruction of an evolving magma chamber beneath Usu volcano since the 1663 eruption. Earth and Planetary Science Letters, 36: 617-636.

Tsuchiyama, A., Takahashi, E., 1983. Melting kinetics of a plagioclase feldspar. Contributions to Mineralogy and Petrology, 84: 345-54.

Tsuchiyama, A., 1985a. Crystallization kinetics in the system $CaMgSi_2O_6$-$CaAl_2Si_2O_8$: development of zoning and kinetic effects on element partitioning. American Mineralogist, 70: 474-486.

Tuschiyama, A., 1985b. Dissolution kinetics of plagioclase in the melt of the system diopside-albite-anorthite, and origin of dusty plagioclase in andesites. Contributions to Mineralogy and Petrology, 89: 1-16.

Wilson, M., 1993. Magmatic differentiation. Journal of the Geological Society, 150: 611-624.

Wilson, M., 1989. Igneous Petrogenesis. Chapman and Hall. New York.

Wilson C.J.N., Hildreth, W., 1997. The Bishop tuff: new insights from eruptive stratigraphy. Journal of Geology, 105: 407-439.

Yoder, H.S., Stewart, D.B., Smith J.R., 1957. Ternary Feldspars. Carnegie Institution of Washington, Year Book 55. pp. 206-214.

Yoder, H.S., Tilley, C.E., 1962. Origin of basalt magmas: an experimental study of natural and synthetic rock systems. Journal of Petrology, 3: 392-532.

Zonenshain, L.P., Kuzmin, M.I., Natapov, L.M., 1990. Geology of the USSR: A Plate Tectonic Synthesis. American Geophysical Union. Washington D.C., 242p.

Zubin, M.I., Nikolaev, A.S., Sheimovich, V.S., 1982. New data about origin of Kurile Lake in Kamchatka. Vulkanologia i Seismologia, 1: 85-88. (in Russian).

APPENDIX A

SAMPLE COLLECTION AND PREPARATION

Collection

Representative pumices and scoria clasts were collected at outcrops. Large, unaltered clasts were collected to reduce contamination and inaccurate analysis due to loss of phenocrysts. When outcrops hosted a variety of lithologies, a representative sample of each type was collected. Pumices with little or no vapor phase alteration or contamination from soil were preferentially collected. Where singular clasts were not large enough for analysis, multiple clasts were collected. Collection of samples at the outcrop was carried out by digging clasts from the outcrop by hand, with a knife, shovel or hammer. Sample locations were determined with a hand-held GPS unit, air photo and 1:50,000 maps.

Cleaning

Samples were cleaned of ash and other contaminants to eliminate possible contamination by soaking samples in deionized (DI) water. The samples were scrubbed with a new, firm bristle toothbrush until it rinsed clean with DI water. Samples were then air dried for one to seven days and placed in labeled clean plastic bags.

Crushing

Rock powders were prepared from cleaned samples by coarsely crushing single pumices or a combination of small pumices enclosed in a plastic bag with a 3lb steel sledge hammer. Coarse material was homogenized, then separated into two aliquots, one for further processing, the other a contingency or for future work. Further crushing was carried out using one of two methods. Small samples were ground using a high-speed agate mill. Other larger samples were ground using a WC-TEMA swing mill. Before each sample was processed, each grinder was cleaned using Ottawa sand standard as a cleaning agent. After this initial cleaning, the mill was cleaned with acetone, dried, and loaded with sample. Samples were ground for approximately 1 minute to less than 400 mesh. Finished samples were then placed in glass jars, plastic pill-type bottles or small plastic zipper bags depending on sample size.

Petrographic Thin Sections

Billets were cut from hand samples using a small diamond wheel cutoff saw and sent to High Mesa Petrographic Service in Los Alamos, NM for preparation into polished thin sections for electron microprobe analysis and petrography.

Table A.1. Sample List

Sample	Lithology	Deposit	Location	Latitude	Longitude	Description
96KAM3	andesite	ignimbrite	Vetvisty River	N 51° 28' 80.0"	E 157° 15' 55.2"	Grey, porphyritic, vesiculated scoria
96KAM4	basaltic andesite	ignimbrite	Vetvisty River	N 51° 28' 80.0"	E 157° 15' 55.2"	Black, porphyritic, vesiculated scoria
96KAM5	mixed	ignimbrite	Vetvisty River	N 51° 28' 80.0"	E 157° 15' 55.2"	Black and white, mixed, prophyritic, vesiculated clast
96KAM6	mixed	ignimbrite	Vetvisty River	N 51° 28' 80.0"	E 157° 15' 55.2"	Black and white, mixed, prophyritic, vesiculated clast
96KAM9	rhyolite	fall	Inkanush River	N 51° 26' 31.6"	E 157° 16' 9.5"	White, porphyritic pumice
96KAM9P2-7	rhyolite	fall	Inkanush River	N 51° 26' 31.6"	E 157° 16' 9.5"	White, porphyritic pumice
96KAM12	basaltic andesite	ignimbrite	Inkanush River	N 51° 26' 60.5"	E 157° 15' 66.5"	Black, porphyritic, vesiculated scoria
96KAM12L	andesite	ignimbrite	Inkanush River	N 51° 26' 60.5"	E 157° 15' 66.5"	Grey, porphyritic, vesiculated scoria
96KAM12W	rhyolite	ignimbrite	Inkanush River	N 51° 26' 60.5"	E 157° 15' 66.5"	White, porphyritic pumice
96KAM12WP1-2	rhyolite	ignimbrite	Inkanush River	N 51° 26' 60.5"	E 157° 15' 66.5"	White, porphyritic pumice
96KAM14	andesite	ignimbrite	Inkanush River	N 51° 26' 60.5"	E 157° 15' 66.5"	Black, porphyritic, vesiculated scoria
96KAM15	rhyolite	ignimbrite	Foot of Illinsky	N/A	N/A	White, porphyritic pumice
96KAM15/2	rhyolite	ignimbrite	Foot of Illinsky	N/A	N/A	White, porphyritic pumice
96KAM18	dacite	ignimbrite	Foot of Illinsky	N/A	N/A	White, porphyritic pumice
96KAM20	mixed	ignimbrite	Foot of Illinsky	N/A	N/A	Black and white, mixed, prophyritic, vesiculated clast
96KAM21	dacite	ignimbrite	Foot of Illinsky	N/A	N/A	White, porphyritic pumice
96KAM22	mixed	ignimbrite	Foot of Illinsky	N/A	N/A	Black and white, mixed, prophyritic, vesiculated clast
97KAM01	rhyolite	fall	OZ1	N 51° 30' 15.6"	E 156° 31' 40.0"	White, porphyritic pumice clasts
97KAM02	rhyolite	fall	OZ1	N 51° 30' 15.6"	E 156° 31' 40.0"	White, porphyritic pumice clasts. Channel Sample
97KAM03	rhyolite	fall	OZ1	N 51° 30' 15.6"	E 156° 31' 40.0"	White, porphyritic pumice clasts. Channel Sample
97KAM04F	rhyolite	ignimbrite	OZ1	N 51° 30' 15.6"	E 156° 31' 40.0"	White, porphyritic pumice
97KAM05F	rhyolite	ignimbrite	OZ3	N 51° 30' 49.4"	E 156° 50' 59.6"	White, porphyritic pumice
97KAM05S	andesite	ignimbrite	OZ3	N 51° 30' 49.4"	E 156° 50' 59.6"	White, porphyritic pumice
97KAM06	rhyolite	ignimbrite	OZ3	N 51° 30' 49.4"	E 156° 50' 59.6"	White, porphyritic pumice
97KAM07	rhyolite	ignimbrite	OZ3	N 51° 30' 49.4"	E 156° 50' 59.6"	White, porphyritic pumice
97KAM08G1	andesite	ignimbrite	OZ3	N 51° 30' 49.4"	E 156° 50' 59.6"	Grey, porphyritic pumice
97KAM08G2	rhyolite	ignimbrite	OZ3	N 51° 30' 49.4"	E 156° 50' 59.6"	Grey, porphyritic pumice
97KAM08W	rhyolite	ignimbrite	OZ3	N 51° 30' 49.4"	E 156° 50' 59.6"	White, porphyritic pumice
97KAM10A	rhyolite	fall	OZ1	N 51° 30' 15.6"	E 156° 31' 40.0"	Ivory fine ash

Table A.1. Sample List

Sample	Lithology	Deposit	Location	Latitude	Longitude	Description
97KAM11	rhyolite	surge	OZ1	N 51° 30' 15.6"	E 156° 31' 40.0"	White, porphyritic pumice clasts. Channel Sample
97KAM12	dacite	surge	OZ1	N 51° 30' 15.6"	E 156° 31' 40.0"	White, porphyritic pumice clasts. Channel Sample
97KAM16L	dacite	ignimbrite	PAU5	N 51° 27' 06.8"	E 156° 49' 29.8"	White, porphyritic pumice
97KAM16S1	basaltic andesite	ignimbrite	PAU5	N 51° 27' 06.8"	E 156° 49' 29.8"	Grey, porphyritic pumice
97KAM17A	rhyolite	fall	PAU5	N 51° 27' 06.8"	E 156° 49' 29.8"	White, porphyritic pumice
97KAM17BF	rhyolite	fall	PAU5	N 51° 27' 06.8"	E 156° 49' 29.8"	White, porphyritic pumice
97KAM17BS	rhyolite	fall	PAU5	N 51° 27' 06.8"	E 156° 49' 29.8"	White, porphyritic pumice
97KAM17CF	rhyolite	fall	PAU5	N 51° 27' 06.8"	E 156° 49' 29.8"	White, porphyritic pumice
97KAM17CS	rhyolite	fall	PAU5	N 51° 27' 06.8"	E 156° 49' 29.8"	White, porphyritic pumice
97KAM17DF	rhyolite	fall	PAU5	N 51° 27' 06.8"	E 156° 49' 29.8"	White, porphyritic pumice
97KAM17DS	dacite	fall	PAU5	N 51° 27' 06.8"	E 156° 49' 29.8"	White, porphyritic pumice
97KAM18F	rhyolite	ignimbrite	TIN2	N 51° 30' 40.0"	E 156° 58' 00.7"	Grey, porphyritic pumice
97KAM18GS	rhyolite	ignimbrite	TIN2	N 51° 30' 40.0"	E 156° 58' 00.7"	Grey, porphyritic pumice
97KAM18H	rhyolite	ignimbrite	TIN2	N 51° 30' 40.0"	E 156° 58' 00.7"	White, porphyritic pumice
97KAM18I	rhyolite	ignimbrite	TIN2	N 51° 30' 40.0"	E 156° 58' 00.7"	White, porphyritic pumice
97KAM19B	rhyolite	ignimbrite	TIN4	N 51° 29' 46.8"	E 156° 59' 52.8"	White, porphyritic pumice
97KAM19C	rhyolite	ignimbrite	TIN4	N 51° 29' 46.8"	E 156° 59' 52.8"	White, porphyritic pumice
97KAM20AF	rhyolite	ignimbrite	TIN5	N 51° 23' 13.3"	E 157° 8' 00.2"	White, porphyritic pumice
97KAM20B	rhyolite	ignimbrite	TIN5	N 51° 23' 13.3"	E 157° 8' 00.2"	White, porphyritic pumice
97KAM20D	rhyolite	ignimbrite	TIN5	N 51° 23' 13.3"	E 157° 8' 00.2"	White, porphyritic pumice
97KAM21AW	dacite	ignimbrite	TIN6	N 51° 30' 13.1"	E 157° 1' 13.6"	White, porphyritic pumice
97KAM21BG	andesite	ignimbrite	TIN6	N 51° 30' 13.1"	E 157° 1' 13.6"	Grey, porphyritic pumice
97KAM21BW	rhyolite	ignimbrite	TIN6	N 51° 30' 13.1"	E 157° 1' 13.6"	White, porphyritic pumice
97KAM21CF	rhyolite	ignimbrite	TIN6	N 51° 30' 13.1"	E 157° 1' 13.6"	White, porphyritic pumice from cored bomb
97KAM21CG	andesite	ignimbrite	TIN6	N 51° 30' 13.1"	E 157° 1' 13.6"	Grey, porphyritic pumice from cored bomb
97KAM21CL	andesite	ignimbrite	TIN6	N 51° 30' 13.1"	E 157° 1' 13.6"	Grey, porphyritic pumice from cored bomb
97KAM21D	rhyolite	ignimbrite	TIN6	N 51° 30' 13.1"	E 157° 1' 13.6"	White pumice core from cored bomb
97KAM22A	rhyolite	ignimbrite	TIN7	N 51° 30' 56.5"	E 157° 2' 54.8"	White, porphyritic pumice
97KAM22B	rhyolite	ignimbrite	TIN7	N 51° 30' 56.5"	E 157° 2' 54.8"	White, porphyritic pumice

Table A.1. Sample List

Sample	Lithology	Deposit	Location	Latitude	Longitude	Description
97KAM22C	rhyolite	ignimbrite	TIN7	N 51° 30' 56.5"	E 157° 2' 54.8"	White, porphyritic pumice
97KAM22D	rhyolite	ignimbrite	TIN7	N 51° 30' 56.5"	E 157° 2' 54.8"	White, porphyritic pumice
97KAM24A	rhyolite	ignimbrite	HAK2	N 51° 22' 07.3"	E 156° 57' 44.7"	White, porphyritic pumice
97KAM24B	rhyolite	ignimbrite	HAK2	N 51° 22' 07.3"	E 156° 57' 44.7"	White, porphyritic pumice
97KAM25A	rhyolite	ignimbrite	HAK4	N 51° 21' 1.9"	E 157° 00' 31.9"	White, porphyritic pumice
97KAM26A	rhyolite	ignimbrite	HAK7	N 51° 23' 32.7"	E 156° 59' 49.5"	White, porphyritic pumice
97KAM26B2	rhyolite	ignimbrite	HAK7	N 51° 23' 32.7"	E 156° 59' 49.5"	White, porphyritic pumice
97KAM26BA	rhyolite	ignimbrite	HAK7	N 51° 23' 32.7"	E 156° 59' 49.5"	White, porphyritic pumice
97KAM26C	rhyolite	ignimbrite	HAK7	N 51° 23' 32.7"	E 156° 59' 49.5"	White, porphyritic pumice
97KAM26D	rhyolite	ignimbrite	HAK7	N 51° 23' 32.7"	E 156° 59' 49.5"	White, porphyritic pumice
97KAM29AB	basaltic andesite	ignimbrite	CNE3	N 51° 22' 32.0"	E 157° 16' 6.9"	Black, porphyritic, vesiculated scoria
97KAM29AL	rhyolite	ignimbrite	CNE3	N 51° 22' 32.0"	E 157° 16' 6.9"	Grey, porphyritic pumice
97KAM29B1	dacite	ignimbrite	CNE3	N 51° 22' 32.0"	E 157° 16' 6.9"	Black, porphyritic, vesiculated scoria
97KAM29CB	basaltic andesite	ignimbrite	CNE3	N 51° 22' 32.0"	E 157° 16' 6.9"	Black, porphyritic, vesiculated scoria
97KAM29CG1	rhyolite	ignimbrite	CNE3	N 51° 22' 32.0"	E 157° 16' 6.9"	Grey, porphyritic pumice
97KAM29CG2	andesite	ignimbrite	CNE3	N 51° 22' 32.0"	E 157° 16' 6.9"	Grey, porphyritic pumice
97KAM29CL	rhyolite	ignimbrite	CNE3	N 51° 22' 32.0"	E 157° 16' 6.9"	Grey, porphyritic pumice
97KAM29CS	rhyolite	ignimbrite	CNE3	N 51° 22' 32.0"	E 157° 16' 6.9"	Grey, porphyritic pumice
97KAM29DB	basaltic andesite	ignimbrite	CNE3	N 51° 22' 32.0"	E 157° 16' 6.9"	Black, porphyritic, vesiculated scoria
97KAM29DG	andesite	ignimbrite	CNE3	N 51° 22' 32.0"	E 157° 16' 6.9"	Grey, porphyritic pumice
97KAM29DL	rhyolite	ignimbrite	CNE3	N 51° 22' 32.0"	E 157° 16' 6.9"	Grey, porphyritic pumice
97KAM29HD	andesite	ignimbrite	CNE3	N 51° 22' 32.0"	E 157° 16' 6.9"	Black, porphyritic, vesiculated scoria
97KAM29HL	rhyolite	ignimbrite	CNE3	N 51° 22' 32.0"	E 157° 16' 6.9"	Grey, porphyritic pumice
97KAM29HW	rhyolite	ignimbrite	CNE3	N 51° 22' 32.0"	E 157° 16' 6.9"	White, porphyritic pumice
97KAM30C	rhyolite	fall	CNE4	N 51° 21' 39.3"	E 157° 16' 18.0"	White, porphyritic pumice
97KAM32A	rhyolite	ignimbrite	CNE6	N 51° 21' 53.7"	E 157° 16' 12.7"	Grey, porphyritic pumice
97KAM32D1	rhyolite	ignimbrite	CNE6	N 51° 21' 53.7"	E 157° 16' 12.7"	White, porphyritic pumice
97KAM32D2	dacite	ignimbrite	CNE6	N 51° 21' 53.7"	E 157° 16' 12.7"	White, porphyritic pumice
97KAM32F	rhyolite	ignimbrite	CNE6	N 51° 21' 53.7"	E 157° 16' 12.7"	White, porphyritic pumice

APPENDIX B

X-RAY FLUORESCENCE ANALYSES

Both major and trace element analysis were made on 95 samples by X-ray fluorescence at New Mexico Institute of Mining and Technology. Major elements were determined on fused glass beads. Trace elements were determined on pressed powder pellets. New Mexico Rhyolite, an in-house standard was prepared in triplicate, along with duplicate and triplicate rock powders to check sample preparation and instrumental accuracy.

Fusion Preparation

Fused glass beads were prepared in the following manner. 1.0000±0.0005 g of whole rock powder was fused with 6.0000±0.001g x-ray flux (adjusted to account for flux loss). X-ray flux consists of 12 parts (35.3%) di-lithium tetraborate ($Li_2B_4O_7$) and 22 parts (64.7%) lithium metaborate ($LiBO_2$). Additions of 0.05±0.001g lithium bromide (LiBr), a non-wetting agent, and 0.05±0.01g ammonium nitrate (NH_4NO_3), an oxidizer were added to aid fusion. The components were mixed dry to eliminate clumping, heated in 95% Pt + 5% Au crucibles to 1100°C for 10 minutes or until completely fused. The molten mixture was then poured into a preheated 95% Pt + 5% Au casting dish and allowed to cool. Finished beads were labeled with a small paper sticker and put in polyethylene bags

Flux weight loss due to heating and removal of H_2O was calculated during each sample preparation run to accurately determine true sample weight/flux weight for each fusion bead preparation.

Pressed Powder Preparation

Pressed powder samples consisted of 7.00±0.1g rock powder mixed with 7-10 drops of polyvinyl alcohol (used as a binder) in a agate mortar and pestle. The rock powder and binder mixture was then poured into a stainless steel die with an aluminum spacer sleeve and hand pressed to initially form a pellet. The aluminum sleeve was then removed, and powdered boric acid was then poured around and over the sample. The stainless steel die was then placed in a hydraulic laboratory press and subjected to 10 tons for one minute. The pellet was then removed from the die. Excess boric acid backing was removed from the pellet. The pellet was labeled on the boric acid backing with a Sharpie type permanent marker and placed on a heating plate to speed drying of the polyvinyl alcohol. Dried and cooled samples were stored in polystyrene boxes.

Loss on Ignition

Samples were dried at 110°C for at least two hours to eliminate absorbed H_2O. Loss-on-ignition (LOI's) for whole-rock powders were determined by heating samples at 1000°C for 2 hours in porcelain crucibles to render samples anhydrous. Loss on ignition data were used in the Phillips WD-XRF analyzing program to correct for sample weight change due to heating during fusion sample preparation.

XRF Analysis

Analysis were made using a Phillips PW2400 wavelength disperse X-ray spectrometer at New Mexico Institute of Mining and Technology. An end-window Rh tube was used to excite the sample. X-rays were measured by a P-10 gas flow detector, Xe counter and scintillation detector. Minor elements are reported as the element name (e.g. nickel=Ni) and in parts per million (ppm). Major elements are reported as oxide (i.e. K_2O) and weight percents. Detection limits, wavelengths and crystals used are reported in table (B.1a,b). Major and trace element determinations are reported in table (C.1)

Table B.1a. XRF Major element settings

Parameters for major element determination and precision expressed as standard deviation experssed as %. Concentrations are in wt.%

Major Element	Count Time (sec)	Tube Voltage (kV)	Tube Current (mA)	Analyzing Crystal	High Conc. (wt.%)	Precision	Low Conc. (wt.%)	Precision
SiO_2	20	30	100	PE C	96.9	0.45	36.7	0.74
TiO_2	20	35	85	LiF200	1.66	3.47	0.003	81.65
Al_2O_3	20	30	100	PE C	23.40	0.92	0.16	11.29
Fe_2O_3	12	45	66	LiF200	14.13	0.92	0.08	12.17
MnO	12	45	66	LiF200	0.26	6.78	0.002	77.46
MgO	30	30	100	PX1	44.66	0.82	0.01	48.04
Cr_2O_3	40	45	66	LiF200	0.64	7.91	0.001	200.00
CaO	12	35	85	LiF200	14.68	0.90	0.04	18.01
Na_2O	60	30	100	PX1	10.89	2.35	0.47	11.35
K_2O	16	30	100	LiF200	9.98	1.27	0.01	47.81
P_2O_5	20	30	100	Ge	0.34	7.71	0.01	53.45
SO_3	40	30	100	Ge	1.01	6.30	0.01	75.59
BaO	100	35	85	LiF200	0.18	23.44	0.002	223.61

Table B.1b. XRF Trace element settings

Trace element operating parameters and expression expressed as standard deviation expressed as %.

Element	Count time (sec.)	Background (sec)	Analyzing Crystal	High (ppm)	Precision	Low (ppm)	Precision
As	60	50	LiF220	228.0	0.51	0.5	10.95
Ba	100	40	LiF200	1651.5	0.25	14.9	2.59
Cr	50	20	LiF200	4653.1	0.10	6.9	2.69
Cu	40	30	LiF200	1038.3	0.20	2.2	4.26
Ga	40	20	LiF200	27.4	1.03	1.9	4.59
Mo	60	50	LiF220	16.0	1.94	2.0	5.48
Nb	60	20	LiF220	567.8	0.33	3.0	4.47
Ni	40	20	LiF200	2701.8	0.12	2.0	4.47
Pb	60	40	LiF200	162.0	0.61	2.7	4.71
Rb	30	40	LiF200	471.0	0.25	2.5	3.46
Sr	30	30	LiF200	772.2	0.20	2.7	3.33
Th	50	40	LiF200	128.1	0.62	3.0	4.08
U	100	60	LiF220	20.9	2.19	1.6	7.91
V	40	32	LiF220	721.9	0.24	1.0	6.32
Y	50	20	LiF220	177.8	0.53	1.5	5.77
Zn	40	20	LiF200	1886.8	0.15	6.0	2.58
Zr	50	20	LiF220	1693.0	0.17	2.5	4.47

APPENDIX C

INSTRUMENTAL NEUTRON ACTIVATION ANALYSIS

Sample Preparation and Irradiation

Approximately 100 mg. of whole rock powders were loaded into pre-cleaned, high-purity vials, weighed, sealed then re-weighed for identification purposes. Vials were washed in DI water and acetone and arranged sequentially and wrapped in an aluminum foil and shipped to the University of Missouri Research Reactor for activation. Activation at UMRR entails exposure to a neutron flux of 2.4×10^{13} n cm^{-2} sec^{-1} for 24 hours. The wrapped samples are placed along the inside wall of a 3.35-inch irradiation container and rotated during the irradiation period to minimize variance in neutron flux distribution. For more detailed explanation of sample preparation, see Hallett and Kyle (1993).

Sample Analysis

Analysis follows that of Hallett and Kyle (1993). Samples were counted on two coaxial p-type, high-purity germanium detectors at The New Mexico Institute of Mining and Technology. Detector resolution ranges are from 1.8keV at 1332keV to 0.6keV at 122 keV. Spectra of 8192 channels were collected using a Nuclear Data 9900 system and reduced by TEABAGS (Trace Element Analysis by Automated Gamma-ray Spectrometry) (10) on a Digital VAXstation 3100 computer. Samples were counted at 7 days after irradiation and then 21 days for longer half-life elements.

TEABAGS is a set of FORTRAN data reduction programs described by Lindstrom and Korotev, (1982) which collectively control, monitor and analyze data collected during INAA. Read Only libraries of possible gamma ray peaks (Table C.1) in the target spectrum are utilized to determine the element being detected. Peaks are analyzed and abundances determined based on peak size and background subtraction. Some data analysis is done the TEABAGS program, but the final analysis is carried out by the operator who determines final validity of the collected data.

Standards Used

Two aliquots of National Institute of Standards and Technology (NIST) SRM 1633a (coal fly ash) were used to standardize most elements. USGS granite standard, G-2 was used to standardize Na_2O (Table C.1).

Table C.1. INAA settings

Element or Oxide Determined	Radionuclide Analyzed	Standard	Accepted Concentration*	Photopeak Lines (keV)			
Na_2O	^{24}Na	G2	4.08	1368.5			
Sc	^{46}Sc	SRM1633a	38.6	889.3	1120.5		
Cr	^{51}Cr	SRM1633a	193	320.1			
FeO^T	^{59}Fe	SRM1633a	12.07	1099.2	1291.6		
As	^{76}As	SRM1633a	145	559.1			
Se	^{75}Se	SRM1633a	10.3	264.7			
Br	^{82}Br	SRM1633a	2.31	554.3	776.5		
Sb-S	^{122}Sb	SRM1633a	6.15	564.1			
Sb-L	^{124}Sb	SRM1633a	6.15	1691			
Cs	^{134}Cs	SRM1633a	10.24	604.7	795.8		
Ba	^{131}Ba	SRM1633a	1320	496.2			
La	^{140}La	SRM1633a	79.1	328.8	487	815.9	1596.5
Ce	^{141}Ce	SRM1633a	168.3	145.4			
Nd	^{147}Nd	SRM1633a	75.7	91.1	531		
Sm	^{153}Sm	SRM1633a	16.83	103.2			
Eu	^{152}Eu	SRM1633a	3.58	244.7	778.9	1408.1	
Tb	^{160}Tb	SRM1633a	2.53	298.6	879.4	966.2	1178
Yb	^{175}Yb	SRM1633a	7.5	282.5	396.3		
Lu	^{177}Lu	SRM1633a	1.08	208.3			
Hf	^{181}Hf	SRM1633a	7.29	482			
Ta	^{182}Ta	SRM1633a	1.93	1189	1221.4	1231	
W	^{187}W	SRM1633a	4.6	479.5	685.8		
Th	^{233}Pa	SRM1633a	24	311.9			
U	^{239}Np	SRM1633a	10.3	228.1			

*wt.% for oxides, otherwise ppm (μg/g)

Table C.2. Whole Rock Major and Trace Element Analyses

SAMPLE	96KAM3	96KAM04	96KAM9	96KAM9P2	96KAM9P3	96KAM9P4	96KAM9P5
SiO_2	60.01	53.18	71.46	72.04	71.66	71.76	70.90
TiO_2	0.71	0.87	0.29	0.27	0.28	0.28	0.30
Al_2O_3	19.86	18.51	14.02	14.24	14.09	14.18	13.90
Fe_2O_3	5.21	9.53	1.91	1.78	1.87	1.85	2.01
MnO	0.13	0.18	0.07	0.07	0.07	0.07	0.07
MgO	1.72	4.56	0.39	0.39	0.42	0.38	0.45
CaO	6.89	9.60	2.42	2.34	2.43	2.52	2.44
Na_2O	4.51	2.88	4.51	4.45	4.44	4.50	4.56
K_2O	0.76	0.45	1.92	2.00	1.96	1.92	1.91
P_2O_5	0.20	0.13	0.05	0.05	0.05	0.05	0.06
LOI	0.49	-0.60	2.85	2.86	3.04	3.04	2.91
Total	100.49	99.29	99.89	100.49	100.31	100.55	99.51
S	50	119	75	77	54	60	75
Sc	15.98	33.70	8.41				
V	80	272	17				
Cr	6.2	39.8	8.0				
Ni	3	13	5				
Cu	13	44	27	21			34
Zn	52	74	39	39		29	40
Ga	19	18	14				
As	5	4	12			12	
Br	0.30	0.37	1.14			0.78	
Rb	12	7	31			32	
Sr	393	335	172	148	162	179	158
Y	21	18	34				
Zr	74	50	172				
Nb	2	2	3				
Mo	1	1	3				
Sb	0.22	0.13	0.42			0.52	
Cs	0.76	0.59	2.11			2.20	
Ba	240	153	423	403	412	414	409
La	5.95		10.64			10.24	
Ce	14.2	8.4	24.9			25.7	
Nd	7.2	4.6	15.0			12.3	
Sm	2.66	2.00	3.94			4.10	
Eu	1.13	0.79	0.94			0.94	
Tb	0.50	0.41	0.72			0.78	
Yb	1.95	1.71	3.65			3.87	
Lu	0.27	0.24	0.54			0.54	
Hf	2.19	1.29	4.98			4.81	
Ta	0.17	0.06	0.17			0.20	
Pb	6	2	9				
Th	0.75	0.59	2.16	2	2	2.15	2
U	0.27		0.88			1.14	

Table C.2. Whole Rock Major and Trace Element Analyses

SAMPLE	96KAM9P6	96KAM9P7	96KAM12	96KAM12L	96KAM12W	96KAM12WP1
SiO_2	70.90	70.88	55.05	58.37	70.64	71.05
TiO_2	0.30	0.28	0.92	0.73	0.26	0.28
Al_2O_3	13.90	14.36	19.29	19.50	14.20	14.32
Fe_2O_3	2.01	1.78	7.36	5.73	1.78	2.01
MnO	0.07	0.07	0.15	0.14	0.07	0.07
MgO	0.45	0.37	3.50	2.01	0.35	0.40
CaO	2.44	2.53	8.85	7.26	2.45	2.55
Na_2O	4.56	4.49	3.29	4.25	4.50	4.44
K_2O	1.91	1.91	0.58	0.73	1.82	1.74
P_2O_5	0.06	0.05	0.13	0.21	0.05	0.05
LOI	2.91	2.90	0.57	1.02	3.34	3.55
Total	99.51	99.62	100.40	99.95	99.44	100.46
S	32	77	177	119	51	43
Sc		8.36	25.41	18.02	7.79	
V			193			
Cr			27.4	13.3	8.8	
Ni			11		5	
Cu			28	43	34	
Zn	38		63	65	38	40
Ga			18		14	
As		11	4	5	10	
Br		1.69		1.28	1.83	
Rb		31	9	11	31	
Sr	176	163	349	382	173	183
Y			19		32	
Zr			58		173	
Nb			2		3	
Mo			1		3	
Sb		0.56	0.23	0.24	0.53	
Cs		2.06	0.63	0.68	2.02	
Ba	403	426	178	222	416	413
La		10.08	4.31	8.76	0.37	
Ce		23.9	11.6	13.4	24.2	
Nd		12.8	5.9	8.1	13.2	
Sm		3.94	2.33	2.73	3.91	
Eu		0.97	0.88	1.12	0.92	
Tb		0.70	0.47	0.48	0.71	
Yb		3.67	1.79	2.03	3.72	
Lu		0.52	0.25	0.35	0.53	
Hf		4.82	1.82	2.17	4.93	
Ta		0.21	0.11	0.10	0.20	
Pb			4		9	
Th	2	2.06	0.58	0.82	2.14	1
U		0.97	0.30	0.30	1.18	

Table C.2. Whole Rock Major and Trace Element Analyses

SAMPLE	96KAM12WP2	96KAM14	96KAM15	96KAM15/2	96KAM18	96KAM20	96KAM21
SiO_2	60.93	56.92	70.18	69.63	64.81	61.70	64.62
TiO_2	0.64	0.78	0.28	0.29	0.52	0.55	0.50
Al_2O_3	19.01	18.97	14.98	14.74	16.24	16.76	15.81
Fe_2O_3	4.51	7.23	2.04	2.01	4.38	5.44	4.18
MnO	0.12	0.15	0.07	0.07	0.11	0.12	0.12
MgO	1.39	3.00	0.37	0.40	1.57	2.60	1.45
CaO	6.24	8.06	2.52	2.58	4.45	6.46	4.02
Na_2O	4.50	3.80	4.45	4.54	3.94	3.47	3.85
K_2O	0.89	0.65	1.76	1.76	1.45	1.20	1.51
P_2O_5	0.18	0.18	0.05	0.06	0.11	0.11	0.11
LOI	1.79	0.08	3.66	3.60	2.55	1.88	3.06
Total	100.20	99.82	100.36	99.68	100.13	100.29	99.23
S	101	117	66	66	100	79	101
Sc	14.24	24.43	8.36	9.20	13.64	19.88	13.63
V		159		10	53		59
Cr		15.0		4.5			9.2
Ni		7		4	5		6
Cu		43	48	18	27	13	19
Zn		65	43	41	46	54	50
Ga		18		14	15	16	15
As	5	4	11	10	8	6	8
Br	1.01	0.39	2.44	2.57	2.10	0.68	0.83
Rb	14	9	35	30	26	20	26
Sr	355	359	217	203	258	260	235
Y		21		33	23	21	25
Zr	116	66		175	127	98	128
Nb		2		3	2	2	3
Mo		1	2	2	2	2	3
Sb	0.11	0.18	0.34	0.53	0.47	0.29	0.45
Cs	0.97	0.53	2.10	1.95	1.69	1.30	1.61
Ba	259	213	455	440	395	294	365
La	6.78	4.92	10.28	10.15	8.42	6.41	10.37
Ce	16.7	12.2	25.4	24.1	19.9	14.3	24.2
Nd		6.9	13.7	14.6	9.0	6.9	11.4
Sm	2.92	2.49	3.92	3.95	2.84	2.48	3.63
Eu	1.17	0.96	0.93	0.94	0.85	0.75	0.97
Tb	0.55	0.48	0.70	0.70	0.53	0.45	0.62
Yb	2.15	1.98	3.50	3.68	2.43	2.16	2.53
Lu	0.37	0.27	0.56	0.54	0.37	0.31	0.36
Hf	2.50	2.09	5.01	4.83	3.48	2.65	3.69
Ta	0.14	0.07	0.20	0.20	0.15	0.14	0.16
Pb		3		9	7	5	7
Th	1.11	0.72	2.31	2.10	2.08	1.34	2.00
U	0.55	0.33	1.11	0.84	0.83	0.66	0.78

Table C.2. Whole Rock Major and Trace Element Analyses

SAMPLE	97KAM01	97KAM02	97KAM03	97KAM04F	97KAM05F	97KAM05S	97KAM06
SiO_2	71.37	69.52	71.26	69.79	69.55	60.00	70.68
TiO_2	0.28	0.29	0.27	0.27	0.34	0.67	0.28
Al_2O_3	14.20	14.41	14.04	14.29	14.61	18.52	14.18
Fe_2O_3	1.86	1.89	1.84	1.85	2.27	4.97	1.86
MnO	0.07	0.07	0.07	0.07	0.08	0.12	0.07
MgO	0.36	0.38	0.36	0.38	0.52	1.67	0.38
CaO	2.37	2.54	2.30	2.31	2.87	6.15	2.46
Na_2O	4.55	4.53	4.51	4.45	4.60	4.39	4.51
K_2O	1.82	1.76	1.83	1.81	1.76	0.87	1.84
P_2O_5	0.06	0.06	0.05	0.05	0.07	0.25	0.06
LOI	3.04	3.73	3.25	3.49	3.43	2.47	3.45
Total	99.98	99.18	99.78	98.76	100.10	100.08	99.75
S	38	61	36	53	49	112	25
Sc		8.92	8.81	8.20	10.18	16.34	8.29
V	10	12	10	13	17	69	13
Cr						5.2	
Ni	2	4	3	3	3	3	3
Cu	9	11	11	9	6	8	5
Zn	39	39	39	37	41	56	38
Ga	13	14	13	13	14	17	14
As	9	12	11	12	10	5	10
Br		1.70	2.61	3.60	2.10	0.22	0.56
Rb	30	30	31	30	27	13	29
Sr	166	182	166	164	191	347	182
Y	33	33	33	32	32	22	31
Zr	175	172	178	178	158	82	165
Nb	1	1	1	1			1
Mo	2	2	2	1	2	2	2
Sb		0.51	0.49	0.48	0.52	0.27	0.53
Cs		1.99	2.11	2.23	1.91	0.94	2.05
Ba	420	422	431	416	405	264	425
La		10.20	10.73	10.77	9.90	6.40	10.22
Ce		25.3	26.4	26.3	23.8	16.7	25.4
Nd		14.6	14.3	15.3	14.4	8.2	12.7
Sm		3.99	4.04	3.98	3.78	2.93	3.80
Eu		0.98	0.95	0.92	1.01	1.16	0.96
Tb		0.78	0.76	0.73	0.72	0.55	0.71
Yb		3.58	3.51	3.47	3.45	2.27	3.59
Lu		0.55	0.57	0.54	0.52	0.34	0.55
Hf		4.85	5.08	5.11	4.43	2.43	5.02
Ta		0.88	0.33	0.63	0.36	0.21	0.43
Pb	10	9	10	10	9	6	8
Th	4	2.19	2.29	2.40	1.94	0.92	2.22
U		0.76	0.78	1.35	0.82	0.52	0.76

Table C.2. Whole Rock Major and Trace Element Analyses

SAMPLE	97KAM07	97KAM08G1	97KAM08G2	97KAM08W	97KAM10A	97KAM11	97KAM12
SiO_2	70.64	59.61	69.77	70.17	68.93	70.09	64.67
TiO_2	0.27	0.70	0.28	0.31	0.30	0.28	0.46
Al_2O_3	14.19	18.85	14.10	14.37	13.98	14.83	16.96
Fe_2O_3	1.85	5.50	1.92	2.03	2.60	1.90	3.75
MnO	0.07	0.12	0.07	0.07	0.08	0.07	0.10
MgO	0.38	1.86	0.44	0.45	0.64	0.38	1.07
CaO	2.45	6.70	2.47	2.68	2.42	2.40	3.47
Na_2O	4.47	4.31	4.50	4.54	4.07	4.46	3.84
K_2O	1.84	0.82	1.84	1.80	1.76	1.79	1.51
P_2O_5	0.05	0.21	0.06	0.06	0.06	0.06	0.07
LOI	4.03	1.71	3.25	3.99	3.87	3.60	3.26
Total	100.24	100.39	98.70	100.47	98.71	99.86	99.16
S	26	127	107	28	87	42	90
Sc	8.85	17.57	8.97	8.51	10.15		
V	11	112	12	6	29	14	60
Cr		6.8					
Ni	3	5	3	2	4	2	4
Cu	9	18	4	8	32	14	23
Zn	39	54	39	43	44	40	50
Ga	13	17	14	14	14	14	16
As	9	7	10	9	11	9	9
Br	0.47	0.27	2.31	0.41	2.70		
Rb	31	12	30	30	31	30	28
Sr	169	346	173	173		191	247
Y	32	21	32	32	36	32	22
Zr	168	77	167	165	169	182	143
Nb	1			1	1	1	1
Mo	2	2	1	2	3	2	3
Sb	0.46	0.30	0.58	0.54	0.56		
Cs	2.05	0.98	2.05	2.11	2.25		
Ba	436	239	417	433	430	452	424
La	10.12	5.98	10.13	10.26	11.00		
Ce	25.1	15.4	25.4	24.8	26.7		
Nd	13.2	7.7	12.9	13.5	14.5		
Sm	3.85	2.67	3.94	3.87	4.44		
Eu	0.95	1.10	0.96	0.95	0.97		
Tb	0.72	0.54	0.68	0.72	0.83		
Yb	3.57	2.13	3.58	3.54	4.02		
Lu	0.55	0.31	0.54	0.55	4.02		
Hf	5.01	2.25	4.93	4.76	4.93		
Ta	0.31	0.52	0.31	0.31	0.19		
Pb	10	5	10	18	11	10	10
Th	2.18	0.91	2.09	2.06	2.27	4	4
U	1.22	0.28	0.78	1.04	0.94		

Table C.2. Whole Rock Major and Trace Element Analyses

SAMPLE	97KAM16L	97KAM16S1	97KAM17A	97KAM17BF	97KAM17BS	97KAM17CF
SiO_2	65.50	54.38	68.46	69.81	70.19	69.19
TiO_2	0.41	0.82	0.28	0.27	0.27	0.29
Al_2O_3	16.38	18.46	15.15	14.69	14.56	15.00
Fe_2O_3	2.97	8.29	1.91	1.87	1.91	2.06
MnO	0.08	0.16	0.07	0.07	0.07	0.07
MgO	0.70	3.87	0.35	0.37	0.36	0.41
CaO	3.03	8.37	2.47	2.32	2.26	2.35
Na_2O	4.19	3.16	4.36	4.36	4.37	4.40
K_2O	1.49	0.56	1.68	1.77	1.79	1.71
P_2O_5	0.06	0.15	0.04	0.04	0.04	0.04
LOI	5.37	1.36	4.48	4.17	4.19	4.25
Total	100.18	99.58	99.25	99.74	100.01	99.77
S	202	142	68	54	80	77
Sc			9.83	8.39	8.08	9.08
V	30	220	14	12	10	14
Cr				5.0		
Ni	4	11	3	3	3	4
Cu	11	38	9	10	11	12
Zn	46	67	37	37	36	41
Ga	15	18	14	14	13	15
As	9	5	11	11	9	12
Br			4.50	2.32	0.59	0.88
Rb	25	7	29	30	30	29
Sr	201	324	175	164	159	165
Y	28	19	32	32	31	32
Zr	165	58	180	179	182	183
Nb			1	1		1
Mo	3	1	2	2	2	2
Sb			0.48	0.51	0.48	0.53
Cs			1.82	2.02	1.99	2.04
Ba	390	386	376	426	402	420
La			9.74	10.31	10.26	10.33
Ce			23.5	26.2	25.2	25.7
Nd			14.2	13.8	11.2	13.2
Sm			3.87	3.84	3.74	3.94
Eu			1.00	0.93	0.93	0.95
Tb			0.72	0.74	0.67	0.72
Yb			3.47	3.45	3.56	3.75
Lu			0.56	0.55	0.58	0.56
Hf			5.13	5.15	5.40	5.19
Ta			0.28	0.29	0.30	0.30
Pb	9	3	10	11	10	10
Th	4	2	2.26	2.44	2.21	2.37
U			1.05	0.95	0.81	0.95

Table C.2. Whole Rock Major and Trace Element Analyses

SAMPLE	97KAM17CS	97KAM17DF	97KAM17DS	97KAM18F	97KAM18GS	97KAM18H
SiO_2	68.77	68.80	64.85	72.28	70.48	71.60
TiO_2	0.30	0.28	0.44	0.32	0.26	0.25
Al_2O_3	15.36	15.41	17.54	14.00	13.76	13.76
Fe_2O_3	2.04	1.96	3.18	2.12	1.76	1.66
MnO	0.07	0.07	0.09	0.07	0.07	0.06
MgO	0.41	0.37	0.84	0.54	0.35	0.30
CaO	2.47	2.28	3.76	2.37	2.29	2.14
Na_2O	4.38	4.32	4.26	4.26	4.48	4.50
K_2O	1.70	1.72	1.31	1.95	1.89	1.92
P_2O_5	0.04	0.04	0.05	0.06	0.05	0.04
LOI	4.43	4.79	4.38	2.50	4.66	3.49
Total	99.97	100.04	100.70	100.47	100.05	99.72
S	77	174	121	118	24	30
Sc	9.40	8.66	11.62	9.95		
V	13	16	36	25	8	10
Cr						
Ni	3	3	4	3	3	3
Cu	12	15	11	28	7	9
Zn	40	39	43	29	37	36
Ga	14	14	15	14	13	13
As	12	11	9	11	9	9
Br	0.92	1.48	1.41	1.78		
Rb	28	28	22	29	31	32
Sr	174	162	242	161	160	154
Y	32	31	26	31	32	32
Zr	182	185	147	166	170	174
Nb	1	1		1		
Mo	2	2	3	3	1	1
Sb	0.58	0.51	0.37	0.54		
Cs	2.03	1.91	1.56	1.86		
Ba	403	417	333	429	424	434
La	9.89	9.56	8.12	10.12		
Ce	24.5	23.8	20.1	24.4		
Nd	10.6	11.9	8.3	13.4		
Sm	3.79	3.60	3.10	3.87		
Eu	0.99	0.95	0.99	0.92		
Tb	0.71	0.68	0.58	0.72		
Yb	3.62	3.47	2.77	3.50		
Lu	0.52	0.54	0.43	0.54		
Hf	5.25	5.17	4.34	4.69		
Ta	0.24	0.25	0.26	0.31		
Pb	10	11	8	8	10	9
Th	2.32	2.39	1.79	2.13	3	3
U	0.84	0.78	0.83	1.01		

Table C.2. Whole Rock Major and Trace Element Analyses

SAMPLE	97KAM18I	97KAM19B	97KAM19C	97KAM19G	97KAM19J	97KAM20AF	97KAM20B
SiO_2	71.04	68.73	69.15	71.87	68.01	71.33	71.62
TiO_2	0.28	0.34	0.29	0.27	0.38	0.27	0.28
Al_2O_3	14.23	14.86	14.42	14.02		14.31	14.56
Fe_2O_3	1.91	2.25	1.92	1.81	3.39	1.87	1.89
MnO	0.07	0.08	0.07	0.07	0.09	0.07	0.07
MgO	0.39	0.53	0.42	0.37	1.28	0.35	0.39
CaO	2.45	2.94	2.61	2.32	3.59	2.45	2.55
Na_2O	4.62	4.42	4.39	4.55	3.83	4.55	4.61
K_2O	1.84	1.75	1.81	1.95		1.87	1.85
P_2O_5	0.06	0.08	0.06	0.05	0.10	0.05	0.06
LOI	3.03	3.99	4.07	2.82	0.65	2.55	2.41
Total	99.92	99.96	99.20	100.10	98.50	99.67	100.27
S	47	36	35	100	50	55	73
Sc							
V	10	13	13	12	50	10	13
Cr							
Ni	3	3	3	3	4	3	3
Cu	9	9	10	10	14	8	9
Zn	36	40	39	32	34	32	35
Ga	13	14	14	14	13	14	14
As	9	8	8	9	6	9	9
Br							
Rb	32	28	28	31		31	30
Sr	161	199	180	162	263	170	177
Y	32	31	32	32	13	32	33
Zr	174	155	163	171	108	173	169
Nb			1	1	1	1	
Mo		1	2	2	4	2	2
Sb							
Cs							
Ba	409	405	411	424	623	427	421
La							
Ce							
Nd							
Sm							
Eu							
Tb							
Yb							
Lu							
Hf							
Ta							
Pb	9	9	10	9	9	9	9
Th	3	3	4	3	5	4	2
U							

Table C.2. Whole Rock Major and Trace Element Analyses

SAMPLE	97KAM20D	97KAM21AW	97KAM21BG	97KAM21BW	97KAM21CFW	97KAM21CG
SiO_2	72.26	62.99	56.27	70.80	69.35	61.53
TiO_2	0.27	0.57	0.84	0.26	0.31	0.66
Al_2O_3	14.21	17.46	19.49	13.91	14.29	18.82
Fe_2O_3	1.85	3.96	6.94	1.80	2.12	4.60
MnO	0.07	0.11	0.14	0.07	0.07	0.12
MgO	0.37	1.23	2.52	0.36	0.46	1.49
CaO	2.45	5.18	7.92	2.36	2.60	6.05
Na_2O	4.57	4.49	3.82	4.37	4.42	4.73
K_2O	1.92	1.16	0.65	1.94	1.81	0.88
P_2O_5	0.05	0.19	0.26	0.05	0.06	0.24
LOI	2.50	2.68	1.64	3.93	4.04	0.84
Total	100.52	100.02	100.49	99.85	99.53	99.96
S	57	81	174	24	69	101
Sc					9.78	
V	10	56	152	7	17	65
Cr						
Ni	3	4	6	4	3	3
Cu	17	12	27	8	10	20
Zn	34	50	61	36	39	56
Ga	14	16	18	13	13	16
As	9		5	8	9	4
Br					0.39	
Rb	31	17	9	32	28	13
Sr	167	303	383	166	177	354
Y	33	26	22	32	32	23
Zr	172	102	61	167	163	83
Nb	1			1		
Mo	2	2	1	2	2	1
Sb					0.53	
Cs					2.07	
Ba	433	300	192	432	398	246
La					9.94	
Ce					25.3	
Nd					13.0	
Sm					3.90	
Eu					0.98	
Tb					0.70	
Yb					3.58	
Lu					0.54	
Hf					4.71	
Ta					0.44	
Pb	9	6	4	10	9	7
Th	3	2	2	4	2.06	2
U					1.03	

Table C.2. Whole Rock Major and Trace Element Analyses

SAMPLE	97KAM21CL	97KAM21D	97KAM22A	97KAM22B	97KAM22C	97KAM22D
SiO_2	60.33	71.23	70.07	68.61	67.76	70.00
TiO_2	0.66	0.25	0.30	0.33	0.27	0.26
Al_2O_3	18.38	13.47	14.57	14.89	15.11	14.17
Fe_2O_3	4.70	1.70	1.97	2.19	1.89	1.81
MnO	0.12	0.07	0.07	0.08	0.09	0.08
MgO	1.56	0.32	0.39	0.50	0.49	0.35
CaO	5.94	2.12	2.58	2.89	2.33	2.21
Na_2O	4.52	4.45	4.48	4.59	4.15	4.26
K_2O	0.91	1.92	1.75	1.63	1.71	1.87
P_2O_5	0.25	0.04	0.06	0.06	0.04	0.04
LOI	2.32	3.82	3.81	3.92	4.78	4.46
Total	99.67	99.39	100.05	99.69	98.62	99.49
S	94	22	54	78	33	71
Sc		7.72				
V	72	6	12	16	13	10
Cr						
Ni	4	3	3	4	4	3
Cu	22	10	10	8	20	12
Zn	56	37	40	43	70	40
Ga	17	13	13	14	15	14
As	5	9	8	8	9	9
Br		0.46				
Rb	13	32	29	27	29	30
Sr	340	148	181	195	191	165
Y	22	32	32	32	31	32
Zr	83	171	168	159	189	179
Nb			1	1		1
Mo	1	1	2	2	2	1
Sb		0.48				
Cs		2.19				
Ba		442	417	388	571	455
La		10.62				
Ce		26.7				
Nd		12.2				
Sm		3.90				
Eu		0.91				
Tb		0.72				
Yb		3.70				
Lu		0.55				
Hf		5.02				
Ta		0.30				
Pb	6	10	10	9	10	10
Th	2	2.26	4	3	4	3
U		1.06				

Table C.2. Whole Rock Major and Trace Element Analyses

SAMPLE	97KAM24A	97KAM24B	97KAM25A	97KAM26A	97KAM26B2	97KAM26BA
SiO_2	70.79	70.90	70.04	71.09	70.37	72.13
TiO_2	0.28	0.28	0.28	0.28	0.32	0.27
Al_2O_3	14.67	14.37	14.85	13.91	14.81	14.02
Fe_2O_3	1.92	1.95	1.97	1.94	2.15	1.93
MnO	0.07	0.07	0.07	0.07	0.07	0.07
MgO	0.40	0.37	0.40	0.39	0.51	0.38
CaO	2.61	2.52	2.50	2.44	2.87	2.40
Na_2O	4.57	4.59	4.42	4.52	4.57	4.63
K_2O	1.76	1.81	1.76	1.87	1.76	1.91
P_2O_5	0.06	0.05	0.04	0.05	0.07	0.05
LOI	2.78	2.90	3.48	3.52	3.00	2.40
Total	99.91	99.81	99.81	100.08	100.48	100.19
S	60	71	52	60	93	113
Sc						
V	14	12	12	11	16	13
Cr						
Ni	3	3	3	3	3	4
Cu	7	19	9	15	9	10
Zn	38	39	39	41	40	35
Ga	14	14	14	13	14	13
As	9	8	10	9	9	9
Br						
Rb	29	29	29	32	29	32
Sr	180	176	179	168	191	166
Y	32	32	34	33	32	33
Zr	167	169	174	171	160	171
Nb		1	1			
Mo	2	1	2	1	2	2
Sb						
Cs						
Ba	424	426	419	426	416	425
La						
Ce						
Nd						
Sm						
Eu						
Tb						
Yb						
Lu						
Hf						
Ta						
Pb	10	9	10	10	9	9
Th	3	2	3	3	3	3
U						

Table C.2. Whole Rock Major and Trace Element Analyses

SAMPLE	97KAM26C	97KAM26D	97KAM29AB	97KAM29AL	97KAM29B1	97KAM29CB
SiO_2	71.55	71.69	54.77	71.38	66.64	54.10
TiO_2	0.27	0.26	0.84	0.28	0.44	0.86
Al_2O_3	14.32	14.09	18.98	14.52	16.13	18.78
Fe_2O_3	1.81	1.79	8.68	1.89	3.10	8.81
MnO	0.07	0.07	0.17	0.07	0.09	0.17
MgO	0.37	0.36	3.91	0.39	0.91	4.08
CaO	2.46	2.40	9.00	2.60	4.05	8.80
Na_2O	4.67	4.53	3.25	4.55	4.55	3.12
K_2O	1.87	1.92	0.49	1.88	1.48	0.52
P_2O_5	0.05	0.05	0.16	0.06	0.13	0.20
LOI	2.31	2.60	-0.09	2.59	2.11	0.66
Total	99.75	99.76	100.14	100.21	99.63	100.07
S	197	224	241	48	124	172
Sc			29.82	8.58		24.12
V	9	12	221	13	37	250
Cr			31.2			25.0
Ni	3	3	10	3	4	10
Cu	10	12	46	8	13	40
Zn	33	34	72	36	43	72
Ga	14	14	18	13	15	18
As	10	11	5	9	8	4
Br			0.76	1.76		0.85
Rb	31	31	7	30	22	8
Sr	171	166	355	179	235	341
Y	32	33	19	33	29	19
Zr	170	173	55	166	135	57
Nb						
Mo	2	1	1	2	3	1
Sb			0.28	0.54		0.21
Cs			0.53	2.01		0.71
Ba	411	424	153	433	358	171
La			3.88	10.32		5.78
Ce			9.8	24.1		13.0
Nd			5.7	13.5		9.0
Sm			2.21	3.87		2.79
Eu			0.90	0.96		1.08
Tb			0.40	0.74		0.53
Yb			1.88	3.53		2.17
Lu			0.26	0.56		0.32
Hf			1.56	4.73		2.01
Ta			0.30	0.32		0.32
Pb	9	8	5	10	7	6
Th	2	2	0.48	2.11	1.00	0.80
U				0.97		

Table C.2. Whole Rock Major and Trace Element Analyses

SAMPLE	97KAM29CG1	97KAM29CG2	97KAM29CL	97KAM29CS	97KAM29DB	97KAM29DG
SiO_2	71.01	58.23	69.86	69.06	51.95	57.56
TiO_2	0.31	0.78	0.32	0.30	0.84	0.73
Al_2O_3	14.70	19.18	14.71	14.32	17.99	19.85
Fe_2O_3	2.10	5.98	2.05	2.00	9.84	5.92
MnO	0.07	0.14	0.07	0.07	0.18	0.14
MgO	0.48	2.16	0.48	0.44	5.02	2.18
CaO	2.82	7.16	2.87	2.61	9.88	7.49
Na_2O	4.59	4.15	4.63	4.41	2.52	4.27
K_2O	1.80	0.76	1.80	1.82	0.45	0.66
P_2O_5	0.07	0.27	0.07	0.07	0.11	0.26
LOI	2.17	1.47	2.47	3.83	0.16	0.87
Total	100.12	100.28	99.33	98.93	98.94	99.92
S	144	122	68	34	288	148
Sc	9.60		10.22	9.22	38.40	18.64
V	16	96	17	13	326	104
Cr					55.6	9.5
Ni	2	5	3	3	12	5
Cu	12	22	12	9	54	28
Zn	36	54	35	39	70	57
Ga	14	17	15	14	17	18
As	11	6	8	8	4	5
Br	1.60		0.48	0.48		0.82
Rb	30	12	29	30	7	9
Sr	187	370	192	181	300	398
Y	32	22	33	32	18	20
Zr	163	73	162	164	49	62
Nb						
Mo	2	2	2	2	1	2
Sb	0.59		0.42	0.43	0.17	0.18
Cs	1.80		1.89	1.99	0.42	0.70
Ba	413	234	410	420	137	205
La	9.81		9.73	9.77	3.37	5.39
Ce	24.2		24.1	24.6	8.4	14.1
Nd	14.3		11.0	11.7	5.5	7.4
Sm	3.87		3.87	3.81	1.95	2.55
Eu	1.00		1.05	0.95	0.71	1.14
Tb	0.71		0.73	0.74	0.38	0.48
Yb	3.41		3.58	3.51	1.73	1.97
Lu	0.53		0.53	0.51	0.24	0.31
Hf	4.54		4.54	4.71	1.55	1.88
Ta	0.41		0.31	0.30	0.25	0.32
Pb	8	6	8	10	6	5
Th	2.05	3	2.17	2.02	0.51	0.91
U	0.90		0.93	0.91	0.18	0.32

Table C.2. Whole Rock Major and Trace Element Analyses

SAMPLE	97KAM29DL	97KAM29HD	97KAM29HL	97KAM29HW	97KAM30C	97KAM32A
SiO_2	70.98	56.77	68.57	69.04	71.62	70.51
TiO_2	0.30	0.82	0.31	0.30	0.27	0.27
Al_2O_3	14.65	18.42	15.15	14.62	14.35	14.16
Fe_2O_3	2.02	7.28	2.16	2.07	1.84	1.82
MnO	0.07	0.16	0.10	0.07	0.07	0.07
MgO	0.42	3.02	0.44	0.48	0.36	0.38
CaO	2.66	7.63	2.79	2.78	2.46	2.47
Na_2O	4.53	3.70	4.46	4.57	4.59	4.54
K_2O	1.93	0.70	1.72	1.74	1.88	1.97
P_2O_5	0.07	0.25	0.09	0.07	0.05	0.05
LOI	2.63	0.25	3.98	3.08	2.63	2.77
Total	100.26	99.00	99.76	98.82	100.12	99.01
S	43	181	73	65	47	294
Sc	9.18	25.03		9.49		8.49
V	14	174	15	15	15	12
Cr		21.2				
Ni	3	8	4	3	2	3
Cu	11	24	16	8	9	10
Zn	39	67	39	40	37	29
Ga	14	17	14	14	14	14
As	10	4	18	8	9	12
Br	2.19	0.70		1.48		1.64
Rb	30	11	28	29	31	31
Sr	182	348	189	192	171	173
Y	32	21	31	32	32	33
Zr	165	69	169	164	171	170
Nb						
Mo	2	2	2	2	2	2
Sb	0.55	0.15		0.49		0.50
Cs	2.02	0.77		1.90		2.03
Ba	410	215	405	424	426	433
La	10.20	5.47		10.27		10.26
Ce	24.8	14.6		24.9		25.6
Nd	12.2			14.7		13.3
Sm	3.88	2.64		3.90		3.88
Eu	1.00	1.00		0.99		0.98
Tb	0.72	0.53		0.75		0.73
Yb	3.58	2.13		3.41		3.45
Lu	0.57	0.32		0.55		0.56
Hf	4.68	1.99		4.62		4.90
Ta	0.44	0.52		0.33		0.30
Pb	9	6	10	10	9	8
Th	2.22	0.84	3	1.98	2	2.19
U	0.91	0.22		0.88		0.68

Table C.2. Whole Rock Major and Trace Element Analyses

SAMPLE	97KAM32D1	97KAM32D2	97KAM32F
SiO_2	69.30	64.35	70.02
TiO_2	0.31	0.55	0.28
Al_2O_3	14.52	17.24	14.44
Fe_2O_3	2.09	3.90	1.91
MnO	0.07	0.11	0.07
MgO	0.51	1.16	0.39
CaO	2.48	5.06	2.61
Na_2O	4.46	4.62	4.47
K_2O	1.82	1.17	1.82
P_2O_5	0.07	0.14	0.06
LOI	3.41	2.37	3.38
Total	99.04	100.67	99.45
S	90	68	41
Sc	9.84		8.55
V	19	41	13
Cr			
Ni	2	3	3
Cu	9	10	7
Zn	38	52	38
Ga	14	16	14
As	10	6	12
Br	0.52		0.41
Rb	31	19	30
Sr	177	300	182
Y	32	26	32
Zr	164	131	166
Nb			
Mo	2	2	2
Sb	0.52		0.50
Cs	1.97		2.04
Ba	421	334	427
La	9.75		9.84
Ce	24.2		25.6
Nd	13.6		9.9
Sm	3.69		3.93
Eu	0.96		0.99
Tb	0.74		0.68
Yb	3.53		3.38
Lu	0.52		0.52
Hf	4.74		4.76
Ta	0.28		0.24
Pb	10	7	10
Th	2.12	2	2.12
U	0.86		0.81

APPENDIX D

ELECTRON MICROPROBE ANALYSES

Major element determinations of mineral phases and glass were measured in twelve samples by a Cameca SX-100 electron microprobe at New Mexico Institute of Mining and Technology.

Sample billets were cut from cleaned hand samples and sent to High Mesa Petrographic Service in Los Alamos, NM for mounting and polishing. Samples were returned after mounting and polishing. Upon arrival, samples were examined by petrographic microscope for petrographic analysis and to determine phases present and relative abundances. Representative samples were selected for microprobe probe analysis based on lithology and texture as well as stratigraphic position. At least two samples of each lithology were selected along with representative samples of clasts showing magma mixing. The following is a list of samples examined and their lithology.

96KAM3:	andesite	96KAM4:	basaltic andesite
96KAM6:	banded clast	96KAM9:	rhyolite
96KAM12l:	andesite	96KAM12b:	basaltic andesite
96KAM14:	banded clast	96KAM18:	dacite
97KAM2:	rhyolite	97KAM17b:	rhyolite
97KAM32a:	rhyolite	97KAM32b:	dacite

After selection, samples were cleaned with DI water and placed in a ultrasonic cleaner for one minute, then dried. Upon drying, samples were cleaned with acetone and

petroleum ether. Cleaned samples were carbon coated to ensure electrical conductivity as per microprobe operating standards.

Samples were secured in the microprobe shuttle and carbon tape was applied to at least two locations on the edges of the sample to ensure electrical continuity with the shuttle. The shuttle and samples were then dusted with pressurized air and placed in the electron microprobe. During the entire cleaning, coating and sample loading process latex gloves were utilized to ensure sample cleanliness

Representative minerals and glasses were analyzed in each sample. Feldspars were chosen based on type, i.e. sieve, euhedral, glomerocrystic, etc. Core to rim relations were determined. Pyroxene was also chosen based on type and size. Core to rim relationships were also determined. Magnetite and ilmenite were analyzed based on proximity. Co-existing pairs were analyzed preferentially over isolated crystals, but isolated crystals were analyzed when co-existing pairs were unavailable. Amphibole was analyzed when found, and core to rim relationships were also determined. Apatite was analyzed when found, as well as quartz. During analysis of mixed samples, care was taken to document which analyses were taken from minerals located in the various glass types in the sample. Glass was analyzed by utilizing the largest beam size possible without including vesicles. This was done to minimize Na volatilization. Sometimes phyric glass analysis incorporate microlites due to the nature of the glass in some samples. In mixed samples, analyses of glass from each lithology was analyzed as close to the contact to establish degree of mixing present.

Pyroxene, magnetite and ilmenite were analyzed by a point beam. Feldspar, apatite and amphibole was analyzed by a 10μm beam and alternately, a 5μm beam for

rim analyses or microlites. Beam current for all minerals was 20 nA. Glass was analyzed with the largest beam possible to prevent Na loss. Glass analysis was made with a 5, 10, 15, 20 or 25μm beam at 10 nA. Individual mineral and glass analysis parameters are listed in D.1-7.

Table D.1. Glass Analyses

Sample	K2-GLS1	K2-GLS2	K2-GLS3	K2-GLS4	K2-GLS5	K2AVG	K3-GLS1	K3-GLS2	K3-GLS3	K3-GLS4	K3-GLS5	K3-GLS6	K3-GLS7
Beam Size (μm)	15	15	15	15	15		10	10	10	10	10	10	10
SiO_2	75.75	76.92	78.07	76.98	77.97	77.14 (0.94)	75.39	74.28	73.73	75.45	73.88	73.43	75.43
TiO_2	0.31	0.43	0.19	0.22	0.23	0.28 (0.10)	0.42	0.35	0.37	0.43	0.44	0.36	0.43
Al_2O_3	13.60	12.95	13.19	12.88	13.38	13.20 (0.30)	14.60	14.45	14.53	14.91	14.63	14.89	14.84
FeO	1.57	1.86	1.28	1.44	1.40	1.51 (0.22)	1.65	2.07	2.24	1.23	2.66	2.42	0.94
MnO	b.d.	b.d.	b.d.	b.d.	b.d.		b.d.	b.d.	b.d.	b.d.	0.12	b.d.	b.d.
MgO	0.30	0.18	0.23	0.21	0.21	0.23 (0.05)	0.29	0.44	0.53	0.13	0.68	0.60	0.10
CaO	1.60	1.40	1.38	1.46	1.42	1.45 (0.09)	2.07	2.25	2.40	1.87	2.49	2.66	1.92
Na_2O	3.85	3.82	4.05	3.80	3.80	3.86 (0.11)	4.46	4.41	4.22	4.61	4.01	4.37	3.50
K_2O	2.03	2.02	2.18	2.14	2.03	2.08 (0.07)	1.85	1.80	1.85	1.92	1.77	1.64	1.87
P_2O_5	0.05	0.02	0.02	0.03	0.01	0.03 (0.02)	0.07	0.09	0.09	b.d.	b.d.	0.09	0.17
SO_2	b.d.	b.d.	b.d.	b.d.	0.03	0.03	b.d.	b.d.	b.d.	b.d.	b.d.	b.d.	b.d.
F	0.08	0.00	0.05	0.02	0.01	0.03 (0.03)	0.09	0.08	0.03	0.00	0.03	b.d.	0.03
Cl	0.13	0.18	0.16	0.15	0.15	0.15 (0.02)	0.11	0.10	0.08	0.11	0.10	0.07	0.12
Total	99.39	99.84	100.83	99.42	100.73	100.04	101.08	100.44	100.19	100.79	100.87	100.62	99.41

Sample	K3-GLS8	K3AVG	K4-GLS1	K4-GLS2	K4-GLS3	K4-GLS4	K4-GLS5	K4-GLS6	K4-GLS7	K4AVG	K6-GLS1	K6-GLS2	K6-GLS3
Beam Size (μm)	10		10	10	10	15	10	10	10		10	10	10
SiO_2	73.50	74.01 (3.19)	65.16	62.73	64.62	64.96	64.55	65.84	65.08	64.71 (0.97)	76.27	71.20	75.15
TiO_2	0.41	0.41 (0.22)	0.86	0.66	0.83	0.80	0.54	0.97	0.86	0.79 (0.14)	0.34	0.52	0.42
Al_2O_3	14.39	14.54 (0.26)	15.56	18.88	15.83	15.04	16.95	14.38	14.44	15.87 (1.60)	13.46	15.11	14.17
FeO	2.49	2.19 (1.30)	5.28	3.74	5.17	5.54	3.90	5.65	6.68	5.14 (1.03)	0.90	2.45	1.78
MnO	b.d.		0.16	0.14	0.12	0.14	b.d.	0.15	0.15	0.14 (0.01)	b.d.	b.d.	b.d.
MgO	0.70	0.55 (0.32)	0.95	0.50	1.33	2.18	0.93	1.07	2.15	1.30 (0.64)	0.11	0.52	0.34
CaO	2.68	2.46 (0.83)	4.17	5.92	4.64	4.09	4.80	3.86	3.80	4.47 (0.74)	1.36	3.38	1.83
Na_2O	4.27	4.25 (0.41)	5.24	5.70	5.16	5.19	5.15	5.07	5.10	5.23 (0.21)	3.71	5.30	4.42
K_2O	1.70	1.76 (0.28)	0.81	0.34	0.60	0.76	1.20	1.20	0.58	0.78 (0.32)	2.31	0.54	2.22
P_2O_5	b.d.		0.28	0.13	0.13	0.16	0.18	0.37	0.28	0.22 (0.09)	0.08	0.12	0.15
SO_2	b.d.		0.03	b.d.	b.d.	b.d.	0.03	b.d.	b.d.		b.d.	b.d.	b.d.
F	0.13	0.09 (0.03)	0.07	0.02	0.07	0.06	b.d.	b.d.	0.06	0.06 (0.02)	0.16	0.04	0.05
Cl	0.08	0.09 (0.03)	0.04	0.05	0.05	0.09	0.08	0.06	0.07	0.06 (0.02)	0.07	0.03	0.11
Total	100.49	100.49	98.61	98.81	98.56	99.03	98.34	98.62	99.26	98.75	98.78	99.29	100.73

Table D.1. Glass Analyses

Sample	K6-GLS4	K6-GLS5	K6-GLS6	K6-GLS7	K6-GLS8	K6-GLS9	K6-GLS10	K6-GLS11	K6-GLS12	K6-GLS13	K6-GLS14	K6-GLS15	K6-GLS16
Beam Size (μm)	10	10	10	10	10	10	10	10	10	10	10	10	10
SiO_2	66.20	71.81	71.60	73.66	76.75	70.17	63.86	70.86	70.29	69.39	70.31	60.22	74.26
TiO_2	0.97	0.60	0.53	0.14	0.29	0.61	1.15	0.56	0.68	0.69	0.67	0.31	0.42
Al_2O_3	15.22	14.89	15.94	16.14	12.75	14.52	14.07	15.02	14.29	15.35	15.20	22.02	14.80
FeO	4.95	3.14	2.26	1.10	1.05	3.84	7.57	2.58	3.33	2.92	3.24	2.49	1.78
MnO	0.20	0.17	b.d.	b.d.	b.d.	b.d.	0.19	b.d.	0.16	0.13	0.16	b.d.	b.d.
MgO	1.02	0.81	0.54	0.15	0.12	0.99	2.40	0.46	0.77	0.62	0.69	0.29	0.35
CaO	4.32	2.61	3.51	2.91	1.25	2.85	3.36	3.22	2.66	3.09	3.10	7.47	2.09
Na_2O	4.72	4.60	5.21	5.07	3.86	4.85	3.58	5.50	5.98	5.30	6.10	5.41	4.46
K_2O	1.11	2.13	1.37	1.83	2.61	1.38	2.37	0.95	0.87	1.34	0.74	0.50	2.43
P_2O_5	0.24	0.13	0.17	b.d.	b.d.	0.16	0.23	0.19	0.13	0.17	0.13	0.09	0.16
SO_2	0.03	b.d.	b.d.	b.d.	b.d.	b.d.	0.04	b.d.	b.d.	b.d.	b.d.	b.d.	b.d.
F	b.d.	0.01	b.d.	b.d.	0.71	0.04	0.27	0.06	0.03	1.21	0.09	0.03	b.d.
Cl	0.04	0.10	0.08	0.06	0.12	0.05	0.07	0.04	0.09	0.04	0.10	0.02	0.08
Total	99.01	101.01	101.30	101.14	99.58	99.56	99.15	99.51	99.29	100.25	100.52	98.89	100.92

Sample	K6-GLS17	K6-GLS18	K6-GLS19	K6-GLS20	K6-GLS21	K6-GLS22	K6-GLS23	K6-GLS24	K6-GLS25	K6-GLS26	K6-GLS27	K6-GLS28	K6-GLS29
Beam Size (μm)	10	10	10	10	10	10	10	10	15	15	15	15	15
SiO_2	76.46	70.10	67.53	66.28	72.03	73.18	73.30	69.99	69.47	68.94	69.35	68.79	77.30
TiO_2	0.30	0.58	0.73	0.73	0.54	0.50	0.38	0.80	0.70	0.62	0.66	0.57	0.27
Al_2O_3	13.07	15.08	15.32	17.11	14.38	13.82	14.14	14.37	15.29	15.91	15.69	16.54	12.76
FeO	1.40	2.63	4.22	3.22	2.60	2.34	1.69	3.55	3.37	3.28	3.67	3.14	0.93
MnO	b.d.	0.12	0.14	b.d.	b.d.	0.11	b.d.	b.d.	b.d.	0.17	0.11	b.d.	b.d.
MgO	0.33	0.32	1.12	1.12	0.52	0.51	0.32	0.79	0.80	0.85	0.94	0.82	0.11
CaO	1.48	3.56	3.70	4.37	3.14	1.81	2.45	3.01	2.98	3.40	3.09	3.74	1.30
Na_2O	3.94	5.68	5.06	5.56	5.19	4.10	5.01	5.27	5.75	5.68	5.80	5.61	3.89
K_2O	2.34	0.49	1.22	0.91	0.81	2.26	1.34	0.99	1.26	1.11	1.22	0.99	2.74
P_2O_5	0.03	0.13	0.24	0.20	0.14	0.12	b.d.	0.32	0.19	0.21	0.25	0.19	b.d.
SO_2	b.d.	b.d.	b.d.	b.d.	b.d.	b.d.	b.d.	b.d.	b.d.	b.d.	b.d.	b.d.	b.d.
F	0.06	b.d.	0.07	b.d.	0.06	0.13	0.06	0.06	0.09	b.d.	0.18	b.d.	b.d.
Cl	0.10	0.06	0.04	0.03	0.03	0.04	0.03	0.02	0.08	0.08	0.07	0.07	0.07
Total	99.58	98.74	99.39	99.60	99.52	98.92	98.86	99.27	100.06	100.24	101.03	100.53	99.46

Table D.1. Glass Analyses

Table

Sample	K6-GLS30	K6-GLS31	K6-GLS32	K6-GLS33	K6-GLS34	K6-GLS35	K6-GLS36	K6-GLS37	K6-GLS38	K9-GLS1	K9-GLS2	K9AVG	K12B-GLS1	K14
Beam Size (μm)	15	20	20	20	20	15	15	15	15	15	20		15	
SiO_2	72.44	69.39	73.93	74.46	67.98	71.48	74.00	67.83	76.98	76.87	77.09	76.98 (0.16)	61.13	
TiO_2	0.20	0.64	0.34	0.33	0.78	0.69	0.23	0.90	0.28	0.21	0.21	0.21 (0.00)	0.69	
Al_2O_3	15.84	15.22	13.19	13.26	14.92	15.43	15.09	14.92	12.93	12.70	12.76	12.73 (0.04)	17.72	
FeO	0.88	3.71	1.38	1.22	4.87	2.80	0.77	4.43	1.08	1.39	1.45	1.42 (0.04)	5.66	
MnO	b.d.	0.17	b.d.	b.d.	0.17	0.13	b.d.	0.16	b.d.	b.d.	b.d.		0.13	
MgO	0.13	0.88	0.20	0.09	1.28	0.44	0.04	1.12	0.15	0.23	0.24	0.24 (0.01)	1.85	
CaO	2.74	2.80	1.10	0.86	2.91	3.49	2.10	3.54	0.97	1.35	1.45	1.40 (0.07)	5.73	
Na_2O	4.66	5.99	3.40	3.27	5.57	5.38	4.63	5.47	3.59	4.32	4.47	4.40 (0.11)	4.73	
K_2O	1.96	1.20	6.56	5.99	1.37	0.09	3.70	1.79	3.57	2.03	2.11	2.07 (0.06)	0.81	
P_2O_5	b.d.	0.18	b.d.	b.d.	0.22	0.26	b.d.	0.36	0.05	b.d.	b.d.		0.22	
SO_2	b.d.	b.d.	b.d.	b.d.	b.d.	b.d.	b.d.	b.d.	b.d.	b.d.	b.d.		0.03	
F	b.d.	0.01	0.01	0.02	0.04	0.05	0.14	b.d.	0.02	b.d.	b.d.		0.13	
Cl	0.07	0.21	0.24	0.21	0.16	0.15	0.17	0.12	0.15	0.14	0.16	0.15 (0.01)	0.07	
Total	99.08	0.40	0.25	0.22	0.41	0.45	0.31	0.48	0.22	99.29	99.94	99.62	98.90	

Sample	K12L-GLS1	K12L-GLS2	K12L-GLS3	K12L-GLS4	K12AVG	K14-GLS1	K14-GLS2	K14-GLS3	K14-GLS4	K14-GLS5	K14-GLS6	K14-GLS7	K14-GLS8	K17B
Beam Size (μm)	15	15	15	15		15	15	15	15	15	15	20	20	
SiO_2	69.73	70.22	69.47	68.68	69.53 (0.64)	62.39	65.31	70.27	69.73	65.79	62.62	66.73	63.97	77.56
TiO_2	0.75	0.72	0.71	0.68	0.72 (0.03)	0.79	0.56	0.69	0.66	0.86	0.70	0.87	0.75	0.17
Al_2O_3	14.34	14.43	14.81	14.38	14.49 (0.22)	17.59	12.62	15.70	15.72	15.91	17.21	15.39	16.81	13.41
FeO	3.38	3.57	3.13	4.24	3.58 (0.48)	4.95	6.74	3.33	3.44	5.02	4.97	4.87	4.81	1.46
MnO	b.d.	b.d.	b.d.	0.14		0.13	0.31	0.14	0.14	0.19	0.13	0.18	0.15	
MgO	0.64	0.67	0.72	1.33	0.84 (0.33)	1.23	5.68	0.94	1.02	1.41	1.37	1.32	1.28	0.25
CaO	2.90	2.96	3.04	2.95	2.96 (0.06)	5.54	2.89	2.96	3.11	4.04	5.23	3.76	4.46	1.51
Na_2O	5.46	5.89	4.88	4.99	5.31 (0.46)	5.26	3.45	4.48	4.72	5.47	5.40	5.73	5.73	3.90
K_2O	1.34	0.89	2.01	1.81	1.51 (0.50)	0.68	1.86	1.91	1.84	0.79	0.66	0.69	0.76	2.03
P_2O_5	0.26	0.31	0.22	0.23	0.26 (0.04)	0.30	0.17	0.16	0.23	0.23	0.33	0.26	0.23	
SO_2	b.d.	0.04	b.d.	b.d.		b.d.	0.03	b.d.	b.d.	b.d.	0.04	0.01	0.01	
F	0.07	0.08	b.d.	b.d.	0.08 (0.01)	0.07	0.02	0.07	0.03	0.09	b.d.	0.04	0.05	0.09
Cl	0.08	0.19	0.09	0.09	0.11 (0.05)	0.06	0.07	0.11	0.08	0.10	0.07	0.07	0.08	0.15
Total	99.02	100.06	99.18	99.51	99.44	99.00	99.70	100.77	100.72	99.92	98.73	99.90	99.09	100

D.1. Glass Analyses

Sample	4-GLS9	K14-GLS10	K14-GLS11	K14-GLS12	K14-GLS13	K14-GLS14	K14-GLS15	K14-GLS16	K14-GLS17	K14-GLS18	K17B-GLS1	K17B-GLS2	K17B-GLS3
Beam Size (μm)	20	20	20	20	20	20	20	20	20	20	15	15	15
SiO_2	66.00	64.88	69.55	65.52	67.75	65.91	68.21	67.25	66.04	71.58	76.95	77.53	78.21
TiO_2	0.75	0.97	0.61	0.76	0.71	0.77	0.64	0.75	0.47	0.56	0.21	0.15	0.16
Al_2O_3	15.45	14.89	15.19	15.50	15.58	15.78	15.53	15.53	19.02	14.82	13.80	13.15	13.28
FeO	5.27	6.46	3.63	4.83	4.11	4.67	3.87	4.69	2.51	3.37	1.45	1.43	1.49
MnO	0.15	0.16	0.12	0.16	0.14	0.07	0.11	0.13	0.03	0.16	b.d.	b.d.	b.d.
MgO	1.46	1.61	1.02	1.35	1.28	1.40	1.06	1.25	0.68	0.85	0.30	0.22	0.23
CaO	3.97	4.10	3.05	3.79	3.61	3.89	2.52	3.56	5.11	2.76	1.75	1.38	1.39
Na_2O	5.63	5.09	4.52	6.01	5.09	5.80	4.39	5.73	5.36	4.85	3.88	3.82	3.99
K_2O	0.70	0.85	2.33	0.53	1.79	0.77	3.25	0.88	1.18	1.89	2.02	2.00	2.08
P_2O_5	0.17	0.19	0.24	0.28	0.23	0.34	0.28	0.26	0.21	0.20	0.06	b.d.	b.d.
SO_2	0.00	0.01	0.02	0.03	0.00	0.03	0.00	0.01	0.02	0.02	b.d.	b.d.	b.d.
F	0.22	0.06	0.07	0.08	0.03	0.03	0.06	0.00	0.00	0.00	b.d.	0.08	0.10
Cl	0.08	0.06	0.05	0.07	0.05	0.07	0.09	0.07	0.06	0.07	0.16	0.15	0.15
Total	99.83	99.33	100.39	98.85	100.36	99.53	99.99	100.10	100.69	101.13	100.61	99.95	101.18

Sample	AVG	K18-GLS1	K18-GLS2	K18-GLS3	K18-GLS4	K18-GLS5	K18-GLS6	K18AVG	K32A-GLS1	K32A-GLS2	K32A-GLS3	K32AVG	K32D-GLS1
Beam Size (μm)		25	20	25	20	20	20		15	15	15		15
SiO_2	(0.63)	75.67	75.89	74.54	76.06	75.38	75.98	75.59 (0.57)	76.73	76.42	75.37	76.17 (0.71)	74.06
TiO_2	(0.03)	0.32	0.37	0.43	0.32	0.30	0.36	0.35 (0.05)	0.29	0.26	0.27	0.27 (0.02)	0.45
Al_2O_3	(0.34)	12.90	13.13	13.05	13.22	13.16	13.14	13.10 (0.11)	13.42	13.23	13.93	13.53 (0.36)	15.02
FeO	(0.03)	1.71	1.69	1.71	1.84	1.72	1.76	1.74 (0.05)	0.90	1.45	1.58	1.31 (0.36)	2.43
MnO		b.d.	b.d.	b.d.	b.d.	b.d.	b.d.		b.d.	b.d.	b.d.		0.11
MgO	(0.04)	0.42	0.37	0.42	0.34	0.37	0.42	0.39 (0.03)	0.21	0.25	0.29	0.25 (0.04)	0.61
CaO	(0.21)	1.94	1.79	1.70	1.87	1.84	1.98	1.85 (0.10)	1.59	1.54	1.45	1.53 (0.07)	2.56
Na_2O	(0.09)	3.91	4.46	3.50	4.29	4.13	4.23	4.09 (0.34)	3.63	3.78	4.44	3.95 (0.43)	2.50
K_2O	(0.04)	1.97	2.02	2.25	2.09	2.08	2.14	2.09 (0.10)	2.24	2.12	2.01	2.12 (0.12)	1.71
P_2O_5		b.d.	b.d.	0.09	b.d.	b.d.	b.d.		b.d.	b.d.	b.d.		0.09
SO_2		b.d.	b.d.	b.d.	b.d.	b.d.	b.d.		b.d.	b.d.	b.d.		b.d.
F	(0.01)	0.59	b.d.	1.37	0.25	0.13	b.d.	0.59 (0.56)	b.d.	0.12	b.d.		0.02
Cl	(0.01)	0.14	0.11	0.13	0.15	0.13	0.13	0.13 (0.01)	0.10	0.11	0.16	0.12 (0.03)	0.11
Total	1.58	99.66	99.97	99.23	100.52	99.30	100.24	99.82	99.23	99.39	99.62	99.41	99.68

Table D.2. Pyroxene Analyses

Sample	K2-PYX1	K2-PYX2	K2-PYX3	K2-PYX4	K2-PYX5	K2-PYX6	K2-PYX7	K2-PYX8	K2-PYX9	K2-PYX10	K2-PYX11	K3-PYX1
Analysis	euhedral	euhedral	euhedral	anhedral	anhedral	euhedral	euhedral	euhedral	euhedral	euhedral	euhedral	glomerocryst
Rock Type	rhyolite	rhyolite	rhyolite	rhyolite	rhyolite	rhyolite	rhyolite	rhyolite	rhyolite	rhyolite	rhyolite	andesite
SiO_2	51.54	50.92	51.41	51.68	52.68	52.52	52.14	51.31	52.00	51.74	52.05	52.42
TiO_2	0.08	0.13	0.12	0.28	0.10	0.16	0.10	0.09	0.11	0.12	0.13	0.17
Al_2O_3	0.32	0.49	0.45	1.37	0.56	0.64	0.35	0.51	0.44	0.48	0.45	0.94
FeO	25.12	25.93	24.79	23.22	22.57	22.96	25.64	25.57	24.68	24.54	23.81	8.55
MnO	1.69	1.83	1.65	1.26	1.29	1.31	1.77	1.76	1.60	1.62	1.62	0.49
MgO	19.53	18.85	19.86	21.06	21.78	21.16	19.44	19.13	19.60	19.67	19.89	14.39
CaO	1.00	1.20	1.08	1.09	1.07	1.12	0.98	1.01	1.05	1.10	1.06	21.48
Na_2O	0.00	0.02	0.02	0.28	0.01	0.04	0.06	0.00	0.49	0.11	0.08	0.29
K_2O	0.01	0.00	0.00	0.01	0.02	0.00	0.00	0.02	0.02	0.00	0.03	0.00
Analyses Total	99.29	99.37	99.38	100.25	100.08	99.91	100.48	99.40	99.99	99.38	99.12	99.59
FeO (calculated)	23.74	23.75	22.87	20.25	21.35	22.18	24.33	24.06	21.80	23.22	23.35	7.75
Fe_2O_3 (calculated)	0.86	1.37	1.21	2.63	0.95	0.74	0.91	1.07	2.30	1.04	0.42	1.55
Total	98.77	98.56	98.67	99.91	99.82	99.87	100.08	98.95	99.41	99.10	99.08	99.47
Wo	2.04	2.44	2.19	2.20	2.14	2.26	1.98	2.06	2.15	2.25	2.18	43.74
En	55.32	53.40	55.97	59.18	60.60	59.46	54.71	54.35	55.83	55.96	56.94	40.77
Fs	42.64	44.16	41.84	38.62	37.27	38.28	43.31	43.59	42.02	41.79	40.88	15.49
Wo+En+Fs	100.00	99.85	99.85	97.91	99.93	99.71	99.55	100.00	96.35	99.18	99.40	97.86
Jd	0.00	0.00	0.00	0.00	0.00	0.00	0.00	0.00	0.00	0.00	0.16	0.18
Ae	0.00	0.15	0.15	2.09	0.07	0.30	0.45	0.00	3.65	0.82	0.44	1.96

Sample	K3-PYX2	K3-PYX3	K3-PYX4	K3-PYX5	K3-PYX6	K3-PYX7	K3-PYX8	K3-PYX9	K3-PYX10	K3-PYX11	K3-PYX12	K3-PYX13
Analysis	microphenocryst	microphenocryst	microphenocryst	microphenocryst	microphenocryst	microphenocryst	microphenocryst	microphenocryst	microphenocryst	microphenocryst	microphenocryst	microphenocryst
Rock Type	andesite	andesite	andesite	andesite	andesite	andesite	andesite	andesite	andesite	andesite	andesite	andesite
SiO_2	51.12	52.78	52.88	53.06	53.06	52.35	52.41	51.76	51.76	51.49	51.56	50.78
TiO_2	0.47	0.20	0.18	0.16	0.17	0.15	0.16	0.29	0.31	0.38	0.35	0.54
Al_2O_3	2.11	0.69	0.77	0.64	0.65	0.80	0.90	1.29	1.40	1.53	1.52	2.34
FeO	8.17	19.52	20.00	19.54	19.38	19.93	19.27	8.13	8.56	8.14	8.08	8.83
MnO	0.42	0.82	0.96	0.91	0.82	0.92	0.73	0.43	0.44	0.50	0.43	0.54
MgO	14.66	23.28	23.06	23.36	23.71	22.93	23.39	14.57	14.43	14.60	14.40	14.15
CaO	20.54	1.28	1.21	1.23	1.22	1.15	1.23	21.33	20.99	20.87	21.27	20.38
Na_2O	0.30	0.02	0.03	0.04	0.01	0.02	0.06	0.31	0.26	0.33	0.33	0.37
K_2O	0.01	0.01	0.00	0.02	0.00	0.01	0.02	0.02	0.01	0.00	0.02	0.01
Analyses Total	98.91	99.00	99.58	99.36	99.64	99.01	99.17	99.60	98.98	99.11	99.25	99.45
FeO (calculated)	7.16	19.08	19.51	19.09	18.94	19.32	18.51	6.98	7.78	7.02	6.93	7.45
Fe_2O_3 (calculated)	1.98	0.71	0.85	0.71	0.68	1.02	1.27	2.24	1.47	2.26	2.30	2.67
Total	98.77	98.87	99.45	99.22	99.26	98.67	98.68	99.22	98.85	98.98	99.11	99.23
Wo	42.48	2.57	2.42	2.46	2.42	2.31	2.46	43.33	43.17	42.82	43.61	42.15
En	42.18	65.03	64.20	65.06	65.48	64.05	65.05	41.18	41.30	41.68	41.08	40.72
Fs	15.34	32.40	33.38	32.48	32.10	33.65	32.49	15.48	15.53	15.51	15.31	17.13
Wo+En+Fs	97.74	99.85	99.78	99.71	99.93	99.85	99.56	97.69	98.06	97.53	97.53	97.20
Jd	0.50	0.00	0.01	0.02	0.00	0.00	0.00	0.00	0.39	0.10	0.11	0.36
Ae	1.77	0.14	0.21	0.28	0.07	0.15	0.44	2.31	1.55	2.37	2.36	2.45

Table D.2. Pyroxene Analyses

Sample	K3-PYX14	K3-PYX15	K3-PYX16	K3-PYX17	K3-PYX18	K3-PYX19	K3-PYX20	K3-PYX21	K3-PYX22	K3-PYX23	K3-PYX24	K3-PYX25
Analysis	microphenocryst	microphenocryst	microphenocryst	microphenocryst	microphenocryst	microphenocryst	microphenocryst	euhedral	microphenocryst	microphenocryst	microphenocryst	microphenocryst
Rock Type	andesite	andesite	andesite	andesite	andesite	andesite	andesite	andesite	andesite	andesite	andesite	andesite
SiO_2	51.19	52.42	51.35	51.55	51.20	50.83	51.39	52.49	52.12	51.85	52.54	51.73
TiO_2	0.40	0.17	0.42	0.32	0.43	0.46	0.42	0.24	0.22	0.25	0.21	0.40
Al_2O_3	1.68	0.81	2.00	1.44	1.98	2.27	1.72	0.95	1.03	1.66	0.95	1.60
FeO	8.03	19.37	8.32	8.43	8.10	7.86	8.56	19.69	20.19	19.96	20.50	8.85
MnO	0.48	0.82	0.43	0.50	0.46	0.47	0.46	0.93	1.00	0.89	1.01	0.49
MgO	14.23	23.41	14.50	14.24	14.57	14.56	14.19	23.20	22.57	22.33	22.60	14.41
CaO	21.36	1.22	20.77	21.18	20.72	20.92	20.84	1.21	1.23	1.67	1.19	20.99
Na_2O	0.34	0.03	0.34	0.34	0.32	0.33	0.34	0.02	0.03	0.04	0.00	0.32
K_2O	0.00	0.02	0.01	0.00	0.02	0.01	0.00	0.01	0.01	0.00	0.01	0.01
Analyses Total	99.24	99.29	99.42	99.33	99.00	99.48	98.82	99.57	99.15	99.56	99.41	100.35
FeO (calculated)	6.72	18.71	7.15	7.24	7.01	6.28	7.69	19.04	19.41	18.96	20.03	7.60
Fe_2O_3 (calculated)	2.64	1.02	2.27	2.37	2.16	3.13	1.63	1.06	1.23	1.65	0.74	2.49
Total	99.04	98.64	99.24	99.17	98.86	99.26	98.68	99.16	98.85	99.30	99.28	100.04
Wo	43.79	2.43	42.74	43.39	42.77	42.86	43.24	2.41	2.48	3.37	2.40	42.56
En	40.59	64.87	41.52	40.59	41.85	41.50	40.96	64.40	63.24	62.64	63.28	40.65
Fs	15.62	32.70	15.74	16.02	15.38	15.64	15.81	33.18	34.29	34.00	34.32	16.79
Wo+En+Fs	97.44	99.78	97.45	97.46	97.59	97.50	97.45	99.85	99.78	99.70	100.00	97.62
Jd	0.00	0.00	0.40	0.03	0.40	0.10	0.62	0.00	0.00	0.04	0.00	0.00
Ae	2.56	0.22	2.15	2.52	2.01	2.40	1.93	0.15	0.22	0.26	0.00	2.38

Sample	K3-PYX26	K3-PYX27	K3-PYX28	K3-PYX29	K3-PYX30	K3-PYX31	K3-PYX32	K3-PYX33	K3-PYX34	K3-PYX35	K3-PYX36	K3-PYX37
Analysis	microphenocryst	microphenocryst	microphenocryst	microphenocryst	microphenocryst	microphenocryst	euhedral	euhedral	euhedral	euhedral	euhedral	euhedral
Rock Type	andesite	andesite	andesite	andesite	andesite	andesite	andesite	andesite	andesite	andesite	andesite	andesite
SiO_2	51.78	51.54	51.69	52.00	51.82	52.03	52.65	52.55	52.51	52.53	52.87	52.81
TiO_2	0.33	0.38	0.38	0.27	0.38	0.31	0.18	0.11	0.12	0.19	0.23	0.14
Al_2O_3	1.36	1.68	1.56	1.37	1.70	1.33	0.88	0.44	0.43	0.87	0.97	0.62
FeO	8.80	8.50	8.58	8.54	8.68	8.71	19.81	22.31	22.42	20.04	19.77	19.99
MnO	0.44	0.50	0.50	0.49	0.47	0.44	0.94	1.32	1.30	0.89	0.91	0.89
MgO	14.61	14.30	14.16	14.43	14.20	14.40	23.15	21.49	21.36	23.06	23.22	23.13
CaO	20.85	21.13	21.11	21.17	21.10	20.95	1.18	1.12	1.09	1.11	1.17	1.19
Na_2O	0.29	0.32	0.35	0.30	0.31	0.31	0.03	0.02	0.03	0.03	0.04	0.02
K_2O	0.00	0.01	0.00	0.02	0.02	0.01	0.01	0.00	0.00	0.00	0.01	0.01
Analyses Total	99.83	99.71	99.37	99.67	99.51	99.27	99.50	100.03	99.79	99.47	99.64	99.39
FeO (calculated)	7.68	7.29	7.63	7.54	7.87	7.97	19.12	21.95	22.07	19.41	19.25	19.50
Fe_2O_3 (calculated)	2.17	2.41	1.85	1.96	1.50	1.40	1.10	0.53	0.49	1.03	0.82	0.74
Total	99.51	99.56	99.23	99.55	99.38	99.15	99.24	99.53	99.40	99.11	99.49	99.06
Wo	42.32	43.20	43.47	43.21	43.48	43.08	2.36	2.24	2.19	2.22	2.34	2.38
En	41.26	40.68	40.57	40.99	40.71	41.20	64.39	59.92	59.83	64.15	64.73	64.29
Fs	16.42	16.13	15.97	15.80	15.82	15.72	33.25	37.84	37.98	33.64	32.93	33.33
Wo+En+Fs	97.84	97.61	97.39	97.77	97.69	97.70	99.78	99.85	99.78	99.78	99.71	99.85
Jd	0.00	0.12	0.41	0.21	0.66	0.54	0.00	0.00	0.00	0.00	0.05	0.00
Ae	2.16	2.28	2.20	2.02	1.65	1.76	0.22	0.15	0.22	0.22	0.24	0.15

Table D.2. Pyroxene Analyses

Sample	K3-PYX38	K3-PYX39	K3-PYX40	K3-PYX41	K3-PYX42	K3-PYX43	K3-PYX44	K3-PYX45	K3-PYX46	K3-PYX47	K3-PYX48	K3-PYX49
Analysis	euhedral	microphenocryst	glomerocryst	glomerocryst	glomerocryst	glomerocryst	glomerocryst	glomerocryst	glomerocryst	glomerocryst	glomerocryst	glomerocryst
Rock Type	andesite	andesite	andesite	andesite	andesite	andesite	andesite	andesite	andesite	andesite	andesite	andesite
SiO_2	52.12	52.95	52.43	51.95	52.61	53.11	51.67	51.90	52.22	52.07	51.19	52.15
TiO_2	0.26	0.16	0.20	0.17	0.16	0.12	0.25	0.20	0.21	0.17	0.33	0.19
Al_2O_3	1.45	0.59	0.94	0.98	0.62	0.52	1.09	0.75	1.15	0.99	1.52	1.06
FeO	19.97	20.50	20.70	21.81	20.26	20.70	9.03	21.17	20.52	20.32	8.09	20.82
MnO	0.76	1.00	0.93	1.10	0.98	1.13	0.62	1.11	0.93	0.89	0.47	1.09
MgO	23.12	22.72	22.51	21.57	22.80	22.78	14.21	21.97	22.60	22.75	14.35	22.33
CaO	1.14	1.15	1.17	1.03	1.13	1.03	20.75	1.16	1.08	1.05	21.01	1.08
Na_2O	0.02	0.03	0.05	0.03	0.03	0.05	0.33	0.03	0.03	0.02	0.33	0.04
K_2O	0.00	0.01	0.02	0.01	0.02	0.01	0.00	0.01	0.01	0.00	0.00	0.00
Analyses Total	100.00	99.35	99.74	99.38	99.23	99.93	99.29	99.33	99.55	99.23	98.63	99.68
FeO (calculated)	18.90	20.21	19.95	21.05	19.78	20.24	8.01	20.55	19.66	19.56	6.91	19.98
Fe_2O_3 (calculated)	1.77	0.43	1.20	1.26	0.74	0.71	2.02	0.84	1.44	1.23	2.39	1.37
Total	99.54	99.24	99.40	99.15	98.87	99.70	98.95	98.52	99.33	98.73	98.50	99.29
Wo	2.27	2.31	2.35	2.09	2.27	2.06	42.42	2.33	2.17	2.11	43.31	2.17
En	64.04	63.60	62.78	60.75	63.66	63.29	40.42	61.40	63.16	63.45	41.15	62.33
Fs	33.70	34.09	34.87	37.16	34.08	34.66	17.16	36.27	34.67	34.44	15.54	35.50
Wo+En+Fs	99.85	99.78	99.63	99.78	99.78	99.64	97.54	99.78	99.78	99.85	97.51	99.70
Jd	0.00	0.05	0.00	0.00	0.00	0.00	0.00	0.00	0.00	0.00	0.07	0.00
Ae	0.15	0.17	0.37	0.22	0.22	0.36	2.46	0.22	0.22	0.15	2.41	0.30

Sample	K3-PYX50	K3-PYX51	K3-PYX52	K3-PYX53	K3-PYX54	K4-PYX1	K4-PYX2	K4-PYX3	K4-PYX4	K4-PYX5	K4-PYX6	K4-PYX7
Analysis	glomerocryst	glomerocryst	glomerocryst	euhedral	microphenocryst	anhedral	anhedral	microphenocryst	microphenocryst	microphenocryst	microphenocryst	microphenocryst
Rock Type	andesite	andesite	andesite	andesite	andesite	basaltic andesite	basaltic andesite	basaltic andesite	basaltic andesite	basaltic andesite	basaltic andesite	basaltic andesite
SiO_2	52.51	52.66	52.73	51.37	52.86	51.61	50.76	51.17	51.43	50.83	49.60	50.79
TiO_2	0.18	0.12	0.07	0.39	0.18	0.43	0.54	0.42	0.40	0.44	0.64	0.48
Al_2O_3	0.61	0.58	0.35	1.71	1.20	1.91	2.22	2.06	1.99	2.32	3.78	2.73
FeO	20.70	20.34	20.07	8.52	19.61	8.08	8.18	8.15	7.88	7.52	7.52	8.03
MnO	1.12	1.07	1.24	0.54	0.89	0.31	0.33	0.37	0.30	0.27	0.29	0.35
MgO	22.53	22.77	23.09	14.38	22.32	14.90	14.33	15.25	15.04	14.89	14.18	14.74
CaO	1.03	1.17	1.01	20.99	1.42	20.15	20.73	19.98	20.58	20.81	20.67	20.51
Na_2O	0.04	0.03	0.02	0.37	0.10	0.30	0.35	0.32	0.27	0.32	0.37	0.29
K_2O	0.01	0.01	0.01	0.01	0.03	0.00	0.00	0.01	0.00	0.00	0.00	0.01
Analyses Total	99.45	99.50	99.55	100.40	99.15	99.13	98.74	99.28	98.80	98.95	98.78	99.33
FeO (calculated)	20.23	19.86	19.68	7.20	19.93	7.91	7.00	6.77	7.03	6.09	5.97	6.76
Fe_2O_3 (calculated)	0.70	0.74	0.46	2.79	0.00	1.33	2.28	2.72	1.64	2.78	3.02	2.47
Total	98.97	99.02	98.66	99.75	98.93	98.84	98.55	99.07	98.68	98.74	98.52	99.13
Wo	2.07	2.34	2.00	42.47	2.91	41.67	43.06	40.91	42.46	42.82	43.42	42.33
En	62.85	63.30	63.75	40.48	63.60	42.88	41.42	43.45	43.17	42.63	41.45	42.33
Fs	35.09	34.36	34.25	17.05	33.49	15.45	15.53	15.65	14.37	14.55	15.13	15.35
Wo+En+Fs	99.71	99.78	99.85	97.24	99.26	97.76	97.35	97.59	97.98	97.58	97.14	97.80
Jd	0.00	0.00	0.00	0.00	0.74	0.81	0.44	0.17	0.59	0.27	0.81	0.51
Ae	0.29	0.22	0.15	2.76	0.00	1.43	2.21	2.24	1.44	2.15	2.05	1.69

Table D.2. Pyroxene Analyses

Sample	K4-PYX8	K4-PYX9	K4-PYX10	K4-PYX11	K4-PYX12	K4-PYX13	K4-PYX14	K4-PYX15	K4-PYX16	K4-PYX17	K4-PYX18	K4-PYX19
Analysis	microphenocryst	microphenocryst	anhedral	anhedral	euhedral	euhedral	euhedral	euhedral	microphenocryst	microphenocryst	microphenocryst	microphenocryst
Rock Type	basaltic andesite	basaltic andesite	basaltic andesite	basaltic andesite	basaltic andesite	basaltic andesite	basaltic andesite	basaltic andesite	basaltic andesite	basaltic andesite	basaltic andesite	basaltic andesite
SiO_2	49.86	51.86	53.21	52.49	51.47	51.29	53.40	53.54	51.00	51.14	51.20	51.31
TiO_2	0.52	0.25	0.21	0.24	0.42	0.39	0.19	0.23	0.48	0.45	0.45	0.46
Al_2O_3	3.43	2.28	1.15	2.27	1.97	1.98	1.49	1.17	2.93	2.52	1.80	1.83
FeO	7.65	17.16	16.80	15.51	7.91	7.58	16.01	16.92	6.79	7.23	7.88	8.04
MnO	0.25	0.52	0.52	0.37	0.38	0.27	0.47	0.58	0.24	0.23	0.40	0.40
MgO	14.29	24.26	25.22	25.59	15.12	15.13	25.26	25.47	14.97	15.14	14.79	14.81
CaO	20.76	1.49	1.35	1.57	20.32	20.63	1.43	1.31	20.76	20.76	20.73	20.53
Na_2O	0.33	0.04	0.04	0.04	0.32	0.32	0.08	0.02	0.28	0.31	0.33	0.36
K_2O	0.01	0.01	0.01	0.00	0.01	0.01	0.01	0.01	0.03	0.01	0.00	0.00
Analyses Total	98.87	98.89	99.03	98.93	98.93	98.88	99.23	99.85	99.14	98.98	98.93	99.03
FeO (calculated)	6.07	16.10	16.24	14.60	6.94	6.39	16.15	16.30	6.39	6.18	6.66	6.89
Fe_2O_3 (calculated)	3.10	1.80	0.93	1.54	1.85	2.30	0.47	1.05	1.78	2.09	2.40	2.30
Total	98.62	98.61	98.89	98.71	98.80	98.71	98.95	99.68	98.86	98.83	98.76	98.89
Wo	43.30	3.00	2.68	3.13	41.92	42.43	2.86	2.58	43.13	42.88	42.62	42.29
En	41.48	67.92	69.77	71.05	43.40	43.29	70.28	69.77	43.27	43.52	42.31	42.44
Fs	15.22	29.09	27.55	25.82	14.68	14.28	26.86	27.66	13.60	13.60	15.06	15.27
Wo+En+Fs	97.45	99.70	99.71	99.71	97.60	97.59	99.42	99.86	97.88	97.66	97.52	97.30
Jd	0.60	0.08	0.07	0.10	0.58	0.35	0.37	0.02	0.88	0.67	0.15	0.28
Ae	1.94	0.22	0.22	0.19	1.82	2.06	0.21	0.12	1.24	1.67	2.34	2.42

Sample	K4-PYX20	K4-PYX21	K4-PYX22	K4-PYX23	K4-PYX24	K4-PYX25	K6-PYX1	K6-PYX2	K6-PYX3	K6-PYX4	K6-PYX5	K6-PYX6
Analysis	euhedral	euhedral	euhedral	euhedral	euhedral	euhedral	euhedral	euhedral	euhedral	euhedral	euhedral	euhedral
Rock Type	basaltic andesite	basaltic andesite	basaltic andesite	basaltic andesite	basaltic andesite	basaltic andesite	dacite	dacite	dacite	dacite	dacite	dacite
SiO_2	49.95	53.41	51.81	50.06	50.86	52.36	52.74	53.36	51.13	52.04	51.98	51.95
TiO_2	0.66	0.16	0.49	0.53	0.40	0.24	0.24	0.26	0.59	0.49	0.39	0.40
Al_2O_3	3.50	1.02	2.31	3.18	2.31	2.22	1.01	0.94	2.54	1.78	1.77	1.79
FeO	8.15	16.00	8.87	7.36	7.42	16.40	20.42	19.34	9.26	9.17	8.92	9.04
MnO	0.25	0.44	0.32	0.27	0.27	0.45	0.92	0.90	0.44	0.43	0.46	0.41
MgO	14.46	25.91	14.53	14.75	14.78	24.64	23.09	23.58	14.48	14.57	14.65	14.91
CaO	20.14	1.42	20.61	20.78	20.78	1.64	1.30	1.24	20.82	21.24	21.17	20.82
Na_2O	0.30	0.02	0.00	0.24	0.36	0.14	0.03	0.01	0.32	0.32	0.34	0.31
K_2O	0.01	0.00	0.01	0.01	0.02	0.02	0.02	0.00	0.02	0.00	0.00	0.01
Analyses Total	98.77	99.01	99.19	98.85	98.71	99.06	99.77	99.63	99.60	100.04	99.68	99.64
FeO (calculated)	6.92	15.33	9.00	5.87	6.11	15.43	19.18	19.25	7.09	7.50	7.13	7.26
Fe_2O_3 (calculated)	2.35	1.15	0.00	2.94	2.67	1.67	1.21	0.00	2.24	1.77	1.87	1.87
Total	98.53	98.86	99.08	98.63	98.56	98.81	99.74	99.54	99.68	100.14	99.76	99.73
Wo	42.24	2.80	42.80	43.00	43.01	3.30	2.60	2.49	42.89	43.34	43.31	42.54
En	42.20	71.09	41.98	42.47	42.57	69.00	64.14	65.81	41.50	41.36	41.70	42.39
Fs	15.56	26.11	15.22	14.53	14.42	27.70	33.27	31.71	15.61	15.30	14.99	15.08
Wo+En+Fs	97.69	99.86	100.00	98.16	97.27	98.97	99.78	99.93	97.59	97.63	97.48	97.70
Jd	0.79	0.01	0.00	0.38	0.45	0.34	0.00	0.07	0.55	0.46	0.53	0.46
Ae	1.51	0.14	0.00	1.47	2.29	0.69	0.22	0.00	1.86	1.91	2.00	1.84

Table D.2. Pyroxene Analyses

Sample	K6-PYX7	K6-PYX8	K6-PYX9	K6-PYX10	K6-PYX11	K6-PYX12	K6-PYX13	K6-PYX14	K6-PYX15	K6-PYX16	K6-PYX17	K6-PYX18
Analysis	euhedral	euhedral	euhedral	euhedral	euhedral	euhedral	euhedral	euhedral	microphenocryst	euhedral	euhedral	euhedral
Rock Type	dacite	dacite	dacite	basaltic andesite	dacite	dacite	dacite	dacite	basaltic andesite	basaltic andesite	basaltic andesite	basaltic andesite
SiO_2	53.22	51.82	49.04	52.59	52.33	51.82	54.27	53.39	51.08	51.45	53.26	52.75
TiO_2	0.20	0.42	0.96	0.31	0.25	0.37	0.19	0.26	0.52	0.43	0.17	0.24
Al_2O_3	1.20	1.58	5.36	1.37	1.10	1.71	1.02	1.85	2.77	2.12	1.26	1.26
FeO	18.77	8.76	8.63	9.08	9.90	9.17	16.34	16.95	8.77	9.18	16.74	17.23
MnO	0.63	0.43	0.24	0.46	0.59	0.47	0.45	0.49	0.32	0.45	0.49	0.64
MgO	23.99	14.50	14.19	14.64	13.88	14.87	26.24	25.74	15.25	14.36	25.82	25.24
CaO	1.60	21.52	20.91	21.21	20.76	20.17	1.36	1.34	21.18	21.34	1.32	1.30
Na_2O	0.02	0.30	0.27	0.27	0.32	0.31	0.03	0.02	0.27	0.37	0.04	0.02
K_2O	0.00	0.00	0.00	0.02	0.00	0.01	0.01	0.00	0.00	0.01	0.00	0.00
Analyses Total	99.63	99.36	99.60	99.95	99.13	98.90	99.91	100.04	100.16	99.71	99.11	98.68
FeO (calculated)	18.15	6.99	5.78	8.06	9.33	7.94	15.84	15.72	5.55	6.66	15.29	15.75
Fe_2O_3 (calculated)	0.54	1.86	2.88	1.06	0.56	1.26	0.47	1.16	3.39	2.63	1.44	1.46
Total	99.55	99.45	99.64	99.99	99.12	98.93	99.89	99.97	100.33	99.83	99.10	98.66
Wo	3.19	44.00	43.95	43.26	43.01	41.68	2.67	2.64	42.79	43.69	2.60	2.58
En	66.59	41.33	41.50	41.55	40.01	42.76	71.62	70.54	42.87	40.91	70.87	69.72
Fs	30.22	14.67	14.56	15.20	16.98	15.56	25.72	26.82	14.34	15.40	26.53	27.70
Wo+En+Fs	99.86	97.77	97.90	98.02	97.64	97.69	99.79	99.86	97.97	97.23	99.71	99.85
Jd	0.07	0.26	0.86	0.71	1.32	0.83	0.10	0.05	0.14	0.34	0.03	0.00
Ae	0.08	1.97	1.24	1.28	1.04	1.47	0.11	0.10	1.89	2.43	0.27	0.14

Sample	K6-PYX19	K6-PYX20	K6-PYX21	K6-PYX22	K6-PYX23	K6-PYX24	K6-PYX25	K6-PYX26	K6-PYX27	K6-PYX28	K6-PYX29	K6-PYX30
Analysis	euhedral	euhedral	anhedral	anhedral	anhedral	anhedral	euhedral	euhedral	anhedral	anhedral	microphenocryst	microphenocryst
Rock Type	basaltic andesite	basaltic andesite	basaltic andesite	basaltic andesite	basaltic andesite	basaltic andesite	basaltic andesite	basaltic andesite	basaltic andesite	basaltic andesite	basaltic andesite	basaltic andesite
SiO_2	52.12	51.06	53.98	53.84	52.13	54.15	51.84	51.91	54.15	53.80	52.09	51.30
TiO_2	0.28	0.55	0.16	0.19	0.16	0.10	0.49	0.49	0.15	0.19	0.31	0.42
Al_2O_3	2.40	2.82	0.78	1.02	2.76	0.50	2.01	2.06	1.02	1.18	1.49	1.64
FeO	18.21	9.00	17.29	17.13	18.68	17.57	8.90	9.02	16.40	15.79	8.96	9.14
MnO	0.55	0.30	0.89	0.80	0.73	0.82	0.41	0.48	0.55	0.41	0.49	0.46
MgO	24.18	14.73	25.01	25.49	24.16	25.89	14.92	14.57	25.96	26.29	14.34	14.55
CaO	1.56	20.51	1.15	1.05	0.66	0.62	20.78	20.79	1.47	1.43	21.26	20.95
Na_2O	0.03	0.28	0.04	0.02	0.03	0.01	0.31	0.34	0.07	0.03	0.34	0.36
K_2O	0.02	0.01	0.00	0.01	0.00	0.00	0.01	0.02	0.01	0.02	0.00	0.01
Analyses Total	99.35	99.26	99.30	99.55	99.31	99.66	99.67	99.68	99.78	99.14	99.28	98.83
FeO (calculated)	16.51	7.28	17.23	16.75	17.48	16.95	7.26	7.70	15.73	15.08	7.61	6.68
Fe_2O_3 (calculated)	1.64	1.75	0.00	0.33	1.07	0.62	1.73	1.34	0.65	0.65	1.37	2.58
Total	99.29	99.29	99.24	99.50	99.18	99.66	99.76	99.70	99.77	99.09	99.30	98.95
Wo	3.13	42.49	2.29	2.08	1.34	1.22	42.57	42.88	2.89	2.82	43.75	43.03
En	67.49	42.46	69.39	70.20	68.00	70.63	42.53	41.81	71.07	72.21	41.06	41.58
Fs	29.38	15.05	28.32	27.72	30.66	28.16	14.90	15.30	26.04	24.97	15.19	15.40
Wo+En+Fs	99.78	97.89	99.71	99.86	99.78	99.93	97.70	97.48	99.50	99.78	97.48	97.29
Jd	0.07	0.82	0.29	0.09	0.13	0.00	0.60	0.99	0.20	0.09	0.75	0.02
Ae	0.15	1.29	0.00	0.06	0.09	0.07	1.70	1.53	0.30	0.13	1.77	2.68

Table D.2. Pyroxene Analyses

Sample	K6-PYX31	K6-PYX32	K6-PYX33	K6-PYX34	K6-PYX35	K6-PYX36	K6-PYX37	K6-PYX38	K6-PYX39	K6-PYX40	K6-PYX41	K6-PYX42
Analysis	microphenocryst	euhedral	euhedral	euhedral	euhedral	euhedral	euhedral	euhedral	euhedral	microphenocryst	microphenocryst	microphenocryst
Rock Type	basaltic andesite	basaltic andesite	basaltic andesite	basaltic andesite	basaltic andesite	basaltic andesite	basaltic andesite	basaltic andesite	basaltic andesite	basaltic andesite	basaltic andesite	basaltic andesite
SiO_2	51.63	52.88	52.90	52.94	52.76	51.13	50.56	51.69	51.49	51.34	52.70	51.90
TiO_2	0.68	0.15	0.33	0.18	0.11	0.48	0.50	0.47	0.43	0.15	0.29	0.27
Al_2O_3	4.48	0.49	0.80	0.63	0.41	2.55	2.98	1.98	1.96	0.66	1.23	1.21
FeO	8.05	22.15	19.58	19.97	20.57	8.31	8.68	8.24	8.51	25.66	9.16	9.12
MnO	0.24	1.37	0.89	1.03	1.10	0.29	0.31	0.39	0.41	1.86	0.55	0.57
MgO	13.69	21.65	23.90	23.28	22.75	14.57	14.82	15.03	14.80	18.48	14.44	14.33
CaO	20.05	1.04	1.24	1.12	1.16	21.15	20.97	21.22	21.02	1.07	21.36	21.36
Na_2O	0.32	0.02	0.02	0.03	0.04	0.26	0.29	0.31	0.33	0.00	0.33	0.00
K_2O	0.05	0.00	0.01	0.00	0.02	0.01	0.02	0.00	0.00	0.01	0.00	0.00
Analyses Total	99.19	99.75	99.67	99.18	98.92	98.75	99.13	99.33	98.95	99.23	100.06	98.76
FeO (calculated)	7.96	21.91	18.22	19.26	19.69	6.88	5.81	6.33	6.61	25.20	8.03	8.75
Fe_2O_3 (calculated)	0.00	0.21	1.00	0.67	0.71	1.47	3.00	1.97	1.96	0.41	1.17	0.31
Total	99.10	99.72	99.31	99.15	98.75	98.78	99.26	99.39	99.02	99.18	100.10	98.70
Wo	44.00	2.10	2.46	2.24	2.33	43.94	43.14	43.42	43.27	2.22	43.56	43.71
En	41.80	60.81	65.88	64.90	63.64	42.11	42.42	42.79	42.39	53.26	40.97	40.80
Fs	14.20	37.09	31.67	32.86	34.03	13.95	14.44	13.79	14.34	44.53	15.47	15.49
Wo+En+Fs	97.52	99.85	99.85	99.78	99.71	98.04	97.79	97.69	97.53	100.00	97.58	100.00
Jd	2.48	0.06	0.00	0.00	0.00	0.84	0.40	0.44	0.51	0.00	0.72	0.00
Ae	0.00	0.08	0.15	0.22	0.29	1.12	1.81	1.87	1.96	0.00	1.70	0.00

Sample	K6-PYX43	K6-PYX44	K6-PYX45	K6-PYX46	K6-PYX47	K6-PYX48	K6-PYX49	K6-PYX50	K6-PYX51	K6-PYX52	K6-PYX53	K6-PYX54
Analysis	microphenocryst	microphenocryst	microphenocryst	microphenocryst	microphenocryst	microphenocryst	microphenocryst	euhedral	euhedral	microphenocryst	microphenocryst	microphenocryst
Rock Type	basaltic andesite	basaltic andesite	basaltic andesite	basaltic andesite	basaltic andesite	basaltic andesite	basaltic andesite	basaltic andesite	basaltic andesite	basaltic andesite	basaltic andesite	basaltic andesite
SiO_2	51.55	51.62	52.00	52.17	52.01	50.88	53.33	53.61	53.42	51.63	51.51	51.77
TiO_2	0.43	0.42	0.44	0.40	0.41	0.55	0.21	0.26	0.25	0.47	0.44	0.46
Al_2O_3	2.07	2.05	1.66	1.38	1.57	2.52	1.51	1.26	2.53	2.36	2.11	1.97
FeO	8.17	8.29	8.50	8.86	8.94	8.63	16.73	17.43	16.35	8.47	8.42	9.52
MnO	0.32	0.39	0.38	0.47	0.47	0.32	0.59	0.73	0.63	0.34	0.36	0.46
MgO	14.75	14.68	14.70	14.73	15.42	15.11	25.16	24.78	23.13	15.01	15.15	14.39
CaO	21.64	21.33	21.09	20.86	20.13	20.47	1.48	1.32	2.21	20.83	21.01	20.72
Na_2O	0.30	0.30	0.33	0.31	0.29	0.27	0.02	0.07	0.19	0.33	0.28	0.32
K_2O	0.00	0.00	0.01	0.01	0.01	0.02	0.01	0.01	0.02	0.01	0.02	0.00
Analyses Total	99.23	99.08	99.11	99.19	99.25	98.77	99.04	99.47	98.73	99.45	99.30	99.61
FeO (calculated)	6.22	6.75	7.33	7.75	7.35	6.47	16.39	17.30	16.26	6.71	6.26	8.09
Fe_2O_3 (calculated)	2.04	1.61	1.19	1.16	1.65	2.27	0.25	0.04	0.00	1.79	2.28	1.48
Total	99.32	99.16	99.14	99.24	99.31	98.88	98.96	99.38	98.64	99.49	99.43	99.66
Wo	44.35	43.95	43.50	42.88	41.14	42.22	2.96	2.64	4.64	42.87	42.93	42.69
En	42.06	42.09	42.19	42.13	43.84	43.36	70.00	68.98	67.54	42.98	43.07	41.25
Fs	13.59	13.97	14.31	14.98	15.02	14.42	27.04	28.38	27.83	14.16	14.01	16.06
Wo+En+Fs	97.76	97.76	97.55	97.71	97.85	97.96	99.86	99.50	98.58	97.54	97.90	97.62
Jd	0.46	0.71	0.89	0.70	0.38	0.43	0.11	0.48	1.42	0.80	0.33	0.79
Ae	1.78	1.53	1.56	1.59	1.77	1.61	0.03	0.03	0.00	1.66	1.76	1.59

Table D.2. Pyroxene Analyses

Sample	K6-PYX55	K6-PYX56	K6-PYX57	K6-PYX58	K6-PYX59	K6-PYX60	K6-PYX61	K6-PYX62	K6-PYX63	K6-PYX64	K6-PYX65	K6-PYX66
Analysis	anhedral	euhedral	euhedral	euhedral	microphenocryst	microphenocryst	microphenocryst	anhedral	microphenocryst	anhedral	anhedral	microphenocryst
Rock Type	basaltic andesite	basaltic andesite	basaltic andesite	basaltic andesite	basaltic andesite	basaltic andesite	basaltic andesite	basaltic andesite	basaltic andesite	basaltic andesite	basaltic andesite	basaltic andesite
SiO_2	51.00	49.95	51.51	48.82	51.85	52.09	51.71	53.52	51.32	51.27	51.86	51.93
TiO_2	0.51	0.70	0.47	0.80	0.48	0.35	0.43	0.21	0.58	0.44	0.30	0.37
Al_2O_3	3.19	4.66	2.67	4.88	2.38	1.89	2.19	0.68	2.60	2.80	1.62	1.60
FeO	7.77	7.78	8.02	8.68	8.38	19.18	18.86	19.45	8.91	7.89	9.03	9.46
MnO	0.24	0.23	0.27	0.27	0.28	0.78	0.70	0.89	0.43	0.24	0.37	0.56
MgO	15.14	14.74	15.24	13.88	14.94	22.52	22.62	23.90	14.73	15.35	14.11	14.58
CaO	21.15	20.89	21.05	21.20	21.09	2.06	2.30	1.25	20.95	21.12	21.69	20.72
Na_2O	0.24	0.29	0.27	0.30	0.32	0.04	0.05	0.04	0.36	0.26	0.32	0.33
K_2O	0.00	0.01	0.00	0.00	0.00	0.00	0.00	0.00	0.00	0.01	0.00	0.01
Analyses Total	99.24	99.25	99.50	98.83	99.72	98.91	98.86	99.94	99.88	99.38	99.30	99.56
FeO (calculated)	5.91	5.59	6.28	5.39	6.93	18.70	17.82	18.80	6.59	5.70	7.38	7.69
Fe_2O_3 (calculated)	1.93	2.23	1.80	3.38	1.48	0.35	0.92	0.61	2.43	2.25	1.68	1.86
Total	99.31	99.29	99.56	98.92	99.75	98.79	98.74	99.90	99.98	99.44	99.33	99.65
Wo	43.64	43.84	43.20	44.63	43.36	4.21	4.69	2.48	42.98	43.26	44.57	42.43
En	43.46	43.04	43.52	40.66	42.74	63.97	64.17	65.99	42.05	43.74	40.34	41.54
Fs	12.90	13.13	13.29	14.71	13.90	31.82	31.14	31.53	14.97	13.00	15.09	16.03
Wo+En+Fs	98.19	97.77	97.98	97.65	97.62	99.70	99.63	99.71	97.30	98.05	97.62	97.55
Jd	0.73	1.09	0.73	0.76	0.97	0.22	0.18	0.03	0.59	0.56	0.56	0.41
Ae	1.08	1.14	1.29	1.60	1.41	0.08	0.19	0.26	2.11	1.39	1.83	2.05

Sample	K6-PYX67	K6-PYX68	K6-PYX69	K6-PYX70	K6-PYX71	K6-PYX72	K6-PYX73	K6-PYX74	K6-PYX75	K6-PYX76	K6-PYX77	K6-PYX78
Analysis	euhedral	euhedral	anhedral	microphenocryst	microphenocryst	microphenocryst	anhedral	euhedral	euhedral	euhedral	euhedral	microphenocryst
Rock Type	basaltic andesite	basaltic andesite	basaltic andesite	basaltic andesite	basaltic andesite	basaltic andesite	basaltic andesite	basaltic andesite	basaltic andesite	basaltic andesite	basaltic andesite	basaltic andesite
SiO_2	52.05	51.26	51.73	51.25	51.30	51.85	51.33	51.88	51.97	51.02	51.69	51.44
TiO_2	0.42	0.56	0.48	0.51	0.44	0.41	0.45	0.45	0.44	0.58	0.50	0.51
Al_2O_3	1.67	2.25	2.08	2.47	2.28	1.82	2.47	1.81	1.88	2.64	2.32	2.14
FeO	8.96	9.34	8.72	9.09	9.02	8.88	9.03	8.77	8.76	8.82	8.58	8.85
MnO	0.48	0.43	0.35	0.45	0.38	0.42	0.42	0.43	0.39	0.38	0.35	0.39
MgO	14.70	14.71	14.94	14.74	14.80	14.73	14.46	14.92	14.79	14.52	14.91	14.81
CaO	20.88	20.80	20.84	20.60	20.39	20.72	20.99	21.07	20.95	21.12	20.75	20.96
Na_2O	0.35	0.29	0.34	0.32	0.33	0.34	0.36	0.35	0.36	0.32	0.30	0.34
K_2O	0.02	0.00	0.01	0.00	0.00	0.01	0.00	0.01	0.03	0.01	0.00	0.00
Analyses Total	99.53	99.64	99.49	99.43	98.94	99.18	99.51	99.69	99.57	99.41	99.40	99.44
FeO (calculated)	7.41	7.07	6.90	7.03	7.20	7.45	6.94	6.66	7.10	6.58	7.28	6.67
Fe_2O_3 (calculated)	1.62	2.39	1.87	2.14	1.85	1.47	2.17	2.19	1.73	2.31	1.34	2.28
Total	99.60	99.76	99.54	99.51	98.97	99.23	99.59	99.77	99.64	99.48	99.44	99.54
Wo	42.87	42.54	42.78	42.42	42.20	42.74	43.29	42.99	43.04	43.54	42.81	42.97
En	41.99	41.86	42.68	42.24	42.61	42.28	41.49	42.35	42.28	41.65	42.80	42.24
Fs	15.14	15.61	14.54	15.34	15.19	14.98	15.22	14.66	14.68	14.81	14.39	14.79
Wo+En+Fs	97.41	97.82	97.47	97.60	97.52	97.47	97.30	97.40	97.33	97.59	97.77	97.46
Jd	0.65	0.28	0.63	0.62	0.75	0.82	0.74	0.32	0.72	0.57	0.96	0.40
Ae	1.95	1.90	1.90	1.79	1.72	1.71	1.97	2.28	1.96	1.85	1.28	2.15

Table D.2. Pyroxene Analyses

Sample	K6-PYX79	K6-PYX80	K6-PYX81	K6-PYX82	K6-PYX83	K6-PYX84	K6-PYX85	K6-PYX86	K6-PYX87	K6-PYX88	K6-PYX89	K6-PYX90
Analysis	microphenocryst	microphenocryst	anhedral	anhedral	euhedral	euhedral	euhedral	euhedral	microphenocryst	microphenocryst	microphenocryst	euhedral
Rock Type	basaltic andesite	basaltic andesite	basaltic andesite	basaltic andesite	basaltic andesite	basaltic andesite	basaltic andesite	basaltic andesite	basaltic andesite	basaltic andesite	basaltic andesite	dacite
SiO_2	50.80	51.92	51.45	51.28	51.47	51.43	51.80	51.84	51.80	53.30	51.95	52.46
TiO_2	0.66	0.45	0.51	0.51	0.40	0.33	0.50	0.46	0.32	0.22	0.37	0.08
Al_2O_3	2.88	1.79	2.20	2.40	2.04	1.84	2.06	1.91	2.31	1.44	1.98	0.26
FeO	9.54	8.74	9.00	8.84	10.52	9.94	8.76	8.86	19.56	18.37	20.11	24.05
MnO	0.44	0.42	0.37	0.36	0.65	0.62	0.41	0.43	0.81	0.66	0.87	1.68
MgO	14.25	14.88	14.45	14.72	13.97	13.94	14.75	14.62	23.62	24.75	21.56	19.37
CaO	20.81	21.00	20.60	20.88	20.27	20.84	20.83	20.75	1.30	1.29	1.89	1.03
Na_2O	0.36	0.32	0.36	0.31	0.38	0.00	0.36	0.39	0.02	0.00	0.00	0.00
K_2O	0.01	0.00	0.00	0.00	0.01	0.02	0.01	0.00	0.00	0.02	0.01	0.01
Analyses Total	99.75	99.52	98.94	99.30	99.71	98.96	99.48	99.26	99.74	100.05	99.74	98.94
FeO (calculated)	6.99	7.07	7.70	6.91	8.47	9.47	7.22	7.42	17.29	17.29	18.71	24.09
Fe_2O_3 (calculated)	2.62	1.73	1.33	2.03	2.10	0.42	1.58	1.47	2.20	1.05	1.31	0.00
Total	99.82	99.57	98.97	99.40	99.76	98.91	99.52	99.30	99.67	100.01	99.65	98.98
Wo	42.97	42.98	42.90	43.01	41.85	42.98	42.94	42.92	2.60	2.55	3.81	2.14
En	40.94	42.38	41.87	42.19	40.13	40.00	42.30	42.08	65.63	68.07	63.20	56.05
Fs	16.09	14.64	15.24	14.80	18.02	17.01	14.76	15.01	31.77	29.38	32.99	41.81
Wo+En+Fs	97.28	97.63	97.31	97.67	97.15	100.00	97.32	97.10	99.85	100.00	100.00	100.00
Jd	0.58	0.51	1.15	0.62	0.64	0.00	0.86	1.00	0.02	0.00	0.00	0.00
Ae	2.14	1.87	1.54	1.71	2.21	0.00	1.81	1.90	0.13	0.00	0.00	0.00

Sample	K6-PYX91	K6-PYX92	K6-PYX93	K6-PYX94	K6-PYX95	K6-PYX96	K9-PYX1	K9-PYX2	K9-PYX3	K9-PYX4	K9-PYX5	K9-PYX6
Analysis	euhedral	euhedral	euhedral	microphenocryst	microphenocryst	euhedral	euhedral	euhedral	microphenocryst	microphenocryst	euhedral	euhedral
Rock Type	dacite	dacite	dacite	dacite	dacite	basaltic andesite	rhyolite	rhyolite	rhyolite	rhyolite	rhyolite	rhyolite
SiO_2	51.92	53.42	52.96	54.15	51.38	52.41	52.79	52.41	52.13	52.27	51.60	52.59
TiO_2	0.11	0.26	0.29	0.24	0.53	0.18	0.16	0.14	0.14	0.16	0.10	0.10
Al_2O_3	0.31	0.89	1.54	1.05	2.40	1.83	0.58	0.55	0.58	0.79	0.40	0.26
FeO	24.31	18.57	18.47	16.38	8.71	16.72	21.56	22.49	22.36	21.70	25.81	24.64
MnO	1.61	0.86	0.80	0.61	0.37	0.62	1.21	1.25	1.21	1.08	1.78	1.62
MgO	19.79	23.69	23.75	25.20	14.59	25.40	22.37	21.58	21.30	22.18	18.88	19.28
CaO	1.03	1.24	1.37	1.34	20.65	1.33	1.09	1.04	1.05	1.10	1.01	1.06
Na_2O	0.18	0.02	0.03	0.05	0.35	0.02	0.03	0.03	0.01	0.00	0.04	0.03
K_2O	0.00	0.00	0.00	0.00	0.02	0.01	0.00	0.00	0.00	0.00	0.01	0.01
Analyses Total	99.26	98.95	99.21	99.02	99.00	98.52	99.79	99.49	98.78	99.28	99.63	99.59
FeO (calculated)	22.98	18.53	18.36	16.34	7.30	14.92	20.53	21.48	21.78	20.49	24.70	24.66
Fe_2O_3 (calculated)	1.01	0.00	0.00	0.00	1.43	1.78	0.85	0.81	0.52	1.06	0.83	0.00
Total	98.94	98.91	99.10	98.98	99.03	98.50	99.62	99.29	98.72	99.13	99.35	99.61
Wo	2.11	2.51	2.77	2.70	42.98	2.65	2.18	2.10	2.14	2.21	2.07	2.19
En	56.41	66.76	66.81	70.59	42.26	70.38	62.25	60.53	60.36	62.03	53.80	55.43
Fs	41.48	30.73	30.42	26.71	14.76	26.97	35.57	37.38	37.50	35.76	44.14	42.38
Wo+En+Fs	98.66	99.85	99.78	99.64	97.38	99.85	99.78	99.78	99.93	100.00	99.70	99.78
Jd	0.00	0.15	0.22	0.36	1.12	0.03	0.00	0.00	0.01	0.00	0.00	0.22
Ae	1.34	0.00	0.00	0.00	1.50	0.12	0.22	0.22	0.07	0.00	0.30	0.00

Table D.2. Pyroxene Analyses

Sample	K9-PYX7	K9-PYX8	K9-PYX9	K9-PYX10	K9-PYX11	K9-PYX12	K9-PYX13	K12L-PYX1	K12L-PYX2	K12L-PYX3	K12L-PYX4	K12L-PYX5
Analysis	euhedral	euhedral	microphenocryst	euhedral	euhedral	euhedral	euhedral	microphenocryst	microphenocryst	microphenocryst	euhedral	euhedral
Rock Type	rhyolite	rhyolite	rhyolite	rhyolite	rhyolite	rhyolite	rhyolite	andesite	andesite	andesite	andesite	andesite
SiO_2	51.90	52.00	53.08	51.52	51.14	51.96	51.87	50.60	53.37	51.02	51.77	51.20
TiO_2	0.02	0.21	0.15	0.11	0.12	0.14	0.10	0.46	0.17	0.49	0.42	0.49
Al_2O_3	0.27	0.88	0.55	0.48	0.36	0.47	0.45	3.08	0.84	2.91	2.34	2.57
FeO	24.76	22.82	20.86	26.14	26.41	25.12	25.15	8.43	19.04	8.49	8.35	8.33
MnO	1.68	1.23	1.10	1.81	1.82	1.66	1.59	0.26	0.92	0.26	0.29	0.26
MgO	19.43	21.13	22.78	18.37	18.63	19.53	19.79	14.82	24.03	14.88	15.54	15.15
CaO	1.06	1.18	1.23	1.06	0.96	1.04	1.05	21.15	1.23	21.17	20.78	21.04
Na_2O	0.03	0.04	0.02	0.03	0.01	0.02	0.03	0.28	0.03	0.27	0.24	0.26
K_2O	0.01	0.01	0.01	0.00	0.01	0.00	0.01	0.01	0.02	0.02	0.00	0.01
Analyses Total	99.16	99.50	99.78	99.52	99.46	99.94	100.04	99.09	99.65	99.51	99.73	99.32
FeO (calculated)	24.14	21.59	20.10	25.52	24.75	24.22	23.58	5.72	18.34	6.13	6.46	6.10
Fe_2O_3 (calculated)	0.55	1.12	0.68	0.55	1.03	0.70	1.08	2.83	0.68	2.46	1.94	2.32
Total	99.10	99.39	99.70	99.45	98.83	99.74	99.55	99.20	99.63	99.60	99.78	99.41
Wo	2.17	2.39	2.46	2.19	1.96	2.12	2.12	43.56	2.45	43.47	42.28	43.08
En	55.46	59.56	63.29	52.75	52.97	55.31	55.66	42.47	66.53	42.51	43.99	43.19
Fs	42.37	38.05	34.25	45.06	45.07	42.58	42.22	13.98	31.02	14.03	13.73	13.73
Wo+En+Fs	99.78	99.70	99.85	99.78	99.92	99.85	99.78	97.87	99.78	97.96	98.21	98.04
Jd	0.00	0.00	0.00	0.01	0.00	0.00	0.00	0.49	0.05	0.54	0.48	0.43
Ae	0.22	0.30	0.15	0.22	0.08	0.15	0.22	1.64	0.17	1.50	1.31	1.52

Sample	K12L-PYX6	K12L-PYX7	K12L-PYX8	K12L-PYX9	K12L-PYX10	K12L-PYX11	K12L-PYX12	K12L-PYX13	K12L-PYX14	K12L-PYX15	K12L-PYX16	K12L-PYX17
Analysis	euhedral	euhedral	euhedral	euhedral	euhedral	euhedral	euhedral	euhedral	microphenocryst	microphenocryst	microphenocryst	microphenocryst
Rock Type	andesite	andesite	andesite	andesite	andesite	andesite	andesite	andesite	andesite	andesite	andesite	andesite
SiO_2	51.57	51.63	51.63	51.34	51.78	51.85	53.66	53.05	53.31	53.30	51.58	50.83
TiO_2	0.47	0.44	0.48	0.57	0.44	0.48	0.22	0.25	0.15	0.26	0.47	0.48
Al_2O_3	2.10	1.77	2.38	2.56	2.06	1.81	1.07	1.31	0.91	0.97	2.37	3.04
FeO	8.76	8.67	8.42	9.22	9.02	8.65	18.14	18.79	19.44	19.28	8.42	8.44
MnO	0.40	0.45	0.33	0.39	0.41	0.41	0.66	0.74	0.80	0.81	0.27	0.23
MgO	15.10	14.82	15.19	14.35	15.12	14.85	24.92	24.29	23.95	24.17	15.15	14.86
CaO	20.84	21.22	20.91	20.75	20.58	21.09	1.46	1.33	1.38	1.32	21.11	21.02
Na_2O	0.26	0.33	0.31	0.36	0.30	0.31	0.03	0.03	0.03	0.03	0.27	0.28
K_2O	0.00	0.00	0.00	0.00	0.00	0.01	0.00	0.01	0.00	0.01	0.01	0.01
Analyses Total	99.50	99.33	99.65	99.54	99.71	99.46	100.16	99.80	99.97	100.15	99.65	99.19
FeO (calculated)	6.78	6.45	6.44	7.57	7.11	7.00	17.15	17.59	18.37	18.08	6.41	6.14
Fe_2O_3 (calculated)	2.08	2.32	2.05	1.68	2.01	1.72	0.98	1.15	1.08	1.15	2.12	2.41
Total	99.59	99.42	99.72	99.57	99.81	99.53	100.14	99.74	99.97	100.10	99.75	99.30
Wo	42.53	43.34	42.78	43.03	42.02	43.19	2.87	2.64	2.73	2.61	43.10	43.37
En	42.87	42.11	43.24	41.41	42.95	42.32	68.24	67.09	65.98	66.41	43.04	42.66
Fs	14.60	14.55	13.98	15.56	15.04	14.49	28.89	30.27	31.29	30.98	13.86	13.97
Wo+En+Fs	98.06	97.54	97.69	97.30	97.77	97.70	99.78	99.78	99.78	99.78	97.98	97.88
Jd	0.34	0.18	0.60	1.02	0.47	0.48	0.03	0.04	0.01	0.00	0.48	0.63
Ae	1.60	2.28	1.71	1.68	1.76	1.83	0.18	0.18	0.21	0.22	1.54	1.49

Table D.2. Pyroxene Analyses

Sample	K12L-PYX18	K12L-PYX19	K12L-PYX20	K12L-PYX21	K12L-PYX22	K12L-PYX23	K12L-PYX24	K12L-PYX25	K12L-PYX26	K12L-PYX27	K12L-PYX28	K12L-PYX29
Analysis	microphenocryst	euhedral	euhedral	euhedral	euhedral	euhedral	euhedral	microphenocryst	euhedral	euhedral	anhedral	euhedral
Rock Type	andesite	andesite	andesite	andesite	andesite	andesite	andesite	andesite	andesite	andesite	andesite	andesite
SiO_2	51.44	53.46	54.24	51.70	51.44	52.29	51.93	51.63	51.47	52.21	51.53	52.02
TiO_2	0.46	0.21	0.18	0.41	0.51	0.22	0.53	0.45	0.45	0.48	0.48	0.33
Al_2O_3	2.42	1.35	1.12	2.27	2.36	1.10	1.94	2.31	2.43	1.80	2.27	1.70
FeO	8.38	17.19	16.73	8.20	8.43	9.70	9.19	8.61	9.24	8.96	8.83	9.33
MnO	0.27	0.57	0.50	0.31	0.31	0.63	0.36	0.33	0.30	0.45	0.35	0.49
MgO	15.17	25.54	26.02	15.43	15.06	14.49	14.68	15.16	15.88	14.93	14.92	14.90
CaO	21.13	1.37	1.50	20.85	21.08	20.97	21.09	20.61	20.92	20.85	21.02	20.79
Na_2O	0.27	0.02	0.02	0.26	0.28	0.33	0.33	0.28	0.30	0.31	0.29	0.31
K_2O	0.01	0.00	0.00	0.01	0.00	0.00	0.01	0.02	0.01	0.01	0.02	0.00
Analyses Total	99.55	99.71	100.31	99.44	99.47	99.73	100.06	99.40	100.00	100.00	99.71	99.87
FeO (calculated)	6.15	16.03	16.03	6.35	6.43	7.79	7.37	6.93	6.79	7.55	6.68	7.27
Fe_2O_3 (calculated)	2.32	1.12	0.66	1.94	2.11	2.01	1.91	1.72	2.54	1.49	2.25	2.15
Total	99.64	99.67	100.26	99.52	99.58	99.83	100.15	99.45	100.08	100.07	99.82	99.96
Wo	43.13	2.70	2.93	42.58	43.14	42.62	43.06	42.33	42.63	42.58	42.94	42.26
En	43.08	69.99	70.77	43.85	42.89	40.98	41.71	43.33	42.19	42.42	42.41	42.15
Fs	13.79	27.31	26.30	13.57	13.97	16.40	15.23	14.34	15.18	15.01	14.65	15.59
Wo+En+Fs	97.98	99.86	99.86	98.06	97.91	97.56	97.55	97.91	97.75	97.71	97.83	97.70
Jd	0.42	0.03	0.05	0.52	0.48	0.05	0.47	0.68	0.39	0.65	0.41	0.29
Ae	1.61	0.11	0.09	1.42	1.62	2.39	1.97	1.41	1.86	1.64	1.76	2.01

Sample	K12L-PYX30	K12L-PYX31	K12L-PYX32	K12L-PYX33	K12L-PYX34	K12L-PYX35	K12L-PYX36	K12B-PYX1	K12B-PYX2	K12B-PYX3	K12B-PYX4	K12B-PYX5
Analysis	euhedral	euhedral	euhedral	euhedral	anhedral	anhedral	euhedral	anhedral	anhedral	anhedral	anhedral	anhedral
Rock Type	andesite	andesite	andesite	andesite	andesite	andesite	andesite	basaltic andesite	basaltic andesite	basaltic andesite	basaltic andesite	basaltic andesite
SiO_2	51.60	51.90	51.56	52.42	52.37	52.86	51.49	52.90	52.73	51.49	51.10	50.85
TiO_2	0.51	0.45	0.46	0.40	0.27	0.26	0.47	0.24	0.28	0.41	0.53	0.47
Al_2O_3	2.21	1.92	2.29	1.69	2.18	1.66	2.27	1.55	1.75	2.15	2.56	2.57
FeO	8.96	8.93	8.86	9.09	18.65	19.07	8.91	17.31	17.82	7.92	8.26	8.15
MnO	0.36	0.45	0.35	0.43	0.56	0.73	0.33	0.50	0.47	0.31	0.28	0.29
MgO	14.88	14.88	15.01	14.93	24.37	23.78	14.96	24.96	24.44	15.43	15.25	15.27
CaO	20.97	21.21	21.23	20.89	1.72	1.46	20.84	1.61	1.79	21.54	21.39	21.41
Na_2O	0.33	0.30	0.29	0.32	0.02	0.05	0.29	0.00	0.02	0.26	0.32	0.29
K_2O	0.00	0.00	0.03	0.01	0.00	0.00	0.00	0.00	0.01	0.00	0.01	0.00
Analyses Total	99.82	100.04	100.08	100.18	100.14	99.87	99.56	99.07	99.31	99.51	99.70	99.30
FeO (calculated)	6.78	6.84	6.23	7.66	16.36	18.07	6.83	16.28	16.71	5.23	5.10	4.86
Fe_2O_3 (calculated)	2.29	2.19	2.75	1.49	2.29	0.93	2.15	1.00	1.07	2.82	3.34	3.51
Total	99.94	100.14	100.20	100.24	100.14	99.80	99.63	99.04	99.27	99.64	99.88	99.51
Wo	42.84	43.08	43.06	42.55	3.40	2.92	42.64	3.20	3.58	43.57	43.41	43.48
En	42.29	42.05	42.36	42.31	66.98	66.16	42.59	69.12	67.91	43.43	43.06	43.14
Fs	14.87	14.88	14.59	15.14	29.63	30.92	14.77	27.68	28.52	13.00	13.53	13.38
Wo+En+Fs	97.54	97.77	97.83	97.65	99.85	99.64	97.83	100.00	99.85	98.05	97.59	97.80
Jd	0.43	0.28	0.22	0.65	0.02	0.15	0.46	0.00	0.05	0.06	0.10	0.07
Ae	2.03	1.95	1.95	1.71	0.13	0.22	1.71	0.00	0.10	1.88	2.31	2.12

Table D.2. Pyroxene Analyses

Sample	K12B-PYX6	K12B-PYX7	K12B-PYX8	K14-PYX1	K14-PYX2	K14-PYX3	K14-PYX4	K14-PYX5	K14-PYX6	K14-PYX7	K14-PYX8	K14-PYX9
Analysis	anhedral	euhedral	microphenocryst	microphenocryst	microphenocryst	euhedral	euhedral	euhedral	euhedral	euhedral	euhedral	euhedral
Rock Type	basaltic andesite	basaltic andesite	basaltic andesite	basaltic andesite	basaltic andesite	basaltic andesite	basaltic andesite	andesite	andesite	andesite	andesite	andesite
SiO_2	51.42	53.27	53.64	53.80	53.1[illegible]	51.19	53.62	50.73	51.50	54.27	53.79	51.84
TiO_2	0.49	0.24	0.21	0.15	0.28	0.48	0.19	0.59	0.38	0.15	0.23	0.30
Al_2O_3	2.61	1.90	1.54	0.55	0.98	3.07	0.99	3.52	2.21	0.95	0.90	1.44
FeO	8.11	16.02	16.10	18.68	18.12	8.50	18.25	8.42	8.28	15.09	17.70	9.59
MnO	0.32	0.42	0.46	0.92	0.84	0.25	0.67	0.27	0.28	0.41	0.83	0.56
MgO	1[illegible]4	25.91	25.94	23.64	24.29	14.74	24.03	14.53	15.35	26.5[illegible]	24.35	14.41
CaO	21.22	1.55	1.41	1.20	1.24	20.63	1.27	20.58	20.30	1.43	1.23	21.09
Na_2O	0.29	0.03	0.02	0.06	0.05	0.28	0.03	0.30	0.28	0.06	0.05	0.39
K_2O	0.00	0.01	0.00	0.01	0.01	0.01	0.03	0.01	0.01	0.01	0.02	0.01
Analyses Total	99.60	99.35	99.32	99.01	98.99	99.15	99.08	98.95	98.59	98.93	99.10	99.63
FeO (calculated)	5.99	15.02	15.63	18.68	17.74	7.25	18.20	7.10	6.83	15.03	17.67	7.08
Fe_2O_3 (calculated)	2.22	0.94	0.40	0.00	0.32	1.23	0.00	1.29	1.47	0.00	0.00	2.63
Total	99.70	99.29	99.25	99.01	98.93	99.13	99.03	98.92	98.61	98.87	99.07	99.75
Wo	43.42	3.07	2.80	2.43	2.49	43.01	2.57	43.25	41.99	2.83	2.48	42.98
En	43.11	71.48	71.57	66.58	67.81	42.75	67.57	42.49	44.18	73.20	68.33	40.86
Fs	13.47	25.45	25.64	30.99	29.71	14.24	29.86	14.26	13.83	23.97	29.19	16.16
Wo+En+Fs	97.83	99.78	99.86	99.56	99.64	97.89	99.78	97.73	97.90	99.57	99.64	97.09
Jd	0.56	0.10	0.10	0.44	0.21	1.19	0.22	1.34	0.83	0.43	0.36	0.00
Ae	1.61	0.12	0.05	0.00	0.16	0.92	0.00	0.94	1.27	0.00	0.00	2.91

Sample	K14-PYX10	K14-PYX11	K14-PYX12	K14-PYX13	K14-PYX14	K14-PYX15	K14-PYX16	K14-PYX17	K14-PYX18	K14-PYX19	K14-PYX20	K17B-PYX1
Analysis	euhedral	euhedral	euhedral	euhedral	euhedral	euhedral	euhedral	euhedral	euhedral	euhedral	euhedral	anhedral
Rock Type	andesite	basaltic andesite	basaltic andesite	basaltic andesite	basaltic andesite	basaltic andesite	andesite	andesite	basaltic andesite	basaltic andesite	basaltic andesite	rhyolite
SiO_2	51.59	50.90	53.25	53.20	52.95	52.91	53.58	50.59	51.42	51.38	52.13	51.44
TiO_2	0.42	0.45	0.28	0.26	0.18	0.26	0.27	0.53	0.48	0.57	0.48	0.14
Al_2O_3	2.00	2.77	1.11	1.11	1.30	2.06	1.53	2.37	2.39	2.51	2.04	0.48
FeO	9.06	9.19	19.03	19.12	16.64	17.27	18.60	9.27	9.06	9.20	8.90	26.03
MnO	0.45	0.40	0.80	0.78	0.52	0.57	0.63	0.45	0.41	0.42	0.45	1.77
MgO	14.86	15.28	24.73	24.82	26.57	26.01	25.05	15.06	15.15	14.82	14.99	18.85
CaO	20.86	20.21	1.20	1.25	1.46	1.52	1.34	20.44	20.52	21.02	20.77	1.03
Na_2O	0.30	0.31	0.01	0.03	0.01	0.04	0.02	0.38	0.29	0.33	0.34	0.05
K_2O	0.00	0.02	0.00	0.00	0.03	0.00	0.01	0.00	0.00	0.00	0.03	0.00
Analyses Total	99.54	99.53	100.41	100.57	99.66	100.64	101.03	99.09	99.72	100.25	100.13	99.79
FeO (calculated)	6.93	6.12	17.30	16.93	13.40	14.21	17.01	5.64	6.75	6.57	7.23	24.54
Fe_2O_3 (calculated)	2.25	3.23	1.48	1.77	2.53	2.94	1.56	3.69	2.39	2.79	1.74	1.04
Total	99.66	99.68	100.16	100.14	98.95	100.52	101.01	99.16	99.80	100.41	100.20	99.34
Wo	42.60	41.28	2.35	2.44	2.82	2.94	2.62	41.73	41.88	42.76	42.45	2.10
En	42.23	43.42	67.34	67.29	71.33	70.08	68.06	42.78	43.02	41.95	42.63	53.55
Fs	15.17	15.30	30.31	30.28	25.85	26.98	29.32	15.50	15.10	15.29	14.93	44.34
Wo+En+Fs	97.76	97.65	99.93	99.78	99.93	99.71	99.86	97.11	97.83	97.53	97.49	99.62
Jd	0.33	0.30	0.00	0.00	0.00	0.00	0.01	0.00	0.39	0.31	0.72	0.00
Ae	1.91	2.05	0.07	0.22	0.07	0.29	0.13	2.89	1.78	2.16	1.80	0.38

Table D.2. Pyroxene Analyses

Sample	K17B-PYX2	K17B-PYX3	K17B-PYX4	K17B-PYX5	K17B-PYX6	K17B-PYX7	K17B-PYX8	K18-PYX1	K18-PYX2	K18-PYX3	K18-PYX4	K18-PYX5
Analysis	anhedral	anhedral	euhedral	euhedral	euhedral	euhedral	euhedral	glomerocryst	glomerocryst	glomerocryst	glomerocryst	glomerocryst
Rock Type	rhyolite	rhyolite	rhyolite	rhyolite	rhyolite	rhyolite	rhyolite	dacite	dacite	dacite	dacite	dacite
SiO_2	51.46	51.65	51.76	51.09	51.75	51.56	52.06	50.54	50.12	52.28	50.90	52.73
TiO_2	0.11	0.13	0.11	0.11	0.11	0.13	0.08	0.62	0.48	0.24	0.18	0.26
Al_2O_3	0.54	0.60	0.42	0.39	0.44	0.35	0.46	3.11	2.07	1.08	0.97	1.12
FeO	24.81	24.58	24.71	26.02	24.92	25.59	24.65	8.50	8.34	8.21	8.40	8.46
MnO	1.62	1.53	1.67	1.87	1.73	1.85	1.60	0.35	0.35	0.40	0.41	0.39
MgO	19.37	19.73	19.81	18.73	19.66	18.95	19.97	14.98	15.39	15.20	15.33	15.15
CaO	1.13	1.06	1.09	1.00	1.08	0.98	1.11	21.81	21.46	22.03	21.83	21.79
Na_2O	0.03	0.00	0.02	0.01	0.09	0.00	0.05	0.32	1.15	0.27	0.30	0.30
K_2O	0.01	0.02	0.01	0.01	0.01	0.01	0.00	0.01	0.02	0.01	0.02	0.01
Analyses Total	99.08	99.35	99.60	99.23	99.79	99.42	99.98	100.24	99.38	99.72	100.34	100.21
FeO (calculated)	23.73	23.53	23.32	24.41	23.20	24.73	23.31	4.37	8.05	5.67	6.19	6.50
Fe_2O_3 (calculated)	0.90	0.87	0.94	1.03	1.22	0.55	0.98	4.36	0.00	2.30	2.14	2.03
Total	98.90	99.17	99.15	98.65	99.29	99.12	99.62	100.47	99.09	99.47	100.27	100.27
Wo	2.32	2.16	2.21	2.05	2.19	2.01	2.25	44.00	43.21	44.15	43.62	43.77
En	55.31	56.19	55.95	53.35	55.54	54.05	56.25	42.05	43.12	42.38	42.63	42.34
Fs	42.37	41.64	41.83	44.60	42.27	43.94	41.51	13.94	13.67	13.48	13.75	13.88
Wo+En+Fs	99.77	100.00	99.85	99.92	99.33	100.00	99.63	97.57	92.27	98.00	97.80	97.80
Jd	0.00	0.00	0.00	0.00	0.00	0.00	0.00	0.00	0.00	0.00	0.00	0.00
Ae	0.23	0.00	0.15	0.08	0.67	0.00	0.37	2.43	0.08	2.00	2.20	2.20

Sample	K18-PYX6	K18-PYX7	K18-PYX8	K18-PYX9	K18-PYX10	K18-PYX11	K18-PYX12	K18-PYX13	K18-PYX14	K18-PYX15	K18-PYX16	K18-PYX17
Analysis	glomerocryst	euhedral	euhedral	euhedral	euhedral	euhedral	euhedral	euhedral	euhedral	euhedral	euhedral	microphenocryst
Rock Type	dacite	dacite	dacite	dacite	dacite	dacite	dacite	dacite	dacite	dacite	dacite	dacite
SiO_2	52.68	51.74	51.47	53.63	53.56	52.34	51.90	52.39	52.66	52.86	52.81	52.92
TiO_2	0.30	0.06	0.10	0.23	0.18	0.20	0.26	0.20	0.24	0.12	0.13	0.20
Al_2O_3	1.21	0.25	0.49	1.28	0.88	1.01	1.30	0.91	1.35	0.45	0.58	0.00
FeO	8.35	25.88	24.82	18.59	19.48	10.73	9.64	10.09	9.68	22.87	22.10	21.90
MnO	0.39	1.89	1.55	0.73	0.91	0.66	0.52	0.59	0.52	1.21	1.02	1.17
MgO	15.16	20.05	20.81	25.55	24.81	14.16	14.42	14.37	14.52	22.01	22.99	22.39
CaO	21.83	0.74	0.83	1.27	1.24	20.66	21.33	21.28	21.50	0.95	0.97	1.55
Na_2O	0.29	0.00	0.00	0.03	0.00	0.29	0.34	0.29	0.31	0.02	0.03	0.01
K_2O	0.01	0.00	0.00	0.02	0.02	0.00	0.00	0.00	0.00	0.01	0.01	0.00
Analyses Total	100.22	100.61	100.07	101.33	101.08	100.05	99.71	100.12	100.78	100.49	100.64	100.14
FeO (calculated)	6.43	23.13	21.70	16.05	17.26	8.97	7.08	7.94	7.71	21.41	19.68	20.23
Fe_2O_3 (calculated)	2.03	1.54	1.88	2.12	1.63	1.87	2.53	2.01	2.06	0.96	1.61	0.68
Total	100.33	99.40	98.83	100.90	100.49	100.15	99.68	99.98	100.87	99.99	99.82	99.15
Wo	43.88	1.47	1.65	2.45	2.40	41.94	43.24	42.89	43.29	1.89	1.90	3.06
En	42.40	55.43	57.47	68.49	66.79	40.00	40.67	40.30	40.68	60.78	62.70	61.42
Fs	13.72	43.10	40.88	29.07	30.81	18.06	16.09	16.81	16.04	37.33	35.40	35.53
Wo+En+Fs	97.87	100.00	100.00	99.78	100.00	97.86	97.47	97.86	97.73	99.85	99.78	99.93
Jd	0.00	0.00	0.00	0.00	0.00	0.03	0.00	0.00	0.17	0.00	0.00	0.00
Ae	2.13	0.00	0.00	0.22	0.00	2.11	2.53	2.14	2.11	0.15	0.22	0.07

Table D.2. Pyroxene Analyses

Sample	K18-PYX18	K18-PYX19	K18-PYX20	K18-PYX1	K18-PYX2	K18-PYX3	K18-PYX4	K18-PYX5	K18-PYX6	K18-PYX7	K18-PYX8	K18-PYX9
Analysis	euhedral	euhedral	microphenocryst	glomerocryst	glomerocryst	glomerocryst	glomerocryst	glomerocryst	glomerocryst	euhedral	euhedral	euhedral
Rock Type	dacite	dacite	dacite	dacite	dacite	dacite	dacite	dacite	dacite	dacite	dacite	dacite
SiO_2	51.51	52.83	52.75	50.54	50.12	52.28	52.90	52.73	52.68	51.74	51.47	53.63
TiO_2	0.15	0.13	0.16	0.62	0.48	0.24	0.18	0.26	0.30	0.06	0.10	0.23
Al_2O_3	0.69	0.41	0.60	3.11	2.07	1.08	0.97	1.12	1.21	0.25	0.49	1.28
FeO	24.12	21.99	22.24	8.50	8.34	8.21	8.40	8.46	8.35	25.88	24.82	18.59
MnO	1.52	1.02	1.18	0.35	0.35	0.40	0.41	0.39	0.39	1.89	1.55	0.73
MgO	21.36	23.18	22.40	14.98	15.39	15.20	15.33	15.[illegible]	15.16	20.05	20.81	25.55
CaO	0.82	1.07	1.04	21.81	21.46	22.03	21.83	21.79	21.83	0.74	0.83	1.27
Na_2O	0.02	0.00	0.00	0.32	1.15	0.27	0.30	0.30	0.29	0.00	0.00	0.03
K_2O	0.00	0.02	0.02	0.01	0.02	0.01	0.02	0.01	0.01	0.00	0.00	0.02
Analyses Total	100.19	100.65	100.42	100.24	99.38	99.72	100.34	100.21	100.22	100.61	100.07	101.33
FeO (calculated)	20.74	19.34	20.60	4.37	8.05	5.67	6.19	6.50	6.43	23.13	21.70	16.05
Fe_2O_3 (calculated)	2.14	1.57	1.14	4.36	0.00	2.30	2.14	2.03	2.03	1.54	1.88	2.12
Total	98.95	99.57	99.92	100.47	99.09	99.47	100.27	100.27	100.33	99.40	98.83	100.90
Wo	1.62	2.09	2.06	44.00	43.21	44.15	43.62	43.77	43.88	1.47	1.65	2.45
En	58.77	62.88	61.72	42.05	43.12	42.38	42.63	42.34	42.40	55.43	57.47	68.49
Fs	39.61	35.04	36.22	13.94	13.67	13.48	13.75	13.88	13.72	43.10	40.88	29.07
Wo+En+Fs	99.85	100.00	100.00	97.57	92.27	98.00	97.80	97.80	97.87	100.00	100.00	99.78
Jd	0.00	0.00	0.00	0.00	0.00	0.00	0.00	0.00	0.00	0.00	0.00	0.00
Ae	0.15	0.00	0.00	2.43	0.08	2.00	2.20	2.20	2.13	0.00	0.00	0.22

Sample	K18-PYX10	K18-PYX11	K18-PYX12	K18-PYX13	K18-PYX14	K18-PYX15	K18-PYX16	K18-PYX17	K18-PYX18	K18-PYX19	K18-PYX20	K32A-PYX1
Analysis	euhedral	euhedral	euhedral	euhedral	euhedral	euhedral	euhedral	microphenocryst	euhedral	euhedral	microphenocryst	microphenocryst
Rock Type	dacite	dacite	dacite	dacite	dacite	dacite	dacite	dacite	dacite	dacite	dacite	rhyolite
SiO_2	53.56	52.34	51.90	52.39	52.66	52.86	52.81	52.92	51.51	52.83	52.78	52.04
TiO_2	0.18	0.20	0.26	0.20	0.24	0.12	0.13	0.20	0.15	0.13	0.16	0.10
Al_2O_3	0.88	1.01	1.30	0.91	1.35	0.45	0.58	0.00	0.69	0.41	0.60	0.27
FeO	19.48	10.73	9.64	10.09	9.68	22.87	22.10	21.90	24.12	21.99	22.24	25.26
MnO	0.91	0.66	0.52	0.59	0.52	1.21	1.02	1.17	1.52	1.02	1.18	1.65
MgO	24.81	14.16	14.42	14.37	14.52	22.01	22.99	22.39	21.36	23.18	22.40	19.50
CaO	1.24	20.66	21.33	21.28	21.50	0.95	0.97	1.55	0.82	1.07	1.04	1.11
Na_2O	0.00	0.29	0.34	0.29	0.31	0.02	0.03	0.01	0.02	0.00	0.00	0.07
K_2O	0.02	0.00	0.00	0.00	0.00	0.00	0.01	0.00	0.00	0.02	0.02	0.01
Analyses Total	101.08	100.05	99.71	100.12	100.78	100.49	100.64	100.14	100.19	100.65	100.42	100.01
FeO (calculated)	17.26	8.97	7.08	7.94	7.71	21.41	19.68	20.23	20.74	19.34	20.60	23.98
Fe_2O_3 (calculated)	1.63	1.87	2.53	2.01	2.06	0.96	1.61	0.68	2.14	1.57	1.14	0.84
Total	100.49	100.15	99.68	99.98	100.87	99.99	99.82	99.15	98.95	99.57	99.92	99.56
Wo	2.40	41.94	43.24	42.89	43.29	1.89	1.90	3.06	1.62	2.09	2.06	2.25
En	66.79	40.00	40.67	40.30	40.68	60.78	62.70	61.42	58.77	62.88	61.72	55.08
Fs	30.81	18.06	16.09	16.81	16.04	37.33	35.40	35.53	39.61	35.04	36.22	42.67
Wo+En+Fs	100.00	97.86	97.47	97.86	97.73	99.85	99.78	99.93	99.85	100.00	100.00	99.48
Jd	0.00	0.03	0.00	0.00	0.17	0.00	0.00	0.00	0.00	0.00	0.00	0.00
Ae	0.00	2.11	2.53	2.14	2.11	0.15	0.22	0.07	0.15	0.00	0.00	0.52

Table D.2. Pyroxene Analyses

Sample	K32A-PYX2	K32A-PYX3	K32A-PYX4	K32A-PYX5	K3?A-PYX6	K32A-PYX7	K32A-PYX8	K32A-PYX9	K32A-PYX10	K32A-PYX11	K32A-PYX12	K32A-PYX13
Analysis	microphenocryst	microphenocryst	microphenocryst	microphenocryst	microphenocryst	microphenocryst	microphenocryst	microphenocryst	euhedral	microphenocryst	euhedral	euhedral
Rock Type	rhyolite	rhyolite	rhyolite	rhyolite	rhyolite	rhyolite	rhyolite	rhyolite	rhyolite	rhyolite	rhyolite	rhyolite
SiO_2	52.21	52.00	51.74	51.35	52.10	52.04	51.58	52.15	51.52	51.40	51.90	51.71
TiO_2	0.10	0.12	0.12	0.14	0.11	0.10	0.10	0.10	0.25	0.21	0.14	0.18
Al_2O_3	0.33	0.32	0.46	0.50	0.33	0.22	0.38	0.32	1.14	1.03	0.44	0.46
FeO	25.15	25.83	24.74	25.10	24.70	24.36	25.75	24.64	9.90	9.82	25.67	25.50
MnO	1.66	1.79	1.50	1.75	1.59	1.64	1.85	1.62	0.66	0.66	1.70	1.79
MgO	19.65	19.40	19.65	19.25	9.68	19.90	19.12	20.03	13.87	14.25	19.87	19.73
CaO	1.05	0.97	1.13	1.07	1.15	1.16	1.01	1.14	21.55	21.51	0.97	1.08
Na_2O	0.00	0.03	0.00	0.03	0.01	0.00	0.03	0.04	0.19	0.32	0.00	0.00
K_2O	0.01	0.00	0.01	0.00	0.01	0.01	0.01	0.02	0.01	0.01	0.01	0.00
Analyses Total	100.16	100.46	99.35	99.19	99.68	99.43	99.83	100.06	99.09	99.21	100.70	100.45
FeO (calculated)	24.36	24.37	23.84	23.81	24.07	23.60	24.21	23.27	7.84	6.40	23.59	23.46
Fe_2O_3 (calculated)	0.56	0.91	0.69	0.93	0.45	0.45	1.00	0.91	1.95	2.82	1.22	1.22
Total	99.93	99.90	99.14	98.83	99.50	99.12	99.30	99.60	98.98	98.62	99.84	99.63
Wo	2.13	1.96	2.31	2.19	2.34	2.36	2.05	2.30	43.89	43.43	1.94	2.17
En	55.42	54.49	55.84	54.85	55.80	56.32	54.10	56.28	39.31	40.04	55.30	55.07
Fs	42.45	43.55	41.86	42.96	41.85	41.32	43.85	41.42	16.80	16.53	42.76	42.77
Wo+En+Fs	100.00	99.78	100.00	99.77	99.93	100.00	99.78	99.70	98.57	97.59	100.00	100.00
Jd	0.00	0.00	0.00	0.00	0.00	0.00	0.00	0.00	0.00	0.00	0.00	0.00
Ae	0.00	0.22	0.00	0.23	0.07	0.00	0.23	0.30	1.43	2.41	0.00	0.00

Sample	K32D-PYX8	K32D-PYX9	K32D-PYX10	K32D-PYX11	K32D-PYX12	K32D-PYX13	K32D-PYX14	K32D-PYX15	K32D-PYX16	K32D-PYX17	K32D-PYX18	K32D-PYX19
Analysis	euhedral	euhedral	euhedral	euhedral	euhedral	euhedral	euhedral	euhedral	euhedral	euhedral	euhedral	euhedral
Rock Type	dacite	dacite	dacite	dacite	dacite	dacite	dacite	dacite	dacite	dacite	dacite	dacite
SiO_2	52.80	52.43	52.99	52.79	53.59	53.17	53.42	53.36	53.29	52.37	52.19	53.09
TiO_2	0.24	0.20	0.10	0.15	0.17	0.13	0.16	0.15	0.21	0.34	0.38	0.21
Al_2O_3	0.86	0.82	0.42	0.96	0.57	0.45	0.52	0.65	0.95	1.57	1.34	0.78
FeO	21.22	21.09	22.35	21.23	21.39	22.33	21.00	19.97	20.60	10.10	9.72	20.74
MnO	1.08	1.09	1.30	1.06	1.22	1.32	1.21	0.91	0.99	0.65	0.63	0.85
MgO	23.00	22.65	21.89	22.78	23.06	22.25	23.06	24.01	23.36	14.20	14.68	23.61
CaO	1.18	1.24	1.04	1.27	1.15	1.04	1.11	1.36	1.28	21.15	21.05	1.31
Na_2O	0.02	0.01	0.05	0.00	0.03	0.72	0.00	0.02	0.00	0.28	0.32	0.01
K_2O	0.01	0.01	0.00	0.01	0.02	0.01	0.01	0.00	0.03	0.01	0.00	0.00
Analyses Total	100.41	99.54	100.14	100.25	101.20	101.42	100.49	100.43	100.71	100.67	100.31	100.60
FeO (calculated)	19.46	19.61	21.47	19.77	20.09	17.72	20.15	18.25	19.39	8.45	7.42	18.85
Fe_2O_3 (calculated)	1.32	1.20	0.74	1.32	0.97	3.50	0.68	1.26	1.15	1.70	2.30	1.36
Total	99.97	99.26	100.01	100.11	100.87	100.32	100.32	99.97	100.65	100.72	100.30	100.08
Wo	2.33	2.48	2.08	2.52	2.26	2.06	2.20	2.66	2.53	42.90	42.47	2.57
En	63.25	62.93	60.95	62.92	63.04	61.34	63.48	65.41	64.18	40.07	41.21	64.39
Fs	34.42	34.59	36.97	34.56	34.70	36.60	34.32	31.93	33.29	17.03	16.31	33.05
Wo+En+Fs	99.85	99.93	99.64	100.00	99.78	94.76	100.00	99.86	100.00	97.94	97.64	99.93
Jd	0.00	0.00	0.00	0.00	0.00	0.00	0.00	0.00	0.00	0.38	0.00	0.00
Ae	0.15	0.07	0.37	0.00	0.22	5.24	0.00	0.15	0.00	1.69	2.37	0.07

Table D.3. Feldspar Analyses

Sample	K2-FSP1	K2-FSP2	K2-FSP3	K2-FSP4	K2-FSP5	K2-FSP6	K2-FSP7	K2-FSP8	K2-FSP9	K2-FSP10	K2-FSP11	K2-FSP12	K2-FSP13	K2-FSP14	K2-FSP15	K2-FSP16
Type	euhedral	euhedral	euhedral	euhedral	euhedral	euhedral	euhedral	euhedral	euhedral	euhedral	euhedral	euhedral	euhedral	euhedral	micro	micro
Location	core	core	core	rim	core	rim	core	middle	rim	core	core	rim	core	rim	core	rim
Host Lithology	rhyolite	rhyolite	rhyolite	rhyolite	rhyolite	rhyolite	rhyolite	rhyolite	rhyolite	rhyolite	rhyolite	rhyolite	rhyolite	rhyolite	rhyolite	rhyolite
SiO_2	55.89	54.47	57.72	54.87	55.96	53.51	55.91	54.29	57.82	56.78	55.12	57.33	54.39	56.85	56.35	56.70
Al_2O_3	28.12	28.86	27.59	29.13	28.70	29.71	28.40	29.42	27.46	27.82	28.24	27.22	28.69	27.74	27.75	27.86
Fe_2O_3	0.38	0.31	0.26	0.40	0.42	0.43	0.40	0.33	0.32	0.35	0.39	0.31	0.32	0.33	0.34	0.29
CaO	9.75	10.45	8.69	10.72	10.11	11.75	10.12	11.22	8.75	9.33	10.06	9.03	10.63	9.21	9.32	9.08
Na_2O	5.95	5.50	6.80	5.57	5.83	4.90	5.85	5.26	6.70	6.25	5.88	6.46	5.50	6.22	6.21	6.37
K_2O	0.15	0.11	0.18	0.12	0.13	0.11	0.15	0.10	0.18	0.13	0.13	0.15	0.12	0.14	0.14	0.14
TOTAL	100.24	99.70	101.25	100.81	101.14	100.41	100.82	100.61	101.22	100.66	99.83	100.49	99.66	100.50	100.10	100.44
Ab	52.0	48.5	58.0	48.2	50.7	42.7	50.7	45.6	57.5	54.4	51.0	56.0	48.0	54.5	54.2	55.5
An	47.1	50.9	41.0	51.2	48.6	56.6	48.5	53.8	41.5	44.9	48.2	43.2	51.3	44.6	45.0	43.7
Or	0.9	0.6	1.0	0.7	0.7	0.6	0.9	0.6	1.0	0.8	0.7	0.8	0.7	0.8	0.8	0.8

Sample	K2-FSP17	K2-FSP18	K2-FSP19	K2-FSP20	K2-FSP21	K2-FSP22	K2-FSP23	K2-FSP24	K2-FSP25	K2-FSP26	K2-FSP27	K2-FSP28	K2-FSP29	K2-FSP30	K2-FSP31	K3-FSP1
Type	euhedral	euhedral	micro	micro	euhedral	euhedral	euhedral	euhedral	euhedral	micro	micro	euhedral	euhedral	euhedral	euhedral	euhedral
Location	core	rim	core	rim	core	middle	rim	core	rim	core	rim	middle	rim	rim	rim	rim
Host Lithology	rhyolite	rhyolite	rhyolite	rhyolite	rhyolite	rhyolite	rhyolite	rhyolite	rhyolite	rhyolite	rhyolite	rhyolite	rhyolite	rhyolite	rhyolite	dacite
SiO_2	54.95	55.37	56.42	57.40	56.71	56.19	57.61	59.84	60.52	58.48	58.92	56.30	56.72	57.31	57.70	52.78
Al_2O_3	28.96	28.45	27.84	26.71	27.83	28.52	26.63	25.74	25.55	26.90	26.93	28.16	27.50	27.51	27.58	29.51
Fe_2O_3	0.33	0.34	0.36	0.30	0.32	0.32	0.30	0.25	0.24	0.32	0.26	0.29	0.32	0.29	0.36	0.96
CaO	10.69	10.06	9.32	8.38	9.27	9.77	8.02	7.05	6.64	7.81	8.03	9.72	8.76	8.76	8.80	11.21
Na_2O	5.43	5.85	6.29	6.76	6.35	5.99	6.83	7.50	7.75	7.08	7.02	6.17	6.53	7.17	6.51	5.92
K_2O	0.12	0.13	0.13	0.17	0.15	0.11	0.18	0.23	0.25	0.18	0.19	0.14	0.15	0.16	0.14	b.d.
TOTAL	100.47	100.20	100.35	99.72	100.63	100.91	99.57	100.61	100.94	100.77	101.35	100.77	99.98	101.20	101.08	100.39
Ab	47.6	50.9	54.6	58.8	54.9	52.3	60.0	65.0	66.9	61.5	60.6	53.0	57.0	59.1	56.8	48.8
An	51.8	48.4	44.7	40.2	44.3	47.1	38.9	33.7	31.7	37.5	38.3	46.2	42.2	40.0	42.4	51.1
Or	0.7	0.7	0.7	1.0	0.9	0.7	1.1	1.3	1.4	1.0	1.1	0.8	0.9	0.9	0.8	0.1

Sample	K3-FSP2	K3-FSP3	K3-FSP4	K3-FSP5	K3-FSP6	K3-FSP7	K3-FSP8	K3-FSP9	K3-FSP10	K3-FSP11	K3-FSP12	K3-FSP13	K3-FSP14	K3-FSP15	K3-FSP16	K3-FSP17
Type	euhedral	sieve	sieve	sieve	sieve	sieve	sieve	sieve	sieve	sieve	sieve	sieve	sieve	sieve	sieve	sieve
Location	middle	rim	rim	core	rim	rim	rim	core	core	middle	middle	middle	middle	middle	middle	core
Host Lithology	dacite	dacite	dacite	andesite	andesite	andesite	andesite	andesite	andesite	andesite	andesite	andesite	andesite	andesite	andesite	andesite
SiO_2	56.25	54.31	54.24	56.85	53.54	53.78	53.57	56.53	56.19	48.35	48.54	49.18	57.65	57.82	57.80	53.89
Al_2O_3	26.99	28.23	27.96	27.41	29.39	29.39	29.37	27.37	27.68	32.77	32.84	32.04	26.68	26.59	26.74	29.32
Fe_2O_3	0.31	0.44	0.45	0.30	0.42	0.42	0.46	0.31	0.33	0.41	0.49	0.41	0.32	0.32	0.32	0.39
CaO	8.65	10.87	10.65	9.12	11.40	11.25	11.52	9.20	9.36	15.23	15.30	14.79	8.40	8.35	8.31	11.27
Na_2O	6.43	5.33	5.35	6.45	5.07	5.12	5.16	6.40	6.19	2.85	2.84	3.20	6.72	6.74	6.74	5.16
K_2O	0.14	0.10	0.10	0.16	0.10	0.12	0.10	0.13	0.13	0.05	0.04	0.06	0.16	0.16	0.17	0.09
TOTAL	98.76	99.28	98.75	100.28	99.92	100.08	100.19	99.95	99.88	99.66	100.04	99.68	99.93	99.97	100.09	100.12
Ab	56.9	46.7	47.4	55.6	44.3	44.9	44.5	55.3	54.0	25.2	25.1	28.1	58.6	58.8	58.9	45.1
An	42.3	52.7	52.0	43.5	55.1	54.4	54.9	43.9	45.2	74.5	74.7	71.6	40.5	40.2	40.1	54.4
Or	0.8	0.6	0.6	0.9	0.5	0.7	0.6	0.7	0.7	0.3	0.2	0.4	0.9	0.9	1.0	0.5

Table D.3. Feldspar Analyses

Sample	K3-FSP18	K3-FSP19	K3-FSP20	K3-FSP21	K3-FSP22	K3-FSP23	K3-FSP24	K3-FSP25	K3-FSP26	K3-FSP27	K3-FSP28	K3-FSP29	K3-FSP30	K3-FSP31	K3-FSP32	K3-FSP33
Type	sieve	sieve	sieve	sieve	sieve	sieve	sieve	sieve	euhedral	euhedral	euhedral	euhedral	euhedral	euhedral	euhedral	euhedral
Location	core	core	middle	middle	middle	rim	rim	rim	core	core	core	middle	middle	middle	rim	rim
Host Lithology	andesite	andesite	andesite	andesite	andesite	andesite	andesite	andesite	andesite	andesite	andesite	andesite	andesite	andesite	andesite	andesite
SiO_2	54.03	53.86	46.40	45.94	46.18	53.51	53.87	53.50	56.92	56.50	57.01	46.99	48.65	48.16	54.93	53.92
Al_2O_3	29.32	29.43	34.32	34.56	34.29	29.56	29.44	29.36	27.05	27.25	27.16	34.03	32.89	33.15	28.47	29.21
Fe_2O_3	0.43	0.37	0.55	0.52	0.46	0.36	0.39	0.43	0.32	0.42	0.36	0.43	0.42	0.43	0.35	0.39
CaO	11.31	11.26	17.08	17.30	17.28	11.31	11.38	11.55	8.88	8.94	8.82	16.61	15.36	15.77	10.23	11.08
Na_2O	5.24	5.19	1.85	1.74	1.80	5.18	5.15	5.13	6.49	6.44	6.52	2.16	2.90	2.63	5.07	5.26
K_2O	0.10	0.09	0.03	0.04	0.03	0.10	0.09	0.09	0.16	0.14	0.15	0.04	0.04	0.05	0.10	0.10
TOTAL	100.44	100.20	100.23	100.10	100.03	100.03	100.32	100.05	99.72	99.68	100.02	100.25	100.26	100.18	99.75	99.96
Ab	45.3	45.2	16.4	15.4	15.8	45.1	44.8	44.3	56.1	56.1	56.8	19.0	25.4	23.1	49.8	46.0
An	54.1	54.2	83.5	84.4	84.0	54.3	54.7	55.2	43.0	43.1	42.4	80.8	74.3	76.6	49.6	53.5
Or	0.6	0.5	0.2	0.2	0.1	0.6	0.5	0.5	0.9	0.8	0.8	0.2	0.2	0.3	0.6	0.6

Sample	K3-FSP34	K3-FSP35	K3-FSP36	K3-FSP37	K3-FSP38	K3-FSP39	K3-FSP40	K3-FSP41	K3-FSP42	K3-FSP43	K3-FSP44	K3-FSP45	K3-FSP46	K3-FSP47	K3-FSP48	K3-FSP49
Type	euhedral	euhedral	glom	glom	glom	glom	glom	glom	glom	glom	glom	sieve	sieve	sieve	sieve	sieve
Location	rim	rim	core	core	core	middle	middle	middle	rim	rim	rim	core	rim	core	core	middle
Host Lithology	andesite	andesite	andesite	andesite	andesite	andesite	andesite	andesite	andesite	andesite	andesite	andesite	andesite	andesite	andesite	andesite
SiO_2	54.34	52.32	45.86	45.73	45.55	55.31	55.44	55.39	53.98	54.20	54.56	54.03	53.97	53.89	54.41	46.34
Al_2O_3	28.63	30.06	34.84	34.83	34.84	28.37	28.08	28.06	29.13	28.79	28.92	28.95	29.01	29.11	29.00	34.41
Fe_2O_3	0.42	0.37	0.36	0.31	0.37	0.38	0.51	0.44	0.38	0.39	0.40	0.37	0.41	0.38	0.42	0.42
CaO	10.84	12.43	17.63	17.39	17.54	10.23	9.86	9.96	11.00	10.81	10.85	10.82	11.01	11.04	10.94	17.20
Na_2O	4.86	4.33	1.63	1.59	1.59	5.78	6.00	5.91	5.36	5.40	5.35	5.44	5.31	5.23	5.41	1.81
K_2O	0.10	0.09	b.d.	0.03	b.d.	0.10	0.14	0.12	0.11	0.09	0.10	0.10	0.12	0.09	0.10	0.03
TOTAL	99.19	99.60	100.32	99.87	99.89	100.17	100.03	99.88	99.96	99.68	100.18	99.70	99.81	99.74	100.27	100.21
Ab	44.5	38.5	14.3	14.1	14.1	50.2	52.0	51.4	46.5	47.2	46.9	47.3	46.3	45.9	47.0	16.0
An	54.9	61.0	85.7	85.7	85.9	49.2	47.2	47.9	52.8	52.2	52.5	52.1	53.1	53.6	52.5	83.9
Or	0.6	0.5	0.0	0.2	0.0	0.6	0.8	0.7	0.6	0.5	0.6	0.6	0.7	0.5	0.5	0.1

Sample	K3-FSP50	K3-FSP51	K3-FSP52	K3-FSP53	K3-FSP54	K3-FSP55	K3-FSP56	K3-FSP57	K3-FSP58	K3-FSP59	K3-FSP60	K3-FSP61	K3-FSP62	K3-FSP63	K3-FSP64	K3-FSP65
Type	sieve	sieve	sieve	sieve	micro	micro	euhedral	micro	micro	micro	euhedral	micro	euhedral	euhedral	euhedral	euhedral
Location	middle	middle	rim	rim	core	core	core	core	rim	rim	rim	rim	core	core	core	middle
Host Lithology	andesite	andesite	andesite	andesite	andesite	andesite	andesite	andesite	andesite	andesite	andesite	andesite	andesite	andesite	andesite	andesite
SiO_2	47.70	46.00	54.31	53.73	53.99	54.60	53.86	54.11	54.60	53.97	54.31	53.37	55.18	55.95	55.89	55.28
Al_2O_3	33.53	34.64	29.02	29.33	29.07	28.49	29.23	28.94	28.68	29.21	28.72	29.26	28.22	27.80	27.62	28.28
Fe_2O_3	0.44	0.40	0.41	0.43	0.43	0.44	0.37	0.36	0.41	0.40	0.40	0.43	0.34	0.38	0.37	0.36
CaO	16.07	17.41	11.01	11.40	11.07	10.56	11.24	10.83	10.66	11.10	10.82	11.25	10.18	9.78	9.54	10.19
Na_2O	2.44	1.68	5.28	4.97	5.26	5.55	5.18	5.41	5.43	5.26	5.35	5.07	5.74	6.16	6.16	5.75
K_2O	b.d.	b.d.	0.11	0.08	0.09	0.11	0.10	0.10	0.10	0.11	0.13	0.09	0.14	0.15	0.15	0.11
TOTAL	100.22	100.16	100.14	99.94	99.91	99.75	99.98	99.74	99.88	100.05	99.72	99.47	99.79	100.22	99.72	99.96
Ab	21.6	14.9	46.2	43.9	46.0	48.4	45.2	47.2	47.7	45.9	46.9	44.7	50.1	52.8	53.4	50.2
An	78.3	85.0	53.2	55.6	53.5	51.0	54.2	52.2	51.7	53.5	52.4	54.8	49.1	46.3	45.7	49.2
Or	0.1	0.1	0.6	0.5	0.5	0.6	0.6	0.5	0.6	0.6	0.7	0.5	0.8	0.8	0.8	0.6

Table D.3. Feldspar Analyses

Sample	K3-FSP66	K3-FSP67	K3-FSP68	K3-FSP69	K3-FSP70	K3-FSP71	K3-FSP72	K3-FSP73	K3-FSP74	K3-FSP75	K3-FSP76	K3-FSP77	K3-FSP78	K3-FSP79	K3-FSP80	K3-FSP81
Type	euhedral	euhedral	euhedral	euhedral	euhedral	micro	micro	euhedral	micro	euhedral	euhedral	euhedral	micro	euhedral	euhedral	micro
Location	middle	middle	rim	rim	rim	core	rim	rim	core	core	core	core	rim	rim	rim	core
Host Lithology	andesite	andesite	andesite	andesite	andesite	andesite	andesite	andesite	andesite	andesite	andesite	andesite	andesite	andesite	andesite	andesite
SiO_2	55.95	54.90	54.64	55.53	54.04	52.59	53.82	55.10	54.22	54.01	53.99	53.54	52.25	53.51	53.41	56.12
Al_2O_3	27.77	28.51	28.75	27.91	28.91	30.11	29.42	28.33	29.10	29.07	28.96	29.28	30.24	29.08	29.10	27.14
Fe_2O_3	0.35	0.36	0.36	0.37	0.35	0.44	0.40	0.39	0.43	0.42	0.35	0.36	0.44	0.44	0.44	0.33
CaO	9.64	10.32	10.67	9.88	10.94	12.25	11.39	10.31	10.94	11.13	10.97	11.54	12.73	11.31	11.13	9.15
Na_2O	6.11	5.69	5.73	5.92	5.27	4.66	5.07	5.54	5.28	5.22	4.99	5.06	4.39	4.82	4.92	6.33
K_2O	0.14	0.13	0.12	0.14	0.09	0.08	0.08	0.11	0.11	0.09	0.10	0.09	0.09	0.09	0.10	0.15
TOTAL	99.95	99.90	100.27	99.75	99.59	100.13	100.17	99.77	100.07	99.94	99.37	99.86	100.14	99.25	99.11	99.21
Ab	53.0	49.6	48.9	51.6	46.3	40.6	44.4	49.0	46.3	45.7	44.9	44.0	38.3	43.3	44.2	55.1
An	46.2	49.7	50.4	47.6	53.2	59.0	55.1	50.4	53.1	53.8	54.5	55.5	61.3	56.2	55.2	44.0
Or	0.8	0.7	0.7	0.8	0.5	0.5	0.5	0.6	0.6	0.5	0.6	0.5	0.5	0.5	0.6	0.9

Sample	K3-FSP82	K3-FSP83	K3-FSP84	K3-FSP85	K3-FSP86	K3-FSP87	K3-FSP88	K3-FSP89	K3-FSP90	K3-FSP91	K3-FSP92	K4-FSP1	K4-FSP2	K4-FSP3	K4-FSP4	K4-FSP5
Type	euhedral	euhedral	euhedral	micro	micro	euhedral	euhedral	euhedral	micro	micro	micro	micro	micro	micro	euhedral	euhedral
Location	rim	rim	rim	core	core	core	core	core	rim	rim	rim	core	core	core	rim	rim
Host Lithology	andesite	andesite	andesite	andesite	andesite	andesite	andesite	andesite	andesite	andesite	andesite	andesite	andesite	andesite	andesite	andesite
SiO_2	53.67	53.57	53.04	57.42	57.79	53.68	54.43	52.29	54.52	53.05	53.72	51.00	45.66	45.97	45.52	45.48
Al_2O_3	29.48	29.15	29.25	26.77	26.62	29.36	28.79	30.02	28.59	29.64	29.37	30.81	34.57	34.63	34.56	35.02
Fe_2O_3	0.42	0.42	0.45	0.34	0.37	0.38	0.40	0.41	0.44	0.44	0.44	0.74	0.65	0.60	0.64	0.61
CaO	11.43	11.18	11.31	8.56	8.37	11.51	10.65	11.96	10.83	11.53	11.38	13.22	17.57	17.31	17.51	17.79
Na_2O	5.03	5.07	5.27	6.26	6.76	4.80	5.57	4.79	5.55	5.02	5.09	3.95	1.51	1.61	1.44	1.30
K_2O	0.09	0.09	0.11	0.16	0.15	0.10	0.12	0.08	0.11	0.10	0.10	0.07	0.03	b.d.	b.d.	b.d.
TOTAL	100.12	99.48	99.42	99.51	100.05	99.82	99.95	99.55	100.03	99.77	100.10	99.79	99.99	100.13	99.70	100.22
Ab	44.1	44.8	45.5	56.4	58.8	42.8	48.3	41.9	47.8	43.8	44.5	35.0	13.4	14.4	13.0	11.7
An	55.4	54.6	53.9	42.6	40.3	56.7	51.0	57.7	51.6	55.6	54.9	64.6	86.4	85.6	86.9	88.2
Or	0.5	0.5	0.6	0.9	0.9	0.6	0.7	0.4	0.6	0.6	0.6	0.4	0.2	0.1	0.1	0.1

Sample	K4-FSP6	K4-FSP7	K4-FSP8	K4-FSP9	K4-FSP10	K4-FSP11	K4-FSP12	K4-FSP13	K4-FSP14	K4-FSP15	K4-FSP16	K4-FSP17	K4-FSP18	K4-FSP19	K4-FSP20	K4-FSP21
Type	euhedral	euhedral	sieve	sieve	sieve	sieve	sieve	sieve	sieve	sieve	sieve	sieve	micro	micro	micro	sieve
Location	core	core	core	core	middle	middle	rim	rim	rim	rim	core	core	core	core	core	rim
Host Lithology	andesite	andesite	andesite	basaltic andesite	basaltic andesite	basaltic andesite	basaltic andesite	basaltic andesite	basaltic andesite	basaltic andesite	basaltic andesite	basaltic andesite	basaltic andesite	basaltic andesite	basaltic andesite	basaltic andesite
SiO_2	44.21	44.40	46.11	45.27	46.77	44.91	46.13	46.11	45.76	46.77	47.11	45.23	45.51	46.08	44.81	47.75
Al_2O_3	35.67	35.59	34.58	35.10	34.08	35.05	34.40	34.37	34.69	33.86	33.62	34.65	34.70	34.20	35.19	33.22
Fe_2O_3	0.60	0.57	0.64	0.59	0.59	0.55	0.59	0.57	0.59	0.59	0.58	0.62	0.61	0.63	0.66	0.57
CaO	18.72	18.55	17.36	18.00	16.77	17.86	17.30	17.10	17.33	16.65	16.51	17.83	17.70	17.19	18.30	16.00
Na_2O	0.79	0.87	1.62	1.26	1.93	1.26	1.74	1.72	1.63	1.98	2.18	1.42	1.42	1.71	1.13	2.45
K_2O	b.d.	b.d.	b.d.	b.d.	b.d.	b.d.	0.03	0.03	0.03	0.03	0.03	0.03	b.d.	0.03	b.d.	0.04
TOTAL	99.99	100.00	100.32	100.24	100.16	99.64	100.18	99.89	100.02	99.88	100.03	99.78	99.96	99.85	100.10	100.02
Ab	7.1	7.8	14.5	11.2	17.2	11.3	15.4	15.3	14.5	17.7	19.3	12.5	12.7	15.2	10.0	21.7
An	92.9	92.1	85.5	88.6	82.7	88.6	84.5	84.5	85.4	82.1	80.6	87.3	87.2	84.6	89.9	78.1
Or	0.0	0.1	0.1	0.1	0.1	0.1	0.1	0.2	0.1	0.2	0.1	0.2	0.1	0.2	0.1	0.2

Table D.3. Feldspar Analyses

Sample	K4-FSP22	K4-FSP23	K4-FSP24	K4-FSP25	K4-FSP26	K4-FSP27	K4-FSP28	K4-FSP29	K4-FSP30	K4-FSP31	K4-FSP32	K4-FSP33	K6-FSP1	K6-FSP2	K6-FSP3	K6-FSP4
Type	micro	euhedral	euhedral	euhedral	euhedral	euhedral	sieve	euhedral	euhedral	sieve	sieve	micro	euhedral	euhedral	euhedral	sieve
Location	core	core	middle	rim	core	core	rim	core	rim	rim	rim	core	rim	rim	core	middle
Host Lithology	basaltic andesite	basaltic andesite	basaltic andesite	basaltic andesite	basaltic andesite	basaltic andesite	basaltic andesite	basaltic andesite	basaltic andesite	basaltic andesite	basaltic andesite	basaltic andesite	basaltic andesite	basaltic andesite	basaltic andesite	basaltic andesite
SiO_2	44.71	45.31	46.50	50.60	49.77	49.99	49.20	49.77	47.25	46.47	46.32	46.17	46.49	46.31	43.98	48.78
Al_2O_3	35.38	34.75	34.01	31.45	31.68	31.51	32.16	32.13	33.49	34.16	33.94	34.20	33.48	33.87	35.61	32.65
Fe_2O_3	0.66	0.65	0.57	0.69	0.59	0.58	0.58	0.55	0.55	0.57	0.67	0.58	0.63	0.59	0.48	0.49
CaO	18.33	17.85	16.76	13.89	14.15	14.03	14.78	14.77	16.42	16.93	16.54	17.15	16.26	16.41	18.64	14.87
Na_2O	1.05	1.36	1.87	3.56	3.44	3.64	3.02	3.25	2.20	1.87	2.03	1.73	2.05	1.94	0.76	2.68
K_2O	b.d.	b.d.	0.03	0.05	0.06	0.07	0.04	0.05	b.d.	0.03	0.05	b.d.	0.03	b.d.	0.03	0.09
TOTAL	100.14	99.93	99.74	100.23	99.69	99.82	99.77	100.52	99.92	100.02	99.54	99.87	98.93	99.14	99.49	99.56
Ab	9.4	12.1	16.8	31.6	30.4	31.8	26.9	28.4	19.5	16.6	18.1	15.6	18.5	17.6	6.9	24.5
An	90.5	87.8	83.0	68.2	69.2	67.8	72.8	71.3	80.4	83.3	81.6	84.3	81.3	82.3	93.0	75.0
Or	0.0	0.1	0.2	0.3	0.4	0.4	0.2	0.3	0.1	0.1	0.3	0.1	0.2	0.1	0.2	0.5

Sample	K6-FSP5	K6-FSP6	K6-FSP7	K6-FSP8	K6-FSP9	K6-FSP10	K6-FSP11	K6-FSP12	K6-FSP13	K6-FSP14	K6-FSP15	K6-FSP16	K6-FSP17	K6-FSP18	K6-FSP19	K6-FSP20
Type	sieve	sieve	sieve	micro	euhedral	euhedral	micro	euhedral	euhedral	euhedral	sieve	sieve	euhedral	euhedral	sieve	sieve
Location	rim	core	rim	core	rim	rim	core	core	middle	rim	middle	rim	core	core	core	middle
Host Lithology	basaltic andesite	basaltic andesite	basaltic andesite	basaltic andesite	basaltic andesite	basaltic andesite	basaltic andesite	dacite	dacite	dacite	basaltic andesite	basaltic andesite	basaltic andesite	basaltic andesite	basaltic andesite	basaltic andesite
SiO_2	49.39	48.17	49.51	54.31	48.41	49.70	51.68	54.49	55.98	55.42	56.35	53.37	45.43	44.94	56.42	55.43
Al_2O_3	32.02	32.74	31.46	27.77	31.72	31.21	30.40	29.30	28.25	28.56	27.18	28.34	34.02	34.47	27.87	28.35
Fe_2O_3	0.49	0.51	0.50	0.45	0.68	0.72	0.76	0.36	0.35	0.37	0.52	0.47	0.63	0.63	0.39	0.57
CaO	14.17	15.21	14.22	10.82	15.15	14.57	13.34	11.16	9.80	10.39	9.49	11.22	17.56	17.78	9.54	10.41
Na_2O	3.32	2.70	3.26	5.30	2.72	3.08	3.85	5.25	5.87	5.66	6.10	5.11	1.46	1.25	6.15	5.62
K_2O	0.04	0.04	0.06	0.08	0.04	0.05	0.05	0.10	0.12	0.09	0.11	0.08	0.03	b.d.	0.09	0.11
TOTAL	99.44	99.37	99.01	98.73	98.70	99.33	100.08	100.66	100.37	100.50	99.75	98.58	99.12	99.09	100.46	100.49
Ab	29.7	24.3	29.2	46.8	24.4	27.5	34.2	45.7	51.6	49.4	53.4	45.0	13.0	11.3	53.6	49.1
An	70.0	75.5	70.4	52.8	75.4	72.2	65.5	53.7	47.7	50.1	45.9	54.6	86.8	88.7	45.9	50.2
Or	0.3	0.2	0.4	0.4	0.2	0.3	0.3	0.6	0.7	0.5	0.7	0.4	0.2	0.0	0.5	0.7

Sample	K6-FSP21	K6-FSP22	K6-FSP23	K6-FSP24	K6-FSP25	K6-FSP26	K6-FSP27	K6-FSP28	K6-FSP29	K6-FSP30	K6-FSP31	K6-FSP32	K6-FSP33	K6-FSP34	K6-FSP35	K6-FSP36
Type	sieve	sieve	sieve	sieve	sieve	sieve	sieve	sieve	euhedral	sieve	euhedral	sieve	sieve	sieve	sieve	sieve
Location	rim	rim	core	core	middle	middle	rim	rim	core	core	middle	middle	middle	rim	rim	core
Host Lithology	basaltic andesite	basaltic andesite	basaltic andesite	basaltic andesite	basaltic andesite	basaltic andesite	basaltic andesite	basaltic andesite	basaltic andesite	basaltic andesite	basaltic andesite	basaltic andesite	basaltic andesite	basaltic andesite	basaltic andesite	basaltic andesite
SiO_2	53.82	51.32	46.03	51.60	45.10	50.52	45.61	51.77	51.88	51.94	52.69	55.54	52.95	52.47	54.94	46.60
Al_2O_3	29.42	31.11	34.57	30.68	35.17	31.55	35.22	30.97	31.16	30.64	30.20	28.08	30.29	30.45	28.90	34.47
Fe_2O_3	0.41	0.47	0.60	0.69	0.62	0.60	0.44	0.46	0.48	0.48	0.43	0.57	0.52	0.45	0.49	0.60
CaO	11.50	13.44	17.11	12.93	17.77	13.95	17.73	13.13	13.30	12.85	12.19	10.07	12.17	12.56	10.79	17.16
Na_2O	5.09	4.06	1.67	4.46	1.35	3.59	1.43	4.14	4.08	4.34	4.62	5.73	4.67	4.44	5.47	1.69
K_2O	0.08	0.08	b.d.	0.06	0.03	0.05	b.d.	0.05	0.06	0.06	0.07	0.09	0.08	0.08	0.08	0.03
TOTAL	100.31	100.47	99.99	100.42	100.04	100.25	100.43	100.52	100.96	100.31	100.21	100.07	100.67	100.45	100.66	100.56
Ab	44.3	35.2	15.0	38.3	12.1	31.7	12.8	36.2	35.6	37.8	40.5	50.5	40.8	38.8	47.6	15.1
An	55.3	64.4	85.0	61.3	87.8	68.0	87.2	63.5	64.1	61.8	59.1	49.0	58.8	60.7	51.9	84.7
Or	0.4	0.4	0.1	0.3	0.1	0.3	0.0	0.3	0.3	0.3	0.4	0.5	0.5	0.4	0.4	0.2

Table D.3. Feldspar Analyses

Sample	K6-FSP37	K6-FSP38	K6-FSP39	K6-FSP40	K6-FSP41	K6-FSP42	K6-FSP43	K6-FSP44	K6-FSP45	K6-FSP46	K6-FSP47	K6-FSP48	K6-FSP49	K6-FSP50	K6-FSP51	K6-FSP52
Type	euhedral	sieve	euhedral	euhedral	euhedral	sieve	sieve	sieve	sieve	sieve	sieve	euhedral	euhedral	euhedral	euhedral	euhedral
Location	core	middle	core	core	core	core	core	middle	middle	rim	rim	core	core	middle	middle	middle
Host Lithology	basaltic andesite	basaltic andesite	basaltic andesite	basaltic andesite	basaltic andesite	basaltic andesite	basaltic andesite	basaltic andesite	basaltic andesite	basaltic andesite	basaltic andesite	basaltic andesite	basaltic andesite	basaltic andesite	basaltic andesite	basaltic andesite
SiO_2	51.78	51.86	47.43	50.60	46.04	46.10	46.95	46.04	46.34	47.94	50.56	53.52	47.23	51.93	51.31	55.02
Al_2O_3	31.04	30.70	32.11	30.42	33.40	33.51	32.56	33.51	33.36	32.46	30.34	28.57	32.50	29.66	29.78	27.47
Fe_2O_3	0.53	0.45	0.72	0.71	0.64	0.57	0.57	0.59	0.54	0.59	0.42	0.36	0.59	0.40	0.34	0.37
CaO	13.21	13.15	16.11	13.53	17.41	17.23	16.17	17.25	17.03	16.05	13.40	11.37	16.18	12.58	12.82	10.14
Na_2O	4.03	4.11	2.31	3.78	1.61	1.67	2.28	1.54	1.74	2.33	3.86	5.13	2.20	4.48	4.22	5.79
K_2O	0.06	0.07	0.04	0.04	0.03	b.d.	0.03	b.d.	0.03	b.d.	0.06	0.10	0.03	0.08	0.06	0.12
TOTAL	100.65	100.34	98.73	99.08	99.12	99.10	98.56	99.04	99.04	99.40	98.63	99.05	98.74	99.13	98.53	98.91
Ab	35.4	35.9	20.6	33.5	14.3	14.9	20.3	14.7	15.6	20.8	34.2	44.7	19.7	39.0	37.2	50.5
An	64.2	63.6	79.2	66.3	85.5	84.9	79.5	85.3	84.2	79.1	65.5	54.7	80.1	60.5	62.4	48.8
Or	0.4	0.4	0.2	0.2	0.2	0.1	0.2	0.0	0.1	0.1	0.3	0.6	0.2	0.5	0.4	0.7

Sample	K6-FSP53	K6-FSP54	K6-FSP55	K6-FSP56	K6-FSP57	K6-FSP58	K6-FSP59	K6-FSP60	K6-FSP61	K6-FSP62	K6-FSP63	K6-FSP64	K6-FSP65	K6-FSP66	K6-FSP67	K6-FSP68
Type	euhedral	euhedral	euhedral	euhedral	sieve	euhedral	euhedral	euhedral	euhedral	euhedral	euhedral	euhedral	euhedral	euhedral	euhedral	euhedral
Location	middle	rim	rim	core	core	core	middle	middle	rim	core	rim	core	core	rim	rim	core
Host Lithology	basaltic andesite	basaltic andesite	basaltic andesite	basaltic andesite	basaltic andesite	basaltic andesite	basaltic andesite	basaltic andesite	basaltic andesite	basaltic andesite	basaltic andesite	basaltic andesite	basaltic andesite	basaltic andesite	basaltic andesite	basaltic andesite
SiO_2	55.45	52.67	53.57	52.19	51.99	55.28	46.44	48.38	53.83	53.83	53.40	47.21	46.84	51.40	53.02	51.79
Al_2O_3	27.20	28.74	28.63	29.34	29.17	27.28	33.13	31.82	28.75	28.17	28.39	32.83	33.10	29.89	28.99	29.83
Fe_2O_3	0.35	0.43	0.48	0.51	0.46	0.36	0.61	0.39	0.45	0.36	0.43	0.51	0.55	0.46	0.47	0.47
CaO	9.52	11.67	11.29	12.18	12.22	9.70	17.25	14.99	11.38	10.97	11.19	16.26	16.57	12.95	11.80	12.79
Na_2O	6.18	4.99	5.05	4.68	4.63	6.03	1.75	2.96	5.22	5.51	5.27	2.20	2.07	4.23	4.86	4.28
K_2O	0.13	0.08	0.08	0.07	0.07	0.11	b.d.	0.04	0.09	0.09	0.10	0.04	b.d.	0.07	0.08	0.08
TOTAL	98.83	98.59	99.11	98.96	98.55	98.75	99.20	98.58	99.72	98.93	98.77	99.05	99.15	99.00	99.23	99.24
Ab	53.6	43.4	44.5	40.9	40.5	52.6	15.5	26.2	45.1	47.4	45.7	19.6	18.4	37.0	42.5	37.5
An	45.6	56.1	55.0	58.8	59.1	46.8	84.4	73.5	54.4	52.1	53.7	80.1	81.5	62.6	57.0	62.0
Or	0.7	0.5	0.5	0.4	0.4	0.6	0.1	0.2	0.5	0.5	0.6	0.2	0.1	0.4	0.5	0.4

Sample	K6-FSP69	K6-FSP70	K6-FSP71	K6-FSP72	K6-FSP73	K6-FSP74	K6-FSP75	K6-FSP76	K6-FSP77	K6-FSP78	K6-FSP79	K6-FSP80	K6-FSP81	K6-FSP82	K6-FSP83	K6-FSP84
Type	euhedral	euhedral	euhedral	euhedral	euhedral	euhedral	euhedral	sieve	sieve	sieve	euhedral	sieve	euhedral	euhedral	euhedral	euhedral
Location	middle	core	rim	rim	rim	core	core	rim	rim	middle	rim	core	core	core	rim	rim
Host Lithology	basaltic andesite	basaltic andesite	basaltic andesite	basaltic andesite	basaltic andesite	basaltic andesite	basaltic andesite	basaltic andesite	basaltic andesite	basaltic andesite	basaltic andesite	basaltic andesite	basaltic andesite	basaltic andesite	basaltic andesite	basaltic andesite
SiO_2	53.26	52.97	52.99	51.98	52.70	52.21	55.20	52.98	49.50	49.33	53.53	50.61	45.84	45.46	51.92	52.40
Al_2O_3	28.82	29.20	28.93	29.37	28.90	29.53	27.32	28.66	30.97	31.20	28.58	30.31	33.96	34.02	29.22	29.06
Fe_2O_3	0.46	0.47	0.46	0.55	0.52	0.42	0.45	0.65	0.58	0.59	0.48	0.55	0.46	0.42	0.48	0.47
CaO	11.81	12.14	11.91	12.34	11.77	12.32	10.05	11.89	14.35	14.30	11.39	13.70	17.51	17.53	12.29	12.06
Na_2O	4.82	4.77	4.74	4.43	4.83	4.54	5.86	4.84	3.32	3.31	5.10	3.84	1.57	1.45	4.58	4.70
K_2O	0.09	0.08	0.09	0.09	0.06	0.05	0.10	0.07	0.04	0.05	0.08	0.04	b.d.	b.d.	0.08	0.08
TOTAL	99.25	99.63	99.11	98.75	98.79	99.06	98.97	99.10	98.76	98.78	99.16	99.05	99.34	98.89	98.57	98.78
Ab	42.3	41.4	41.7	39.2	42.5	39.9	51.1	42.3	29.4	29.4	44.6	33.6	13.9	13.0	40.1	41.2
An	57.2	58.1	57.8	60.3	57.2	59.8	48.4	57.3	70.3	70.3	55.0	66.2	86.0	87.0	59.5	58.4
Or	0.5	0.5	0.5	0.5	0.3	0.3	0.5	0.4	0.2	0.3	0.5	0.2	0.0	0.0	0.4	0.5

Table D.3. Feldspar Analyses

Sample	K6-FSP85	K6-FSP86	K6-FSP87	K6-FSP88	K6-FSP89	K6-FSP90	K6-FSP91	K6-FSP92	K6-FSP93	K6-FSP94	K6-FSP95	K6-FSP96	K6-FSP97	K6-FSP98	K6-FSP99	K6-FSP100
Type	micro	micro	micro	micro	micro	euhedral	micro	euhedral	euhedral	euhedral	euhedral	euhedral	euhedral	euhedral	euhedral	euhedral
Location	core	core	core	core	rim	rim	core	rim	rim	core	core	core	core	core	core	core
Host Lithology	basaltic andesite	basaltic andesite	basaltic andesite	basaltic andesite	basaltic andesite	basaltic andesite	basaltic andesite	basaltic andesite	basaltic andesite	basaltic andesite	basaltic andesite	basaltic andesite	basaltic andesite	basaltic andesite	basaltic andesite	basaltic andesite
SiO_2	52.56	51.74	52.13	52.47	53.30	52.03	53.28	53.62	53.84	53.89	53.90	45.49	45.89	46.07	44.63	50.38
Al_2O_3	29.48	29.86	29.38	29.09	28.71	29.73	28.82	28.31	28.39	28.39	28.57	33.71	33.56	33.23	35.84	31.94
Fe_2O_3	0.45	0.51	0.47	0.45	0.42	0.79	0.42	0.38	0.50	0.36	0.41	0.76	0.68	0.75	0.48	0.51
CaO	12.24	12.80	12.23	11.92	11.41	12.81	11.55	11.14	11.19	11.01	11.16	17.42	17.29	17.12	18.02	13.61
Na_2O	4.71	4.34	4.61	4.75	5.07	4.16	5.12	5.19	5.36	5.29	5.32	1.54	1.61	1.72	0.98	3.67
K_2O	0.08	0.08	0.08	0.09	0.08	0.06	0.09	0.05	0.05	0.06	0.06	b.d.	0.03	b.d.	b.d.	0.04
TOTAL	99.53	99.33	98.90	98.77	99.00	99.58	99.27	98.69	99.33	98.99	99.41	98.93	99.06	98.90	99.96	100.14
Ab	40.9	37.9	40.4	41.7	44.4	36.9	44.3	45.6	46.3	46.4	46.2	13.8	14.4	15.3	8.9	32.7
An	58.7	61.7	59.2	57.8	55.2	62.7	55.2	54.1	53.4	53.3	53.5	86.1	85.5	84.5	91.0	67.0
Or	0.4	0.4	0.4	0.5	0.5	0.4	0.5	0.3	0.3	0.3	0.3	0.1	0.1	0.1	0.1	0.2

Sample	K6-FSP101	K6-FSP102	K6-FSP103	K6-FSP104	K6-FSP105	K6-FSP106	K6-FSP107	K6-FSP108	K6-FSP109	K6-FSP110	K6-FSP111	K6-FSP112	K6-FSP113	K6-FSP114	K6-FSP115	K6-FSP116
Type	sieve	sieve	euhedral	euhedral	euhedral	euhedral	euhedral	euhedral	euhedral	euhedral	euhedral	euhedral	sieve	sieve	sieve	sieve
Location	core	rim	core	core	rim	rim	core	rim	middle	middle	rim	rim	core	core	rim	rim
Host Lithology	basaltic andesite	basaltic andesite	basaltic andesite	basaltic andesite	basaltic andesite	basaltic andesite	basaltic andesite	basaltic andesite	basaltic andesite	basaltic andesite	basaltic andesite	basaltic andesite	basaltic andesite	basaltic andesite	basaltic andesite	basaltic andesite
SiO_2	52.39	46.94	46.41	47.20	46.55	46.24	46.29	47.91	47.87	45.36	50.28	50.04	49.89	49.22	49.60	50.30
Al_2O_3	30.46	33.94	34.92	34.39	34.69	34.76	34.85	33.69	33.43	35.29	32.31	32.17	32.65	33.41	32.78	32.06
Fe_2O_3	0.71	0.50	0.52	0.54	0.59	0.57	0.61	0.57	0.55	0.52	0.51	0.52	0.52	0.53	0.56	0.53
CaO	12.69	16.26	16.94	16.50	16.88	17.01	16.70	15.56	15.67	17.51	14.10	13.85	14.48	14.80	14.54	13.86
Na_2O	4.02	1.87	1.83	2.12	1.84	1.63	1.80	2.33	2.72	1.34	3.47	3.56	3.20	3.11	3.27	3.57
K_2O	0.10	b.d.	b.d.	b.d.	b.d.	b.d.	b.d.	0.04	0.03	b.d.	0.04	0.05	0.03	0.05	0.05	0.04
TOTAL	100.38	99.52	100.62	100.75	100.57	100.23	100.26	100.09	100.26	100.02	100.72	100.18	100.77	101.12	100.80	100.36
Ab	36.3	17.2	16.3	18.8	16.5	14.8	16.3	21.3	23.9	12.2	30.8	31.7	28.5	27.5	28.8	31.7
An	63.2	82.8	83.6	81.1	83.4	85.2	83.6	78.5	76.0	87.8	69.0	68.1	71.3	72.3	70.9	68.0
Or	0.6	0.0	0.0	0.1	0.1	0.1	0.1	0.2	0.1	0.0	0.2	0.3	0.2	0.3	0.3	0.2

Sample	K6-FSP117	K6-FSP118	K6-FSP119	K6-FSP120	K6-FSP121	K6-FSP122	K6-FSP123	K6-FSP124	K6-FSP125	K6-FSP126	K6-FSP127	K6-FSP128	K6-FSP129	K6-FSP130	K6-FSP131	K6-FSP132
Type	sieve	sieve	sieve	sieve	euhedral	euhedral	sieve	micro	sieve	sieve	micro	micro	euhedral	euhedral	euhedral	sieve
Location	core	core	rim	rim	rim	core	core	core	middle	rim	core	rim	rim	core	rim	core
Host Lithology	basaltic andesite	basaltic andesite	basaltic andesite	basaltic andesite	basaltic andesite	basaltic andesite	basaltic andesite	basaltic andesite	basaltic andesite	basaltic andesite	basaltic andesite	basaltic andesite	basaltic andesite	dacite	basaltic andesite	basaltic andesite
SiO_2	49.27	48.65	49.83	48.51	51.21	44.63	50.06	47.44	46.63	50.80	49.44	49.21	50.94	56.65	53.45	47.21
Al_2O_3	32.97	33.29	32.60	33.45	31.56	36.06	32.32	34.08	34.65	31.86	32.79	32.48	31.83	26.61	28.85	33.01
Fe_2O_3	0.53	0.53	0.49	0.52	0.46	0.55	0.60	0.49	0.57	0.53	0.56	0.59	0.50	0.35	0.46	0.59
CaO	14.81	15.05	14.21	15.35	13.26	18.12	14.23	15.95	16.83	13.56	14.32	14.54	13.53	8.62	10.94	15.81
Na_2O	2.50	2.70	3.30	2.69	4.06	0.98	2.88	2.29	1.90	3.84	3.34	3.23	3.88	6.31	5.15	2.41
K_2O	0.03	b.d.	0.04	0.03	0.06	b.d.	0.04	0.03	b.d.	0.05	0.03	0.03	0.06	0.18	0.09	0.04
TOTAL	100.11	100.23	100.48	100.56	100.62	100.36	100.13	100.27	100.60	100.63	100.47	100.07	100.74	98.73	98.93	99.07
Ab	23.4	24.5	29.5	24.0	35.5	8.9	26.8	20.6	16.9	33.8	29.6	28.6	34.0	56.4	45.8	21.6
An	76.5	75.4	70.2	75.8	64.1	91.0	73.0	79.2	83.0	66.0	70.2	71.2	65.6	42.6	53.7	78.2
Or	0.2	0.1	0.3	0.2	0.4	0.1	0.3	0.2	0.1	0.3	0.2	0.2	0.4	1.1	0.5	0.2

Table D.3. Feldspar Analyses

Sample	K6-FSP133	K6-FSP134	K6-FSP135	K6-FSP136	K6-FSP137	K6-FSP138	K6-FSP139	K6-FSP140	K6-FSP141	K6-FSP142	K6-FSP143	K6-FSP144	K6-FSP145	K6-FSP146	K6-FSP147	K6-FSP148
Type	sieve	sieve	sieve	sieve	sieve	euhedral	euhedral	euhedral	euhedral	euhedral	euhedral	euhedral	euhedral	euhedral	euhedral	euhedral
Location	rim	core	rim	core	rim	core	rim	rim	core	rim	core	rim	core	rim	core	rim
Host Lithology	basaltic andesite	basaltic andesite	basaltic andesite	basaltic andesite	basaltic andesite	basaltic andesite	basaltic andesite	dacite	dacite	dacite	dacite	dacite	dacite	dacite	dacite	dacite
SiO_2	48.59	50.86	51.48	48.09	47.66	54.70	56.17	56.61	58.60	57.85	58.25	57.56	59.13	59.40	56.30	56.70
Al_2O_3	32.04	30.78	30.38	32.41	32.82	28.13	27.01	26.86	25.76	26.21	25.98	26.22	25.21	25.40	27.99	27.74
Fe_2O_3	0.59	0.44	0.50	0.62	0.56	0.38	0.36	0.28	0.24	0.28	0.29	0.31	0.26	0.27	0.33	0.34
CaO	14.90	13.06	12.64	15.11	15.40	10.03	8.82	8.61	7.32	7.82	7.71	7.92	6.88	6.73	9.46	9.26
Na_2O	3.01	3.93	4.18	2.87	2.58	5.57	6.21	6.39	7.06	6.80	6.99	6.75	7.38	7.38	6.25	6.26
K_2O	0.03	0.05	0.08	0.03	0.04	0.13	0.16	0.17	0.20	0.18	0.19	0.17	0.25	0.26	0.15	0.15
TOTAL	99.16	99.13	99.26	99.12	99.06	99.04	98.72	98.91	99.19	99.15	99.41	98.93	99.11	99.43	100.49	100.43
Ab	26.7	35.2	37.3	25.6	23.2	50.2	55.5	56.8	62.8	60.5	61.4	60.1	65.1	65.5	54.0	54.6
An	73.1	64.5	62.3	74.3	76.6	49.1	43.6	42.3	36.0	38.4	37.4	39.0	33.5	33.0	45.2	44.6
Or	0.2	0.3	0.5	0.1	0.2	0.7	0.9	1.0	1.2	1.1	1.1	1.0	1.4	1.5	0.8	0.9

Sample	K6-FSP149	K6-FSP150	K6-FSP151	K6-FSP152	K6-FSP153	K6-FSP154	K9-FSP1	K9-FSP2	K9-FSP3	K9-FSP4	K9-FSP5	K9-FSP6	K9-FSP7	K9-FSP8	K9-FSP9	K9-FSP10
Type	sieve	sieve	euhedral	euhedral	euhedral	euhedral	euhedral	euhedral	euhedral	euhedral	euhedral	euhedral	euhedral	euhedral	euhedral	euhedral
Location	core	rim	core	core	core	core	core	core	rim	rim	rim	core	rim	rim	core	rim
Host Lithology	basaltic andesite	basaltic andesite	basaltic andesite	basaltic andesite	basaltic andesite	basaltic andesite	rhyolite	rhyolite	rhyolite	rhyolite	rhyolite	rhyolite	rhyolite	rhyolite	rhyolite	rhyolite
SiO_2	50.77	48.31	54.03	51.82	50.87	53.61	59.98	56.33	57.68	57.65	54.58	54.39	56.06	56.63	59.22	59.84
Al_2O_3	31.36	33.29	29.12	30.34	31.75	29.66	25.82	27.88	27.08	27.29	28.89	29.18	28.21	27.49	26.08	26.04
Fe_2O_3	0.57	0.62	0.62	0.56	0.70	0.56	0.25	0.35	0.29	0.35	0.37	0.35	0.34	0.32	0.29	0.24
CaO	13.84	15.64	11.01	12.48	13.74	11.79	6.89	9.24	8.48	8.35	10.52	10.96	9.54	8.93	7.27	7.05
Na_2O	3.72	2.65	5.21	4.44	3.75	4.94	7.76	6.41	6.99	6.91	5.54	5.40	6.26	6.58	7.58	7.73
K_2O	0.05	0.05	0.10	0.07	0.07	0.08	0.22	0.14	0.18	0.19	0.10	0.11	0.13	0.14	0.21	0.17
TOTAL	100.30	100.56	100.08	99.70	100.88	100.65	100.92	100.35	100.70	100.73	100.00	100.38	100.55	100.08	100.64	101.07
Ab	32.6	23.4	45.9	39.0	32.9	42.9	66.3	55.3	59.3	59.3	48.5	46.8	53.9	56.7	64.6	65.8
An	67.1	76.3	53.6	60.6	66.7	56.6	32.5	44.0	39.7	39.6	50.9	52.5	45.4	42.5	34.2	33.2
Or	0.3	0.3	0.6	0.4	0.4	0.5	1.2	0.8	1.0	1.1	0.6	0.6	0.8	0.8	1.2	1.0

Sample	K9-FSP11	K9-FSP12	K9-FSP13	K9-FSP14	K9-FSP15	K9-FSP16	K9-FSP17	K9-FSP18	K9-FSP19	K9-FSP20	K9-FSP21	K9-FSP22	K9-FSP23	K9-FSP24	K9-FSP25	K9-FSP26
Type	euhedral	euhedral	euhedral	euhedral	euhedral	euhedral	euhedral	euhedral	euhedral	euhedral	euhedral	euhedral	euhedral	micro	micro	euhedral
Location	rim	core	core	rim	rim	core	core	core	core	rim	rim	core	rim	core	rim	core
Host Lithology	rhyolite	rhyolite	rhyolite	rhyolite	rhyolite	rhyolite	rhyolite	rhyolite	rhyolite	rhyolite	rhyolite	rhyolite	rhyolite	rhyolite	rhyolite	rhyolite
SiO_2	59.11	55.96	56.18	59.28	58.15	56.01	54.93	55.03	55.06	59.67	59.08	58.96	58.90	59.40	58.19	55.69
Al_2O_3	26.37	27.76	28.35	25.70	26.67	28.27	28.57	28.89	28.76	25.60	26.23	26.42	25.92	26.05	26.31	28.60
Fe_2O_3	0.29	0.31	0.33	0.28	0.33	0.34	0.35	0.32	0.33	0.28	0.28	0.25	0.27	0.27	0.26	0.34
CaO	7.39	9.35	9.46	7.06	7.90	9.49	9.93	10.37	10.19	6.81	7.36	7.49	7.11	7.19	7.78	9.75
Na_2O	7.61	6.44	6.35	7.67	7.18	6.30	6.00	5.81	5.89	7.76	7.64	7.52	7.60	7.57	7.34	5.99
K_2O	0.21	0.13	0.13	0.22	0.18	0.13	0.11	0.12	0.12	0.22	0.20	0.20	0.19	0.20	0.18	0.10
TOTAL	100.97	99.95	100.79	100.20	100.41	100.54	99.89	100.54	100.34	100.34	100.80	100.84	100.00	100.68	100.06	100.47
Ab	64.4	55.1	54.5	65.5	61.5	54.1	51.9	50.0	50.8	66.5	64.5	63.8	65.2	64.9	62.4	52.4
An	34.5	44.2	44.8	33.3	37.5	45.1	47.5	49.3	48.6	32.3	34.3	35.1	33.7	34.0	36.6	47.1
Or	1.2	0.8	0.7	1.2	1.0	0.7	0.6	0.7	0.7	1.2	1.1	1.1	1.1	1.1	1.0	0.6

Table D.3. Feldspar Analyses

Sample	K9-FSP27	K9-FSP28	K9-FSP29	K9-FSP30	K9-FSP31	K9-FSP32	K9-FSP33	K9-FSP34	K9-FSP35	K9-FSP36	K9-FSP37	K9-FSP38	K9-FSP39	K9-FSP40	K9-FSP41
Type	euhedral	euhedral	euhedral	euhedral	euhedral	euhedral	euhedral	euhedral	euhedral	euhedral	euhedral	euhedral	euhedral	euhedral	euhedral
Location	rim	rim	rim	core	core	rim	rim	rim	core	middle	middle	rim	core	rim	middle
Host Lithology	rhyolite	rhyolite	rhyolite	rhyolite	rhyolite	rhyolite	rhyolite	rhyolite	rhyolite	rhyolite	rhyolite	rhyolite	rhyolite	rhyolite	rhyolite
SiO_2	55.12	54.94	45.21	55.98	56.14	57.50	57.06	57.03	53.84	56.32	57.55	54.28	45.13	55.54	55.48
Al_2O_3	28.27	28.72	35.28	27.78	27.70	27.28	27.53	27.13	28.38	27.02	26.57	28.29	35.00	27.68	27.47
Fe_2O_3	0.33	0.32	0.47	0.32	0.32	0.30	0.32	0.33	0.35	0.34	0.35	0.33	0.31	0.34	0.34
CaO	9.75	10.06	17.29	9.27	9.22	8.34	8.75	8.78	10.67	8.88	8.38	9.91	17.68	9.38	8.90
Na_2O	6.09	5.97	1.44	6.38	6.50	6.90	6.68	6.23	5.23	6.19	6.57	5.65	1.48	6.05	6.41
K_2O	0.12	0.13	b.d.	0.14	0.14	0.17	0.15	0.14	0.11	0.16	0.16	0.14	0.03	0.14	0.17
TOTAL	99.68	100.14	99.70	99.86	100.03	100.49	100.49	99.64	98.58	98.91	99.58	98.60	99.63	99.13	98.75
Ab	52.7	51.4	13.1	55.0	55.6	59.4	57.5	55.7	46.7	55.3	58.1	50.4	13.1	53.4	56.0
An	46.6	47.9	86.8	44.2	43.6	39.7	41.6	43.4	52.7	43.8	41.0	48.8	86.7	45.8	43.0
Or	0.7	0.8	0.1	0.8	0.8	0.9	0.8	0.8	0.7	0.9	0.9	0.8	0.1	0.8	1.0

Sample	K12L-FSP1	K12L-FSP2	K12L-FSP3	K12L-FSP4	K12L-FSP5	K12L-FSP6	K12L-FSP7	K12L-FSP8	K12L-FSP9	K12L-FSP10	K12L-FSP11	K12L-FSP12	K12L-FSP13	K12L-FSP14	K12L-FSP15
Type	sieve	sieve	euhedral	sieve	sieve	sieve	sieve	sieve	sieve	sieve	euhedral	euhedral	euhedral	euhedral	euhedral
Location	core	rim	core	core	core	middle	core	middle	rim	rim	rim	core	rim	rim	core
Host Lithology	andesite	andesite	andesite	andesite	andesite	andesite	andesite	andesite	andesite	andesite	andesite	andesite	andesite	andesite	andesite
SiO_2	45.86	50.31	46.67	52.36	52.26	54.53	47.85	55.25	52.40	52.26	45.67	52.20	45.94	53.38	46.14
Al_2O_3	33.63	30.24	32.77	29.39	29.43	27.76	32.08	27.31	28.99	29.14	33.78	29.22	33.41	28.42	33.32
Fe_2O_3	0.61	0.64	0.57	0.43	0.47	0.36	0.53	0.39	0.48	0.60	0.58	0.56	0.55	0.75	0.73
CaO	17.33	13.86	16.54	12.36	12.19	10.56	15.68	10.17	12.10	12.14	17.38	12.13	17.03	11.51	17.02
Na_2O	1.55	3.42	1.95	4.38	4.44	5.45	2.61	5.63	4.51	4.48	1.51	4.41	1.61	4.92	1.57
K_2O	b.d.	0.05	b.d.	0.07	0.07	0.09	0.04	0.11	0.05	0.06	b.d.	0.06	b.d.	0.09	b.d.
TOTAL	99.00	98.51	98.51	99.00	98.85	98.75	98.78	98.86	98.53	98.69	98.93	98.58	98.55	99.07	98.80
Ab	13.9	30.8	17.6	38.9	39.6	48.1	23.1	49.7	40.2	39.9	13.6	39.6	14.6	43.4	14.3
An	85.9	68.9	82.4	60.7	60.1	51.4	76.7	49.6	59.5	59.7	86.3	60.1	85.3	56.1	85.6
Or	0.1	0.3	0.0	0.4	0.4	0.5	0.2	0.6	0.3	0.4	0.1	0.4	0.1	0.5	0.1

Sample	K12L-FSP16	K12L-FSP17	K12L-FSP18	K12L-FSP19	K12L-FSP20	K12L-FSP21	K12L-FSP22	K14-FSP1	K14-FSP2	K14-FSP3	K14-FSP4	K14-FSP5	K14-FSP6	K14-FSP7	K14-FSP8
Type	euhedral	sieve	sieve	sieve	sieve	sieve	sieve	sieve	sieve	euhedral	euhedral	euhedral	euhedral	sieve	sieve
Location	rim	rim	rim	core	rim	rim	core	core	rim	core	rim	core	rim	core	rim
Host Lithology	andesite	andesite	andesite	andesite	andesite	andesite	andesite	basaltic andesite	basaltic andesite	andesite	andesite	andesite	andesite	andesite	andesite
SiO_2	51.51	52.21	51.84	46.51	49.97	46.39	46.49	45.81	52.68	47.19	49.82	47.84	50.34	46.84	46.94
Al_2O_3	29.67	29.44	29.36	32.77	30.55	33.09	33.11	33.63	29.02	33.40	31.52	32.54	30.83	33.12	33.05
Fe_2O_3	0.68	0.56	0.38	0.65	0.65	0.64	0.64	0.54	0.59	0.45	0.56	0.66	0.53	0.53	0.61
CaO	12.91	12.42	12.59	16.78	14.22	16.76	16.97	16.76	11.63	16.44	14.27	15.65	13.52	16.43	16.11
Na_2O	3.93	4.40	4.38	1.88	3.30	1.79	1.75	1.77	4.78	2.04	3.16	2.40	3.49	1.90	2.02
K_2O	0.07	0.08	0.09	b.d.	0.06	b.d.	0.04	0.02	0.08	0.03	0.03	0.03	0.05	0.02	0.04
TOTAL	98.77	99.11	98.64	98.60	98.75	98.69	98.99	98.53	98.78	99.55	99.36	99.12	98.76	98.84	98.77
Ab	35.4	38.9	38.4	16.9	29.5	16.2	15.7	16.0	42.5	18.3	28.5	21.7	31.7	17.3	18.5
An	64.2	60.7	61.0	83.0	70.1	83.7	84.1	83.8	57.1	81.5	71.3	78.1	67.9	82.6	81.3
Or	0.4	0.5	0.5	0.1	0.3	0.1	0.2	0.1	0.5	0.2	0.2	0.2	0.3	0.1	0.2

Table D.3. Feldspar Analyses

Sample	K14-FSP9	K14-FSP10	K14-FSP11	K14-FSP12	K14-FSP13	K14-FSP14	K14-FSP15	K14-FSP16	K14-FSP17	K14-FSP18	K14-FSP19	K14-FSP20	K17B-FSP1	K17B-FSP2	K17B-FSP3
Type	sieve	sieve	sieve	euhedral	euhedral	euhedral	euhedral	euhedral	euhedral	sieve	sieve	sieve	euhedral	euhedral	euhedral
Location	core	rim	rim	core	rim	core	rim	core	rim	core	rim	rim	core	rim	core
Host Lithology	basaltic andesite	basaltic andesite	basaltic andesite	basaltic andesite	basaltic andesite	andesite	andesite	andesite	andesite	basaltic andesite	basaltic andesite	basaltic andesite	rhyolite	rhyolite	rhyolite
SiO_2	48.12	47.14	50.94	45.44	52.72	49.54	54.61	52.11	54.44	45.72	50.20	55.29	55.69	56.56	60.44
Al_2O_3	32.56	32.72	30.05	33.77	29.34	31.69	28.37	29.79	28.14	34.05	31.57	28.00	28.84	27.51	25.79
Fe_2O_3	0.62	0.67	0.64	0.75	0.70	0.56	0.54	0.42	0.56	0.60	0.56	0.53	0.30	0.32	0.24
CaO	14.92	16.20	12.99	17.15	12.03	14.52	10.74	12.14	10.67	17.25	14.34	10.60	10.15	9.03	6.95
Na_2O	2.70	2.04	3.88	1.42	4.43	3.10	5.36	4.44	5.38	1.51	3.15	5.49	5.85	7.65	7.66
K_2O	0.03	0.04	0.04	0.04	0.07	0.03	0.06	0.06	0.07	0.02	0.03	0.09	0.13	0.16	0.22
TOTAL	98.95	98.81	98.54	98.57	99.29	99.44	99.68	98.96	99.26	99.15	99.85	100.00	100.95	100.24	101.29
Ab	24.6	18.5	35.0	13.0	39.8	27.8	47.3	39.7	47.5	13.7	28.4	48.1	50.7	56.6	65.8
An	75.2	81.3	64.8	86.7	59.8	72.0	52.3	60.0	52.1	86.2	71.4	51.3	48.6	42.5	33.0
Or	0.2	0.2	0.2	0.3	0.4	0.2	0.4	0.4	0.4	0.1	0.2	0.5	0.7	0.9	1.3

Sample	K17B-FSP4	K17B-FSP5	K17B-FSP6	K17B-FSP7	K17B-FSP8	K17B-FSP9	K17B-FSP10	K17B-FSP11	K17B-FSP12	K17B-FSP13	K17B-FSP14	K17B-FSP15	K17B-FSP16	K17B-FSP17	K17B-FSP18
Type	euhedral	euhedral	euhedral	euhedral	euhedral	euhedral	euhedral	euhedral	euhedral	euhedral	euhedral	euhedral	euhedral	euhedral	euhedral
Location	rim	core	rim	core	middle	rim	core	rim	core	rim	core	rim	core	rim	core
Host Lithology	rhyolite	rhyolite	rhyolite	rhyolite	rhyolite	rhyolite	rhyolite	rhyolite	rhyolite	rhyolite	rhyolite	rhyolite	rhyolite	rhyolite	rhyolite
SiO_2	59.11	59.37	58.45	55.78	56.07	59.02	56.36	56.64	56.13	56.87	57.09	57.46	48.29	56.38	58.70
Al_2O_3	26.21	25.93	26.57	28.84	28.47	26.45	28.24	27.86	28.04	27.59	27.55	27.78	33.45	27.46	26.79
Fe_2O_3	0.35	0.28	0.29	0.33	0.36	0.29	0.33	0.33	0.30	0.33	0.32	0.31	0.38	0.31	0.30
CaO	7.60	7.22	7.77	10.34	9.68	7.64	9.54	9.22	9.67	8.97	9.00	9.12	15.92	9.09	8.06
Na_2O	7.25	7.32	6.95	5.74	6.03	7.20	6.21	6.36	6.08	6.39	6.43	6.48	3.10	6.32	7.03
K_2O	0.19	0.20	0.21	0.13	0.14	0.21	0.15	0.18	0.13	0.15	0.16	0.15	0.05	0.13	0.20
TOTAL	100.70	100.32	100.23	101.15	100.74	100.80	100.82	100.58	100.35	100.30	100.54	101.29	101.19	99.70	101.08
Ab	62.7	64.0	61.1	49.7	52.6	62.3	53.6	55.0	52.8	55.8	55.9	55.8	26.0	55.3	60.5
An	36.3	34.9	37.7	49.5	46.6	36.5	45.5	44.0	46.4	43.3	43.2	43.4	73.7	44.0	38.4
Or	1.1	1.1	1.2	0.7	0.8	1.2	0.8	1.0	0.8	0.9	0.9	0.9	0.3	0.8	1.1

Sample	K18-FSP1	K18-FSP2	K18-FSP3	K18-FSP4	K18-FSP5	K18-FSP6	K18-FSP7	K18-FSP8	K18-FSP9	K18-FSP10	K18-FSP11	K18-FSP12	K18-FSP13	K18-FSP14	K18-FSP15
Type	euhedral	euhedral	euhedral	euhedral	euhedral	euhedral	euhedral	euhedral	euhedral	glom	glom	micro	euhedral	euhedral	euhedral
Location	rim	rim	rim	core	rim	core	rim	core	rim	rim	core	euhedral	core	rim	core
Host Lithology	dacite	dacite	dacite	dacite	dacite	dacite	dacite	dacite	dacite	dacite	dacite	dacite	dacite	dacite	dacite
SiO_2	47.26	54.90	55.66	56.73	55.69	47.81	51.02	55.65	56.35	53.47	53.06	56.47	51.00	50.85	53.96
Al_2O_3	32.68	27.43	27.43	27.10	27.60	32.10	30.42	27.66	26.78	28.26	28.76	27.17	30.35	30.40	28.03
Fe_2O_3	0.42	0.45	0.42	0.34	0.37	0.51	0.48	0.35	0.33	0.57	0.44	0.40	0.57	0.53	0.57
CaO	16.22	10.06	9.90	9.45	10.19	15.35	13.08	10.35	9.20	11.45	11.46	9.74	13.66	13.40	10.65
Na_2O	2.10	5.60	5.88	6.01	5.62	2.68	4.06	5.63	6.14	4.95	4.81	6.02	3.71	3.74	5.40
K_2O	b.d.	0.14	0.14	0.14	0.13	0.05	0.09	0.13	0.16	0.10	0.12	0.14	0.06	0.05	0.13
TOTAL	98.70	98.58	99.43	99.77	99.59	98.50	99.15	99.77	98.96	98.80	98.65	99.93	99.34	98.97	98.73
Ab	19.0	49.7	51.4	53.1	49.6	23.9	35.8	49.3	54.2	43.6	42.9	52.4	32.8	33.4	47.5
An	81.0	49.4	47.8	46.1	49.7	75.8	63.7	50.0	44.9	55.8	56.4	46.8	66.8	66.2	51.8
Or	0.1	0.8	0.8	0.8	0.7	0.3	0.5	0.7	0.9	0.6	0.7	0.8	0.3	0.3	0.7

Table D.3. Feldspar Analyses

Sample	K32A-FSP1	K32A-FSP2	K32A-FSP3	K32A-FSP4	K32A-FSP5	K32A-FSP6	K32A-FSP7	K32A-FSP8	K32A-FSP9	K32A-FSP10	K32A-FSP11	K32A-FSP12
Type	euhedral	euhedral	euhedral	euhedral	euhedral	euhedral	euhedral	euhedral	euhedral	euhedral	euhedral	euhedral
Location	core	core	middle	rim	core	rim	core	rim	core	rim	core	rim
Host Lithology	rhyolite	rhyolite	rhyolite	rhyolite	rhyolite	rhyolite	rhyolite	rhyolite	rhyolite	rhyolite	rhyolite	rhyolite
SiO_2	56.28	54.20	46.01	56.49	58.26	57.44	59.71	57.89	51.00	56.17	54.76	58.46
Al_2O_3	26.79	28.79	34.10	27.72	25.83	26.41	26.19	27.45	31.96	28.24	27.89	27.29
Fe_2O_3	0.35	0.35	0.53	0.30	0.28	0.34	0.32	0.34	0.39	0.44	0.30	0.26
CaO	8.59	10.50	17.08	9.46	7.38	7.89	7.26	8.45	13.95	9.82	9.57	8.50
Na_2O	6.65	4.60	2.86	6.56	7.62	7.06	7.51	6.82	3.83	6.07	6.27	6.38
K_2O	0.17	0.12	0.03	0.16	0.23	0.19	0.18	0.17	0.08	0.13	0.15	0.17
TOTAL	98.83	98.56	100.61	100.68	99.59	99.33	101.17	101.11	101.20	100.86	98.93	101.06
Ab	57.8	43.9	23.2	55.2	64.3	61.2	64.5	58.8	33.0	52.4	53.8	57.0
An	41.2	55.3	76.6	44.0	34.4	37.8	34.5	40.3	66.5	46.9	45.4	42.0
Or	1.0	0.8	0.2	0.9	1.3	1.1	1.0	1.0	0.4	0.7	0.8	1.0

Sample	K32A-FSP13	K32D-FSP1	K32D-FSP2	K32D-FSP3	K32D-FSP4	K32D-FSP5	K32D-FSP6	K32D-FSP7	K32D-FSP8	K32D-FSP9	K32D-FSP10	K32D-FSP11
Type	euhedral	micro	euhedral	micro	micro	euhedral	euhedral	euhedral	euhedral	euhedral	micro	euhedral
Location	core	core	rim	core	rim	core	rim	core	core	core	rim	core
Host Lithology	rhyolite	dacite	dacite	dacite	dacite	dacite	dacite	dacite	dacite	dacite	dacite	dacite
SiO_2	56.21	55.29	56.25	56.66	55.46	54.36	55.71	55.04	56.69	56.29	59.91	47.10
Al_2O_3	27.20	28.74	28.45	28.39	29.36	29.78	28.92	29.33	27.92	28.57	26.31	34.56
Fe_2O_3	0.25	0.34	0.38	0.51	0.50	0.48	0.39	0.34	0.38	0.35	0.30	0.41
CaO	8.95	10.18	9.86	9.79	10.62	11.19	10.48	10.89	9.50	9.98	7.46	16.79
Na_2O	6.76	5.43	5.98	5.43	5.44	5.14	5.47	5.43	6.18	5.95	5.96	2.10
K_2O	0.16	0.12	0.13	0.11	0.10	0.09	0.11	0.12	0.15	0.13	0.22	0.03
TOTAL	99.53	100.10	101.04	100.90	101.47	101.04	101.07	101.14	100.82	101.28	100.16	100.99
Ab	57.2	48.8	51.9	49.7	47.8	45.1	48.3	47.1	53.6	51.5	58.2	18.4
An	41.8	50.5	47.3	49.6	51.6	54.3	51.1	52.2	45.5	47.7	40.3	81.4
Or	0.9	0.7	0.7	0.7	0.6	0.5	0.6	0.7	0.9	0.8	1.5	0.2

Sample	K32D-FSP12	K32D-FSP13	K32D-FSP14	K32D-FSP15	K32D-FSP16	K32D-FSP17	K32D-FSP18	K32D-FSP19	K32D-FSP20	K32D-FSP21	K32D-FSP22	K32D-FSP23
Type	euhedral	euhedral	euhedral	euhedral	euhedral	micro	micro	euhedral	euhedral	euhedral	euhedral	euhedral
Location	rim	core	rim	core	rim	core	rim	core	core	rim	rim	core
Host Lithology	dacite	dacite	dacite	dacite	dacite	dacite	dacite	dacite	dacite	dacite	dacite	dacite
SiO_2	54.84	55.66	56.22	46.57	54.08	59.75	60.97	48.29	48.83	58.04	58.77	47.23
Al_2O_3	29.59	28.59	28.65	34.84	29.27	27.23	26.30	33.56	33.27	26.96	26.63	34.55
Fe_2O_3	0.44	0.36	0.31	0.43	0.43	0.32	0.28	0.38	0.35	0.26	0.24	0.41
CaO	11.13	10.22	9.79	17.07	11.08	8.15	7.16	15.71	15.29	8.39	8.02	16.76
Na_2O	5.30	5.67	6.06	1.92	5.32	5.02	4.74	2.58	2.89	6.64	6.62	2.06
K_2O	0.10	0.12	0.13	b.d.	0.09	0.20	0.21	0.05	0.05	0.18	0.19	0.03
TOTAL	101.40	100.62	101.15	100.84	100.28	100.66	99.67	100.55	100.68	100.47	100.48	101.04
Ab	46.0	49.7	52.5	16.9	46.3	52.0	53.7	22.8	25.4	58.3	59.2	18.2
An	53.4	49.5	46.8	83.1	53.2	46.6	44.8	76.9	74.3	40.7	39.6	81.6
Or	0.6	0.7	0.7	0.0	0.5	1.4	1.6	0.3	0.3	1.0	1.1	0.2

Table D.4. Magnetite Analyses

Sample	K2-MAG1	K2-MAG2	K2-MAG3	K3-MAG1	K3-MAG2	K3-MAG3	K3-MAG4	K3-MAG5	K3-MAG6	K3-MAG7	K3-MAG8	K3-MAG9	K3-MAG10
Host Lithology	rhyolite	rhyolite	rhyolite	andesite	andesite	andesite	andesite	andesite	andesite	andesite	andesite	andesite	andesite
TiO_2	9.13	9.14	9.11	10.12	10.06	9.94	9.89	9.95	10.07	10.06	10.23	10.26	10.12
Al_2O_3	1.58	1.60	1.59	1.56	2.09	2.00	1.49	1.58	1.86	1.88	1.83	1.02	1.88
Cr_2O_3	b.d.	b.d.	b.d.	0.10	0.06	b.d.	0.09	0.05	0.05	0.07	0.05	0.07	0.05
Fe_2O_3	49.59	49.13	49.69	48.38	48.31	48.33	48.81	48.51	48.63	48.51	48.62	48.64	48.49
FeO	37.35	37.31	37.49	36.25	36.25	36.58	36.79	36.99	36.34	36.39	36.59	36.56	36.57
MnO	0.63	0.58	0.57	0.57	0.54	0.56	0.53	0.51	0.60	0.55	0.51	0.55	0.50
MgO	1.05	1.00	1.01	1.79	1.71	1.40	1.39	1.26	1.72	1.69	1.79	1.83	1.66
CaO	b.d.	b.d.	b.d.	b.d.	b.d.	b.d.	b.d.	0.04	b.d.	b.d.	0.03	0.03	b.d.
Total	99.33	98.77	99.48	98.80	99.05	98.83	98.99	98.89	99.29	99.17	99.65	98.96	99.26
Usp	0.26	0.26	0.26	0.29	0.29	0.29	0.28	0.29	0.29	0.29	0.29	0.29	0.29

Sample	K3-MAG11	K3-MAG12	K4-MAG1	K4-MAG2	K4-MAG3	K4-MAG4	K4-MAG5	K4-MAG6	K4-MAG7	K4-MAG8	K4-MAG9	K4-MAG10	K4-MAG11
Host Lithology	andesite	andesite	basaltic andesite	basaltic andesite	basaltic andesite	basaltic andesite	basaltic andesite	basaltic andesite	basaltic andesite	basaltic andesite	basaltic andesite	basaltic andesite	basaltic andesite
TiO_2	10.00	10.13	11.44	9.41	10.67	10.20	10.90	11.38	11.27	11.66	11.30	8.39	9.95
Al_2O_3	1.86	1.69	2.97	3.83	3.22	3.94	2.82	2.83	2.74	2.95	2.87	4.45	3.62
Cr_2O_3	0.06	0.05	0.06	0.31	0.07	0.15	0.12	0.06	0.07	0.03	0.08	0.15	0.08
Fe_2O_3	48.53	48.19	43.87	46.75	44.84	45.34	44.90	44.06	43.99	43.49	44.12	48.29	46.23
FeO	36.21	36.27	37.54	34.97	36.58	35.74	36.99	37.57	37.33	37.42	37.28	33.96	35.63
MnO	0.55	0.51	0.45	0.39	0.36	0.36	0.54	0.55	0.51	0.60	0.58	0.35	0.25
MgO	1.72	1.75	2.23	2.94	2.66	2.97	2.25	2.24	2.34	2.46	2.34	3.20	2.96
CaO	0.03	b.d.	b.d.	b.d.	0.12	b.d.	b.d.	0.03	b.d.	b.d.	b.d.	b.d.	0.03
Total	98.95	98.60	98.57	98.61	98.52	98.72	98.52	98.72	98.25	98.63	98.58	98.79	98.75
Usp	0.29	0.29	0.34	0.28	0.32	0.31	0.32	0.33	0.33	0.34	0.33	0.25	0.30

Sample	K4-MAG12	K6-MAG1	K6-MAG2	K6-MAG3	K6-MAG4	K6-MAG5	K6-MAG6	K6-MAG7	K6-MAG8	K6-MAG9	K6-MAG10	K6-MAG11	K6-MAG12
Host Lithology	basaltic andesite	dacite	dacite	dacite	dacite	dacite	basaltic andesite	basaltic andesite	basaltic andesite	basaltic andesite	dacite	dacite	dacite
TiO_2	9.99	11.40	11.38	9.14	11.30	11.08	8.32	8.48	8.58	8.74	10.22	10.17	8.98
Al_2O_3	3.62	2.82	2.84	4.14	2.86	2.75	4.59	4.61	4.60	2.23	2.49	2.48	4.18
Cr_2O_3	0.13	0.09	0.06	0.27	0.07	0.07	0.08	0.10	0.12	0.06	0.05	b.d.	0.14
Fe_2O_3	45.95	44.39	44.10	47.31	44.43	44.83	49.50	49.15	49.08	49.49	46.88	47.10	47.21
FeO	35.36	38.03	38.10	35.17	37.65	37.56	34.65	34.97	35.18	36.15	37.46	37.48	35.68
MnO	0.30	0.54	0.41	0.28	0.56	0.44	0.19	0.30	0.23	0.53	0.47	0.45	0.35
MgO	2.86	2.21	2.14	2.98	2.32	2.29	3.18	3.02	3.03	1.62	1.85	1.87	2.44
CaO	0.33	0.03	b.d.	b.d.	b.d.	0.04	b.d.	b.d.	b.d.	0.40	b.d.	b.d.	b.d.
Total	98.54	99.51	99.04	99.31	99.20	99.05	100.52	100.64	100.83	99.22	99.43	99.57	98.99
Usp	0.30	0.33	0.34	0.28	0.33	0.33	0.25	0.25	0.26	0.25	0.30	0.30	0.27

Table D.4. Magnetite Analyses

Sample	K6-MAG13	K6-MAG14	K6-MAG15	K6-MAG16	K6-MAG17	K6-MAG18	K6-MAG19	K6-MAG20	K6-MAG21	K6-MAG22	K6-MAG23	K6-MAG24	K6-MAG25
Host Lithology	dacite	dacite	dacite	basaltic andesite	basaltic andesite	basaltic andesite	basaltic andesite	basaltic andesite	basaltic andesite	basaltic andesite	dacite	basaltic andesite	dacite
TiO_2	9.13	10.13	10.26	9.27	9.20	10.62	8.67	10.05	8.47	8.63	10.76	8.35	10.73
Al_2O_3	4.25	2.58	2.43	3.74	3.99	3.23	4.31	3.85	4.28	4.21	2.94	4.46	2.73
Cr_2O_3	0.21	0.00	0.05	0.31	0.30	0.07	0.15	0.15	0.23	0.19	0.11	0.15	0.10
Fe_2O_3	46.75	47.25	46.81	48.32	47.09	46.52	48.52	46.91	48.86	48.67	46.11	49.96	46.35
FeO	36.00	37.43	37.37	35.53	34.99	37.23	34.84	36.29	34.44	34.76	37.09	34.63	37.54
MnO	0.35	0.50	0.54	0.39	0.36	0.35	0.32	0.36	0.31	0.33	0.48	0.35	0.54
MgO	2.35	1.88	1.87	2.95	2.99	2.67	3.01	2.98	3.13	3.02	2.60	3.22	2.26
CaO	b.d.	b.d.	b.d.	b.d.	0.03	0.12	0.09	b.d.	0.04	b.d.	b.d.	b.d.	b.d.
Total	99.05	99.78	99.33	100.52	98.95	100.82	99.91	100.60	99.75	99.83	100.11	101.12	100.22
Usp	0.28	0.29	0.30	0.27	0.28	0.31	0.26	0.31	0.54	0.26	0.31	0.25	0.31

Sample	K6-MAG26	K6-MAG27	K6-MAG28	K6-MAG29	K6-MAG30	K6-MAG31	K6-MAG32	K6-MAG33	K6-MAG34	K6-MAG35	K6-MAG36	K6-MAG37	K6-MAG38
Host Lithology	dacite	basaltic andesite	basaltic andesite	dacite	dacite	basaltic andesite	basaltic andesite	dacite	dacite	dacite	dacite	dacite	dacite
TiO_2	11.23	9.43	9.26	11.23	11.32	9.85	10.55	10.82	11.22	11.31	11.14	7.78	9.81
Al_2O_3	2.74	3.94	3.90	2.96	2.81	3.90	2.54	2.62	2.75	2.86	2.78	3.90	3.63
Cr_2O_3	0.06	0.12	0.16	0.06	0.06	0.15	b.d.	0.07	0.07	b.d.	0.08	0.10	0.08
Fe_2O_3	45.64	47.87	48.13	45.52	45.25	47.26	47.22	46.69	45.67	44.95	45.70	50.84	47.81
FeO	38.12	35.71	35.55	37.60	37.77	36.50	37.45	37.92	37.98	37.76	37.83	34.03	36.19
MnO	0.55	0.41	0.33	0.45	0.43	0.29	0.59	0.62	0.51	0.60	0.57	0.30	0.25
MgO	2.25	2.92	2.94	2.65	2.53	2.80	2.24	2.13	2.35	2.37	2.35	2.99	2.97
CaO	0.03	b.d.	0.03	b.d.	b.d.	b.d.	b.d.	0.03	b.d.	b.d.	b.d.	0.20	0.03
Total	100.61	100.40	100.31	100.48	100.17	100.76	100.60	100.89	100.56	99.87	100.46	100.14	100.76
Usp	0.32	0.28	0.29	0.33	0.33	0.29	0.29	0.31	0.32	0.33	0.32	0.23	0.29

Sample	K6-MAG39	K6-MAG40	K6-MAG41	K6-MAG42	K6-MAG43	K6-MAG44	K6-MAG45	K6-MAG46	K6-MAG47	K6-MAG48	K6-MAG49	K6-MAG50	K6-MAG51
Host Lithology	dacite	dacite	dacite	basaltic andesite	dacite	basaltic andesite	basaltic andesite	basaltic andesite	basaltic andesite	basaltic andesite	basaltic andesite	dacite	dacite
TiO_2	9.64	9.31	11.18	9.05	11.59	9.06	9.09	9.05	8.05	8.44	8.16	9.59	11.61
Al_2O_3	3.63	3.79	2.78	1.61	2.82	1.57	1.61	1.60	1.60	1.66	1.67	1.92	2.86
Cr_2O_3	0.13	0.33	0.06	0.07	0.05	b.d.	0.05	b.d.	b.d.	b.d.	b.d.	b.d.	b.d.
Fe_2O_3	47.26	48.05	45.45	49.93	44.05	49.99	49.73	50.04	51.09	50.84	50.72	49.20	44.27
FeO	35.81	35.45	38.09	37.32	37.82	37.37	37.39	37.49	36.09	36.65	36.20	37.53	38.23
MnO	0.30	0.34	0.45	0.65	0.59	0.64	0.59	0.58	0.56	0.65	0.59	0.55	0.58
MgO	2.87	3.03	2.24	1.09	2.39	1.06	1.06	1.04	1.08	1.07	1.06	1.49	2.25
CaO	0.33	b.d.	b.d.	0.09	0.07	0.03	0.03	0.03	0.14	0.13	0.28	0.09	0.07
Total	99.97	100.31	100.26	99.81	99.38	99.71	99.54	99.82	98.61	99.43	98.68	100.37	99.87
Usp	0.29	0.28	0.33	0.31	0.34	0.26	0.26	0.26	0.23	0.24	0.24	0.27	0.34

Table D.4. Magnetite Analyses

Sample	K6-MAG52	K6-MAG53	K6-MAG54	K6-MAG55	K6-MAG56	K6-MAG57	K6-MAG58	K6-MAG59	K6-MAG60	K6-MAG61	K9-MAG1	K9-MAG2	K9-MAG3
Host Lithology	basaltic andesite	basaltic andesite	basaltic andesite	basaltic andesite	basaltic andesite	basaltic andesite	basaltic andesite	basaltic andesite	basaltic andesite	basaltic andesite	rhyolite	rhyolite	rhyolite
TiO_2	9.97	9.90	9.87	9.85	9.94	10.23	9.95	9.88	10.13	10.12	9.21	9.05	9.35
Al_2O_3	2.27	2.13	2.17	2.39	2.16	2.23	2.31	2.32	2.36	2.41	1.99	2.03	2.01
Cr_2O_3	b.d.	0.09	0.05	0.07	b.d.	0.06	b.d.	0.07	0.06	0.05	0.05	0.09	b.d.
Fe_2O_3	47.95	47.24	47.19	47.12	47.44	46.81	47.22	47.17	47.21	47.22	48.66	48.80	48.35
FeO	36.98	37.02	37.25	37.07	37.07	37.40	37.38	37.87	37.46	37.41	36.96	36.86	36.93
MnO	0.63	0.63	0.63	0.61	0.64	0.61	0.59	0.65	0.63	0.59	0.49	0.56	0.52
MgO	1.71	1.65	1.49	1.65	1.70	1.70	1.58	1.19	1.71	1.77	1.37	1.27	1.42
CaO	b.d.	b.d.	0.04	0.04	b.d.	b.d.	b.d.	b.d.	b.d.	b.d.	0.03	0.10	b.d.
Total	99.52	98.66	98.68	98.80	98.96	99.05	99.05	99.15	99.55	99.56	98.76	98.76	98.59
Usp	0.29	0.29	0.29	0.29	0.29	0.30	0.29	0.29	0.29	0.29	0.27	0.26	0.27

Sample	K9-MAG4	K9-MAG5	K9-MAG6	K9-MAG7	K9-MAG8	K9-MAG9	K9-MAG10	K9-MAG11	K9-MAG12	K9-MAG13	K14-MAG1	K14-MAG2	K14-MAG3
Host Lithology	rhyolite	rhyolite	rhyolite	rhyolite	rhyolite	rhyolite	rhyolite	rhyolite	rhyolite	rhyolite	andesite	andesite	andesite
TiO_2	9.36	9.57	9.38	9.09	9.02	8.31	8.58	9.14	9.04	9.18	9.43	10.23	9.16
Al_2O_3	1.98	2.00	2.00	1.99	1.81	1.69	1.64	1.77	1.78	1.82	2.74	2.70	4.22
Cr_2O_3	b.d.	0.11	0.08	0.08	b.d.	0.05	0.05	0.07	0.06	0.09	0.07	0.06	0.11
Fe_2O_3	48.68	47.98	48.62	49.29	49.30	50.65	50.31	49.14	49.24	48.91	49.31	48.04	48.72
FeO	37.08	37.37	37.23	36.91	37.03	36.41	36.73	37.21	37.11	37.22	36.78	37.43	35.52
MnO	0.45	0.57	0.45	0.54	0.56	0.57	0.55	0.60	0.61	0.61	0.56	0.48	0.36
MgO	1.46	1.29	1.41	1.40	1.18	1.10	1.10	1.14	1.09	1.12	2.11	2.29	3.10
CaO	0.03	b.d.	b.d.	0.03	0.11	0.04	0.03	b.d.	0.08	0.11	b.d.	b.d.	0.03
Total	99.02	98.91	99.18	99.32	99.00	98.82	98.99	99.07	99.00	99.06	100.99	101.24	101.21
Usp	0.27	0.28	0.27	0.26	0.26	0.24	0.25	0.26	0.26	0.27	0.27	0.29	0.27

Sample	K14-MAG4	K14-MAG5	K14-MAG6	K14-MAG7	K14-MAG8	K14-MAG9	K14-MAG10	K14-MAG11	K14-MAG12	K14-MAG13	K14-MAG14	K14-MAG15	K14-MAG16
Host Lithology	basaltic andesite	basaltic andesite	basaltic andesite	basaltic andesite	basaltic andesite	andesite	andesite	andesite	basaltic andesite	andesite	andesite	andesite	andesite
TiO_2	9.19	11.14	11.24	10.85	10.70	11.01	10.10	11.02	10.24	10.65	10.61	10.35	10.52
Al_2O_3	4.20	3.04	2.94	2.62	2.59	2.75	2.88	2.75	2.96	2.53	2.59	2.45	2.57
Cr_2O_3	0.15	b.d.	0.05	b.d.	b.d.	0.05	0.05	0.05	0.09	0.05	0.07	b.d.	b.d.
Fe_2O_3	48.47	45.89	45.76	46.82	47.04	42.52	43.07	42.58	42.92	42.87	42.93	43.48	42.83
FeO	35.63	37.67	37.69	37.95	37.48	42.68	40.07	42.32	40.07	39.75	40.19	39.38	39.52
MnO	0.34	0.42	0.46	0.56	0.55	0.49	0.46	0.35	0.47	0.50	0.47	0.53	0.48
MgO	3.03	2.65	2.67	2.20	2.36	2.23	2.20	2.29	2.58	2.78	2.21	2.99	2.57
CaO	0.03	0.04	0.04	b.d.	b.d.	b.d.	0.03	b.d.	b.d.	b.d.	b.d.	0.03	0.03
Total	101.03	100.86	100.84	101.00	100.72	101.72	98.84	101.36	99.35	99.15	99.09	99.19	98.52
Usp	0.27	0.27	0.32	0.32	0.31	0.34	0.31	0.34	0.32	0.33	0.33	0.32	0.32

Table D.4. Magnetite Analyses

Sample	K14-MAG17	K18-MAG1	K18-MAG2	K18-MAG3	K18-MAG4	K18-MAG5	K18-MAG6	K18-MAG7	K18-MAG8	K18-MAG9	K18-MAG10	K17B-MAG1	K17B-MAG2
Host Lithology	andesite	dacite	dacite	dacite	dacite	dacite	dacite	dacite	dacite	dacite	dacite	rhyolite	rhyolite
TiO_2	10.64	8.33	8.17	8.84	8.65	8.37	8.20	8.14	8.30	8.39	8.36	8.05	9.42
Al_2O_3	2.81	1.97	1.89	2.16	2.33	1.91	1.93	1.69	1.96	2.01	1.97	2.20	1.60
Cr_2O_3	0.05	0.08	0.05	0.08	0.09	0.08	0.07	0.08	0.11	0.10	0.08	0.18	b.d.
Fe_2O_3	42.49	50.46	50.28	48.43	48.51	50.51	50.23	50.54	49.76	49.97	49.89	51.77	48.99
FeO	39.34	38.64	38.21	38.84	38.67	38.76	38.17	38.19	38.27	38.49	38.43	36.05	37.63
MnO	0.42	0.46	0.46	0.39	0.39	0.40	0.57	0.41	0.47	0.53	0.47	0.56	0.61
MgO	2.75	n.a	n.a	n.a	n.a	n.a	n.a	n.a	n.a	n.a	n.a	1.56	1.05
CaO	0.04	b.d.	0.04	b.d.	b.d.	b.d.	0.05	b.d.	0.05	b.d.	b.d.	0.09	b.d.
Total	98.54	99.94	99.09	98.75	98.64	100.03	99.21	99.05	98.93	99.51	99.20	100.46	99.30
Usp	0.33	0.24	0.24	0.26	0.26	0.24	0.24	0.24	0.24	0.25	0.25	0.23	0.27

Sample	K17B-MAG3	K17B-MAG4	K17B-MAG5	K17B-MAG6	K32A-MAG1	K32A-MAG2	K32A-MAG3	K32A-MAG4	K32A-MAG5	K32A-MAG6	K32A-MAG7	K32A-MAG8	K32A-MAG9
Host Lithology	rhyolite	rhyolite	rhyolite	rhyolite	rhyolite	rhyolite	rhyolite	rhyolite	rhyolite	rhyolite	rhyolite	rhyolite	rhyolite
TiO_2	9.06	9.15	9.00	9.12	8.70	8.72	9.27	9.12	9.16	8.69	8.79	8.61	8.79
Al_2O_3	1.68	1.65	1.61	1.64	1.60	1.54	1.68	1.75	1.61	1.61	1.79	1.80	1.61
Cr_2O_3	0.05	b.d.	b.d.	b.d.	b.d.	b.d.	b.d.	b.d.	b.d.	b.d.	b.d.	b.d.	b.d.
Fe_2O_3	49.68	49.57	49.63	49.56	51.34	51.36	49.85	50.21	49.70	50.49	50.25	50.41	50.99
FeO	37.50	37.47	37.09	37.37	37.26	37.34	37.75	37.60	37.47	36.99	36.91	36.80	37.43
MnO	0.58	0.60	0.65	0.66	0.72	0.65	0.60	0.63	0.55	0.56	0.63	0.59	0.63
MgO	0.99	1.05	1.07	1.03	1.05	1.04	1.09	1.12	1.10	1.08	1.20	1.14	1.02
CaO	0.04	b.d.	0.03	b.d.	b.d.	0.03	b.d.	b.d.	0.18	0.17	0.12	0.12	0.04
Total	99.57	99.50	99.07	99.41	100.67	100.69	100.24	100.43	99.77	99.58	99.69	99.46	100.50
Usp	0.26	0.26	0.26	0.26	0.24	0.25	0.26	0.26	0.26	0.25	0.25	0.25	0.25

Sample	K32D-MAG1	K32D-MAG2	K32D-MAG3	K32D-MAG4	K32D-MAG5	K32D-MAG6	K32D-MAG7	K32D-MAG8	K32D-MAG9	K32D-MAG10	K32D-MAG11	K32D-MAG12	K32D-MAG13
Host Lithology	dacite	dacite	dacite	dacite	dacite	dacite	dacite	dacite	dacite	dacite	rhyolite	dacite	rhyolite
TiO_2	9.03	9.03	10.45	10.45	8.99	8.99	8.94	8.94	9.03	9.03	10.92	10.92	10.52
Al_2O_3	1.61	1.61	2.44	2.44	1.56	1.56	1.61	1.61	1.57	1.57	2.47	2.47	2.40
Cr_2O_3	0.07	0.07	0.09	0.09	0.05	0.05	b.d.	b.d.	b.d.	b.d.	b.d.	b.d.	0.05
Fe_2O_3	49.70	49.70	47.30	47.30	50.06	50.06	50.32	50.32	50.14	50.14	46.16	46.16	46.84
FeO	37.30	37.30	38.11	38.11	37.48	37.48	37.40	37.40	37.43	37.43	38.22	38.22	37.75
MnO	0.67	0.67	0.58	0.58	0.56	0.56	0.67	0.67	0.67	0.67	0.56	0.56	0.51
MgO	1.00	1.00	1.76	1.76	0.99	0.99	1.00	1.00	1.02	1.02	1.89	1.89	1.93
CaO	b.d.	b.d.	0.03	0.03	b.d.	b.d.	b.d.	b.d.	b.d.	b.d.	b.d.	b.d.	0.06
Total	99.37	99.37	100.76	100.76	99.69	99.69	99.95	99.95	99.88	99.88	100.23	100.23	100.06
Usp	0.26	0.26	0.30	0.30	0.26	0.26	0.25	0.25	0.26	0.26	0.32	0.32	0.30

Table D.5. Ilmenite Analyses

Sample	K2-ILM1	K2-ILM2	K2-ILM3	K2-ILM4	K3-ILM1	K3-ILM2	K3-ILM3	K3-ILM4	K3-ILM5	K3-ILM6	K3-ILM7	K3-ILM8	K3-ILM9	K3-ILM10
Host Lithology	rhyolite	rhyolite	rhyolite	rhyolite	andesite	andesite	andesite	andesite	andesite	andesite	andesite	andesite	andesite	andesite
TiO_2	44.31	44.51	44.70	45.02	43.17	43.24	43.47	43.50	43.48	43.59	43.16	43.20	43.36	43.32
Al_2O_3	0.15	0.14	0.15	0.15	n.a.	n.a.	n.a.	n.a.	n.a.	n.a.	n.a.	n.a.	n.a.	n.a.
Cr_2O_3	b.d.	b.d.	b.d.	b.d.	b.d.	b.d.	b.d.	b.d.	0.05	b.d.	b.d.	b.d.	b.d.	b.d.
Fe_2O_3	16.06	15.98	15.43	15.17	18.92	19.05	18.41	18.44	19.11	18.96	19.24	19.15	19.10	18.86
FeO	35.26	35.54	35.78	35.95	33.33	33.28	33.41	33.60	33.38	33.41	33.31	33.26	33.42	33.59
MnO	0.91	0.91	0.98	1.04	0.59	0.74	0.66	0.62	0.68	0.72	0.57	0.65	0.63	0.65
MgO	2.12	2.06	1.99	2.02	2.74	2.72	2.82	2.75	2.83	2.84	2.76	2.78	2.77	2.64
CaO	b.d.	b.d.	0.06	b.d.	b.d.	b.d.	b.d.	b.d.	0.03	b.d.	b.d.	b.d.	b.d.	b.d.
Total	98.83	99.19	99.13	99.35	98.76	99.05	98.79	98.94	99.55	99.53	99.07	99.09	99.32	99.08
Ilm	0.83	0.83	0.84	0.84	0.80	0.80	0.80	0.80	0.80	0.80	0.79	0.79	0.80	0.80

Sample	K3-ILM11	K3-ILM12	K3-ILM13	K3-ILM14	K3-ILM15	K3-ILM16	K3-ILM17	K3-ILM18	K3-ILM19	K4-ILM1	K4-ILM2	K4-ILM3	K4-ILM4	K4-ILM5
Host Lithology	andesite	andesite	andesite	andesite	andesite	andesite	andesite	andesite	andesite	basaltic andesite	basaltic andesite	basaltic andesite	basaltic andesite	basaltic andesite
TiO_2	43.17	43.24	43.48	43.47	43.45	43.79	43.61	42.69	43.29	43.29	42.87	43.38	43.31	43.12
Al_2O_3	n.a.	n.a.	n.a.	n.a.	n.a.	n.a.	n.a.	n.a.	n.a.	0.29	0.37	0.39	0.34	0.27
Cr_2O_3	b.d.	b.d.	b.d.	b.d.	b.d.	b.d.	b.d.	b.d.	b.d.	b.d.	b.d.	b.d.	b.d.	b.d.
Fe_2O_3	19.44	18.81	18.48	18.53	18.43	18.18	18.43	19.40	18.73	18.20	18.96	18.31	18.21	18.84
FeO	33.26	33.52	33.63	33.50	33.60	33.90	33.61	33.44	33.46	32.50	32.20	32.60	32.72	32.30
MnO	0.59	0.61	0.70	0.68	0.63	0.67	0.73	0.73	0.71	0.73	0.57	0.72	0.53	0.66
MgO	2.79	2.67	2.67	2.75	2.72	2.70	2.74	2.37	2.66	3.32	3.46	3.31	3.30	3.38
CaO	b.d.	b.d.	0.05	b.d.	b.d.	b.d.	0.04	0.05	b.d.	0.14	0.12	0.13	0.15	0.12
Total	99.29	98.88	99.01	98.94	98.86	99.25	99.19	98.68	98.85	98.47	98.55	98.84	98.56	98.69
Ilm	0.79	0.80	0.80	0.80	0.80	0.81	0.80	0.79	0.80	0.80	0.79	0.80	0.80	0.79

Sample	K4-ILM6	K6-ILM1	K6-ILM2	K6-ILM3	K6-ILM4	K6-ILM5	K6-ILM6	K6-ILM7	K6-ILM8	K6-ILM9	K6-ILM10	K6-ILM11	K6-ILM12	K6-ILM13
Host Lithology	basaltic andesite	basaltic andesite	basaltic andesite	dacite	dacite	dacite	dacite	dacite	basaltic andesite	basaltic andesite	dacite	dacite	dacite	dacite
TiO_2	42.83	42.22	42.57	41.56	41.56	41.86	41.73	42.75	43.27	43.28	42.69	43.29	42.46	41.69
Al_2O_3	0.36	0.27	0.28	0.29	0.26	0.27	0.29	0.31	0.29	0.29	n.a.	n.a.	0.36	0.37
Cr_2O_3	0.05	b.d.	b.d.	b.d.	b.d.	b.d.	0.05	0.06	b.d.	b.d.	b.d.	b.d.	b.d.	b.d.
Fe_2O_3	18.89	20.36	19.71	21.94	21.93	21.55	21.98	19.65	18.65	18.21	19.37	18.70	20.40	21.33
FeO	32.17	32.62	32.81	32.12	32.00	32.26	32.12	31.62	32.31	32.50	33.44	33.46	32.29	31.38
MnO	0.66	0.55	0.58	0.55	0.58	0.60	0.63	0.53	0.46	0.82	0.73	0.71	0.39	0.50
MgO	3.36	2.79	2.85	2.75	2.79	2.79	2.81	3.66	3.55	3.31	2.37	2.66	3.24	3.30
CaO	0.20	0.10	0.22	b.d.	b.d.	b.d.	0.07	0.03	b.d.	0.14	0.05	b.d.	b.d.	0.10
Total	98.52	98.90	99.02	99.22	99.14	99.32	99.68	98.61	98.53	98.55	98.65	55.54	99.17	98.67
Ilm	0.79	0.80	0.79	0.76	0.76	0.77	0.80	0.78	0.79	0.80	0.79	0.80	0.78	0.76

Table D.5. Ilmenite Analyses

Sample	K6-ILM14	K6-ILM15	K6-ILM16	K6-ILM17	K6-ILM18	K6-ILM19	K6-ILM20	K6-ILM21	K6-ILM22	K6-ILM23	K6-ILM24	K6-ILM25	K6-ILM26	K6-ILM27
Host Lithology	dacite	dacite	dacite	dacite	basaltic andesite	basaltic andesite	basaltic andesite	basaltic andesite	basaltic andesite	basaltic andesite	basaltic andesite	basaltic andesite	basaltic andesite	basaltic andesite
TiO_2	46.26	46.56	41.85	44.14	44.75	42.76	42.53	41.43	45.25	45.09	44.80	44.64	44.45	44.48
Al_2O_3	n.a.	n.a.	0.39	n.a.	0.13	0.32	0.37	0.39	0.14	0.14	0.16	0.15	0.17	0.15
Cr_2O_3	b.d.	b.d.	0.08	b.d.	b.d.	b.d.	b.d.	b.d.	b.d.	b.d.	b.d.	b.d.	b.d.	b.d.
Fe_2O_3	11.16	10.43	21.82	16.25	15.95	20.60	22.23	21.85	15.83	15.62	15.78	15.95	16.00	15.73
FeO	36.55	36.63	31.55	34.99	35.54	32.48	31.77	31.04	36.08	35.80	35.65	35.64	35.36	35.35
MnO	4.47	4.62	0.48	0.98	0.93	0.62	0.53	0.54	0.98	0.93	1.01	0.95	1.03	0.99
MgO	0.30	0.32	3.31	2.08	2.17	3.13	3.48	3.34	2.09	2.20	2.09	2.04	2.07	2.10
CaO	b.d	b.d.	0.10	0.11	0.05	0.15	0.09	0.22	0.05	0.05	0.03	b.d.	0.06	0.05
Total	52.47	52.00	99.59	54.42	99.53	100.05	101.00	98.80	55.16	54.72	54.71	54.74	54.69	54.37
Ilm	0.88	0.88	0.76	0.83	0.83	0.78	0.76	0.76	0.83	0.84	0.82	0.83	0.83	0.83

Sample	K9-ILM1	K9-ILM2	K9-ILM3	K9-ILM4	K9-ILM5	K9-ILM6	K9-ILM7	K9-ILM8	K9-ILM9	K9-ILM10	K9-ILM11	K9-ILM12	K9-ILM13	K9-ILM14
Host Lithology	rhyolite	rhyolite	rhyolite	rhyolite	rhyolite	rhyolite	rhyolite	rhyolite	rhyolite	rhyolite	rhyolite	rhyolite	rhyolite	rhyolite
TiO_2	44.56	44.46	44.74	44.75	44.83	44.51	42.81	42.74	43.74	44.41	43.90	43.88	43.91	43.98
Al_2O_3	0.19	0.16	0.17	0.14	0.16	0.14	0.26	0.25	0.17	0.18	0.16	0.16	0.18	0.15
Cr_2O_3	b.d.	b.d.	b.d.	b.d.	b.d.	b.d.	b.d.	b.d.	b.d.	b.d.	b.d.	b.d.	b.d.	b.d.
Fe_2O_3	15.64	15.50	15.46	15.40	14.71	15.87	19.71	19.89	16.75	15.86	16.98	16.93	17.05	16.63
FeO	35.56	35.38	35.66	35.59	36.30	35.43	33.14	33.20	34.70	35.24	34.74	34.88	34.90	34.72
MnO	0.87	0.96	0.90	0.92	0.96	0.99	0.73	0.60	0.91	0.95	0.97	0.91	0.88	0.98
MgO	2.12	2.09	2.12	2.15	1.77	2.07	2.79	2.69	2.15	2.17	2.17	2.12	2.15	2.22
CaO	b.d.	b.d.	0.03	b.d.	0.03	0.05	0.04	b.d.	0.08	0.07	0.03	b.d.	0.03	0.08
Total	98.99	98.56	99.09	98.95	98.78	99.05	99.42	99.39	98.51	98.92	98.95	98.90	99.12	98.75
Ilm	0.83	0.83	0.84	0.84	0.85	0.82	0.79	0.79	0.82	0.83	0.82	0.82	0.82	0.82

Sample	K14-ILM1	K14-ILM2	K14-ILM3	K14-ILM4	K14-ILM5	K14-ILM6	K14-ILM7	K14-ILM8	K14-ILM9	K14-ILM10	K14-ILM11	K14-ILM12	K14-ILM13	K14-ILM14
Host Lithology	andesite	andesite	andesite	andesite	andesite	andesite	andesite	andesite	basaltic andesite	basaltic andesite	basaltic andesite	andesite	andesite	andesite
TiO_2	43.79	43.74	43.32	43.63	43.68	43.47	43.48	43.70	41.47	41.63	41.67	41.98	41.65	43.03
Al_2O_3	0.33	0.35	0.37	0.34	0.37	0.34	0.37	0.34	0.29	0.35	0.34	0.33	0.35	0.36
Cr_2O_3	b.d.	b.d.	b.d.	b.d.	b.d.	b.d.	b.d.	b.d.	b.d.	b.d.	b.d.	b.d.	b.d.	b.d.
Fe_2O_3	20.09	20.41	20.67	20.12	20.02	20.29	20.59	20.15	23.06	21.82	21.81	21.14	21.89	19.23
FeO	32.86	32.46	32.26	32.71	32.49	32.36	32.46	32.54	31.93	30.67	30.40	31.04	30.96	31.96
MnO	0.51	0.63	0.54	0.62	0.59	0.54	0.50	0.62	0.53	0.52	0.55	0.60	0.48	0.48
MgO	3.50	3.64	3.60	3.46	3.63	3.60	3.59	3.58	2.83	3.65	3.70	3.56	3.51	3.65
CaO	b.d.	b.d.	0.05	b.d.	b.d.	0.03	0.06	0.05	0.14	b.d.	0.03	b.d.	0.03	0.03
Total	101.08	101.23	100.81	100.87	100.77	100.63	101.05	100.98	100.25	57.00	98.49	98.65	98.87	98.73
Ilm	0.78	0.78	0.77	0.77	0.78	0.79	0.78	0.78	0.75	0.76	0.76	0.76	0.76	0.78

Table D.5. Ilmenite Analyses

Sample	K17B-ILM1	K17B-ILM2	K17B-ILM3	K17B-ILM4	K17B-ILM5	K17B-ILM6	K17B-ILM7	K17B-ILM8	K18-ILM1	K18-ILM2	K18-ILM3	K18-ILM4
Host Lithology	rhyolite	rhyolite	rhyolite	rhyolite	rhyolite	rhyolite	rhyolite	rhyolite	dacite	dacite	dacite	dacite
TiO_2	44.90	44.44	45.21	44.82	44.94	45.03	44.69	45.05	38.37	38.30	40.19	40.02
Al_2O_3	0.17	0.16	0.15	0.13	0.14	0.16	0.16	0.15	0.46	0.59	0.21	0.23
Cr_2O_3	b.d.	b.d.	b.d.	b.d.	b.d.	b.d.	b.d.	b.d.	b.d.	b.d.	b.d.	b.d.
Fe_2O_3	15.32	15.94	15.13	15.58	15.86	15.00	16.01	15.35	25.83	25.84	24.15	24.39
FeO	35.84	35.32	36.23	35.71	35.83	36.06	35.69	35.97	30.18	30.18	31.63	31.54
MnO	0.89	0.88	0.93	1.08	1.01	0.99	0.92	0.98	0.66	0.63	0.58	0.52
MgO	2.11	2.16	2.02	2.02	2.05	1.99	2.07	2.05	2.20	2.19	2.29	2.29
CaO	0.03	b.d.	b.d.	0.03	b.d.	0.11	0.19	0.06	0.86	0.83	0.28	0.31
Total	99.28	98.92	99.69	99.38	99.84	99.34	99.74	99.61	98.55	98.57	99.33	99.31
Ilm	0.84	0.83	0.84	0.84	0.83	0.84	0.83	0.84	0.72	0.72	0.74	0.74

Sample	K18-ILM5	K18-ILM6	K18-ILM7	K32A-ILM1	K32A-ILM2	K32A-ILM3	K32A-ILM4	K32A-ILM5	K32A-ILM6	K32A-ILM7	K32A-ILM8	K32A-ILM9
Host Lithology	dacite	dacite	dacite	rhyolite	rhyolite	rhyolite	rhyolite	rhyolite	rhyolite	rhyolite	rhyolite	rhyolite
TiO_2	40.75	40.51	40.47	44.47	44.00	45.25	45.02	45.02	44.32	44.76	44.41	44.42
Al_2O_3	0.23	0.24	0.22	0.17	0.00	0.14	0.32	0.32	0.13	0.00	0.15	0.17
Cr_2O_3	b.d.	b.d.	b.d.	b.d.	b.d.	b.d.	b.d.	b.d.	b.d.	b.d.	b.d.	b.d.
Fe_2O_3	24.98	24.52	24.71	16.30	17.32	16.12	16.23	16.23	16.29	16.65	17.59	17.03
FeO	32.04	31.99	31.57	35.63	34.06	35.96	35.88	35.88	35.43	35.60	35.17	35.13
MnO	0.55	0.52	0.69	1.04	1.03	1.01	0.97	0.97	1.07	0.83	0.93	0.91
MgO	2.36	2.29	2.41	1.92	2.51	2.14	2.16	2.16	1.93	2.14	2.21	2.26
CaO	0.03	b.d.	0.03	0.23	0.16	0.04	b.d.	b.d.	0.22	0.05	0.08	0.09
Total	100.93	100.06	100.11	99.76	99.10	100.67	100.61	100.61	99.41	100.03	100.56	100.02
Ilm	0.74	0.77	0.74	0.83	0.81	0.77	0.83	0.83	0.83	0.83	0.82	0.82

Sample	K32A-ILM10	K32A-ILM11	K32A-ILM12	K32A-ILM13	K32D-ILM1	K32D-ILM2	K32D-ILM3	K32D-ILM4	K32D-ILM5	K32D-ILM6	K32D-ILM7
Host Lithology	rhyolite	rhyolite	rhyolite	rhyolite	dacite	dacite	dacite	dacite	dacite	dacite	dacite
TiO_2	44.35	44.52	44.17	44.21	42.91	43.36	44.51	44.45	44.13	43.84	43.61
Al_2O_3	0.16	0.14	0.16	0.14	0.31	0.32	0.12	0.13	0.15	0.26	0.26
Cr_2O_3	b.d.	b.d.	b.d.	0.05	b.d.	b.d.	b.d.	b.d.	b.d.	b.d.	b.d.
Fe_2O_3	16.65	16.70	16.55	17.37	20.94	19.86	16.77	16.19	16.84	18.52	18.71
FeO	35.44	35.36	34.64	34.40	31.83	32.53	35.53	35.61	35.32	33.49	33.38
MnO	0.85	1.04	1.03	0.99	0.61	0.57	1.03	0.94	0.93	0.75	0.67
MgO	2.07	2.09	2.33	2.52	3.57	3.42	1.98	1.97	1.98	3.01	2.99
CaO	0.25	0.08	0.10	0.07	b.d.	0.03	b.d.	0.06	0.03	0.03	0.07
Total	99.77	99.92	98.97	99.75	100.18	100.10	99.97	99.37	99.40	99.89	99.69
Ilm	0.824	0.82	0.82	0.81	0.77	0.78	0.82	0.83	0.82	0.80	0.80

Table D.6. Amphibole Analyses

SAMPLE	K2-AMP1	K2-AMP2	K2-AMP3	K2-AMP4	K2-AMP5	K2-AMP6	K2-AMP7	K2-AMP8	K2-AMP9	K17-AMP1
SiO_2	47.19	48.12	47.18	46.35	47.03	46.82	46.27	47.64	47.00	47.10
TiO_2	1.66	1.44	1.73	1.91	1.76	1.76	1.84	1.55	1.72	1.73
Al_2O_3	7.01	6.37	7.15	7.38	7.29	7.08	7.83	6.42	6.74	6.84
FeO	13.93	14.24	14.02	14.27	14.55	13.94	14.84	14.85	14.39	14.28
MnO	0.50	0.51	0.46	0.46	0.45	0.46	0.45	0.48	0.51	0.49
MgO	14.75	14.82	14.63	14.31	14.34	14.73	13.90	14.22	14.47	14.59
CaO	11.04	10.80	10.89	10.99	10.86	10.96	10.97	10.88	10.94	10.96
Na_2O	1.66	1.50	1.74	1.72	1.86	1.65	1.81	1.52	1.63	1.87
K_2O	0.21	0.19	0.20	0.22	0.22	0.18	0.24	0.19	0.19	0.19
F	0.25	0.25	0.33	0.34	0.28	0.24	0.31	0.33	0.27	0.36
H_2O*	1.93	1.93	1.89	1.87	1.92	1.92	1.89	1.88	1.91	1.87
Total	100.11	100.18	100.22	99.81	100.55	99.74	100.35	99.96	99.75	100.28
Pressure calculations (kbar)										
Johnson	2.16	1.65	2.46	2.74	2.46	2.23	3.01	1.90	2.03	2.28
Hammarstrom	2.76	2.16	3.12	3.45	3.12	2.84	3.77	2.45	2.61	2.91
Hollister	2.73	2.05	3.13	3.50	3.13	2.82	3.86	2.39	2.56	2.89

SAMPLE	K17B-AMP2	K17B-AMP3	K17B-AMP4	K17B-AMP5	K32A-AMP1	K32A-AMP2	K32A-AMP3	K32A-AMP4	K32A-AMP5	K32A-AMP6
SiO_2	46.43	46.86	46.23	48.98	45.37	48.04	47.61	46.09	45.37	46.26
TiO_2	1.84	1.85	1.77	1.34	1.74	1.46	1.66	1.72	1.74	1.71
Al_2O_3	7.26	7.45	7.23	5.52	7.18	6.19	6.86	6.91	7.18	6.84
FeO	14.37	14.07	14.61	14.30	14.62	14.33	14.41	14.57	14.62	14.45
MnO	0.43	0.44	0.45	0.53	0.49	0.46	0.50	0.46	0.49	0.48
MgO	14.38	14.45	14.04	15.01	14.16	14.07	14.53	14.34	14.16	14.40
CaO	10.97	11.07	11.06	10.92	11.14	11.10	11.10	11.12	11.14	11.19
Na_2O	1.73	1.77	1.75	1.47	1.88	1.53	1.68	1.69	1.88	1.65
K_2O	0.21	0.22	0.24	0.19	0.17	0.18	0.19	0.21	0.17	0.22
F	0.29	0.24	0.31	0.33	0.35	0.29	0.24	0.27	1.84	0.37
H_2O*	1.89	1.94	1.87	1.90	1.84	1.90	1.94	1.89	0.35	1.85
Total	99.80	100.35	99.55	100.48	98.93	99.54	100.73	99.26	98.93	99.39
Pressure calculations (kbar)										
Johnson	2.52	2.48	2.58	1.08	2.70	1.62	2.01	2.22	2.70	2.39
Hammarstrom	3.19	3.15	3.26	1.48	3.40	2.12	2.58	2.83	3.40	3.03
Hollister	3.21	3.16	3.29	1.29	3.45	2.01	2.53	2.81	3.45	3.03

Pressures calculated by the methods of Johnson and Rutheford, (1988); Hammarstrom and Zen, (1985) and Hollister (1983).

* H_2O reported is theoretical and determined from the amphibole structural formula.

Table D.7. Apatite Analyses

Sample	K3-APT1	K3-APT2	K3-APT3	K3-APT4	K3-APT5	K3-APT6	K3-APT7	K3-APT8	K3-APT9	K3-APT10	K3-APT11	K3-APT12
Host Lithology	andesite	andesite	andesite	andesite	andesite	andesite	andesite	andesite	andesite	andesite	andesite	andesite
FeO	0.55	0.58	0.72	0.68	0.37	0.36	0.80	1.44	0.28	1.21	0.60	0.51
MnO	0.12	0.12	0.17	0.18	0.17	0.11	0.15	0.16	0.13	0.14	0.15	0.12
CaO	54.24	54.34	54.30	53.64	53.85	54.01	53.51	52.99	53.52	53.71	53.60	53.81
P_2O_5	42.22	42.31	41.96	40.61	40.73	41.07	40.69	40.87	41.07	40.49	40.98	40.78
F	2.60	2.42	2.81	2.32	2.19	1.73	2.18	2.50	2.47	2.32	2.03	2.03
Cl	0.73	0.72	0.71	0.69	0.68	0.71	0.71	0.71	0.70	0.55	0.71	0.73
Total	100.81	100.94	100.92	98.57	98.51	98.73	98.55	99.04	98.54	98.91	98.66	98.57

Sample	K3-APT13	K4-APT1	K6-APT1	K6-APT2	K6-APT3	K6-APT4	K6-APT5	K6-APT6	K6-APT7	K6-APT8	K6-APT9	K6-APT10
Host Lithology	andesite	basaltic andesite	basaltic andesite	basaltic andesite	dacite	dacite	dacite	basaltic andesite	basaltic andesite	basaltic andesite	basaltic andesite	dacite
FeO	1.42	1.64	0.86	0.62	0.67	1.10	0.41	0.56	0.88	0.81	0.42	0.42
MnO	0.12	b.d.	0.16	0.17	0.16	0.19	b.d.	b.d.	b.d.	b.d.	b.d.	b.d.
CaO	53.32	53.82	52.50	53.53	53.39	52.86	54.44	54.62	54.50	54.62	53.87	53.74
P_2O_5	40.82	41.79	42.34	42.35	42.30	42.47	42.20	41.84	41.68	41.83	41.54	41.30
F	2.49	2.29	2.03	3.55	2.18	1.85	2.17	2.44	2.06	2.26	2.01	1.97
Cl	0.60	0.52	0.68	0.75	0.68	0.72	0.56	0.57	0.59	0.58	0.53	0.59
Total	99.17	100.61	99.19	100.97	99.94	99.90	100.38	100.49	100.34	100.66	99.03	98.67

Sample	K6-APT11	K6-APT12	K6-APT13	K6-APT14	K6-APT15	K9-APT1	K9-APT2	K9-APT3	K9-APT4	K9-APT5	K9-APT6	K9-APT7
Host Lithology	basaltic andesite	basaltic andesite	dacite	dacite	basaltic andesite	rhyolite	rhyolite	rhyolite	rhyolite	rhyolite	rhyolite	rhyolite
FeO	0.45	0.57	0.33	0.86	1.49	b.d.	b.d.	0.24	0.29	0.25	0.28	0.39
MnO	b.d.	b.d.	b.d.	b.d.	b.d.	b.d.	b.d.	0.11	0.13	0.11	0.13	b.d.
CaO	54.10	54.05	54.00	53.98	54.25	51.69	51.24	52.03	53.55	52.98	52.82	53.58
P_2O_5	41.08	41.02	40.92	40.57	41.05	41.20	41.61	42.04	43.04	42.42	42.40	41.71
F	3.10	2.83	2.84	2.33	2.57	6.51	6.55	3.44	3.30	2.81	2.94	2.07
Cl	0.95	0.99	0.97	0.52	0.51	b.d.	b.d.	0.89	0.58	0.70	0.68	0.85
Total	99.71	99.61	99.19	98.75	100.27	99.45	99.41	98.74	100.88	99.27	99.26	99.15

Sample	K9-APT8	K9-APT9	K9-APT10	K12L-APT1	K12L-APT2	K12L-APT3	K12L-APT4	K12L-APT5	K12L-APT6	K14-APT1	K14-APT2	K32A-APT1
Host Lithology	rhyolite	rhyolite	rhyolite	andesite	andesite	andesite	andesite	andesite	andesite	andesite	basaltic andesite	rhyolite
FeO	0.80	0.32	0.30	0.36	0.38	0.39	0.35	0.40	0.36	0.71	0.44	0.53
MnO	b.d.	b.d.	b.d.	b.d.	b.d.	b.d.	b.d.	b.d.	b.d.	b.d.	b.d.	b.d.
CaO	53.69	53.90	54.20	54.44	54.33	54.41	54.38	54.32	54.51	53.86	54.40	54.37
P_2O_5	41.41	41.98	41.59	42.59	42.23	42.42	41.92	42.11	41.40	42.45	42.21	41.77
F	2.29	3.00	2.24	0.66	2.34	2.13	2.67	2.48	2.47	2.59	2.22	3.05
Cl	0.86	0.81	0.84	0.51	0.51	0.52	0.52	0.53	0.50	0.55	0.50	0.96
Total	99.50	100.14	99.64	99.90	100.32	100.50	100.22	100.30	99.70	100.57	100.37	100.75

Table D.8. Electron Microprobe Settings

Pyroxene microprobe calibration settings

Beam Current: 20keV
Beam Size: 15μm

Major Element	Line	Analyzing Crystal	Standard	Detection Limit (wt.%)
Na	Ka	TAP	Albite	0.023
Mg	Ka	TAP	Diopside	0.019
Al	Ka	TAP	Al2O3	0.017
Si	Ka	TAP	Orthoclase	0.019
K	Ka	PET	Orthoclase	0.026
Ca	Ka	PET	Beeson apatite	0.028
Ti	Ka	PET	Ilmenite	0.037
Cr	Ka	LLIF	Cr2O3	0.049
Mn	Ka	LLIF	MnO	0.051
Fe	Ka	LLIF	Magnetite	0.058
Ni	Ka	LLIF	Ni	0.02

Amphibole microprobe calibration settings

Beam Current: 20keV
Beam Size: 15μm

Major Element	Line	Analyzing Crystal	Standard	Detection Limit (wt.%)
Na	Ka	TAP	Albite	0.023
F	Ka	TAP	Phlogopite	0.141
Mg	Ka	TAP	Forsterite	0.018
Al	Ka	TAP	Anorthite	0.017
Si	Ka	TAP	Orthoclase	0.019
K	Ka	PET	Orthoclase	0.026
Ca	Ka	PET	Beeson apatite	0.026
Ti	Ka	PET	Ilmenite	0.035
Fe	Ka	LLIF	Magnetite	0.056
Mn	Ka	LLIF	MnO	0.048

Feldspar microprobe calibration settings

Beam Current: 20keV
Beam Size: 15μm

Major Element	Line	Analyzing Crystal	Standard	Detection Limit (wt.%)
Na	Ka	TAP	Albite	0.021
Al	Ka	TAP	Phlogopite	0.008
Si	Ka	TAP	Diopside	0.021
K	Ka	TAP	Orthoclase	0.024
Ca	Ka	TAP	Orthoclase	0.023
Fe	Ka	PET	Beeson apatite	0.05

Apatite microprobe calibration settings

Beam Current: 20keV
Beam Size: 15μm

Major Element	Line	Analyzing Crystal	Standard	Detection Limit (wt.%)
F	Ka	TAP	Phlogopite	0.22
P	Ka	PET	Beeson apatite	0.041
Cl	Ka	PET	Scapolite	0.027
Ca	Ka	PET	Beeson apatite	0.033
Fe	Ka	LLIF	Fe	0.055

Magnetite microprobe calibration settings

Beam Current: 20keV
Beam Size: 15μm

Major Element	Line	Analyzing Crystal	Standard	Detection Limit (wt.%)
Mg	Ka	TAP	Diopside	0.025
Al	Ka	TAP	Orthoclase	0.022
Ca	Ka	PET	Diopside	0.027
Ti	Ka	PET	Ilmenite	0.038
Cr	Ka	LLIF	Cr2O3	0.046
Mn	Ka	LLIF	MnO	0.055
Fe	Ka	LLIF	Magnetite	0.067

Glass microprobe calibration settings

Beam Current: 10keV
Beam Size: 5-25μm

Major Element	Line	Analyzing Crystal	Standard	Detection Limit (wt.%)
Na	Ka	TAP	Albite	0.041
F	Ka	TAP	Fluorphlogopite	0.22
Mg	Ka	TAP	Orthoclase	0.037
Al	Ka	TAP	Orthoclase	0.038
Si	Ka	TAP	Diopside	0.041
P	Ka	LLIF	Magnetite	0.072
S	Ka	PET	Pyrite	0.028
Cl	Ka	PET	Scapolite	0.027
K	Ka	PET	Orthoclase	0.049
Ca	Ka	PET	Beeson apatite	0.055
Ti	Ka	PET	Ilmenite	0.078
Mn	Ka	PET	MnO	0.106
Fe	Ka	LLIF	Magnetite	0.101

Ilmenite microprobe calibration settings

Beam Current: 20keV
Beam Size: 15μm

Major Element	Line	Analyzing Crystal	Standard	Detection Limit (wt.%)
Mg	Ka	TAP	Diopside	0.023
Al	Ka	TAP	Al2O3	0.019
Ca	Ka	PET	Diopside	0.027
Ti	Ka	PET	Ilmenite	0.041
Cr	Ka	LLIF	Cr2O3	0.049
Mn	Ka	PET	MnO	0.055
Fe	Ka	LLIF	Magnetite	0.063

Table D.9. Electron Microprobe Standard Analyses and Accepted Values

	Albite		Anorthite		Orthoclase		VG-568		Kaersutite		Kakanui Hornblende	
N	12	Acc. Value[1]	17	Acc. Value[1]	13	Acc. Value[1]	12	Acc. Value[2]	23	Acc. Value[3]	17	Acc. Value[2]
SiO_2	68.77 (0.67)	68.24	44.09 (0.17)	44.17	64.48 (0.26)	64.79	76.69 (0.27)	76.71	38.74 (0.18)	39.30	40.04 (0.18)	40.37
TiO_2							0.07 (0.04)	0.12	4.35 (0.07)	4.14	4.82 (0.08)	4.72
Al_2O_3	20.34 (0.17)	19.90	35.41 (0.59)	34.95	16.67 (0.08)	16.72	12.43 (0.42)	12.06	15.69 (0.10)	15.37	14.62 (0.13)	14.90
FeO^T	0.01 (0.01)		0.39 (0.04)	0.57	1.77 (0.05)	1.77	1.16 (0.10)	1.82	9.26 (0.10)	8.90	10.79 (0.39)	10.89
MnO							0.03 (0.02)	0.03	0.10 (0.02)	0.10	0.09 (0.02)	0.09
MgO							0.02 (0.01)		13.61 (0.26)	13.89	12.45 (0.26)	12.80
CaO	0.02 (0.01)	0.03	18.73 (0.14)	18.63	0.01 (0.01)		0.44 (0.02)	0.50	12.28 (0.10)	12.54	10.10 (0.12)	10.30
Na_2O	12.31 (0.48)	11.94	0.64 (0.18)	0.79	0.95 (0.13)	0.91	4.14 (0.43)	3.75	2.31 (0.10)	2.36	2.58 (0.07)	2.60
K_2O	0.02 (0.01)	0.04	0.02 (0.01)	0.05	15.29 (0.19)	15.49	4.90 (0.14)	4.89	1.24 (0.02)	1.36	2.06 (0.04)	2.05
P_2O_5							0.01 (0.01)		0.03 (0.02)	0.04	0.02 (0.02)	
F							0.20 (0.05)			0.26		
SO_2							0.01 (0.01)					
H_2O*							0.10 (0.02)		n.a.	1.38	n.a.	0.94

[1] Donovan, (pers. comm.) [2] Jarosewich et al. (1980) [3] Reay et al. (1989)

*H2O is determined by stoichometery

Numbers in parentheses represent 1 standard deviation.

N=number of analyes

APPENDIX E

FIELD NOTES AND STRATIGRAPHIC SECTIONS

This appendix contains field notes and measured section illustrations made during the 1997-1998 field seasons. The text includes thickness, general unit description, color, hardness and depositional features. Pumice, lithics and ash are described in terms of size, shape, color, crystallinity, and frequency. Other features such as fossil fumeroles, secondary craters and lacustrine deposits are also included with unit descriptions. Contacts are described between unit descriptions. Samples collected are denoted in the unit description.

Each location was given a name such as OZ-1, denoting the first field site at or near Ozernaya. TINRO station field localities are denoted by TIN#; Pauzhetka by PAU#; Hakutsen River camp by HAK#; Cnezhiny River camp by CNE#, and Pacific Ocean camp by PAC#. Each section has an accompanying latitude and longitude determined by GPS.

OZ1 Location: N 51° 30' 15.6", E 156° 31' 40.0"

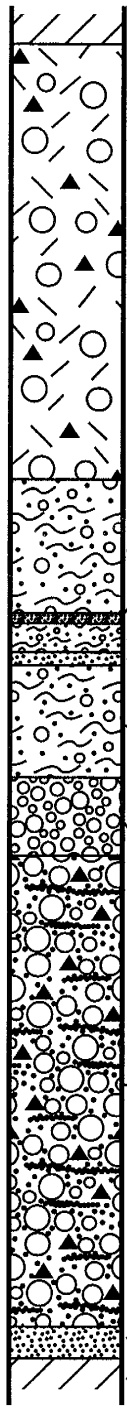

Top of Section

2m lapilli tuff, massive, structureless, poorly sorted, orange-tan. Pumice (15% of unit) are tan and mixed grey and tan, usually 1-6cm in diameter, sub-angular to sub-rounded, crystal content 5%; plagioclase, 90%, pyroxene+hornblende, 10%. Lithics, (5% of unit) are grey and black, scoria, usually 1/2cm in diameter and sub angular. Matrix ash and crystals comprise 80% of unit. Crystal content consists of plagioclase 70%, hornblende and pyroxene 30%, quartz trace. Top eroded. 97KAM4, 97KAM15

Sharp contact

17cm coarse ash tuff, moderately sorted with imbrication and layering of pumice. Pumice is white and comprises 80% of unit. Pumices are too small to determine crystallinity, Crystals (20% of unit), plagioclase 75%, pyroxene and hornblende 24%, quartz trace, Top of unit has some imbrication of pumices, no crossbeds visible, some variable pumice size through section. 97KAM11

Sharp contact

1cm, dark tan-grey, unit similar to first fine ash surge layer, without parting.

Sharp contact

3cm, unit similar to first surge bed, finer grained.

Transitional contact

2cm fine ash tephra, laminated, grey tan, well sorted, no pumice or lithics, trace of small dark crystals Pyroxene and hornblende? Sandy parting lamination in the center. 97KAM12

Sharp contact

15cm coarse ash tuff, well sorted, incipiently crossbedded, dark grey base grading to light grey top. Pumices, small, white, 7%. Crystal rich matrix, plagioclase 70%, pyroxene and hornblende, 20% quartz trace. Lithics, 1-2%, concentrated in bottom half of unit. Some lamination present, top of unit coarsest, weak crossbedding present at top of unit, possible mixed surge-fall unit. Poorly defined laminated beds defined by coarser pumices. 97KAM13

Sharp contact

10cm coarse ash lapilli tuff, uniform thickness well sorted, massive. Pumice are small, mixed white and black and white up to 1/2 cm. Crystals 7-12%, 60-70% plagioclase, 35% hornblende and pyroxene, quartz trace, up to 6cm diameter, usually 2cm, platy shaped. Some lithics present, 2-3%, black and red. 97KAM1, 97KAM2, 97KAM14

Sharp contact

60cm lapilli tuff, well sorted, uniform thickness, coarsening upward to mid-unit then fining to contact. Lapilli sized pumice, white and mixed, plagioclase, pyroxene, and hornblende present in undetermined amounts. Small lithics, black and red. Crystal rich matrix, shower bedded, plagioclase 60%, pyroxene and hornblende 30%; remainder glass ash. 97KAM3, 97KAM3a, 97KAM3b

Sharp contact

4cm very fine ash bed, well sorted, no lithics, crystals or pumice, coarsening upwards to fine ash, grey-tan with some iron stains. Small black specks (possible lithics or crystals) and thin laminations present. Thickness irregular. 97KAM10, 97KAM10a

Sharp contact

Sharp contact with 3-5cm organic rich paleosol. Paleosol grades downward to brown horizon. Black soil layer is irregular in thickness.

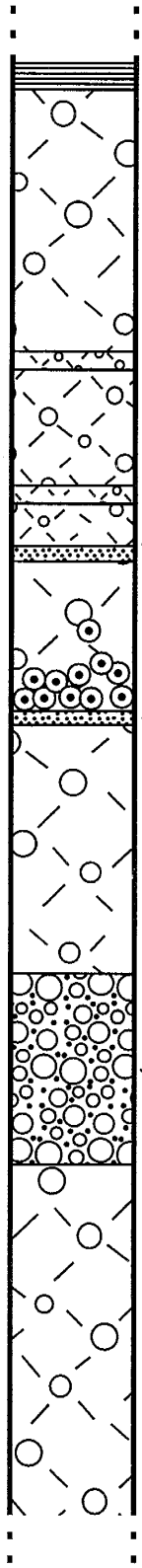

OZ3 Location: N 51° 30' 49.4" E 156° 50' 59.6

Laminar deposits

Contact sharp and irregular

20m blocky lapilli tuff, poorly sorted, massive, structureless, matrix dominated. Pumice 15-20cm, white, KO type, angular. Lithics absent. Poorly defined contacts. Lower contact marked by 40cm thick ash bed. 97KAM5

Contact obscured

15m blocky lapilli tuff, poorly sorted, reverse graded in places, (fluidized?), irregular thickness. Pumice, white, KO type, 10-15 cm diameter. Base 15cm of this unit is finer and grades downward into an ash unit, poorly sorted, lapilli tuff unit of irregular thickness, 30-40 cm thick. 97KAM6.

Sharp contact

15cm lensoid layer, irregular thickness, same components as above, poorly sorted, slight reverse grading. Pumice, white, KO type, up to 10 cm, sub-angular. No lithics.

Sharp contact

8m lapilli tuff, massive, poorly sorted, weak columnar jointing. Pumice concentrated in the lower half of unit, 2% of overall unit, up to 8cm in diameter, grey, rounded to sub-rounded, white fibrous pumice, 40% crystals, plagioclase 50%, pyroxene and hornblende 50%. Lithics 2%, up to 1-2cm in size, black and orange, angular. Accretionary lapilli are up to 3cm diameter. Lower 30cm of unit fine grained tuff: reverse graded, 2a layer, irregular thickness, up to 18cm with rare pumice, eroded contact, 1-2% lithics, black. 97KAM7

Sharp contact

5cm lapilli tuff, composed of 50% accretionary lapilli in a coarse ash matrix with rare pumice lapilli.

Gradational contact

15m lapilli tuff, massive, poorly sorted, grey base, brown top. Pumice 10%, up to 10cm in diameter, usually 5cm, white and light grey KO type, sub-angular. No lithics. Accretionary lapilli are round, brown and up to 1/2 cm in diameter. Matrix is ash with few crystals.

Sharp contact

1.5-3m massive pyroclastic breccia, moderately sorted, reverse graded, massive pumice concentration zone. Pumice 60%, sub-rounded to sub-angular, 60% pumice, up to 50cm in diameter, usually 10-20cm, white pumice, crystals 5% plagioclase 50%, hornblende and pyroxene 50%, grey pumice are dense, but highly vesiculated, grey and white mixed pumice present. No lithics. Fine ash matrix, crystal poor. Rare charcoal observed and sampled. 97KAM8

Sharp contact

20m lapilli tuff, poorly sorted, massive. Pumice 15%, 10-20cm in diameter, white KO type with rare grey pumice, sub-angular to sub-rounded. Lithics increase upward from none to 2%. Ash dominated, crystal poor ash.

PAU5 Location: N51°27'06.8", E156°49'29.8"

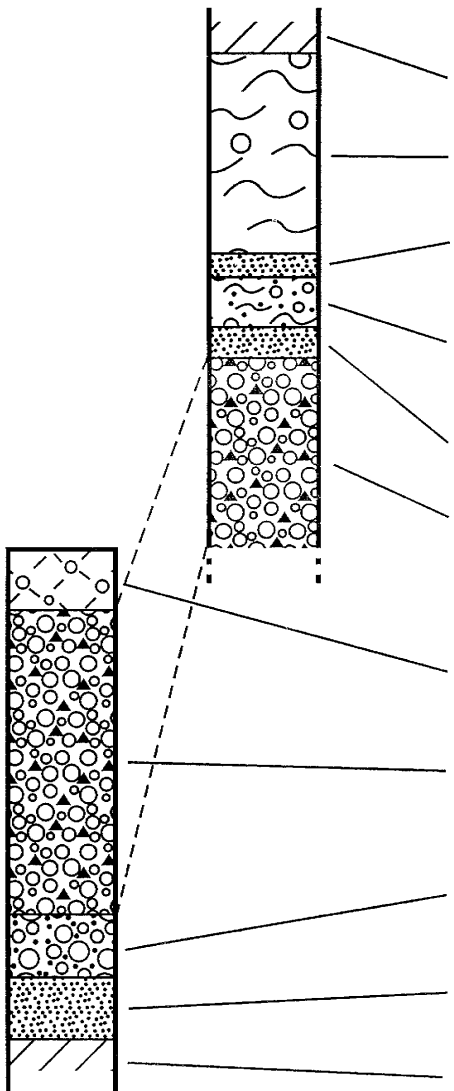

Upper Exposure

Soil cover

Sharp contact

20-0cm coarse ash tephra, well sorted, crossbedded, tan to grey. Pumice, up to 3cm, platy, subangular, white, KO type. Crystal rich matrix, lithics poor.

Sharp contact

1-3cm fine ash tephra, massive, brown. Crystal, pumice and lithic poor. Seems to be glass ash.

Sharp contact

10cm well sorted, coarse ash tephra with occasional laipili pumice, weakly crossbedded, tan. Pumices up to 3cm, platy, subangular to subrounded, white KO type. Lithics poor. Ash rich, 70% crystals: plagioclase, 80%, dark minerals 20%.

Sharp contact

5-7cm ash tephra, well sorted, brown, massive with sandy parting. Pumice and lithics absent.

Sharp contact

35cm coarse ash and fine lapilli tephra, well sorted, crystal shower beds, normal graded. Pumice 3-5cm diameter, white, 5% crystals, hornblende and pyroxene 20%, plagioclase 70%, sub-rounded to sub-angular, Crystal shower beds, plagioclase, 70% pyroxene/hornblende, 30%. Rare mixed and small grey pumices. Lithics 3%, 1-2cm, black, red and grey. Base of unit is more lithic rich.

Lower Exposure

12cm lapilli and fine ash tephra, poorly sorted, massive, matrix supported, grey base, tan top. Pumice 5-7%, white KO type. Ash, glass with few crystals.

Sharp contact

75cm coarse ash and fine lapilli tephra, well sorted, crystal shower beds, normal graded. Pumice 3-5cm diameter, white, 5% crystals, hornblende and pyroxene 20%, plagioclase 70%, sub-rounded to sub-angular, Crystal shower beds, plagioclase, 70% pyroxene/hornblende, 30%. Rare mixed and small grey pumices. Lithics 3%, 1-2cm, black, red and grey. Base of unit is more lithic rich. 97KAM17a-c

Sharp contact

3cm fine ash and fine lapilli tephra, bi-modal sorting, massive, clast supported ash is grey with no crystals or lithics, Pumice are white, up to 3cm in diameter, KO type, angular to sub-angular.

Sharp wavy contact

3cm fine ash tephra, some laminations present, grey with iron stains.

Sharp contact

Paleosol

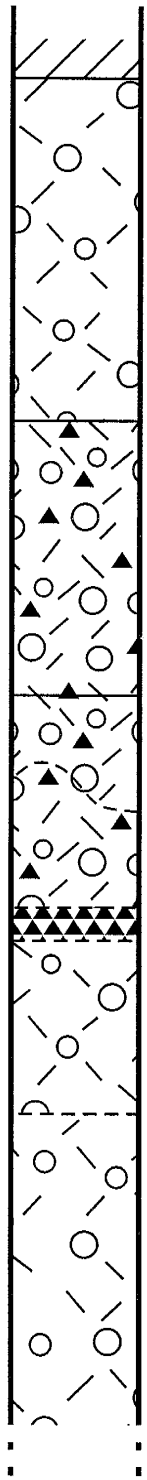

TIN2 Location N51° 30' 40.0" E156° 58' 0.7"

Soil cover

Inferred sharp contact

10m grey ignimbrite top with possible breaks. Possible accretionary lapilli found downslope in float. Unit not directly observed due to slope instability.

Gradational contact

18m tuff breccia, ash supported, massive, dense, indurated, poorly sorted. Pumices up to 12cm, usually 2-3cm, 35-40%, sub-angular to sub rounded, white and orange, crystals 5%, plagioclase, 90%, pyroxene and hornblende 10%. Lithics 5%, usually 1-2cm diameter, black, angular. Ash matrix, indurated, white-orange, angular crystal fragments, ~15%, plagioclase 50%, pyroxene and hornblende 50%. Entire unit highly fractured but no jointing pattern present. Induration may be from vapor phase alteration. 97KAM18a-d

Contact sharp and irregular

6m block and ash tuff breccia, massive, matrix supported, poorly sorted, grey. Pumice 20cm, grey and white, angular to sub-angular, crystal poor, less than 5%, plagioclase 50%, pyroxene and hornblende 50%. Lithics 2-4%, up to 3cm in diameter, tan, grey and black, rounded. 97KAM18e

Contact sharp

6m block and ash tuff breccia, massive, poorly sorted, matrix supported. Pumice 10%, 5cm in diameter, white and grey, crystals 7%, 60% plagioclase, 40% pyroxene and hornblende, sub-angular to sub-rounded. Lithics 20% in zones, up to 15cm diameter, black, grey and tan, rounded, Ash orange, mostly glass.

Gradational contact

12m, coarse ash and lapilli tephra, massive, poorly sorted, matrix supported. Pumices are fragile, highly expanded with few crystals, up to 2cm in diameter, usually .5cm sub-rounded to round. Lithics less than 2%, rounded, black and tan. 97KAMf-g

Base covered

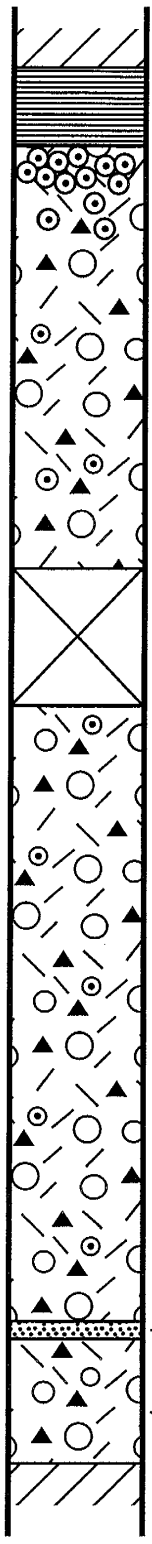

TIN4 Location N51° 29' 46.8" E156° 59' 52.8"

Block and ash flow of Dikii Greben

Contact sharp

71cm Finely laminated, well sorted, lake sediments, grey brown, laminations 1-2mm to centimeter thick, continuous, sometimes marked by coarser ash bed, some layers in the lower 1/3, contain accretionary lapilli .5 cm diameter. Top of bed has soft sediment deformation in the upper 3cm. Light tan layers at the base may be tephra due to presence of accretionary lapilli. Lower 10cm contains numerous ash layers. Thick layer at 18cm is a light brown tephra layer. See lake bed description on the next page for more detail. 97KAM19h

Contact sharp

35m block and ash tephra, massive, poorly sorted, indurated, matrix supported. Pumice 5%, white, rare glassy pumice, up to 7cm diameter usually 3cm, crystals 7%, plagioclase 40%, pyroxene and hornblende 60%, sub-angular to sub-rounded. Lithics are rare. Grey pumice with vapor phase alteration rare. Accretionary lapilli, rare, 2cm diameter, increasing upward to 10%. 97KAM19c

Obscured 20m

40m block and lapilli tephra, massive, poorly sorted, indurated, matrix supported. Pumice 5-7cm, 15% at base, 5% for the rest of the exposure, white, crystals 10%, plagioclase 50%, pyroxene, and amphibole 50%, sub-angular to sub-rounded. Lithics, 1%, black, rounded, 1cm maximum, grading to 3cm upwards. Rare accretionary and coated pumice lapilli, 3cm diameter. 97KAM19b

Contact sharp and irregular

2-3cm ash tephra, poorly bedded, irregular thickness, tan. Pumice 3%, 1cm in diameter. white. 2a layer

Contact sharp

5m exposed, ash and lapilli tephra, massive, slightly indurated, matrix supported, some pumice concentration in lenses, brown. Pumices 15%, 5cm, white, crystal content is 10%, plagioclase 40%, pyroxene and hornblende 60%. Lithics, 2cm in diameter, rounded, black. Rare accretionary lapilli ~2cm diameter.

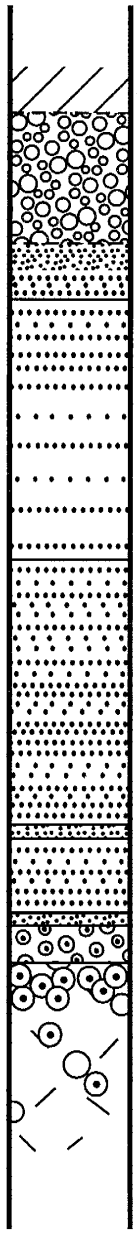

Lake bed description from the top of TIN4

Block and ash from Dikii Greben.

Diffuse gradational contact.

14cm coarse ash tuff, massive, unbedded, white-light grey.

Contact sharp

3cm light brown and dark brown alternating finely laminated sand-silt. Well bedded with some pinch and swell structure. Possible cross bedding present. Soft sediment deformation from DG1 block and ash flow above.

Contact sharp

29cm fine sand and silt, laminated dark brown to grayish. Parallel bedding with lamina from mm thick to cm scale.

Contact sharp

30cm laminated sediments, sand to silt, alternating black, light brown and dark brown to pinkish layers. Black layers seem to be composed of black sub-angular sand. Bedding is 2mm to 10mm thick. 11cm from base of this unit there is a light brown tephra layer.

Contact sharp.

9cm light brown tuffaceous, parallel bedded sediment, light brown. 3 to 4 beds total from 6mm to 25mm thick. Clay and silt sized particles with accretionary lapilli. Possible fine ash tephra associated with secondary explosions. Appears to be fine ash tephra.

Contact sharp.

Above Kurile Lake ignimbrite, conformable, no erosion. Top has small pumice concentration zones at boundary.

TIN 5 Location N51° 23' 13.3" E157° 8' 0.2"

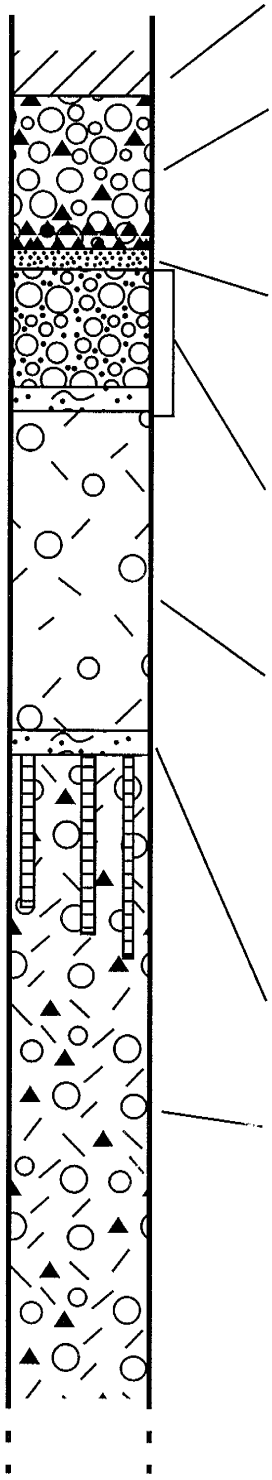

Soil Top

Sharp contact

3m lapilli tuff, massive, poorly sorted, unconsolidated, matrix supported, dark grey. Pumice 10%, grey, 1cm in diameter with rare blocks, crystals 3%, plagioclase, 40%, pyroxene and amphibole 60%. Lithics, 20%, 20cm, red and black, angular to sub-angular. 97KAM20d

Contact sharp

4-6cm ash and coarse ash, complexly crossbedded, irregular thickness, some crossbeds are dark red-orange coarse ash or coarse, lithic rich ash beds at base. Base lithic rich reddish, transition from light grey laminated ash into main unit.

Wavy contact

8m Coarse ash tuff, unconsolidated, massive, grading to a base sandy 2a layer. Pumice 15%, 1-3mm, grey. No lithics, Ash, 85%, glass and crystals. Base layer (2a) has irregular thickness and can contain pumice and light/dark grey sand. 97KAM20C

Wavy contact

15m blocky lapilli tuff, fines depleted, unconsolidated, massive, with pumice rich channel-like concentration at top, 1m x 3m long dark grey, darker than base ignimbrite. Pumice 30% in main part of layer, channel concentration is 50%, grey with rare mixed varities, crystals in grey pumice; 5%, 1/2 plagioclase, 1/2 pyroxene, mixed pumices are grey and black. Lithic poor <1%. Crossbeds at top of ignimbrite. Thin and wavy medium-sized ash bed with laminations and crossbeds, water stained, possible 3 layer. Same color grey as ignimbrite below and grades into lower unit. 97KAM20B

Contact sharp

3cm weakly crossbedded ash bed with sandy parting, secondary water staining, blotchy, altered orange/brown, crossbedded pockets at top.

Sharp contact

35m exposed blocky lapilli tuff, massive, poorly sorted, unconsolidated, dark grey. Pumice, 25% lower unit increasing to 50% at top, white and grey, crystal poor. Pumices lower in unit are more uniform in size than top, up to 9cm usually 2-5cm diameter, sub-rounded to subangular, Pumices show fumerolic alteration in large vesicles. Lithics, 3% 0.5cm-2cm, black and red. Ash is plagioclase and pyroxene 10%, glass 90%. Unit contains fossil fumeroles, 5-7cm in diameter, and altered black ash clumps, black and orange blotchy stains at top of unit. Fumeroles terminate at upper unit and may indicate time break. Fumerole pipes have red- fumerole pipes, are continuous downward and are depleted of fines. 97KAM20A

Base contact covered.

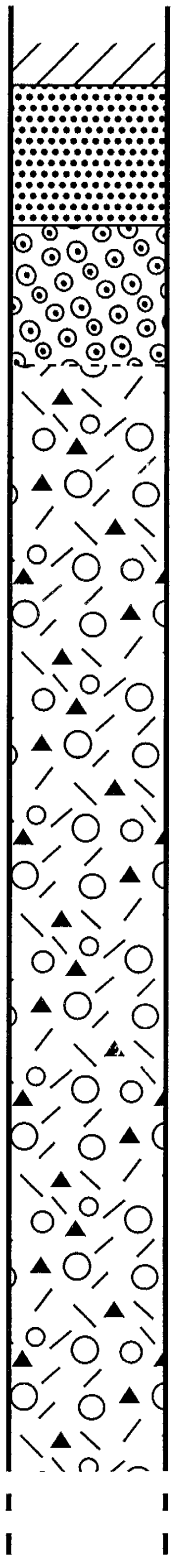

TIN6 Location N51° 30' 13.1" E157° 1' 13.6"

Eruptive units of Dikii Greben

Sharp contact

Lacustrine beds like those of TIN4 suite overlain by Dikii Greben eruptive units.

Sharp contact

60cm accretionary lapilli at top of lapilli tuff, mottled grey tan, well sorted ash with rare pumice. Pumice layers in accretionary lapilli zone may be an explosive fall. Top 2cm is a pumice lapilli layer under 20 cm of reworked material, with small pumices. Iron stains present.

Contact gradational

30m no base exposed blocky lapilli tuff, poorly sorted, unconsolidated, massive, tan. Pumice, 5-10%, white 75%-grey, 25%, pumice concentrations from base are 20% to 10% upwards, angular to sub angular, equant. Grey pumices are banded and dense, plagioclase 5-10% pyroxene trace. White pumices, 15% crystals, plagioclase 75%, pyroxene 25%, light and highly expanded. Lithics, 2%, sub rounded to sub-angular, black and red, 3-5cm in diameter. Ash, fine to coarse ash pumice, crystals and lithics, Pumice blocks are concentrated in middle of unit base 3 meters, 3m above drops to 8%, less than 5% in upper. Top of unit may have increase in block sized pumice. Large 60cm cored bomb found in upper 1/3rd of the exposure. Description: light grey outside, dark grey variable vesiculation dense, high vesiculation, white dense pumice inclusions up to 11cm, usually 2cm diameter, white core has 7-10% crystals, mostly plagioclase with a trace of dark minerals. Not mixed into dark pumice, angular contact with breadcrust fractures throughout. Grey pumice: 10-12% crystals, plagioclase 1/3, pyroxene 2/3, somewhat mixed with dark grey material. Dark grey pumice is glassy and dense, crystal rich 15-18%, plagioclase 1/2, pyroxene/hornblende 1/2, Bomb is angular and intact in deposit.
97KAMA-C

Base of section covered

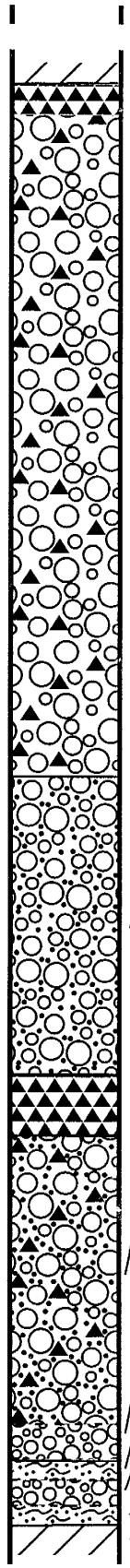

Base of TIN7 (correlated)

1.9m blocky lapilli tuff, shower bedded, typical plinian fall, with zones of coarser lapilli and blocks with occasional lithic rich zones. Pumice, white, 20cm in diameter, KO-type, sub-angular. Lithics up to 10cm 15% abundance in lithic rich zones, overall lithic content is 2-5%, lower 20cm 10% lithics, middle 20cm 15-20% decreasing upwards until lithic zone to 2-5% of unit. At 1.9m from base is a distinct lithic rich zone with large lithic fragments up to 15cm in diameter. Diffuse 10cm wide iron stained band in middle of unit, possible old groundwater level. 97KAM22B

Contact sharp

30cm lapilli tuff bi-modal sorted, fine ash and clay sized, altered. Pumices are coated giving unit dirty appearance. Fine ash approximately 5-10% of unit. Pumice, 85% lapilli and coarse ash pumice up to 5cm in diameter, and blocky, typical KO type pumice, crystal poor, 5% phenocrysts, plagioclase and pyroxene 50/50. Lithics up to 5cm in diameter, with fine ash and clay coatings, grey, red, brown and mixed.

Contact sharp

6cm lithic and ash rich layer. Lithics up to 3cm in diameter, angular, red and black. Ash is very fine and contains ash sized lithic fragments, black and red. Pumice absent.

Sharp contact

10cm lapilli tuff, well sorted. Pumice 75%, white, up to 4cm in diameter. Lithics, 25% red, brown and grey lithics, blocky, 0.5-1cm in diameter.

Diffuse contact

1.5cm diffuse fine ash bed mixed with bracketing units. Ash appears to be altered to clay. Possible rain-flush beds

Diffuse contact

2cm coarse ash tephra, well sorted. Pumice, 70%, angular. Lithics, 30% , black red and grey.

Contact sharp and irregular

2cm coarse ash tephra, well sorted. Pumice, 85%, white, up to 1cm in diameter. 15% lithics, black and red, 0.5cm.

Sharp contact

1.5cm thick fine ash bed, light brown, 1cm from base is a coarse sand layer, unevenly distributed. Possible phreatomagmatic surge layer

Sharp contact,

Base paleosol.

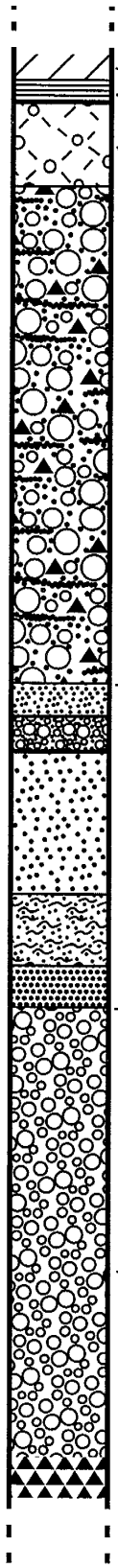

TIN7 Location N51° 30' 56.5" E157° 2' 54.8"

Soil cover

45 cm thinly bedded, well sorted, coarse to fine ash. Reworked. Contains rare pumice and lithics.

Contact sharp.

8-10 cm lapilli tuff, poorly sorted, grey and orange, mottled, coarsening upward from ash (5cm thick) at base to 15% white pumice at top 4 cm. Pumices are 2-3 cm in diameter, white, with secondary oxide staining, sub-rounded, rare lithics, <5%, black. May possibly be an ignimbrite.

Sharp contact

1.4m lapilli tuff, bedded, well sorted, pumice lapilli rich layers up to 10 cm in thickness, subordinate 2-5cm coarse ash beds, color variable, white-light grey, some red-orange iron staining in zones. Upper 35 cm white pumice lapilli up to 5cm diameter with coarse ash matrix of crystals and lithics. Same unit has 5% lithics 5% coarse ash, 90% pumice lapilli and coarse ash pumices. Overall appearance is shower-bedded. More individual beds present but not described due to time constraints.

Sharp contact

70cm variably bedded unit. Distinctive pink layer in lower 18 cm shows weak crossbedding within fine ash beds. Small pockets of coarser ash, possibly surge bed. 40cm of fine ash uniform throughout except upper 10 cm which contains floating pumice lapilli up to 4cm. Well sorted, massive, no bedding, color change slight from darker base to lighter top. Irregular, 1-3cm coarse ash layer at top of pumice layer has pumice, crystals, and lithics up to 10 cm in diameter, distinct pink fine ash with pumice rich lower 3cm and occasional pumice in upper 2cm. Possible fine ash fall deposit and fall in co-ignimbrite.

Contact sharp

2.2m lapilli and tuff breccia, well sorted, white. Upper 15 cm is ~7 beds of alternating, variable colored fine ash layers 1-2 cm thick. Layers are white, yellow, green, pink and orange, upper 8cm coarse ash tephra with pumice lapilli 10%. Pumice, 90%, 3-10cm in diameter, white, KO type, sub-angular. Lower 15cm to lithic zone resembles previous sections top. Plinian deposit. 97KAM22A

Contact correlated across drainage. See next page.

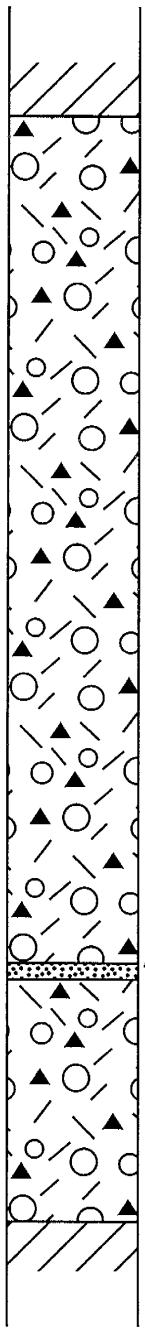

HAK 2 Location N 51° 22' 7.3" E 156° 57' 44.7"

Soil cover

Sharp contact

10m poorly sorted, massive, blocky lapilli tuff, tan, coarsening downward. Pumices, white, 7-10%, up to 15cm in diameter, usually 3-7cm, equant. Lithics, black, up to 2cm, sub-angular. Pumices increase at base 1m to 15%. Pumices sink in water. Carbon sampled. 97KAM24A

Contact sharp and irregular.

0.5cm irregular, wavy, very fine ash marked by iron stain, well sorted, some pumices from lower unit cross contact. Possible 2A layer.

Wavy sharp contact

1m coarse lapilli tuff, pink, poorly sorted, massive. Pumice, 7-10%, white KO type and rare grey 10cm in diameter, sub-angular, equant. Lithics, 2%, black and red, up to 5cm, usually 0.5cm. 97KAM24B

Contact Sharp

Paleosol

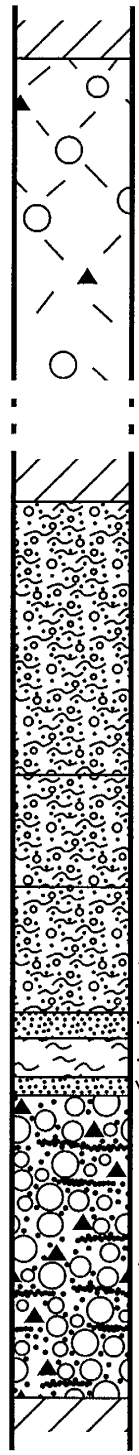

HAK4 N51°21'01.9" E157°00'31.9"

Soil cover

Sharp contact

2.5m exposed grey, coarse lapilli tuff, poorly sorted, structureless. Pumices, 7-10%,up to 10-17cm, usually 7cm, slightly flattened aspect, subrounded, white KO type. Lithics, 2%, 0.5cm. diameter, black, angular. 97KAM25A

Base contact covered, but correlated with a similar outcrop (HAK4.5) downslope 200m.

HAK4.5

Soil/Pyroclastic cover

Contact sharp and wavy

17cm fine lapilli tuff, incipient to well defined cross beds at base, poorly sorted overall. Crossbed lenses consist of well sorted ash. Crossbeds 1cm x 17 to 20cm. Fine ash rich lenses with lapilli pumices, white KO type, mid-section seems more fine ash rich. Top 3cm has 2 discontinuous brown layers, 1cm maximum thickness. Ash in lenses is grey, ash otherwise tan.

Contact gradual

7cm black and orange trough crossbeds, 25cm long 7cm thick. Ash alternates from black and orange to lithic rich. Lithics are 2.5cm in diameter up to 5cm, about 20%, angular. No pumice present. Ash is crystal rich, plagioclase 30%, pyroxene and hornblende 10%.

Contact gradual

6-8cm variable thickness, lapilli tuff, orange, incipient crossbeds or shower beds present. White pumice, KO type, up to 2.5cm usually 4mm. 97KAM25C

Sharp wavy contact

1.5-2cm fine ash bed, well sorted, grey, wavy, structureless.

Sharp wavy contact.

2-3cm lapilli tuff, well sorted, thin, wavy. Pumices are KO type and up to 1cm in diameter.

Sharp wavy contact

3cm fine ash, grey, top 1/2 cm orange. Base 1.5cm is weakly bedded and parallels top bedding plane.

Sharp wavy contact

16-20cm, lapilli tuff, well sorted, shower bedded, pumices up to 5cm in diameter. Orange overall, pumices white KO type, rounded, sub-rounded lithics 3% up to 3cm in diameter usually less than 1cm. 97KAM25b

Contact sharp

Paleosol

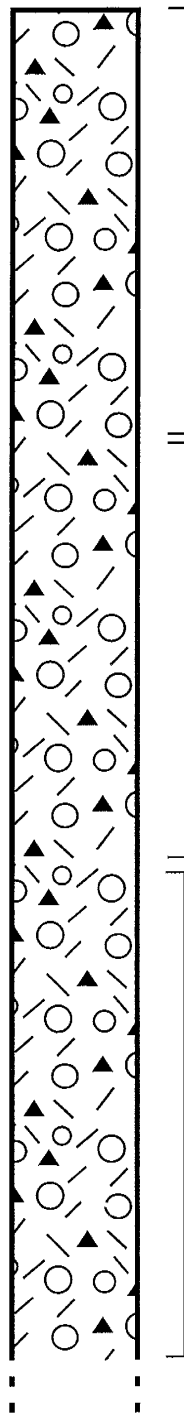

HAK7 Location N51^{o} 23' 32.7" E156^{o} 59' 49.5"

General description: 150m contactless ignimbrite without base exposure. Entire exposure heavily cut with linear gullies and covered in loose ash wash.

Top 1/3rd: Same general description as base. No definite contact, erosional surface is more brownish instead of grey, like base. 97KAM26D

Middle 1/3: Same general description as below. Pumice, 10-13%, 10cm grading to 20cm upwards, same crystallinity as below. Lithics, 10-13%, maximum 3cm in diameter. 97KAM26C upper part of mid-section, 97KAM26B lower part of mid-section

Base 1/3 of section: Massive coarse ash lapilli tuff, poorly sorted, pink-grey. Pumices, 3-7%, light grey and mixed white and grey, coarse ash to blocks 20cm in diameter up to 70cm, sub-rounded to sub-angular, equant to slightly platy. Lithics, 2%, size from coarse ash to 25cm, angular, equant, tan, black, Ash 91-95%, lithics 10%, crystals ~20%, glass ash 70%, Crystals in ash are mostly plagioclase. Outcrop here is drier than most before, and may seem only to be more fines rich than the others. 97KAM26A

Base covered.

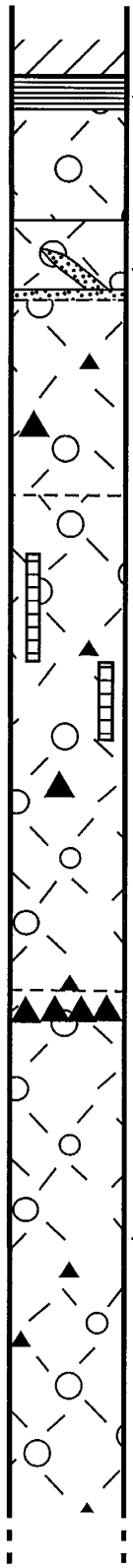

CNE3 Location N51° 22' 32.0" E157° 16' 6.9"

Soil cover

Contact sharp

3.5m grey, massive, structureless, well sorted, fine ash tephra, light grey. Pumices, small 1-3cm in diameter, rounded, KO type. No lithics. 97KAM29H, 97KAM29I

Contact sharp

2m lapilli tuff, massive, grey, poorly sorted. Pumice 3-5%, 2cm, equant, sub-rounded. No lithics. Unit contains beds of fine ash at angles to horizontal ~1cm thick ~30cm long each, possibly fossil fumeroles or crossection of a secondary explosion crater. 97KAM29G

Contact gradational.

30m poorly sorted, blocky lapilli tuff, massive, poorly consolidated, tan, darker at base half and lightens upwards. Pumices, 20-50%, are black, mixed, white, up to 50cm, usually 3-10cm in diameter, fining upward, more dark pumice at the base half. Lithics, 15%, sub-angular to sub-rounded, black, up to 15cm in diameter, usually 2-5cm. 97KAM29D.1, 97KAM29F

Contact gradational

90m blocky lapilli tuff, poorly consolidated, poorly sorted, dark grey. Pumices, 15% to 2% upwards, black, grey, and mixed, white pumice are rare, sub-rounded to sub-angular, up to 70cm but commonly 3-20cm in diameter. Lithics common, 15-20%, increasing upwards to 30%, sub-angular to sub-rounded, various lithologies, commonly 2.5-5cm in diameter up to 10cm. Ash becomes more tan at upper 1/4 of unit into the 3.5m thick upper unit. Unit may contain fossil fumeroles; erosional nature is curtain-like, fin type. Other finger-like remnants in exposure to the east. 97KAM29C, 97KAM29E

Contact gradational over 5cm due to ash color

90m poorly sorted, blocky lapilli tuff, massive, tan, ash matrix, fines depleted. Pumices, 40%, white 80%, black and mixed varieties 20% becoming exclusively white at the base. Pumices up to 50cm, sub-angular, usually 3-10cm, grey black and white, mixed, grey and white, grey and black, and black and grey and white. Lithics 10-15%, usually 7-10cm, sub-rounded to sub-angular, variety of lithologies, lithics increase to small blocks upwards, usually 5-7cm in diameter up to 20cm, sub-angular to subrounded. White pumice rare towards upper contact, grey 40%, black 30%, mixed 30%, ash depleted in fines. Vapor phase alteration common Break in ash color is marked by a lithic rich layer about 10cm thick at the top of this unit.
97KAM29A, 97KAM29B, 97KAM29D.2

Base contact covered

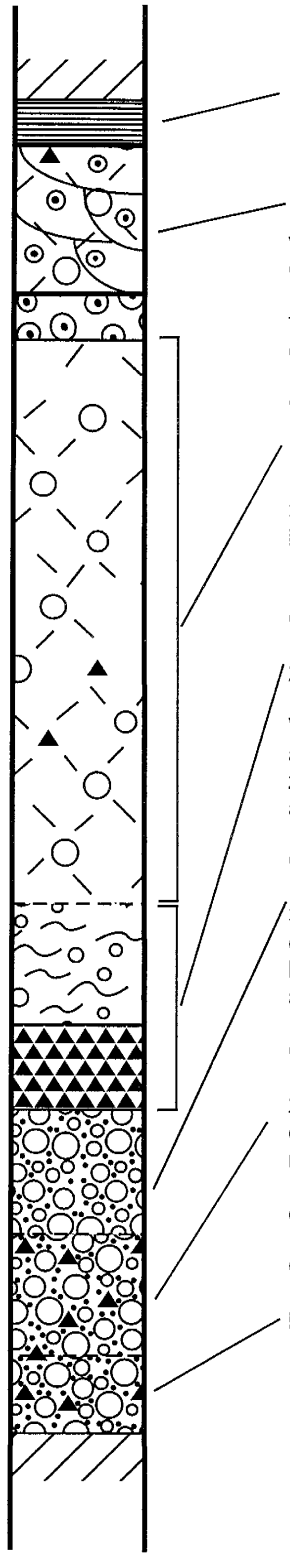

CNE4 Location N51° 21' 39.3" E157° 16' 18.0"

Soil cover

Contact sharp

1m crossbedded, poor to moderately sorted tuff. Base 25cm is tan with weak bedding. Some large pumices at base contact, 3%. Top concentration is 7-10%, mixed and white pumice varieties. Accretionary lapilli ~1%, small, up to 0.5cm throughout. Pumices are sub-rounded, up to 20cm usually 2-5cm, KO type. Top contact is ash and very small lapilli crossbeds, dark grey, 3cm thick with 10° N apparent dip.

Contact sharp

10m coarse lapilli tuff, poorly sorted, massive, tan. Pumice, 7%, 10% mixed, 20% grey, 70% white, angular to sub-rounded, up to 20cm, usually 3-5cm. Lithic concentration 2%, sub-angular to sub-rounded, usually <1cm in diameter to ash sized. Ash tan. Accretionary lapilli at top 1/3rd 2% up to 1-1.5 cm usually 0.25cm, base covered, top sharp contact. 97KAM30B

Contact covered; inferred

20m fine ash lapilli with occasional blocks, massive, poorly sorted, tan. Pumices, white, up to 35-40cm, usually 3-5cm. Lithics rare to 2% at base. Weak surge beds present below lithic zone and grade into ignimbrite above. Ash poor at base, grading into ash rich above 30cm. Lithic rich zone 7cm thick, <20cm from contact. Lithic fragments angular, basalt and andesite, 7cm long. 97KAM30A

Contact Sharp over 2cm

30cm coarse ash, pumice lapilli , well sorted, massive, orange. Ash, 50/50 crystal and lithic ash. Crystals: plagioclase, 75%, pyroxene, 15% 10% hornblende? Pumices, rare ~2%, 1cm in diameter, KO type. Lithics angular to subrounded, black and red, up to 2cm in diameter

Contact gradational

20cm coarse ash lapilli tuff, well sorted, massive. Pumice, 30%, bimodal crystal poor white variety and normal KO type, 4-8cm in diameter, sub-rounded, equant to platy. Crystal poor variety is highly elongated. Lithics, 10%, 2-3cm diameter, black and red. Fine ash in matrix with same components as ash above. Top is pumice poor. 97KAM30C

Contact Sharp

Paleosol

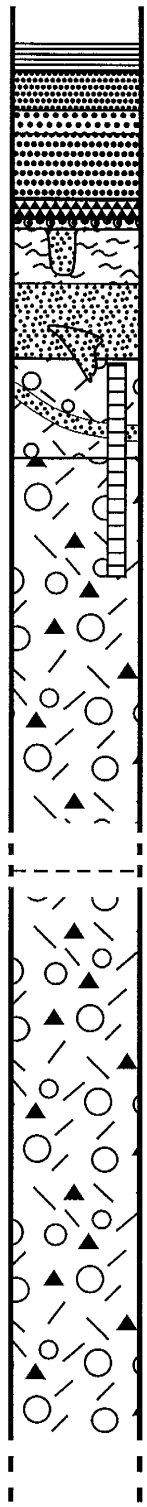

CNE6 Location N51° 21' 53.7" E157° 16' 12.7"

Soil Cover

Contact sharp

3m laminar beds, sand and silt sized, well sorted, alternating tan and brown. Laminations range from mm thick to massive beds 10cm or more thick. Half way up the unit is a 10cm thick accretionary lapilli bearing layer which contains lapilli up to 7-8mm in diameter. Base of unit is sandy with irregular pinch and swell structure. Some lenses of crystal rich material are present above fossil fumeroles. 97KAM32G

Contact sharp

30cm lapilli tuff, tan to grey upwards, poorly sorted, massive. Pumice, white 25%, usually 3-5cm in diameter, round and very light with few phenocrysts. Lithics, trace. Ash, tan, fines poor, contains 15x30cm and 5x30cm pipes which crosscut the contact into lakebeds. Some mineralization staining on the pumices in the pipes. Fines absent in the pipes. Fine ash layer at a 15-20o angle cuts this unit. It is 7-10cm thick, tan, well sorted and contains 2% white pumice identical to the pumice found in the rest of this unit. This layer may represent a secondary explosion crater. below this bed trhe exposure is described as blocky lapilli tuff, tan, massive, poorly sorted. Pumices, white, ~15% sub-rounded, equant, some mixed black and white and grey ~1-2%, Pumices very crystal poor, but some are more crystal rich. Ash, fines depleted. Also contains fossil fumerole:
Fossil Fumerole: 1/2m observed length. Slight yellowing around feature in all layers. This fumerole pipe is present up to the lake beds. May be a secondary explosion crater. 97KAM32D, 97KAM32E, 97KAM32F

Contact covered

100m blocky lapilli tuff, poorly sorted, massive, loosely consolidated, with vegetative cover. Pumice, 30% grey black and white, usually 3cm up to 14cm, equant, sub-angular to sub-rounded. Ash, fines depleted. Lithics, 5%, 2cm, angular, black. Pumices show vapor phase alteration. Pumice concentration increases up to 30% at top. 97KAM32C

Covered contact

50m blocky lapilli tuff, massive, weakly columnar, poorly sorted, loosely consolidated, grey. Pumice, 7-10%, grey, usually 5-7cm in diameter up to 25cm, sub-rounded to sub-angular, equant to platy, crystal poor, 2% plagioclase, and a trace of black minerals. Some pumices are highly expanded others are glassy. Ash, grey and crystal rich. Lithics, 3%, sub-angular to angular, equant, usually 3-4cm in diameter up to 7cm, lack. Pumices: Grey, no black or white evident. 40m grey ignimbrite exposure inferred. 97KAM32A, 97KAM32B

Base covered

This thesis is accepted on behalf of the faculty

of the institute by the following committee:

Philip R. Kyle

Advisor

Nina W. Dunbar

Kenneth R. Lowder

18 Oct 1999

Date